THE UNIVERSITY
of EDINBURGH

The Role of MiR-148b in Angiogenesis and Endothelial Cell Plasticity

Vladislav Miscianinov

Submitted for the degree of Doctor of Philosophy

University of Edinburgh 2018

DECLARATION

The thesis herein is solely my own work. Apart from where stated the experiments were performed entirely by me. I confirm that this work has not been previously submitted for any other degree.

……

ACKNOWLEDGMENTS

I am absolutely grateful to everyone who accompanied me in the exciting and rewarding journey of my PhD. I would like to say huge thank you to my supervisor Andrea Caporali, who did everything he could and even more to make my PhD interesting and productive. Andrea helped me to develop my scientific curiosity and has taught me how to be a good scientist. I would like to thank my second supervisor Gillian Gray for her constant support and advice, which were helping me throughout my PhD. I also thank Mellisa Cudmore for her wise feedback during my yearly review meetings, which was very useful.

I was fortunate to work closely with my colleague and good friend Andrea Martello, who I would like to thank for valuable input in my project and for routine conversations about science.

Finally, I want to say a special thank you to my family for supporting me and believing in me. My family was always there for me, which made me strong and I am immensely grateful for that.

ABSTRACT

Endothelial cells (ECs) have a well-established role in the maintenance of vascular physiology. Moreover, ECs participate in many physiological processes such as angiogenesis, blood homeostasis, inflammatory response, lipid metabolism and many more. Angiogenesis is one of the most studied functions of endothelium, where ECs participate in the formation of the new blood vessels. Additionally, ECs can also exhibit a form of plasticity called endothelial-to-mesenchymal transition (EndMT), which is characterized by the loss of endothelial-specific morphology and markers and acquisition of mesenchymal-like phenotype. Both angiogenesis and EndMT can be regulated by physiological cues, such as inflammation and haemodynamic forces, as well as number of molecular stimuli, such as TGF-β. Interestingly, recent evidence suggests that angiogenesis and EndMT can be orchestrated by miRNAs. This thesis aims to address the hypothesis that miR-148b is a modulator of angiogenesis and endothelial cell plasticity in the form of EndMT.

The preliminary high-throughput miRNA screen has identified miR-148b as a strong enhancer of HUVEC proliferation. Subsequent bioinformatic analysis and validation demonstrated that TGFB2 and SMAD2 are direct targets of miR-148b in ECs. Further experiments using gain- and loss-of-function approaches demonstrated that miR-148b regulates EC function. Specifically, overexpression of miR-148b enhanced EC migration, proliferation and *in vitro* angiogenesis, whereas its inhibition promoted EndMT, decreasing the expression of CD31 and VE-Cadherin and elevating collagen 1. Furthermore, inflammatory cytokine challenge decreased miR-148b levels in ECs, promoting EndMT, via upregulation of SMAD2, and enhancing reactive

oxygen species production, all of which were abrogated by exogenous miR-148b. Finally, in a mouse model of skin wound healing, delivery of miR-148b mimics promoted wound angiogenesis and accelerated wound closure. In contrast, inhibition of miR-148b enhanced EndMT in wounds impairing wound closure, which is reverted by SMAD2 silencing.

Together, the data in this thesis supports the hypothesis that miR-148b regulates angiogenesis and endothelial cell plasticity, and provides the evidence that miR-148b upregulation enhances both *in vitro* and *in vivo* angiogenesis, while its knockdown promotes EndMT. This thesis demonstrates for the first time that miR-148b could be a key factor controlling EndMT and vascularization, thus opening a new avenue for therapeutic application of miR-148b in diseases that require vascular and tissue repair.

LAY SUMMARY

The human body is composed by a complex network of blood vessels, which supply every tissue and every organ with nutrients and oxygen. When there is a need for new blood vessels, a process is initiated in the body, called angiogenesis. From Ancient Greek the word “angio” means vessel while “genesis” means creation. During angiogenesis new blood vessels are formed from pre-existing vessels, which is important for different processes in the body such as development and wound healing.

This thesis describes a novel role of a small molecule, called microRNA-148b, to induce the process of angiogenesis. MicroRNAs are naturally found in the body, where they regulate different genes and processes. This study demonstrates that microRNA-148b activates the endothelial cells and makes them form capillary networks “in a dish” as well as new blood vessels. When microRNA-148b is applied on mice surgical wounds, it can accelerates the process of wound healing.

On the other hand, when microRNA-148b is removed, the endothelial cells change into different type, mesenchymal cells – a process also known as differentiation. This process is harmful and can occur due to chronic inflammation, when the immune system is overstimulated. What is more, in mice, the loss of micoRNA-148b leads to poor wound healing due to reduction in endothelial function.

In conclusion, the novel findings in this thesis can be used to create new medicines to promote angiogenesis and to treat non-healing wounds.

PRESENTATIONS AND PRIZES

"MiR-148b: the missing link between inflammation and endothelial-to-mesenchymal transition". Winner of the Early Career Researcher Prize, Cardiovascular Science Symposium, University of Edinburgh, June 20th, 2017.

"MicroRNA-148b regulates endothelial-mesenchymal transition through TGF-beta signalling". Oral presentation at the Scottish Cardiovascular Forum, University of Glasgow, February 4th, 2017.

"Functional role of miRNA-148b in vascular disease". Poster presentation at the Cardiovascular Science Symposium, University of Edinburgh, June 16th, 2016.

Runner-up prize for an oral business plan presentation at Biotechnology Young Entrepreneurs Scheme competition, Stevenage BioScience Catalyst, GSK, October 19-21, 2015.

PUBLICATIONS

Miscianinov, V. et al. (2018). MicroRNA-148b Targets the TGF-beta Pathway to Regulate Angiogenesis and Endothelial-to-Mesenchymal Transition during Skin Wound Healing. Molecular Therapy.

Caporali, A., Martello, A., **Miscianinov, V.**, Maselli, D., Vono, R., Spinetti, G. (2017) Contribution of pericyte paracrine regulation of the endothelium to angiogenesis. Pharmacology & Therapeutics, Mar;171:56-64.

Caporali, A., **Miscianinov, V.**, Saif, J., Emanueli, C. (2017) MicroRNA transport in cardiovascular complication of diabetes. Biochimica et Biophysica Acta (BBA), Dec;1861(12 Pt B):2111-2120.

PATENTS

Miscianinov, V., Caporali, A. 2018. Method of treatment of soft tissue wounds. United Kingdom Priority Patent Application No 1806569.8, filed 23 Apr 2018. Patent Pending.

TABLE OF CONTENTS

LIST OF FIGURES

LIST OF TABLES

CHAPTER 1: INTRODUCTION

1.1 Endothelial cells and EC plasticity

1.1.1 Endothelial cell biology

One of the first organs systems to develop during embryogenesis is vasculature, serving as a fundament for correct functioning and survival of all other organs in the body. The composition of a blood vessel includes the inner and luminal layer, which are formed by endothelial cells, surrounded by a vessel wall made from smooth muscle cells. Notably, endothelial cells are the first ones to develop during the formation of the blood vessel, which, following a rapid expansion, are remodelled into a circulatory network that subsequently forms a vasculature within different organ systems such as brain, retina, kidney and liver. What is more, vascular endothelium participates in development of blood and the heart, where endothelial cells also undergo a differentiation, also known as transition, into hematopoietic cells as well as cardiac mesenchyme, respectively (Dejana et al., 2017).

After the gastrulation process is finished in the extraembryonic yolk sac, vasculogenesis is initiated, which gives rise to the primordial endothelial cells. When mesodermal progenitor cells receive the signal from visceral endoderm, they form the endothelial cells, which then merge into vascular plexi that are remodelled into capillary networks during angiogenesis. There are number of molecular signals that facilitate endothelial cells formation and differentiation. Specifically, fibroblast growth factor 2, such as FGF2 and bFGF, and bone morphogenic protein 4 (BMP4) not only promote mesoderm formation, but also contribute to endothelial cell differentiation (Marcelo et al., 2013). Moreover, BMP4 in turn mediates Indian hedgehog (IHH) signalling, which drives the development of endothelial cells (Marcelo et al., 2013). One of the most potent regulators of vasculogenesis is vascular endothelial growth factor

(VEGF-A), which interacts with its receptors, VEGFR1 (Flt-1) and VEGFR2 (KDR) that is essential for the development of vascular plexus (Chung and Ferrara, 2011). Interestingly, embryonic stem cells, isolated from the double negative mutant mouse for VEGFR2$^{-/-}$, can give rise to endothelial cells, but they are not able to expand *in vitro*, suggesting that VEGF-A regulates survival and propagation of endothelial cells, rather than differentiation (Dejana et al., 2017). Furthermore, endothelial cell development is tightly orchestrated by transcription factors. Specifically, the majority of the promoters and enhancers of endothelial-specific genes contain binding sites for the transcription regulators from ETS family (De Val and Black, 2009, Birdsey et al., 2015). Notably, ETS variant 2 (Etv2) modulates the cell fate change from mesodermal progenitors to endothelial cells (De Val et al., 2008).

1.1.2 Angiogenesis

Angiogenesis is defined as a following step of remodelling of the primary vascular plexus into the circulatory network as well as formation if new blood vessels from pre-existing ones (Risau, 1997). In a healthy adult body, endothelial cells are guarded from the stimuli such as VEGF, NOTCH, angiopoietin-1 (ANG-1) and FGFs. However, when quiescent endothelial cells are subjected to angiogenic signals listed before as well as chemokines released by inflammatory, tumour or hypoxic cells, the pericytes, which normally surround the endothelium and suppress its proliferation, start to migrate from the vessel wall via proteolytic degradation facilitated by matrix metalloproteinases (MMPs) (Fig. 1 a) (Carmeliet and Jain, 2011). In particular, hypoxia-inducible factor 1α (HIF-1α) makes endothelial cells sensitive to angiogenic cues. In addition to the loss of endothelial cell junctions, which are normally composed by VE-cadherin and claudins, and the resulting vessel dilation, the endothelial cell layer permeability increases in response to VEGF;

this in turn facilitates the increased deposition of the extracellular matrix (ECM) proteins, which form the scaffold for the migrating endothelial cells following the integrin signalling (Fig. 1 a) (Carmeliet and Jain, 2011). Notably, one endothelial cell, known as a tip cell, is selected to lead the tip in response to stimuli such as VEGF, neuropilins (NRPs), DLL4 and JAGGED1 (Fig. 1.1 a); the tip cell is followed by the remodelled and dividing neighbouring endothelial cells, which form the elongating stalk in presence of NOTCH signalling, WNT, FGFs and placental growth factor (PIGF), and build the lumen of the new vessel facilitated by VEGF, hedgehog, CD34, sialomucins and VE-cadherin (Carmeliet and Jain, 2011). The filopodia that resides on the tip cells facilitates the response to environmental signals such as ephrins and semaphorins; on the other hand, the stalk cells release the signals such as EGFL1 into the extracellular matrix scaffold in order to provide the positional information of the adjacent endothelial cells to promote further stalk elongation (Fig. 1.1 b) (Carmeliet and Jain, 2011). The blood flow is established following the assembly of the bridge between two nascent vessels made from myeloid cells (Fig. 1.1 c); the endothelial cells are then put back into quiescent state followed by coverage with pericytes in response to stimuli such as transforming growth factor-β (TGF-β), platelet-derived growth factor B (PDGF-B), ephrin-B2, NOTCH and ANG-1 (Carmeliet and Jain, 2011). Finally, the basement membrane is reassembled as a result of the action of protease inhibitors, such as tissue inhibitors of metalloproteinases (TIMPs) and plasminogen activator inhibitor-1 (PAI-1), followed by formation of cell-to-cell junctions, which ensure the correct blood flow through newly made vessels (Fig. 1.1 c) (Carmeliet and Jain, 2011).

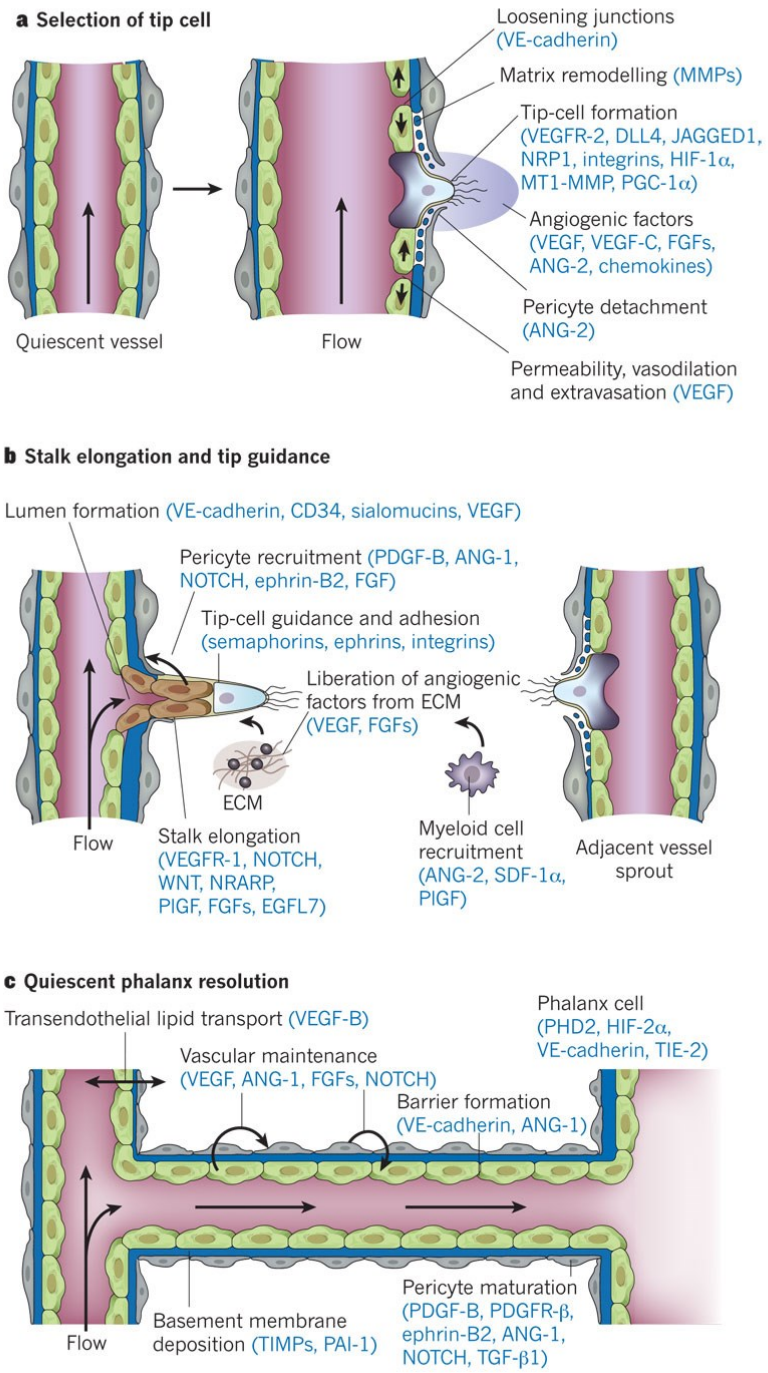

Figure 1.1| Molecular basis of angiogenesis. The key steps of the vessel branching are displayed with the key molecules, which facilitate angiogenesis. **a.** After the stimulation with angiogenic stimuli, the quiescent vessel dilates followed by the formation of the tip cell, which

directs the subsequent branch formation. The degradation of basement membrane, loosening of endothelial cell junctions and pericytes detachment are needed for tip cell assembly. Enhanced permeability of the endothelium contributes to the deposition of ECM proteins and formation of the scaffold. **b.** Tip cells follow the navigation of the angiogenic signals and attach to ECM in order to migrate. The lumen is formed by the stalk cells that proliferate and elongate resulting into fusion of the sprouts that form the nascent vessel. **c.** Following the joining of the neighbouring branches, the blood flow is established and the endothelial cells become quiescent (reproduced with permission from Carmeliet and Jain 2011).

There is a direct link between inflammation and endothelial cell biology as well as angiogenesis. The first evidence of the association between inflammation and angiogenesis came from the study in 1995, where it was demonstrated that the infiltrating monocytes, associated to capillary sprouting after microembolization in the ischemic porcine myocardium, express the proangiogenic insulin growth factor-1 (IGF-1) (Kluge et al., 1995). Under ischemic conditions, the inflammatory cells start to secrete proangiogenic stimuli, such as VEGF and TNF-α, which lead to an increase in vascular permeability as well as attract more inflammatory cells (Grivennikov et al., 2010, Costa et al., 2007, Eltzschig and Carmeliet 2011, Konisti et al., 2012). Moreover, leukocytes and macrophages are able to secrete MMPs, plasminogen and cathepsins, which facilitate the remodelling of extracellular matrix allowing the formation of neovessels (Rüegg, 2006, Kundu and Surh, 2012). Another link between inflammation and angiogenesis is a production of reactive oxygen species (ROS) by inflammatory cells, which can acutely promote angiogenesis (Reuter et al., 2010, Guzik et al., 2003).

1.1.3 Models for evaluation of angiogenesis

In the past 20 years a significant progress has been made in generation of *in vitro* methods to analyse angiogenesis. The most widely used approach is the model of endothelial cells tubulogenesis, in which ECs form tube structures

and cellular networks in 3D matrixes, such as type I collagen and fibrin (Simons et al., 2015). In short, endothelial cells are seeded into 3D matrix that come together and assemble into tubes with a lumen; the tubes then can be analysed using electron and confocal microscopy. Notably, tube formation also produces physical tunnel spaces within the 3D matrix which are generated by the action of MT1-matrix metalloproteinase that degrades the extracellular matrix (Davis et al., 2011). Alternatively, another *in vitro* method is a sprouting model, which involves seeding endothelial cells into a collagen or fibrin matrix to facilitate sprouting and lumen-forming capillary-like structures formation (Simons et al., 2015). This process can be assisted by coating endothelial cells with microcarrier beads, which enables the visualization of endothelial cell growth over time (Nehls and Drenckhahn, 1995). One of the most reproducible *in vitro* angiogenic assays is a 2D sprouting assay using a rich in laminin Matrigel matrix, which allows endothelial cells to form capillary-like lumenless structures (Ponce, 2009).

In terms of *in vivo* methods, one of the most easy to manipulate, visual and physiologically significant postnatal angiogenic assays is a wound healing model (Simons et al., 2015). Wound healing is a tightly organised physiological reparative response to the skin injury and involves a cascade of complex and synergic cellular processes such as hemostasis, inflammation, proliferation and remodelling. Angiogenesis plays a crucial role during the proliferative stage of wound healing, which supplies the granulation tissue with oxygen and nutrients. Notably, the change in vessel density during the wound repair is in a form of a bell-shaped curve. Specifically, during intense wound healing angiogenic response is very strong peaking at ~5 days post-injury, where vessel density is many-fold higher than in uninjured skin; moreover, after the healing processed is finished the vascular density returns to control levels

(Simons et al., 2015). In a mouse model of punch wound repair (Dunn et al., 2013), the vascularization is the most elevated in a period between 4 and 8 days post-injury, thus before and during this peak the model of wound healing represents the angiogenic response (Simons et al., 2015). Moreover, the inflammatory stage of the healing is to be under stringent control as excessive or prolonged inflammatory response is detrimental for the healing process. Failure in regulation of angiogenesis and inflammation during wound healing causes poor wound closure and might lead to skin ulceration.

1.1.4 Endothelial-to-mesenchymal transition

In a healthy blood vessel, the endothelial cell is maintained endothelial via a number of different mechanisms and signalling pathways. Spacial localization of the endothelial cell strongly determines the endothelial phenotype. A quiescent endothelial cell resides in the tight contact with neighbouring endothelial cells via receptors such as VE-Cadherins, CD31 and VEGFR2 as well with the basement membrane via the integrins α/β. The integrins, in turn, activate FAK/ILK cascade, promotes endothelial cell homeostasis (Fig. 1.2) (Krenning et al., 2016). Moreover, the signalling via ALK1/TGFβR2 in response to the binding of the ligands, including TGF-β and BMPs, induces the phosphorylation of SMAD1/SMAD5 complex, which maintains the endothelial cell function, such as angiogenesis (Fig. 1.2) (Gonzalez-Nunez et al., 2013). Importantly, shear stress induced by the blood flow is another strong modulator of the endothelial fate. When endothelial cells are subjected to laminar shear stress, it is sensed by the mechanoreceptors, which activate MEK5-ERK5-MEF2 signalling cascade that, in turn, promotes the expression of KLF2 transcription factor leading to endothelial phenotype maintenance (van Thienen et al., 2006).

On the other hand, endothelial-to-mesenchymal transition (EndMT) is a process by which endothelial cells lose their endothelial specific markers and acquire mesenchymal-like phenotype (Piera-Velazquez and Jimenez, 2012). Specifically, EndMT is characterized by the loss of endothelial cell markers such as VE-cadherin (VE-cad), von Willebrand factor (vWF) and platelet-endothelial cell adhesion molecule 1 (PECAM-1, CD31), and elevated expression of α-SMA, vimentin, N-cadherin and extracellular matrix (ECM) proteins such as collagen type I and III (Table 1) (Arciniegas et al., 2007). What is more, during the process of EndMT, the endothelial cells exhibit cytoskeleton rearrangement resulting in a change in cell polarity and leading to acquisition of stretched and more fibroblast-like morphology (Arciniegas et al., 2007). As a consequence, these phenotypical and morphological alterations during EndMT lead to the disruption of endothelial cell monolayer.

Depending on the final EndMT markers, which are expressed by the differentiated cells, it is now believed that the transition program has three possible outcomes: mesenchymal cells, fibroblasts and smooth muscle cells (Fig. 1.2). Specifically, mesenchymal "stem" cells start to express proteins such as FSP1 and Sca1; fibroblasts become enriched in fibronectin, N-cadherin, vimentin and collagen (mostly type I and III); smooth muscle cells acquire markers of cytoskeleton rearrangement such as α-SMA, SM22α as well as smooth muscle-specific calponin (SM-calponin) and Notch3 (Table 1) (Chen and Simons, 2016).

Markers of EndMT	
Downregulated	**Upregulated**
CD31, VE-Cadherin, eNOS, von Willebrand factor (vWF), Tie-1, Tie-2	α-SMA, Sca1, Vimentin, Collagen I/III, FSP-1, SM22α, N-Cadherin, SM-calponin, Fibronectin, Notch3, MMP2, MMP9, VCAM, ICAM1

Table 1| Selected markers of EndMT. (Dejana et al., 2017, He et al., 2013)

It is widely accepted that transforming growth factor beta (TGF-β) is the main inducer of EndMT, which binds to its heteromeric receptor (TGFβR), consisting of activin-like kinase 5 (ALK5, also known as TGF-β type I receptor, TGFBR1) and the TGFβ type II receptor (TGFBR2); ALK5 phosphorylation triggers formation Smad 2/3/4 complex and its translocation to the nucleus where it induces EndMT gene expression (van Meeteren and ten Dijke, 2012) (Fig. 1.2).

The first claim that endothelial cells enter the process of endothelial-to-mesenchymal transition was made by Arciniegas et al. (Arciniegas et al., 1992), who has demonstrated that bovine aortic endothelial cells (BAEC) are able to differentiate into smooth muscle cells (SMCs) *in vitro*. The study showed that stimulation with TGF-β1 facilitated the expression of α-SMA and loss of coagulation factor VIII (FVIII) in the endothelial cells (Arciniegas et al., 1992). Notably, TGF-β1-induced EndMT is firmly modulated by the transcription factors Snail and Slug and occurs partially via TGF-β receptor 1 (TGF-βR1), due to the fact that its inhibition by small molecule drug can to decrease but not stop the transition program (Diez et al., 2010). Similarly, TGF-β2 is able to promote EndMT program in Snail-mediated manner and lead to downregulation of endothelial-specific markers and increase in smooth muscle cell-specific proteins such as α-SMA, SM22-α and calponin (Kokudo et

al., 2008). It is important to point out that TGF-β2 can switch on the EndMT program in endothelial cells via activation of Smad signalling pathway; the induction of this cascade in turn leads to overexpression of Snail transcription factor (Medici et al., 2011). Both TGF-β1- and TGF-β2-induced transition programs can be inhibited by the action of FGF signalling, which occurs via FGF receptor (FGF-R) and its adaptor FRS2. In particular, the silencing of FRS2 in human umbilical artery endothelial cells (HUAECs) led to elevation in the expression of markers of smooth muscle cells such as α-SMA, SM22-α, SM-calponin and Notch3; moreover, the levels of both mediators of EndMT, TGF-β1 and TGF-β2, were upregulated (Chen et al., 2012).

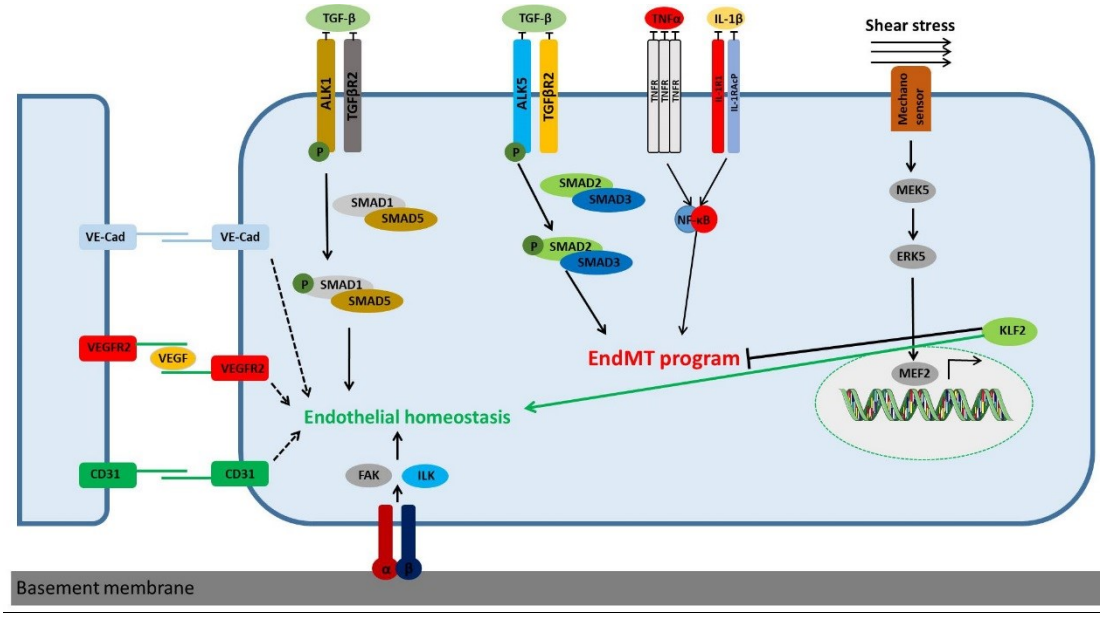

Figure 1.2| Stimuli determining EC behaviour and EndMT. The cell-to-cell contact between the ECs via interactions of VE-Cadherins, CD31 as well as VEGFR2 maintains the endothelial phenotype. The signalling pathway TGFβR2/ALK1, upon the interaction with the ligand such as TGF-β, induces the activation of SMAD1/SMAD5 leading to the maintenance of the endothelial homeostasis. Endothelial cells' spacial sensing of the basement membrane via the integrins α/β induces FAK/ILK signalling, enhancing the endothelial characteristics. The molecular cascade TGFβR-Smad2/Smad3 upon interaction with the ligands, BMP6 and TGFβ1/TGFβ2, lead to induction of EndMT program. The inflammatory pathways induced by TNF-α and IL-1β actvates the NF-κB signalling, which promotes EndMT. The shear stress

induced by laminar blood flow is sensed by mechano-receptors leading to the induction of MEK5/ERK5/MEF2 cascade, promoting KLF2 expression, which enhances the endothelial cell phenotype and blocks EndMT.

Specifically, FGF signalling via its receptor, FGFR1, induces the expression of let-7 miRNA, which directly targets TGFβR and inhibits its expression, leading to the blockage of the EndMT program (Fig. 1.2) (Chen et al., 2012); inflammation and shear stress are strong modulators of FGFR1, which can reactivate EndMT via silencing of the receptor.

In addition, to the discussed above inducers of EndMT, there are other known modulators of transition program such as miRNAs (Ghosh et al., 2012a), shear stress (Moonen et al., 2015) and inflammation (Perez et al., 2017). In particular, it has been recently shown that inflammatory cytokines, such as tumour necrosis factor alpha (TNF-a) and interleukin-1 beta (IL-1β), can trigger EndMT process via binding to their receptors, TNF-R and IL-R1 respectively, and inducing NF-κB translocation to the nucleus, where it drives the expression of EndMT-specific genes (Fig. 1.2) (Mahler et al., 2013, Chaudhuri et al., 2007, Arciniegas et al., 2008). Romero et al. has demonstrated for the first time that IL-1β is able to facilitate phenotypic changes in endothelial cells such as acquisition of spindle-shaped morphology, cytoskeleton rearrangements and loss of endothelial-specific CD31 and von Willebrand factor markers (Romero et al., 1997); these findings were then validated by a number of studies stating that IL-1β can induce EndMT (Rieder et al., 2011, Maleszewska et al., 2013). Similarly, TNF-α has been reported to activate EndMT program in the endothelial cells via activation of NF-κB signalling (Mahler et al., 2013). Notably, both IL-1β and TNF-α are able to promote skin fibrosis (Romero et al., 1997, Chaudhuri et al., 2007).

Importantly, the presence of high laminar shear stress attenuates EndMT program via expression of KLF2 transcription factor (Fig. 1.2). As a result, EndMT can only occur when the endothelial cells within the blood vessel are subjected to the low shear stress, mainly via Snail upregulation (Mahmoud et al., 2017).

Notably, EndMT can occur as a partial or a complete transition. Partial or early EndMT is characterized by the downregulation or partial loss of endothelial-cell specific markers and dismantled adherens junctions as well as by the acquisition of early mesenchymal markers, such as αSMA, SM22α and Fsp1. On the other hand, a complete or late EndMT is characterized by a strong downregulation or complete loss of endothelial markers and upregulation of late mesenchymal or fibroblast markers, such as SM-calponin, Fibronectin, Collagen III, Vimentin, Notch3, SCA1, ZEB2, MMP2 and 9, VCAM and ICAM1 (Dejana et al., 2017). It could be speculated that a partial EndMT can be reverted, when the cells are subjected to pro-endothelial stimuli and laminar shear stress, whereas the cells, which entered a complete transition program will remain mesenchymal.

1.1.3 Endothelial-to-mesenchymal transition in cardiovascular disease

This thesis discusses the literature on EndMT at the point the current study was initiated. During the last four decades, EndMT has been reported to play an important role in cardiac as well as pulmonary artery development during the embryonic stages by promoting endothelial cells to maintain a mesenchymal-like state (Krug et al., 1985, Armstrong and Bischoff, 2004, Arciniegas et al., 2005). However, it has been recently demonstrated that EndMT occurs in adults as well by showing that mature bovine endothelial cells can differentiate into smooth muscle cells (Frid et al., 2002). Moreover,

currently it is believed that EndMT plays an important role in pathological conditions such as cancer progression and organ fibrosis. Specifically, Zeisberg et al. showed that not only does EndMT participate in promoting tumour growth and progression, but also in generation of fibroblasts *in vivo* in mouse model of cardiac fibrosis (Zeisberg et al., 2007a, Zeisberg et al., 2007b). What is more, it has been reported that detrimental consequences of EndMT, such as impaired endothelial cell junctions, loss of cell polarity and enhances migratory ability (Kalluri and Weinberg, 2009), lead to cardiovascular disorders including atherosclerosis (Chen et al., 2015), neointima formation (Chen et al., 2012), cavernous cerebral malformations (CCM) (Maddaluno et al., 2013) and tissue fibrosis (Piera-Velazquez et al., 2011).

Recently, EndMT process has been assigned to be involved in atherosclerotic lesions as well as in transplant atherosclerosis, which both share the same feature, which is a formation of neointima that is primarily composed of a combination of immune and inflammatory cells, smooth muscle cells, fibroblasts and extracellular matrix (Dejana et al., 2017). Together, they are strongly induced by chronic vascular inflammation resulted from mechanical forces as well as deposition of lipids during atherosclerosis (Baeyens and Schwartz, 2016) and immune mismatches in the case of transplant artheriopathy (Tellides and Pober, 2015). Strikingly, it has been reported that in a mouse acute transplant rejection model, 80% of neointimal and 60% luminal endothelial cells were enriched in EndMT markers; in addition to that, almost 80% of coronary artery luminal endothelial cells from the rejected hearts of the patients were exhibiting EndMT program (Chen et al., 2012). What is more, EndMT was also confirmed in coronary (Evrard et al., 2016) as well as carotid artery atherosclerotic plaques (Moonen et al., 2015). Interestingly, a solid association has been observed between the severity of

coronary artery disease and the level of EndMT being exhibited by luminal endothelial cells in the coronary artery (Evrard et al., 2016).

Another serious cardiovascular disorder is the cardiac fibrosis, which can ultimately lead to pathologies such as hypertension and ischemic heart disease. On itself, cardiac fibrosis can affect the cardiac output due to distorted relaxation of the heart chambers (Dejana et al., 2017). There is still a major debate on the exact origin of the cardiac fibroblasts (Kong et al., 2013). The study using lineage tracing mice has confirmed that EndMT occurs during heart fibrosis (Zeisberg et al., 2007b); however, it has been later reported that EndMT is not the major contributor for cardiac fibroblasts (Moore-Morris et al., 2014).

Cavernous cerebral malformations is a serious vascular condition that targets venous microvasculature in retina and central nervous system; due to the fact that malformations lack the integrity from mural cells, they often bleed and lead to a range of neurological disorders from headaches to stroke (Fischer et al., 2013). The prevalence of CCM is just 0.5% of world population and can be in a hereditary or sporadic form (Dejana et al., 2017). The genetic form of the disease is an autosomal dominant disorder characterized by the loss-of-function of *Ccm 1*(*Krit1*), *Ccm 2* (*Osm*) and *Ccm 3* (*Pdcd10*) genes, with the sole treatment being a neurosurgery (Draheim et al., 2014). The studies, utilizing a mouse model with endothelial-specific aberration of any of three of the genes, have reported that inactivation of *Ccm1* or *Ccm3* leads to loss of cell-to-cell junctions and EndMT phenotype in the luminal endothelium in cavernomas; in particular, this phenotypic transitional program can be associated with CCM disease characteristics, as the EndMT-related disorganisation of endothelium contributes to the generation of disordered lumen of cavernomas (Maddaluno et al., 2013, Bravi et al., 2015).

1.2 TGF-β pathway

1.2.1 Characterization of TGF-β pathway

Transforming growth factor-β (TGF-β) signalling exerts a number of important roles on mammalian cells, ranging from regulation of development and differentiation to modulating cellular responses. After the introduction of TGF-β signalling, there was some ambiguity about pathway; the downstream effects of TGF-β differed between cell types and environments with the stronger association with cellular context (Massague, 2012). Eventually, the mechanism of the pathway was mostly uncovered with TGF-β receptor system and SMAD transducers, which also act as a substrate for the receptors; moreover, disease-causing mutations in the cascade were identified that highlighted the medical importance of TGF-β pathway (Massague, 2012). It is now clear that the pathway plays a vital role in the processes of inflammation, immunity, fibrosis, cancer and homeostasis (Massague, 2012).

The main regulatory method of TGF-β signalling is modulation of gene expression, which range from a couple of genes in pluripotent ES cells to numerous in differentiated cells; moreover, the effect of the signalling cascade can be either positive or negative, depending on the cell type and target genes (Mullen et al., 2011). The versatile mode of TGF-β-based regulation of gene expression is demonstrated by the fact that the inhibitor of differentiation 1 (*ID1*) is downregulated by TGFβ in epithelial cells (Kang et al., 2003); on the other hand, TGF-β upregulates *ID1* expression in metastatic breast cancer cells (Padua et al., 2008).

There are more than 30 members of TGF-β family in humans, the orthologues of which can be traced to metazoans (Huminiecki et al., 2009). The complexity of the TGF-β signalling cascade is demonstrated on the Figure 1.3 Upon

binding of the TGF-β ligand, the TGF-β receptor complex is assembled from the signal propagating type I component and the activator type II component (Fig. 1.3), which are both Ser/Thr protein kinases (Massague, 2012). In total, there are seven type I and five type II receptors in human organism. Following the assembly, TGF-βR2 phosphorylates the type I receptor, which activates the signalling cascade (Fig. 1.3) (Wrana et al., 1994). Specifically, the phosphorylation results in replacing the occupied by FKBP12, kinase silencer, site on TGF-βR1 with SMAD proteins, promoting their phosphorylation (Huse et al., 2001). Phosphorylated SMAD transcription factors promote the expression of transcriptionally active genes, but are also able to open the silenced chromatin (Fig. 1.3) (Massague, 2012). SMAD proteins are constituted by MH1 and MH2 domains; MH1 contains DNA-binding moiety while MH2 mainly interacts with cytoplasmic adaptor proteins, phosphorylated TGF-β receptors and various transcription factors (Massague, 2012). Different types of SMADs are activated by different phosphorylated receptors: SMAD1, SMAD5 and SMAD8 are activated by BMP type I receptors (such as ALK1) while SMAD2/SMAD3 are phosphorylated by TGF-β type I receptor (such as ALK5), activin and Nodal (Fig. 1.3) (Massague, 2012). Specifically, phosphorylation of SMAD2/SMAD3 (receptor-regulated SMAD proteins (R-SMAD proteins)) produces a knob on its MH2, which interacts with MH2 of SMAD4 protein resulting in the assembly of the functional unit that drives gene expression assisted by context-dependent transcription factors (Massague, 2012). Interestingly, activated SMAD2/SMAD3 can also interact with TRIM33, which is a histone-binding protein (He et al., 2006). The complex signalling pathway is regulated by different miRNAs, which target the main players within the cascade (Table 1).

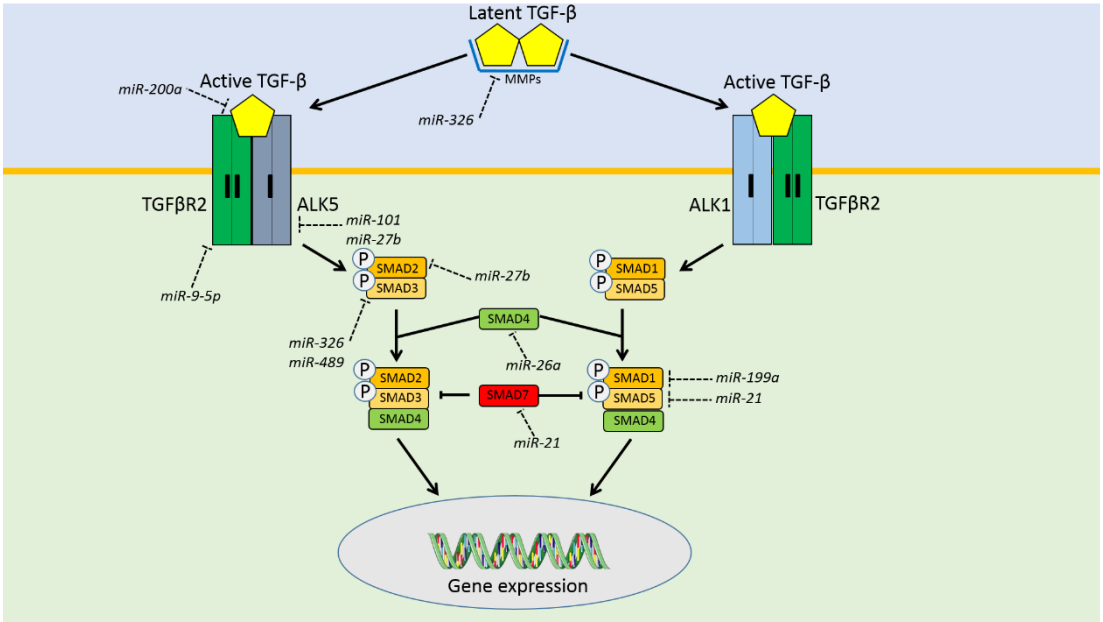

Figure 1.3| Canonical TGF-β signalling cascade. A hetero-tetrameric TGF-β receptor complex is assembled consisting of two subunits of type I and two subunits of type II components upon interaction with activated TGF-β ligands. The signal propagator subunit I then phosphorylates the SMADs. Activated SMADs can then form a transcriptional complex with SMAD4 and other transcription factors, which regulates the expression of specific genes. The whole signalling network is tightly regulated by miRNAs.

In addition to protein interaction domains, TRIM33 also possesses a plant homeodomain as well as bromodomain, which both are able to interact with histones and transduce TGF-β signals via chromatin opening (Xi et al., 2011). Furthermore, SMAD proteins also play important role in modulating miRNA biogenesis. In particular, in human vascular smooth muscle cells (VSMC), phosphorylated SMAD3 is able to bind DDX5 RNA helicase, which is a part of miRNA microprocessor Drosha; as a result, this leads to enhanced processing of primary transcript of miR-21 (pri-miR-21) into precursor miR-21 (pre-miR-21), which in turn upregulates cellular miR-21 levels and downregulated its target gene *PDCD4* thereby inducing the contractile phenotype of VSMCs (Davis et al., 2008).

miRNA	Target	Reference
miR-21	SMAD7	(Liu et al., 2010)
miR-101	TGFβR1	(Huang et al., 2017)
miR-326	SMAD3	(Das et al., 2014)
miR-27b	TGFβR1, SMAD2	(Zeng et al., 2017)
miR-26a	SMAD4	(Liang et al., 2014)
miR-489	SMAD3	(Wu et al., 2016)
miR-9-5p	TGFβR2	(Fierro-Fernandez et al., 2015)
miR-199a	SMAD1	(Lin et al., 2009a)
miR-200a	TGF-β2	(Lu et al., 2015)

Table 2| Regulation of TGF-β signalling pathway by miRNAs.

1.2.2 TGF-β pathway and angiogenesis

The role of TGF-β in regulating angiogenesis is quite contradictory. In fact, the effect of TGF-β on angiogenic response seems to be dose-dependent: specifically, TGF-β increases endothelial cell proliferation at low dose, but attenuates EC proliferation at high doses (Viloria-Petit et al., 2013). The dual effect of TGFβ on angiogenesis can be explained by the interchange between ALK1 and ALK5 type I receptors. Specifically, ALK1 activation promotes endothelial cell proliferation as well as migration at the initial phase of angiogenesis; this effect is achieved through upregulation of Id1 protein, which is required for migration and proliferation (Goumans et al., 2002). On the other hand, ALK5 exerts anti-proliferative effect on the angiogenesis; *in vitro* studies have shown that in endothelial cells ALK5 activation leads to induction of plasminogen activator inhibitor (PAI)-1, which promotes vessel maturation by attenuating the degradation of extracellular matrix around the growing vessel (Goumans et al., 2002). What is more, while there is much

evidence that ALK1 facilitates endothelial cell sprouting, it has been demonstrated that ALK5 pathway makes endothelial cells less sensitive to VEGF stimulus that is important for the resolution step of angiogenesis (Viloria-Petit et al., 2013). Nevertheless, some studies report that ALK1 exerts anti-proliferative and anti-migratory effects on endothelial cells (Lamouille et al., 2002), which is possibly due to differential regulation in different cell types (Holderfield and Hughes, 2008). Thus, it is clear that the balance between ALK1 and ALK5 is vital for the regulation of angiogenesis.

1.2.3 TGFβ pathway in cardiovascular disease

The cardiovascular system (CVS) is tightly regulated by the proteins in TGF-β superfamily: specifically, by TGF-β1, TGF-β2, BMP4, BMP6 and BMP7, which are highly expressed in CVS (Bobik, 2006). It is quite evident that TGF-β superfamily is vital for cardiovascular development because knock-out mice for members such as *TGFB1*, *TGFB2*, *TGFBR3* and *SMAD4* are embryonic lethal due to cardiac defects as well as high inflammatory response in the heart (Kulkarni and Karlsson, 1993, Sanford et al., 1997, Stenvers et al., 2003, Compton et al., 2007).

In particular, Hereditary Hemorrhagic Telangiectasia (HHT), a disorder characterized by vascular dysplasia, telangiectasia as well as arteriovenous malformations, is caused by mutation in co-receptor endoglin (*ENG*) and *ALK1* (Fernandez et al., 2006). Patients affected by HHT develop skin telangiectases, nose bleeds, gastrointestinal bleeding, neurological disorders, as a consequence of arteriovenous malformations, as well as heart failure (Shovlin and Letarte, 1999). The disease has two forms, HHT1 and HHT2, which account for almost 80% of all cases; HHT1 type occurs as a result of *ENG* mutation is associated with pulmonary, hepatic and cerebral arteriovenous

malformations while HHT2 is caused by *ALK1* mutation and is characterized by vascular liver disorders (Gordon and Blobe, 2008, Fernandez et al., 2006). It is also speculated that mutation in *SMAD4* makes up remaining 20% of the cases of HTT (Abdalla and Letarte, 2006).

Alterations in TGF-β signalling are also responsible for disorders within the aorta. Specifically, somatic mutations in the serine/threonine kinase domains of *TGFBR1* and *TGFBR2* genes cause Loeys-Dietz syndrome, which is characterized by aortic aneurysms, arterial dissections, widely spaces eyes, cleft palate, general arterial tortuosity and structural brain abnormalities (Loeys et al., 2005). Similarly, familial thoracic aortic aneurysm syndrome (TADD) is caused by the germline mutations in *TGFBR2* kinase domain and *TGFBR1* cytoplasmic domain and leads to massive arterial aneurysms, severe aortic dissection and, ultimately, significant blood loss (Pannu et al., 2006, Matyas et al., 2006). Finally, arterial tortuosity syndrome (ATS) causes elongation of major arteries, general tortuosity and hyperflexibility of joints and is a result of *GLUT10* loss-of-function mutations, which upregulate the TGF-β pathway in arterial wall (Coucke et al., 2006).

Furthermore, dysregulation in TGF-β cascade is responsible for the primary pulmonary arterial hypertension (PAH), which can cause cardiac arrest due to remodelling of small pulmonary arteries, increased arterial pressure and right ventricular heart failure (Gordon and Blobe, 2008, Eddahibi et al., 2002). Pulmonary arterial hypertension exists in two forms: idiopathic PAH (IPAH) and familial PAH (FPAH); both variants of disease are associated with heterozygous germline mutation in *BMPR2* (Machado et al., 2006).

TGF-β signalling plays important role in biology of atherosclerosis, which is characterized by endothelial dysfunction, accumulation of lipids, vascular

inflammation, increased oxidation and cellular debris, which lead to formation of plaques within the arteries (Gordon and Blobe, 2008). Atherosclerosis acts as a major cause of cardiovascular disease, stroke and myocardial infarction. Moreover, the expression pattern of the members of TGF-β cascade is very prevalent in the cells contributing to the formation of the plaque: smooth muscle cells, endothelial cells, macrophages and T-cells (Bobik et al., 1999b). It is interesting to note that the role of TGF-β cascade remains controversial in the setting of atherosclerosis: there is little evidence supporting pro-atherosclerotic action of TGF-β pathway (Bobik et al., 1999a, Tang et al., 2013), while most findings demonstrate that TGF-β signalling is in fact inhibiting the progression of atherosclerosis. In particular, activation of TGF-β pathway is sufficient to attenuate the proliferation as well as migration of endothelial cells and vascular smooth muscle cells and is able to decrease the immune response (Gordon and Blobe, 2008). It has been demonstrated before that upregulation of TGF-β signalling by tamoxifen inhibits the formation of atherosclerotic plaques (Grainger et al., 1995). On the other hand, inhibition of TGF-β cascade using neutralizing anti-TGF-β1, -β2 and -β3 antibodies facilitates the development of atherosclerotic lesions and weakens the stability of the plaques (Mallat et al., 2001). In fact, TGF-β1 is able to stabilize atherosclerotic plaques due to promoting the production and release of collagen (Cipollone et al., 2004).

The last example, which is important to mention are fibrotic diseases as a result of poor TGF-β signalling regulation. Fibrosis is complex tissue disorder, which is characterized by excessive expression and secretion of extracellular matrix (ECM) proteins, such as collagen, fibronectin, vitronectin and laminin, and by activation and recruitment of myofibroblasts (Gordon and Blobe, 2008, Verrecchia and Mauviel, 2007). In particular, myofibroblasts get differentiated

from fibroblasts during the process of wound healing (Krieg et al., 2007). In this case if extracellular matrix proteins get accumulated in vital organs such as kidney, liver, skin and lungs, it can ultimately cause organ failure. Specifically, it has been shown that in a mouse model of scleroderma, which is characterized by early inflammation and vascular injury, followed by progressive fibrosis, deletion of *SMAD3* is able to decrease collagen deposition and attenuate skin fibrosis (Lakos et al., 2004).

1.3 MiRNA

1.3.1 MiRNA biogenesis

MicroRNAs (miRNAs) are short non-coding RNAs (ncRNAs) of ~22 nucleotides that facilitate gene silencing through interaction with 3′ untranslated region (UTR) of the target mRNAs. MiRNAs bind 3′ UTR of the mRNAs primarily through Watson–Crick pairing between by the miRNA "seed region", which is usually 7-8 nt long facilitating target recognition. Moreover, miRNAs are assembled into families based on their target genes profile and its specificity depends on the miRNA seed region (Bartel, 2009).

MiRNAs are the most abundant small RNAs in somatic tissues. In humans, the largest part of miRNA are encoded within the introns of coding and non-coding sequences in the genome; nevertheless, a small portion of miRNAs is encoded in exons (Ha and Kim, 2014). In particular, miRNAs that are found in the introns of protein-coding genes can be transcribed from the same promoter as a host gene; it has been also demonstrated that sometimes miRNA possess more than one transcription start site (Ozsolak et al., 2008) and can be also transcribed by a promoter different from the gene they reside in (Monteys et al., 2010). Commonly, miRNAs are transcribed by RNA polymerase II (Pol II) and the process is regulated by RNA Pol II-related transcriptional regulators

(Lee et al., 2004); moreover, some viral miRNAs can also be transcribed by RNA polymerase III (Pfeffer et al., 2005). The product of the transcription is a long primary miRNA (pri-miRNA) almost 1 kb in length and is composed of stem-loop structure (Fig. 1.4). Moreover, a number of miRNAs can be transcribed as one pri-miRNA, if they reside in close proximity and at the same cluster genomically (Gebert and MacRae, 2019).

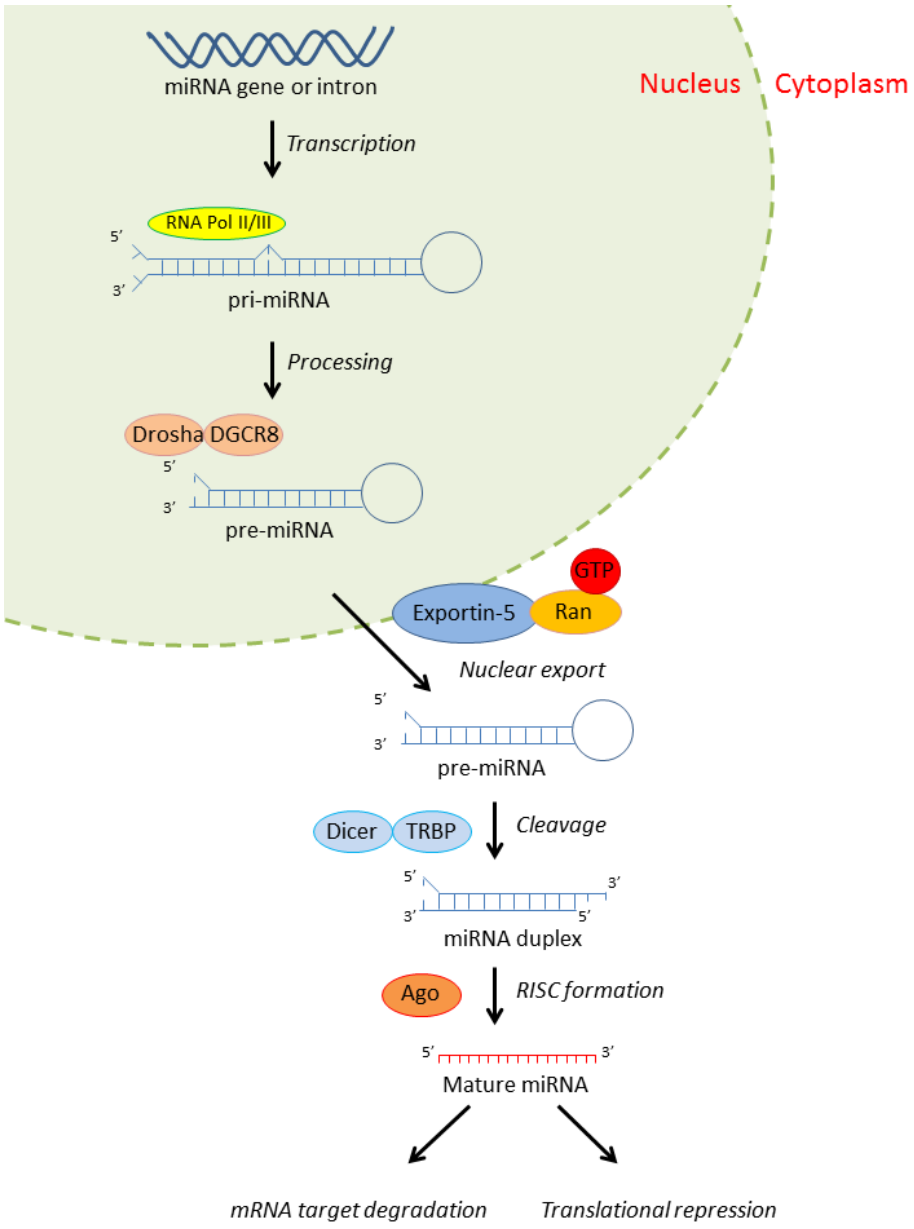

Figure 1.4| Canonical miRNA biogenesis pathway. Primary miRNA transcript (pri-miRNA) is transcribed in the nucleus by RNA polymerase II or III and can originate from miRNA

coding gene or from an intron. Microprocessor complex consisting of Drosha and DGCR8 (Pasha) proteins then cleaves pri-miRNA into a precursor pre-miRNA, which is then exported into cytoplasm by Exportin-5-Ran-GTP. A cytoplasmic pre-miRNA is then bound by Dicer/TRBP complex and cleaved into a double-stranded miRNA molecule. After that, one of the strands is loaded with Argonaute (Ago) to generate a RNA-induced silencing complex (RISC), which can silence the expression of the gene via degradation of its mRNA via deadenylation or repression of translation. Modified from (Winter et al., 2009).

After that, pri-miRNA is bound by RNase III enzyme Drosha, which crops the stem-loop construct and generates smaller precursor miRNA (pre-miRNA) molecule that has a hairpin shape and consists of around 65 nucleotides (Fig. 1.4) (Lee et al., 2003). Specifically, this step is achieved after formation of Microprocessor complex, which consists of Drosha and its partner protein DGCR8 (Pasha). The next step after precursor miRNA processing, pre-miRNA is exported into cytoplasm to initiate the further maturation step. Transport complex is formed by exportin 5 protein, which specifically bind dsRNA, GTP-binding nuclear cofactor, Ran-GTP, and pre-miRNA (Fig. 1.4); after construct is translocated through nuclear pore complex, the GTP is hydrolysed, which induces the disassembly of the pre-miRNA-protein complex and release of pre-miRNA into cytoplasm (Fig. 1.4) (Bohnsack et al., 2004, Lund et al., 2004). Once cytoplasmic, pre-miRNA is bound by Dicer enzyme, which produces a smaller double-stranded miRNA molecule (Knight and Bass, 2001) (Fig. 1.4); moreover, Dicer interacts with TAR RNA-binding protein (TRBP), which regulates the cleavage and guides the proper length of miRNA duplex (Fig. 1.4) (Fukunaga et al., 2012). The mature miRNA comprises a 5p strand, which is generated from the 5′ arm of the pre-miRNA hairpin and a 3p strand, arising from the 3′ arm (Gebert and MacRae, 2019). Finally, the processed double-stranded miRNA is bound by Argonaute protein generating RNA-induced silencing complex (RISC) (Fig. 1.4). Interestingly, in humans there is no

stringent sorting system and the majority of miRNA duplexes can interact with all four AGO proteins (AGO1-4) (Huntzinger and Izaurralde, 2011). The AGO-bound miRNA duplex is then unwinded and the 5p or 3p strand is selected and incorporated into mature RISC complex. It is important to point out, that Ago-independent miRNA strand is not always cleaved that the new findings suggest that both 5p or 3p strands of many miRNAs can be detected in different types of tissues; moreover, miRNA that have more than one sequences in the genome can have both strands, which are processed independently (Meijer et al., 2014). Moreover, AGO proteins are subjected to a number of post-translational modification with phosphorylation being the best characterized one. In particular, Ser387-specific phosphorylation of human Ago2 enhances miRNA activity by facilitating miRISC generation (Lopez-Orozco et al., 2015). On the other hand, Tyr393-specific phosphorylation of Ago2 attenuates the assembly of the miRISC function (Yang et al., 2014). Similarly, Ago2 phosphorylation on Tyr529 also prevents loading of miRNA into Ago2, due to the fact that Tyr529 interacts with the 5′ phosphate and first nucleotide of miRNAs undergoing the loading (Rudel et al., 2011, Schirle and MacRae, 2012). The mature RISC-bound miRNA molecule is then involved in post-transcriptional gene silencing. The target recognition occurs via binding between miRNA seed sequence and 3′ UTR of target mRNA. In some instances, miRNA seed sequence can also bind to the 5′ UTR as well the open reading frame (OFR) of the mRNA (Bartel, 2018). Specifically, miRNA can silence gene expression via degradation of its target mRNA or by repression of translation (Fig. 1.4). It has been demonstrated that mRNA degradation accounts for 66-90% of miRNA-modulated gene silencing (Jonas and Izaurralde, 2015). During this process, the target mRNA is first deadenylated by PAN2-PAN3 and CCR4-NOT deadenylase complexes

(Wahle and Winkler, 2013), followed by decapping by DCP2; the pathway is finished by mRNA degradation by the major cytoplasmic nuclease XRN1 (Fabian and Sonenberg, 2012). Translational repression, on the other hand, accounts for 6-26% of miRNA-induced gene silencing (Eichhorn et al., 2014). The mechanism behind this process has been unclear for many years, however the ribosome profiling has shown that translational repression is achieved due to inhibition of cap-dependent translation at initiation via RNA helicases such as eIF4A and DDX6 (Jonas and Izaurralde, 2015).

Strikingly, each of the 90 conserved miRNA families have >300 binding sites to the seed regions consisted of 7-8 nts and >500 binding sites to the seed regions of 6 nt in length (Friedman et al., 2009). Moreover, one miRNA can target some 3′ UTRs more than once. Nevertheless, the average number of conserved target mRNAs per miRNA family is more than 400, and more than half of 3′ UTRs of the human mRNAs are conserved targets of miRNAs (Friedman et al., 2009). What is more, taking into account the miRNA binding sites in ORFs of the mRNA, the number of conserved targets rises to 60% of all human mRNAs. Interestingly, when a certain miRNA family is inhibited experimentally, it is observed that many mRNA targets with conserved binding sites for that miRNA family become downregulated (Bartel, 2018). It is therefore clear that every process happening in the cell is influenced by miRNA regulation. Furthermore, even though the single contribution of a noncanonical low-affinity interaction miRNA:mRNA is weak, in sum they do contribute to target downregulation. Due to this redundancy, the abundance of target mRNAs target normally exceeds the number of miRNAs (Denzler et al., 2016). Therefore, due to this target abundance, which are competing for miRNA binding, a lot of 3′ UTRs remain unsaturated resulting in a further

downregulation of already repressed targets in response to upregulation of certain miRNAs, which are ultimately sponged up (Denzler et al., 2016).

1.3.2 Role of miRNAs in angiogenesis

The first evidence of a possible miRNA involvement in angiogenesis was back in 2006, where it has been demonstrated that specific miRNAs are expressed in endothelial cells (Poliseno et al., 2006). In particular, the study has shown that 15 of highly expressed miRNAs in HUVECs have the receptors of angiogenic factors as potential target genes; both miR-221 and miR-222 target *c-Kit* expression, which is responsible for endothelial cell migration, tube formation and survival (Poliseno et al., 2006). Later on, the expression of 200 miRNA has been elucidated in endothelial cells; after analysing different expression studies, 28 miRNAs have been confirmed to be common in the majority of the studies, which include examples such as *let-7* family, miR-17~92, miR-126, miR-210, miR-221/222 and others (Heusschen et al., 2010).

Specifically, miR-126 is quite highly expressed in human endothelial cells as well as in tissues with dense vasculature such as lungs and heart (Wang et al., 2008); *in vitro* studies have shown that it facilitates proliferation, stability and migration of endothelial cells (Fish et al., 2008) while inhibition of miR-126 attenuates angiogenic response both *in vitro* and *in vivo* (Wang et al., 2008, Kuhnert et al., 2008). MiR-126's proangiogenic effect can be attributed to its target genes, *Spred-1* and *PIK3R2*, which are both negative regulators of VEGF and FGF signalling pathways (Fish et al., 2008, Wang et al., 2008). On the other hand, it has been reported that miR-17~92 cluster exhibits anti-angiogenic effects on endothelial cells both in cellular and *in vivo* models, which is mediated via targeting the S1PR1, p21 and Jak1 protein kinase (Doebele et al., 2010).

Interestingly, it has been found that miR-210 is being upregulated during hypoxic conditions (Fasanaro et al., 2008). Moreover, during normal oxygen levels, miR-210 facilitates migration and cellular network formation of endothelial cells in response to VEGF, while inhibition of this miRNA leads to anti-angiogenic effects under hypoxic environment (Fasanaro et al., 2008). Specifically, HIF1α acts as a messenger between hypoxia and miR-210 expression induction, which downregulates anti-angiogenic Ephrin-A3 (Fasanaro et al., 2008). As expected, Gene Ontology analysis has elucidated HIF1α pathway as the most enriched miR-210-regulated pathway (Fasanaro et al., 2009). Therefore, it can be concluded that an angiogenic program, switched on by VEGF stimulus, that occurs in response to ischemia is modulated by miR-210.

On the other hand, *Caporali et al.* has found that miR-503 is strongly downregulated in endothelial cells in response to high glucose in combination with low growth factors in the medium, increasing the expression of miR-503 target genes *cdc25A* and *CCNE1* (Caporali et al., 2011). Moreover, the study has demonstrated that miR-503 is a strong inhibitor of angiogenesis, which is upregulated during diabetes mellitus. Specifically, *in vivo* inhibition of miR-503 is able to improve the diabetes-induced impairment of post-ischemic angiogenesis and restore the blood perfusion in ischemic adductor of diabetic mice (Caporali et al., 2011).

Finally, it has been also demonstrated that inflammatory cytokines are able to modulate miRNA-dependent angiogenic response. Specifically, in a model of intraplaque neovascularization the inflammatory cells, which reside in neointima, release pro-angiogenic cytokines and growth factors such as IL-3 and bFGF that are able to modulate differential expression of specific miRNAs (Dentelli et al., 2010). In particular, miR-222 is strongly downregulated upon

exposing the endothelial cells to acute inflammatory stimuli; miRNA gain-of-function results into impairment in proliferation and migration of endothelial cells subjected to IL-3 and bFGF (Dentelli et al., 2010). What is more, it has been demonstrated that miR-222 is able to negatively modulate neoangiogenesis in mice and intraplaque vessel formation in humans via targeting signal transducer and activator of transcription 5A (STAT5A) expression (Dentelli et al., 2010).

1.3.3 MiRNA and EndMT

In these subchapters only the literature at the point of the start of the study is being discussed.

There are only a few examples of the role of miRNA to modulate EndMT. The first prominent example of miRNA-dependent regulation of EndMT came from the study in 2012 (Kumarswamy et al., 2012). Firstly, it has been reported that miR-21, which is highly abundant in cardiac fibroblasts, is being upregulated in endothelial cells following TGF-β stimulation leading to induction of EndMT program in HUVECs (Kumarswamy et al., 2012). Interestingly, *PTEN* gene is a direct target of miR-21 and also is an inhibitor of Akt, which acts as an inducer of EndMT program; therefore, the TGF-β-modulated miR-21 upregulation promotes EndMT phenotype in HUVEC via silencing the expression of *PTEN*, which in turn upregulates Akt and decreases the expression of *PECAM1* (*CD31*) and endothelial nitric oxide synthase (*eNOS*) (Kumarswamy et al., 2012). Moreover, in a mouse model of transaortic constriction (TAC) surgery, the ventricular pressure overload induces cardiac fibrosis due to overexpression of miR-21 and partial EndMT induction (Kumarswamy et al., 2012).

Next example on miRNA involvement in EndMT comes from a study carried out at the same year. In particular, the group has demonstrated that basal FGF signalling is able to block TGF-β-induced EndMT via inducing the expression of *let-7* miRNA, which targets TGF-βR1 (Chen et al., 2012). Specifically, it has been elucidated that the knockdown of fibroblast growth factor receptor substrate 2 (*FRS2*) attenuates the expression of *let-7* family leading to EndMT phenotype (Chen et al., 2012). Moreover, *in vivo* downregulation of *let-7* increases vimentin expression while decreasing CD31 levels in mice liver sections, thus promoting the transition program (Chen et al., 2012). Another novelty of this study was their discovery that inflammatory cytokine IFN-γ is able to downregulate *let-7* and induce EndMT in the endothelial cells *in vitro* and together with TNF-α and IL-1β inhibit the expression of FGF receptors (Chen et al., 2012). Finally, the group was able to demonstrate that EndMT occurs in the models of mouse atherosclerosis as well as human graft arteriosclerosis, where downregulation of *let-7* increased the expression of EndMT markers in neointima such as α-SMA, collagen 1 and Notch3, which were decreased upon *let-7* overexpression (Chen et al., 2012).

1.3.4 Dysregulation of miRNAs in cardiovascular disease

The significance of miRNAs in cardiovascular biology has been elucidated by deletion of *Dicer* gene in specific tissues: in particular, *Dicer* knockout was lethal after its deletion in vascular and myocardial systems (Albinsson et al., 2010, Chen et al., 2008).

The multi-regulatory properties of miRNA make them perfect modulators of heart formation, which requires very complex and precise orchestration of different cell types. Interestingly, in the heart only the highest expressed miRNAs have been assigned a functional role, probably due to functional

redundancy (Small and Olson, 2011). The most enriched miRNA in cardiomyocytes is miR-1, which was the first one reported to regulate heart development (Zhao et al., 2007). MiR-1 and miR-133 are both from the same miRNA family and are transcribed in the embryonic heart under the regulation of serum response factor (SRF) and myocyte enhancer factor-2 MEF2 transcription factors (Liu et al., 2007, Zhao et al., 2005). These miRNAs facilitate differentiation of mesoderm and inhibit development of endodermal and ectodermal cell types (Ivey et al., 2008). Notably, miR-1 and miR-133 exhibit opposite roles in the adult heart, where miR-1 induces while miR-133 attenuates differentiation of cardiomyocytes (Ivey et al., 2008). Moreover, there seems to be a compensatory mechanism between miR-1 and miR-133 as only 50% of mice, lacking either of these miRNA in cardiomyocytes, are lethal (Small and Olson, 2011).

The role of specific miRNAs in certain cardiovascular pathologies has been elucidated using knockout mice. Specifically, miR-1, miR-133 and miR-208a are involved in arrhythmias (Yang et al., 2007, Callis et al., 2009b), miR-21 and miR-29 play role in fibrosis (Thum et al., 2008, van Rooij et al., 2008), and miR-133 and miR-208 in pressure-induced remodelling (van Rooij et al., 2007, Care et al., 2007). One of the most described family of miRNAs, which modulates the expression of stress-induced genes, consists of miR-208a, miR-208b and miR-499 and is encoded by myosin heavy chain (*MHC*) genes; this miRNA family is called MyomiRs (van Rooij et al., 2009). Specifically, MyomiRs modulate a number of transcriptional repressors and signalling proteins, which tune the expression of MHC and responsiveness of cardiomyocytes to stress (van Rooij et al., 2009). Moreover, *Mir208a* loss-of-function prevents the re-activation of fetal *β-MHC* induced by haemodynamic cardiac stress, thus attenuating cardiac hypertrophy (Callis et al., 2009a). Similarly, antagomir

silencing of miR-23a expression, which is upregulated by cardiac-stress inducing NFATc3, is able to decrease heart hypertrophy (Lin et al., 2009b). Interestingly, myocardial infarction inhibits the expression of miR-29 family, which normally targets certain collagens and ECM proteins thus attenuating fibrosis (van Rooij et al., 2008). In addition to this, in a model of hypoxia preconditioning, miR-199 family is repressed in cardiomyocytes in response to hypoxia, thereby re-activating the expression of its target genes Sirtuin 1 and HIF-1α (Rane et al., 2009). In another example inhibition of miR-21, which a positive modulator of fibrosis and cardiac hypertrophy, is able to decrease heart remodelling upon thoracic aortic constriction (Thum et al., 2008). This protective effect is achieved due to miR-21-induced repression of sprouty homologue 1 (*Spry1*), which enhances ERK–MAP kinase activity modulating fibroblast survival and controlling cardiac hypertrophy (Thum et al., 2008). MiR-21 has been also reported to negatively regulate migratory capacity and promote the dysfunction of angiogenic progenitor cells in patients with coronary artery disease (Fleissner et al., 2010). What is more, ischemia-facilitated angiogenesis is induced by silencing of miR-92a (Bonauer et al., 2009) and attenuated by inhibition of miR-126 (van Solingen et al., 2009). MiR-126 is also involved in exerting protective effects from atherosclerosis via upregulation of the CXC chemokine CXCL12 upon silencing its repressor *RGS16* (Zernecke et al., 2009). Finally, it has been demonstrated that miR-145 is downregulated upon neointimal lesion formation and restoration of its expression is able to inhibit neointimal growth (Cheng et al., 2009).

1.4 Preliminary studies

1.4.1 MiRNA high throughput phenotypic screening

Due to the evident importance of miRNA in regulating angiogenesis, miRNA high throughput phenotypic screening has been carried out in BHF Centre for Cardiovascular Target Discovery in University of Oxford (unpublished). The purpose of the screen was to identify miRNA, which enhance or inhibit proliferation of HUVECs. Specifically, HUVECs were transfected with a library of 1500 miRNA mimics and the effect of each miRNA mimic on cellular proliferation was analysed using cellHTS2 package (Open source). Figure 1.5a shows a scatter plot distribution representing the effect of each miRNA mimic on HUVEC proliferation by B-score, which is a number of standard deviations from the mean accounting for within-plate systematic effects (Brideau et al., 2003).

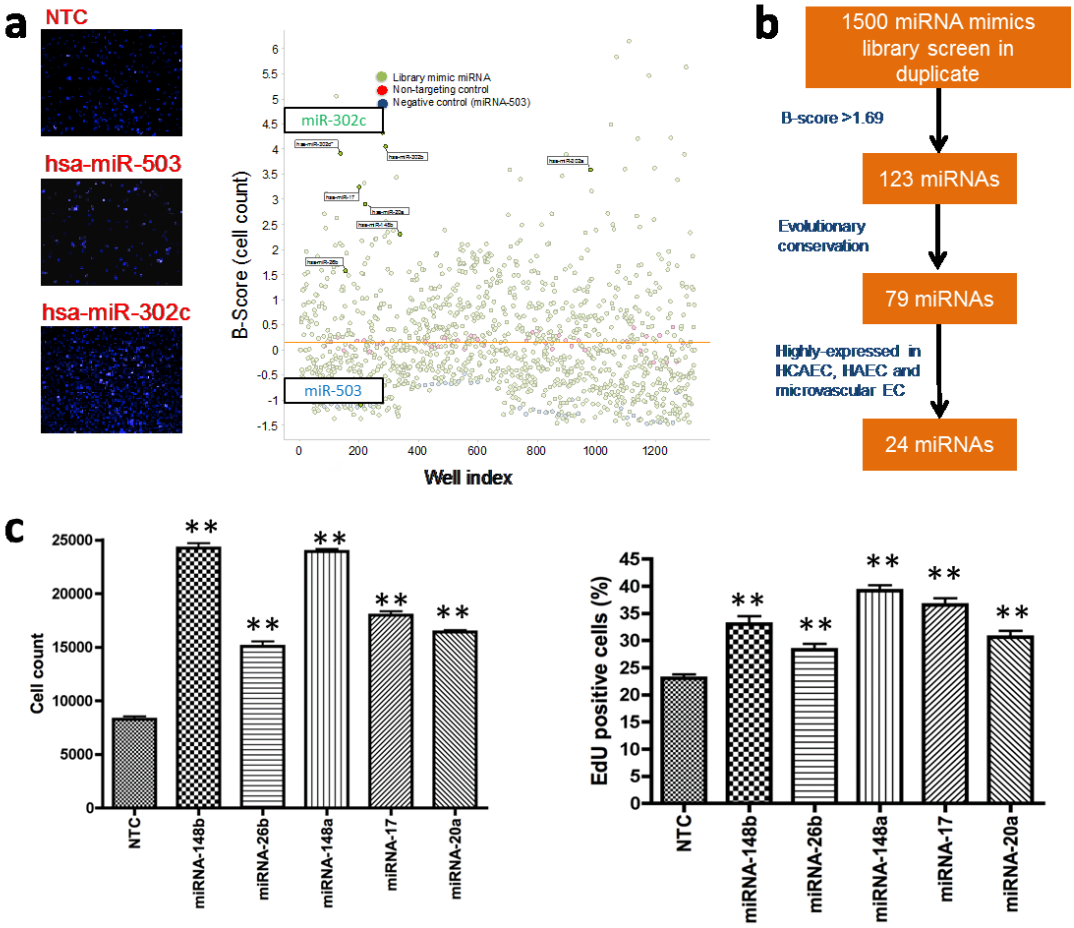

Figure 1.5| Phenotypic-screen of human miRNA mimics library for regulators of endothelial cell growth. a. *Right panel*: Scatter plot distribution showing the B-score of endothelial cell count. The cell count reading values were normalized according to B-score method using CellHTS2 package (Open source). The selection enhancer hit cutoff was set at +1.69; miR-302c was used as a positive control (green); miR-503 was used as a negative control (blue); *left panel*: representative fluorescent images showing DAPI stained HUVECs treated with Non-targeting miRNA mimic control (NTC), negative control (miR-503) and an example of a positive enhancer hit (miR-302c). **b.** Screening summary shows the enhancer hit selection workflow. **c.** Secondary cell-based assays to validate the effect of selected enhancer hits on the endothelial cell proliferation; *left panel*: cells count after transfection with selected miRNA mimics; *right panel*: results from EdU incorporation assay performed with HUVECs transfected with selected set of miRNA mimics. Unpublished data.

During this study, the miRNAs which were above the hit cut-off line (+1.69) established between positive control miR-302c and negative control miR-503,

were considered to be enhancers of HUVEC proliferation (Fig. 1.5 a). Next, 123 miRNA enhancers were selected and based on their evolutionary conservation the 79 miRNA were prioritized; finally, the selection was narrowed down to 24 miRNAs based on high expression level in endothelial cells (Fig. 1.5 b). During this investigation, secondary functional cellular assays have validated the strongest enhancers, miR-148b, miR-26b, miR-148a, miR-17 and miR-20a, as potent inducers of HUVEC proliferation (Fig. 1.5 c). Given the fact that miR-148b is one of the strongest enhancers of proliferation out of this list above and that it hasn't been reported to play a role in angiogenesis or endothelial cell plasticity, it has been selected as a strongest candidate for subsequent characterization.

1.4.2 MiR-148b characterization

MiR-148b, together with miR-148a and miR-152, comprises the miR-148/152 family. MiR-148b is genomically located at chromosome 12q13 with a genomic size of 22 bp (UCSC Genome Browser). Importantly, miR-148b is located genomically within the first and the longest intron of COPZ1 host gene (UCSC Genome Browser). Interestingly, COPZ1 gene is encoding a coatomer subunit zeta-1 protein that constitutes a coatomer protein complex I (COPI) in the cytoplasm, which is involved in the assembly of coated vesicles on Golgi membranes, retrograde transport of luminal and membrane cargo proteins in the ER-Golgi secretory pathway, maturation of the endosome, autophagy (Beck et al., 2009, Razi et al., 2009) as well as lipid homeostasis (Beller et al., 2008). Moreover, it was later demonstrated that the knockdown of COPZ1 leads to apoptosis, accumulation of unfolded proteins, attenuated autophagy and ER stress and, ultimately, to thyroid tumor cell death (Anania et al., 2017). Importantly, miR-148b-3p targets 802 mRNAs with 889 conserved and 268 poorly conserved sites (TargetScan 7.2).

1.4.2 MiR-148b in the literature

Table 3 summarises current known miR-148b target genes as well as their involvement in different physiological conditions and pathologies.

The first time miR-148b has been reported in literature was in 2008, where the study has found miR-148b expression was significantly upregulated among other miRNAs in osteoblast-like cells in response to culturing with plastic polymer, porous polyethylene (Palmieri et al., 2008).

Later, it has been described that miR-148b plays a role in modulating innate immunity (Kotake et al., 2010). Specifically, the study demonstrated that Toll-like receptors (TLR) agonists are able to induce the expression of miR-148a, miR-148b and miR-152, which constitute miR-148 family, in dendritic cells (Kotake et al., 2010). Moreover, the overexpression of miR-148b decreases the production of inflammatory cytokines, IL-6, TNF-a, IL-12, and IFN-b, in LPS-stimulated dendritic cells, suggesting that miR-148/152 might act as a suppressor of TLR-induced innate immune response (Kotake et al., 2010). Finally, it has been shown that miR-148/152 targets the expression of calcium/calmodulin-dependent protein kinase II (*CaMKII*) and, thereby, attenuating the maturation and proliferation of dendritic cells (Kotake et al., 2010).

The most reported role of miR-148b is the involvement in modulation of tumor development. The first study to demonstrate this has been carried out in 2011, which has reported that miR-148b is significantly downregulated in 106 gastric cancer tissues and has a strong correlation with tumor size (Song et al., 2011). Moreover, it has been elucidated that miR-148b is able to suppress gastric cancer cell proliferation via targeting cholecystokinin-B receptor (*CCKBR*) (Song et al., 2011). Later, the same group reported that miR-148b is also

suppressed in colorectal cancer tissues, where it could inhibit tumorigenicity via blocking the expression of cholecystokinin-2 receptor gene (CCK2R) (Song et al., 2012). On the other hand, Chang et al. reported that miR-148b is strongly overexpressed in ovarian cancer tissues (Chang et al., 2012). Interestingly, miR-148b is able to elevate the radiosensitivity of non-Hodgkin's lymphoma cells possibly via facilitating radiation-induced apoptosis (Wu et al., 2012). What is more, in pancreatic cancer tissues miR-148b is downregulated, while its overexpression is able to supress pancreatic cancer cell proliferation and invasion through targeting AMP-activated protein kinase α1 (*AMPKα1*) (Zhao et al., 2013).

Notably, miR-148b has also been reported to play a role in regeneration and tissue repair. Specifically, Qureshi et al. demonstrated that photoactivated miR-148b mimic oligonucleotide delivery using silver nanoparticle complexes leads to differentiation of human autologous adipose derived mesenchymal stromal/stem cells (hASCs) into an osteogenic linage via enhancement of alkaline phosphatase (ALP) activity, which results in rapid calcification of hASCs (Qureshi et al., 2013). The fate change of hASCs into osteogenic cell type was also confirmed by upregulation of osteogenic markers RunX2 and osteocalcin (OCN) upon delivery of conjugated miR-148b mimic oligonucleotides (Qureshi et al., 2013). These findings were confirmed by another study, which showed that miR-148b overexpression using baculovirus induced the hASCs osteogenesis (Liao et al., 2014).

miRNA	Target gene	Physiological response/Pathology	Reference
hsa-miR-148b-3p	HLA-G	Asthma	(Tan et al., 2007)
hsa-miR-148b-3p	CCKBR	Gastric cancer	(Song et al., 2011)
hsa-miR-148b-3p	ITGA5	Breast cancer	(Cimino et al., 2013)
hsa-miR-148b-3p	ROCK1	Breast cancer	(Cimino et al., 2013)
hsa-miR-148b-3p	PIK3CA	Breast cancer	(Cimino et al., 2013)
hsa-miR-148b-3p	NRAS	Breast cancer	(Cimino et al., 2013)
hsa-miR-148b-3p	CSF1	Breast cancer	(Cimino et al., 2013)
hsa-miR-148b-3p	CaMKIIα	Innate immunity	(Kotake et al., 2010)

Table 3. MiR-148b and its target genes in disease and physiology.

1.5 Hypothesis

Given the preliminary data demonstrating that miR-148b is able to strongly enhance endothelial cell proliferation and its potential involvement in differentiation from previous findings, the main goal of this thesis is to test the hypothesis that:

"MiR-148b is a modulator of angiogenesis and endothelial cell plasticity"

1.6 Aims

1. Elucidate miR-148b target genes

2. Determine whether miR-148b overexpression enhances angiogenesis *in vitro* and *in vivo*

3. Determine whether inhibition of miR-148b attenuates angiogenesis and modulates endothelial cell function *in vitro* and *in vivo*

4. Determine the physiological modulator of miR-148b expression

CHAPTER 2: METHODS

2.1 Techniques for *in vitro* studies

2.1.1 MiR-148b target analysis

Computational prediction of miR-148b target genes was done using published algorithm TargetScan (www.targetscan.org). miRpath v.3 (http://diana.imis.athena innovation.gr/DianaTools/index.php?r=mirpath) has been used to perform gene set enriched analysis of miR-148b target genes. The prediction was based on Targetscan parameters such as Context score and Conservation score.

2.1.2 Cells and Cell culture

Human umbilical vein ECs (HUVECs; Lonza) were grown in EGM-2 (EBM-2 added with growth factors and other supplements) with 2% Foetal Bovine Serum. Confluent HUVECs were treated with 10 ng/ml TNF-α, IL-1β, TGFβ2 (PeproTech); medium and cytokines were changed every two days. HEK293T cells (ATCC®, CRL-11268) were cultured in D-MEM with 10% FBS (Life Technologies).

2.1.3 Cell transfection

HUVECs and HEK293T were plated in a 6-well plate in a density of 100,000-120,000 cells per well and transfected using lipofectamine RNAiMAX (Thermo Scientific™, 13778075) (for RNA oligonucleotides) and/or lipofectamine 3000 (Thermo Scientific™, L3000008) (for plasmid DNA) in the Opti-MEM® I Reduced Serum Medium (Thermo Scientific™, 31985062). MiRIDIAN miR-148b Mimic (Dharmacon, MI0000811) 25 nM, miRIDIAN microRNA Mimic Negative Control (Dharmacon, CN-001000-01-05) 25nM, miRCURY LNA™ anti-miR-148b (Exiqon) 75 nM, miRCURY LNA™ microRNA Antisense Control (Exiqon) 75 nM and SMAD2 siRNA (Thermo Scientific™) were used

to transfect HUVECs; pMIR-REPORT miRNA Expression Reporter Vector control (Thermo Scientific™, AM5795) and with cloned 3'UTR of TGFB2 and SMAD2 genes were used to transfect the cells. The medium was changed after 5 hours post-transfection to EGM-2 for HUVECs and D-MEM for HEK293T cells. Then, the medium was changed every 2 days. After 6 days of transfection the cells were detached with Trypsin-EDTA (0.25%) (Thermo Scientific™, 25200056) for subsequent experiments.

2.1.4 Cellular proliferation assay

Cell proliferation was analysed using Cell Proliferation ELISA, BrdU (colorimetric) assay (Roche, 11647229001). Next, 10 μM BrdU was added to transfected HUVECs and incubated for 24 hours in 96-well plate. Then, the cells were fixed and the DNA was denatured by adding FixDenat solution and anti-BrdU-POD was applied to the cells. After 3 washes with dPBS 100 μl of Substrate solution was added and the cells were incubated at room temperature for 5-30 min. After the addition of 25 μl stop solution the absorbance was measured at 450 nm with reference wavelength of 690 nm using the Infinite® M1000 PRO plate reader (Tecan). A standard curve method was used to quantify the results.

2.1.5 Migration and membrane capacitance assays

The assays were carried out using ECIS® (Electric Cell-substrate Impedance Sensing) (Applied BioPhysics) method. For migration assay HUVECs were cultured on the 8W2LE array. At time point 0 a wound was carried out using electric charge followed by migration of cells, which was detected by the change in impedance over the period of 24 hours. The values were expressed as migration speed in μm/h. For membrane capacitance assay the cells were plated on 8W10E+ array at time point 0 and the cell membrane capacitance

(C_m) was measured over the period of 24 hour, which was expressed in $\mu F/cm^2$. The data was quantified using ECIS Zθ (Theta) software.

2.1.6 Matrigel assay

In vitro angiogenesis was measured by Matrigel assay. For this, 10,000 cells were plated onto the Matrigel Matrix (Corning) in 96-well plate, which was solidified in 37°C for 30 min. The cells were incubated for 5-6 hours at 37°C and then fixed with 4% PFA in dPBS. The images of the cells were taken using EVOS inverted digital microscope. The images were then processed using ImageJ software with Angiogenesis Analyser plug-in. The parameters used for analysis were total length of the cellular networks and number of nodes.

2.1.7 RNA extraction

HUVECs were centrifuged at 1000 RPM for 5 minutes at 22°C. The medium above the cell pellet was removed and 700 µl of QIAzol® Lysis Reagent (QIAGEN, Cat No./ID: 79306) was added to each pellet and the content was transferred to RNase-free Microfuge Tubes; at this step the lysed cell pellet in QIAzol can be stored at -80°C. Then, 140 µl of chloroform was added to each tube, vortexed and incubated at room temperature for 5 minutes. After that, each microfuge tube was centrifuged for 15 min at 12,000 x g at 4°C. After the centrifugation the tubes were placed on ice and the upper aqueous phase was transferred to the new RNase-free Microfuge tubes. Then, 1.5 volumes of 100% ethanol was added to the tubes and mixed thoroughly by inverting the tubes around 10 times. Next, 700 µl of each sample was pipetted into an RNeasy® Mini column (QIAGEN, cat. No. 217004) in a 2 ml collection tube and all samples were centrifuged at 8000 x g for 15 s at room temperature. Following the discarding of the flow-through the previous step was repeated with the remainder of the samples. Next, 700 µl of the RWT buffer (QIAGEN, Cat

No./ID: 1067933) was added to each RNease Mini column, which were then centrifuged for 15 s at 8000 x g. Following the discarding of the flow-through 500 µl of the RPE buffer (QIAGEN, Cat No./ID: 1018013) was added to each RNease Mini column, which were then centrifuged for 15 s at 8000 x g. The previous step was repeated two more times (the centrifugation time increases to 2 min during the second repeat). Following the discarding of the flow-through all RNease Mini columns were centrifuged for 1 min at 21,000 x g at room temperature to dry the membrane. Then all RNease Mini columns were placed under the air-flow hood with lids open for 20 minutes to dry out the remaining traces of ethanol. After that 30 µl of RNase-free water was pipetted into each RNease Mini column, which were then placed in the new RNase-free Microfuge Tubes, incubated for 1 min at room temperature and centrifuged for 2 min at 8000 x g. The eluted RNA was then stored at -80°C.

2.1.8 Reverse transcription polymerase chain reaction (RT-PCR) and Real-Time PCR (qPCR) with TaqMan and LightCycler 480 Roche

Firstly, the extracted RNA was quantified using NanoDrop 1000 Spectrophotometer (Thermo Fisher Scientific) and the concentration of RNA was expressed as ng/µl. RT-PCR was carried out using High-Capacity cDNA Reverse Transcription Kit (Applied Biosystems™, Catalog number: 4368814). Specifically, for each sample a master mix was prepared using the following amount of reagents: nuclease free water 2.08 µl, dNTP mix 0.075 µl, 10x RT Buffer 0.75 µl, RNase inhibitor 0.095 µl and multiscribe RT enzyme 0.5 µl. Then the RT-PCR reactions were prepared in PCR tubes using these amounts of reagents: 3.5 µl of the RT master mix, 2.5 µl of diluted RNA (5 ng) and 1.5 µl of TaqMan RT primers (hsa-miR-148b, Cat. # 4427975; U6 snRNA, Cat. # 4427975) to make up 7.5 µl total reaction. The PCR tubes with the reaction mixes were then placed into the PCR thermocycler and the following program

was inputted: Hold 30 min at 16°C, hold 30 min at 42°C, hold 5 min at 85°C and then hold at 4°C.

Further, the cDNA from previous reaction was used for qPCR using LightCycler® 480 Probes Master kit (4707494 - Roche Applied Science). First of all, a qPCR master mix was prepared for each sample using the following quantities: LightCycler probe 5.00 µl, nuclease free water 3.83 µl and TaqMan primers 0.5 µl (hsa-miR-148b, Cat. # 4427975; U6 snRNA, Cat. # 4427975). After that, 9.33 µl of master mix was added to each well of 384-well white PCR plate, to which was then added 0.67 µl of miRNA-cDNA to make up to 10 µl of total reaction volume; each sample was done in duplicate. The PCR plate was then covered with transparent film, centrifuged for 2 min at 1500 RPM. The plate was then placed into LightCycler® 480 Instrument and the following program was selected: Mono Color Hydrolysis Probe – Pre-Incubation at 95°C, Amplification for 45 cycles (95°C for 10 sec, 60°C for 30 sec and 72°C for 1 sec) and Cooling at 40°C for 10 sec. After the qPCR run was finished, the results were analysed by selecting "Abs Quant/2nd Derivative Max" type of analysis and "amplification" program. Then, the calculated CT values were copied and used for further analysis of relative gene expression.

2.1.9 Reverse transcription polymerase chain reaction (RT-PCR) using genomic DNA wipeout method

For this technique QuantiTect Reverse Transcription Kit (QIAGEN, Cat. # 205311) was used. First of all, usually 300-500 ng of extracted RNA was diluted in RNase-free water to make up a total of 12 µl in the PCR tubes placed on ice. Then, 2 µl of gDNA Wipeout Buffer, 7x was added to each sample. The reverse-transcription master mix was prepared using following amounts of reagents per sample: Quantiscript Reverse Transcriptase 1 µl, Quantiscript RT

Buffer, 5x 4 µl, RT Primer Mix 1 µl. After that, each PCR tube was placed in the PCR thermocycler and the following RT-PCR program was set up: incubation for 2 min at 42°C, hold for 4 min at 4°C (6 µl of the master mix was added to each sample and mixed by pipetting during this step), incubation for 30 min at 42°C, incubation for 3 min at 95°C and hold at 4°C. Finally, cDNA was used for qPCR or can be stored at -20°C.

2.1.10 Real-Time PCR (qPCR) with AB SYBR Green for gene expression

Power SYBR® Green PCR Master Mix (Applied Biosystems, Cat. # 4367659) was used for the following qPCR protocol. A master mix was for each sample was prepared using the following quantities: 5 µl of Power SYBR® Green PCR Master Mix, 3 µl of RNase-free water and 1 µl of specific primer mix (10 µM). Then, 9 µl of the prepared master mix was added into each well of 384-well white PCR plate, to which 1 µl of the cDNA was added. The plate was then placed into LightCycler® 480 Instrument and the following program was selected: pre-incubation for 10 min at 95°C; 45 cycles of amplification for 15 sec at 95°C then for 30 sec at specific annealing temperature for each primer pair and 30 sec at 72°C; cooling for 30 sec at 40°C. After the qPCR run was finished, the results were analysed by selecting "Abs Quant/2nd Derivative Max" type of analysis and "amplification" program. Then, the calculated CT values were copied and used for further analysis of relative gene expression. Pre-designed from Sigma (KiCqStart™ Primers) were used for TGFB2, SMAD2, NOX2, CD31, VE-Cadherin, COL1A1, COL1A2, COL3A1, αSMA and 18S rRNA.

2.1.11 Analysis of the qPCR data

The double delta Ct analysis method was used to analyse all qPCR data in this study. The average of the Ct values for the housekeeping gene and for the gene of interest was taken, which generates 4 values: average experimental gene of

interest Ct value, average experimental housekeeping gene Ct value, average control gene of interest Ct value and average control housekeeping gene Ct value. Next, the differences between the Ct values of gene of interest and housekeeping gene were calculated for both experimental and control conditions, respectively, which generates delta Ct (ΔCt) values. After that, the differences between experimental and control ΔCts was calculated to generate the double delta Ct values (ΔΔCt). Finally, the following formula (2^-ΔΔCt) was used to calculate the expression fold change due to the fact that the Ct values were in logarithm base 2. The housekeeping gene used to calculate the expression of miR-148b was U6 snRNA; the housekeeping gene to calculate the expression of all target genes and EndoMT marker genes was 18S ribosomal RNA.

2.1.12 Protein extraction from cell pellet

Firstly, the cells were centrifuged at 1000 RPM for 5 minutes at 22°C. The medium on top of the pellet was removed and the cell pellet was then resuspended in 100 µl of 1x RIPA buffer (10x RIPA lysis buffer (Millipore, 20-188), 20x cOmplete ULTRA protease inhibitor cocktail, 100 mM PMSF, 100 mM Na_3VO_4 and 10x 1M NaF) and placed on ice for 15 min for lysis; each tube was vortexed periodically to facilitate the lysis. Next the tubes with lysed pellet in 1x RIPA were placed in 4°C centrifuge and centrifuged for 20 min at 17,000 x g. After centrifugation the supernatant with the lysed protein was pipetted into new tubes and placed on ice or frozen at 20°C.

2.1.13 Protein quantification by BCA assay

For this assay BCA™ Protein Assay kit (Pierce, 23225) was used. The principle of this assay is the ability of proteins to reduce Cu^{+2} to Cu^{+1} in an alkaline solution, which generates a purple colour formation by bicinchoninic acid.

Amino acids, such as cysteine or cystine, tyrosine, and tryptophan are able to reduce copper. Firstly, 2 μl of each protein extract was pipetted into each well of transparent 96-well plate in duplicate. Secondly, 0.25, 0.5, 1, 2 and 3 μl of Pierce™ Bovine Serum Albumin (BSA) Standard 2 mg/μl was pipetted into corresponding wells in duplicate. Then 200 μl of BCA™ Protein Assay Reagent mix (Reagent A + 50x of Reagent B) was added in each well and the plate was placed in 37°C incubator for at least 1 h. After the incubation the plate was placed into OptiMax™ microplate reader and the absorbance of each well was read at 560 nm. First of all, the averages of the BSA absorbance values of each duplicate were summed together and divided by the total amount of mg of BSA standard that was assayed, which was 13.5 mg, to give a value equal to absorbance of standard per mg of protein. After that the average of the duplicates of the sample proteins was divided by this ratio (OD of standard/mg) and then divided by 2 (because the concentration of the BSA standard was 2 mg/μl. The resulting value was expressed in mg/μl of the sample protein.

2.1.14 Sample preparation for Western Blot

Usually, 20 μg of protein was used for the Western Blot and the volume of the protein extract corresponding to this amount was mixed with 5x loading buffer (Bromophenol blue (0.25%), Bromophenol blue (0.25%), Glycerol (50%), SDS (sodium dodecyl sulfate; 10%)) and the total volume was calibrated with 1x RIPA buffer in order to make the uniform volume for all protein samples. Next, each tube was vortexed and placed in the 99°C heating block for 5 min. After that, the samples were centrifuged for 1 min at maximum speed in table-top centrifuge.

2.1.15 Western Blot

First of all, the SDS-Polyacrylamide gel electrophoresis (PAGE) gel was prepared. Firstly, 10% loading gel was prepared following this recipe: 6.25 ml of dH_2O, 5 ml of Protogel 30% (w/v) Acrylamide:0.8% (w/v) Bis-Acrylamide (National Diagnostics, EC-890), 3.75 ml of Tris/SDS pH=8.8, 50 µl of 10% Ammonium persulfate (APS) and 10 µl of TEMED; the mix was poured into Mini PROTEAN® System glass plate and left polymerising for 20 min. During the polymerisation of the loading gel, the stacking gel was prepared following this recipe: 6.1 ml of dH_2O, 1.3 ml of Protogel 30% (w/v) Acrylamide:0.8% (w/v) Bis-Acrylamide (National Diagnostics, EC-890), 2.5 ml of Tris/SDS pH=6.8, 50 µl of 10% Ammonium persulfate (APS) and 10 µl of TEMED and poured on top of the loading gel followed by placing the comb. After 20 min the glass plate with the SDS-PAGE gel was placed into the chamber, filled with 1x Tris-Glycine-SDS Buffer (250 mM Tris, 1.92 M glycine and 1% SDS). Then the comb was removed and the prepared protein sample and the PageRuler™ Prestained Protein Ladder (Thermo Scientific™, 26616) were added into each well. Finally, the voltage equal to 60V was applied on the chamber. When the sample enters the loading gel, the voltage was increased to 100V.

2.1.16 Protein transfer on the nitrocellulose membrane

After the running of the gel was stopped, the glass plate with the SDS-PAGE gel was opened and, following the separation of the stacking gel, the loading gel was soaked in Tris-Glycine Buffer with 5% methanol. In parallel, sandwich consisting of Whatman paper – gel – nitrocellulose membrane – whatman paper was prepared and assembled into transfer apparatus and filled with Tris-Glycine Buffer with 5% methanol buffer. After this, 100 mA of electrical current was applied and the transfer was carried out overnight.

2.1.17 Ponceau staining, membrane blocking and incubation with primary antibody

After the transfer was finished, the membrane was stained with Ponceau S solution to detect the protein loading on the nitrocellulose membrane. Then, 0.03% trichloroacetic acid was applied onto the membrane to remove unspecific Ponceau S staining. After the picture was taken for future records, the membrane was washed in Tris-buffered saline, 0.1% Tween 20 (TBST) for 5 min and then blocked with 5% non-fat milk in TBST for 1 hour. Following the blocking, the membrane was incubated overnight with a corresponding primary antibody diluted in 3% Bovine Serum Albumin (Sigma, A9647) in TBST. The list of primary antibodies used:

Antibody	**Brand**	**Lot. Num.**	**Dilution**
TGFβ2	Abcam Ltd	ab36495	1:1000
SMAD2	SantaCruz	#3102	1:1000
CD31	Abcam Ltd	ab28364	1:1000, 1:50
VE-Cadherin	Abcam Ltd	ab33168	1:1000
COL1A1	Abcam Ltd	ab138492	1:200
FSP-1	Abcam Ltd	ab41532	1:50
α-SMA	Sigma	A2547	1:100
β-actin	Abcam Ltd	ab16039	1:4000
GAPDH	GeneTex	GT239	1:1000
HDAC3	GeneTex	GTX113303	1:500

Table 4. List of antibodies used.

When using COL1A1 antibody no blocking step was carried prior to incubation with the primary antibody

2.1.18 Incubation with a secondary antibody, ECL-based Western blots detection

Then, the membrane was washed 3 times with TBST and the corresponding secondary antibody was applied in 5% non-fat milk in TBST and incubated for 1 hour. The list of secondary antibodies used: rabbit anti-mouse (Abcam Ltd., ab97046, 1:5000) and goat anti-rabbit (Abcam Ltd., ab6721, 1:10000). Following the incubation with the secondary antibody, the membrane was washed 3 times in TBST. Then, the membrane was incubated in EMD Millipore Immobilon™ Western Chemiluminescent HRP Substrate (ECL) (EMD Millipore, WBKLS0500) for 5 min and applied onto exposure cassette. The following steps were carried out in the dark room: CL-XPosure Film (Thermo Scientific, 34089) was applied on top of the membrane in the cassette, which was then being exposed for a specific time, starting from 1 minute. Following the exposure, the film was loaded onto Konica medical film processor (Konica, SRX-101A). Finally, the molecular weights of the protein were assigned and the film was scanned to analyse the results on the PC.

2.1.19 Immunofluorescence

Cells were plated on the glass coverslips in a 24-well plate in a density of 50,000 cells per well. Cells were fixed using 4% paraformaldehyde in PBS at room temperature for 15 min. Then, the cells were washed with PBS 3 times for 5 mins. After that, cells were blocked for 1 hour in 3% BSA/PBS with either 0.5% Triton X-100 or 0.1% Saponin (for membrane protein immunofluorescence). Following the blocking, the primary antibody was applied on the cells in 1% BSA/PBS with 0.5% Triton X-100 or 0.1% Saponin at 4°C in the dark overnight. The following primary antibodies were used: CD31 (Abcam Ltd., 1:50), VE-Cadherin (Abcam Ltd. ab33168, 1:100), COL1A1 (Abcam Ltd., ab138492,

1:100). Following the incubation with primary antibody, the cells were washed in PBS or 1% BSA/PBS with 0.1% Saponin (for membrane protein immunofluorescence) and the secondary antibody in 1% BSA/PBS with 0.5% Triton X-100 or 0.1% Saponin was applied onto the cells for 1 hour at the dark. This list of secondary antibodies was used: Alexa-Fluor-488-conjugated antibody to rabbit IgG (Life Technologies, Carlsbad, CA, # A11070) and Alexa-Fluor-594-conjugated antibody to rabbit IgG (Life Technologies, Carlsbad, CA, #A11072). Then, the washing step was repeated and the cells were incubated with DAPI (1:2000) in PBS for 5 min. After that, the washing step was repeated again and the glass coverslips were mounted with Fluoromount™ (Sigma, F4680) on the glass slides (Surgipath, 08001E). The slides were then mounted in the dark overnight and were ready to be visualized under the microscope.

2.1.20 Amplification of 3'UTR of *TGFB2* and *SMAD2* genes

The primers for 3'UTR of TGFB2 and SMAD2 were designed using Primer3Plus online software (http://www.bioinformatics.nl/cgi-bin/primer3plus/primer3plus.cgi). The sequences of the primers are the following: TGFβ2 3'UTR: Forward 5'-ATAAAGCTTATTTGCCACATCATTGCAGA-3', Reverse 5'-ATAACTAGTGGGAATAAAAAGACGGCACA-3'; SMAD2 3'UTR: Forward 5'-ATAAAGCTTTGATCCAGCTAAGGTAACTGATGTT-3', Reverse 5'-ATAACTAGTTGGTAAACAACTCAAATGGCTTTC-3'. SuperScript III First-Strand Synthesis kit (Thermo Scientific™, 18080400) was used to amplify 3'UTR of TGFB2 and SMAD2 from total RNA isolated from HUVECs cultured in EGM-2. The mutant truncated version of TGFB2 and SMAD2 3'UTR has been amplified from generated pMIR-TGFB2 3'UTR and pMIR-SMAD2 3'UTR using following primers: TGFβ2 3'UTR mut: Forward 5'-ATAAAGCTTATTTGCCACATCATTGCAGA-3', Reverse 5'-

ATAACTAGTCCTATCTGAGAGGAAAATGTCTGC-3'; SMAD2 3'UTR mut: Forward 5'- ATAAAGCTTTGATCCAGCTAAGGTAACTGATGTT-3', Reverse 5'- ATAACTAGTGGACTTCCAGAGGGAAACAA-3'.

2.1.21 DNA restriction digestion

The plasmid DNA (pMIR-report) and 3'UTR of TGFB2, TGFB2 mut, SMAD2 and SMAD2 mut were digested with HindIII (NEB, R0104S) and SpeI (NEB, R0133S) enzymes. The procedure: 1 μg of DNA, 5 μ of 10X NEBuffer 2.1, 1 μl of each enzyme to 50 μl with nuclease-free water. The reaction was carried out at 37°C for 2 hours.

2.1.22 DNA separation using agarose gel electrophoresis

Firstly, 1% agarose gel was made by melting 2 g of agarose (Bioline, BIO-41025) in 200 ml of 1x Tris-acetate-EDTA (TAE) buffer (242 g Tris free base, 18.61 g Disodiumn EDTA, 57.1 ml Glacial Acetic Acid, DDI H_2O to 1 liter). After that, 10 μl of GelRed™ (Biotium, #41003) was added to the cooled gel, which was then poured into the gel electrophoresis caster and left to solidify. DNA samples were mixed with 10x Orange-G loading buffer (20 g sucrose, 100 mg Orange-G in 100 ml of dH_2O) and loaded inside the well of the agarose gel together with 7 μl of 1 kb DNA ladder (NEB, N3232L). Then, 80-100 V was applied and the samples were run until the Orange-G bands reach the bottom edge of the gel. Specific DNA bands, corresponding to HindIII/SpeI cut pMIR-report and HindIII/SpeI cut 3'UTR of TGFB2 and SMAD2, were excised with a scalpel under UV for subsequent DNA gel extraction.

2.1.23 DNA gel extraction

HindIII/SpeI cut pMIR-report and HindIII/SpeI cut 3'UTR of TGFB2 and SMAD2 were extracted using this method. For this, The QIAquick Gel

Extraction Kit (Qiagen, 28704) was used. Firstly, 3 volumes of Buffer QG were added to 1 volume of gel, following by incubation at 50°C for 10 min. After the gel was completely melted, 1 gel volume of isopropanol was added and mixed. Then the sample was applied in a QIAquick spin column and centrifuged for 1 min full speed. After that, 500 μl of Buffer QG was applied in the column and centrifuged for 1 min full speed. Finally, 750 μl of Buffer PE was added to the column, centrifuged for 1 min full speed. After final centrifugation step, the column was left for air-dry and then 30 μl of nuclease-free water was added and centrifuged for 1 min full speed. The DNA was then stored at -20°C.

2.1.24 DNA ligation

Ligation was carried out using 3:1 ratio of insert (HindIII/SpeI cut 3'UTR of TGFB2, TGFB2 mut, SMAD2 and SMAD2 mut) to the vector (HindIII/SpeI cut pMIR-report), 2 μl of T4 DNA Ligase Buffer (10X), 1 μl of T4 DNA ligase (NEB, M0202) in a final volume of 20 μl with nuclease-free water. The reaction was carried out at room temperature for 1-2 hours.

2.1.25 Bacterial transformation

Competent high efficiency NEB 5-alpha *E.coli* (NEB, C2987H) were thawed on ice for 15 min. After that, 1-7 μl containing around 100 ng of plasmid DNA (pMIR-TGFB2 3'UTR, pMIR-TGFB2 3'UTR mut, pMIR-SMAD2 3'UTR and pMIR-SMAD2 3'UTR mut) were added to the cell mixture. The tube was carefully flicked 5 times and placed on ice for 30 min. Then, the sample was heat shocked for 30 sec at 42°C and placed on ice immediately for 5 min. Next, 950 μl of SOC (NEB, B9020S) medium was added to cell-DNA mixture and tube was placed at 37°C for 1 hour and shaken at 250 rpm. Following the warming of selection plates containing LB agar with antibiotic (Ampicilin) to

37°C, 100 µl of bacteria was spread onto the plate and incubated overnight at 37°C.

2.1.26 Plasmid DNA Purification using the QIAprep Spin Miniprep Kit

Overnight bacterial culture (pMIR-TGFB2 3'UTR, pMIR-TGFB2 3'UTR mut, pMIR-SMAD2 3'UTR and pMIR-SMAD2 3'UTR mut) in a volume of 5-7 ml was centrifuged for 5 min at 4500 x g. The bacterial pellet was then resuspended in 250 µl buffer P1 and transferred to a microcentrifuge tube. After that 250 µl of lysis buffer P2 was added, mixed by inverting 10 times. After 5 min of lysis, N3 buffer was added to each tube and mixed by inverting 10 times. Next, the sample was centrifuged for 10 min at 13,000 rpm in a table-top microcentrifuge. The supernatant was then applied to Qiaprep 2.0 spin column by pipetting and centrifuged for 1 min. After that, the flow-through was discarded and 0.5 ml of PB buffer was applied to the column and centrifuged for 1 min. The column was then washed with 0.75 ml of buffer PE and centrifuged for 1 min. The flow-through was then discarded and the column I centrifuged at maximum speed for 1 min to remove the residual buffer. The column was then left on the bench to allow the residual ethanol to dry out. Finally, 30 µl of nuclease-free water was applied to the column and centrifuged for 1 min. The samples were then stored at -20°C.

2.1.27 Quantification of the DNA/RNA concentration

Quantification was done using NanoDrop 1000 Spectrophotometer and ND-1000 software (Thermo Fisher Scientific). Firstly, 1 µl sample was pipetted onto the end of a fiber optic cable, following by blanking with 1 µl of nuclease-free water. DNA/RNA reads at 260 nm OD. The values for 260/280 nm and 260/230 nm was around 2.

2.1.28 Luciferase assay

HEK293T cells were transfected with 2ng of pMIR-control, pMIR-TGFB2 3'UTR, pMIR-TGFB2 3'UTR mut, pMIR-SMAD2 3'UTR, pMIR-SMAD2 3'UTR mut, 100 ng of CMV-b-galactosidase plasmid (Clontech Laboratories), and 25 nM of either MiRIDIAN miR-148b Mimic (Dharmacon, MI0000811) or miRIDIAN microRNA Mimic Negative Control (Dharmacon, CN-001000-01-05). After 3 days of transfection, the cells were lysed with 1X Passive Lysis Buffer (Promega) for 15 min at room temperature. The protein was quantified using BCA assay and 2 μg of each sample was loaded on the 96-well solid white plate (Corning). Then, 100 μl of luciferase assay substrate (Promega, E151A) was added to each sample simultaneously using multichannel pipette. Immediately after, the absorbance was read at 560 nm (for Firefly luciferase) using Infinite® M1000 PRO plate reader (Tecan). Separately, 50 μl of β-Galactosidase Enzyme Assay buffer (Promega, E2000) was added to 2 μg of protein extract and incubated at 37°C; the reaction was stopped 15-20 min later with 150μl of 1M Sodium Carbonate and the absorbance was read at 420 nm using Infinite® M1000 PRO plate reader (Tecan). The values of luciferase assay were normalised to the values of β-Galactosidase assay and expressed as luciferase/β-Galactosidase ratio.

2.1.29 ELISA assay

Human TGF-beta 2 Quantikine ELISA Kit (R&D, DB250) was used for this assay. Prior to the sample preparation the working standards were prepared at the concentrations of 1000 pg/mL, 500 pg/mL, 250 pg/mL, 125 pg/mL, 62.5 pg/mL, 31.3 pg/mL. After that, 100 μl of Assay Diluent RD1-17 is added to each well on the assay plate. Next, 100 μl of standard, control, or activated sample is added to each well, covered with adhesive strip, incubated for 2 hours at

room temperature. After the incubation, each well is aspirated and washed three times with 300 µl wash buffer (diluted in PBS). Next, 200 µL of Human TGF-β2 Conjugate is added to each well, covered with a new adhesive strip and left for incubation for 2 hours at room temperature. The washing step is repeated and 200 µL of Substrate Solution (Color Reagents A and B should be mixed together in equal volumes within 15 minutes of use) is added to each well, incubated for 20 minutes at room temperature, while protected from light. After addition of 50 µL Stop Solution to each well, the plate is put into the Infinite® M1000 PRO plate reader (Tecan) and the absorbance is read at 450 nm with wavelength correction set to 540 nm or 570 nm. The results are calculated using standard curve method and expressed as a concentration in ng/mL.

2.1.30 Statistical analysis

Comparisons between different conditions were assessed using 2-tailed Student's t test. Differences among groups were elicited using ANOVA followed by Bonferroni post-hoc analyses as appropriate. Continuous data are expressed as mean ± SD of three independent experiments, each performed in triplicate or quintuplicate. P value <0.05 was considered statistically significant. Analyses were performed using GraphPad Prism v5.0.

2.2 Techniques for *in vivo* studies

The *in vivo* work has been performed by Dr Andrea Caporali and assisted by Dr Marco Meloni, Lorraine Rose and myself.

2.2.1 Animal work

The experiments involving mice were performed in accordance with the Guide for the Care and Use of Laboratory Animals prepared by the Institute

of Laboratory Animal Resources and with the prior approval of the UK Home Office and the University of Edinburgh ethic committee. CD-1 female mice (7–10 weeks old) were randomly assigned a treatment group and anaesthetized with isofluorane. Two full-thickness excisional wounds were made to the shaved dorsal skin. Full-thickness excisional wounds were made by picking up a fold of skin and using a sterile, disposable 5-mm biopsy punch (Kai Industries), resulting in generation of one wound on each side of the midline. MiRIDIAN miR-148b Mimic (Dharmacon, MI0000811), miRIDIAN microRNA Mimic Negative Control (Dharmacon, CN-001000-01-05), miRCURY LNA™ anti-miR-148b (Exiqon) 75 nM, miRCURY LNA™ microRNA Antisense Control (Exiqon) (1 ug/wound) were delivered topically by pipette into the wound cavity immediately after wounding and every two days (20µl in a vehicle of 30% Pluronic F-127 gel [is liquid at 4°C but solidifies at body temperature]; Sigma Aldrich). Wounds were photographed with an Olympus camera on days 0, 2, 4, 6, and 7 after wounding. To this aim, two perpendicular diameters of the wound were measured by using a Vernier caliper and wound area was calculated using a standard formula for the area of an ellipse (semi-major diameter X semi-minor diameter X Pi).

2.2.2 Histology

Wounds were harvested on days 5 or 7 post-wounding, fixed in 10% buffered formalin (16h at 4°C, Sigma) for embedding in paraffin. Wounds were sectioned through the wound beyond the midpoint and wound centres identified by staining with Haematoxylin and Eosin (Sigma). Sections were deparaffinised, rehydrated and stained with rat anti-mouse polyclonal CD31 (Abcam), rabbit anti-mouse FSP-1 (fibroblast specific protein-1, Abcam), and Cy3-conjugated α-vascular smooth actin (Sigma) all antibodies overnight at 4°C.

CHAPTER 3: THE ROLE OF MIR-148B IN REGULATION OF *IN VITRO* AND *IN VIVO* ANGIOGENESIS

3.1 INTRODUCTION

Angiogenesis is the subsequent remodelling of the primary vascular plexus formed during vasculogenesis, and the assembly of new vessels from pre-existing ones (Risau, 1997). A number of recent studies have provided great insight into the molecular mechanisms underlying this process, and led to an established mechanistic framework of vessel branching (Carmeliet and Jain, 2011, Potente et al., 2011). Together with the key drivers such as hypoxia, inflammation and haemodynamic forces, angiogenesis is tightly orchestrated by molecular stimuli such as VEGF, NOTCH, ANG-1, FGFs, TGF-β and PDGF-B (Carmeliet and Jain, 2011). In addition to the molecular signals angiogenesis can be also positively or negatively modulated by miRNAs (Landskroner-Eiger et al., 2013).

MiRNAs are small (~22 nucleotides) conserved RNA molecules that function as post-transcriptional regulators of gene expression and modulate all known biological processes, from cell proliferation, growth and differentiation to homeostasis, development and metabolism (Ameres and Zamore, 2013). Using computational prediction algorithms and genome-wide elucidation of miRNA targets, it has been estimated that each miRNA molecule can bind to hundreds target mRNAs, modulating various networks and cascades of different proteins. As a result, an impaired regulation of miRNA biogenesis and function can lead to severe disorders and pathologies (Hesse and Arenz, 2014).

Endothelial cells exert a high expression of miRNAs (Poliseno et al., 2006) and recent findings imply that they can modulate vascular development as well as angiogenesis (Landskroner-Eiger et al., 2013). Depending on their target genes, miRNAs expressed in endothelial cells can be either positive or negative

regulators of angiogenesis. Specifically, miR-126 and miR-210 are enhancers of angiogenic response, targeting *Spred-1* and *PIK3R2*, and *Ephrin-A3*, respectively, which abrogate cellular responsiveness to angiogenic stimuli like VEGF (Fish et al., 2008, Wang et al., 2008, Fasanaro et al., 2008). On the other hand, miR-17~92 cluster exerts anti-angiogenic effects on the endothelial cells via blocking the expression of pro-angiogenic *S1PR1*, *p21* and *Jak1* protein kinase (Doebele et al., 2010). Similarly, diabetes-induced miR-503 is able inhibit the angiogenic response in endothelial cells (Caporali et al., 2011).

Recent study carried out in BHF Centre for Cardiovascular Target Discovery in University of Oxford (unpublished) describes a high-throughput miRNA phenotypic screen, in which 1500 miRNA mimics have been assayed on their capacity to modulate proliferation of HUVECs. Specifically, using miR-302c as a positive control and miR-503 as a negative control, a subset of proliferation enhancer miRNAs and inhibitor miRNAs have been identified. Out of the strongest enhancers 24 miRNAs were conserved and highly expressed in the endothelial cells, including miR-148b, miR-26b, miR-148a, miR-17 and miR-20a. Notably, post-screening analysis has demonstrated that between this list miR-148b is the strongest enhancer of HUVEC proliferation. In addition to this, miR-148b has not been reported before to regulate endothelial cell biology or angiogenesis. In particular, limited number of studies describe the involvement of miR-148b in different types of cancer (Song et al., 2011, Song et al., 2012, Chang et al., 2012, Wu et al., 2012, Zhao et al., 2013) as well as osteogenesis (Qureshi et al., 2013, Liao et al., 2014).

3.1.1 Hypothesis

In light of the novel findings on the capacity of miR-148b to strongly enhance HUVEC proliferation, the main goal of this chapter was to the hypothesis that:

"Overexpression of miR-148b facilitates *in vitro* and *in vivo* angiogenesis"

3.1.2 Aims

The aims of this chapter were:

1. Identify miR-148b target genes

2. Determine whether miR-148b overexpression enhances HUVEC proliferation, migration and cellular network formation *in vitro*

3. Determine whether overexpression of miR-148b is able to induce angiogenesis *in vivo*

3.2 METHODS

3.2.1 Cells and Cell Culture

Human umbilical vein ECs (HUVECs; Lonza) were grown in EGM-2 (comprising EBM-2 with growth factors and other supplements) with 2% Foetal Bovine Serum. HEK293T cells (ATCC®, CRL-11268) were cultured in D-MEM with 10% FBS (Life Technologies).

3.2.2 miR-148b Target Analysis

Computational prediction of miR-148b target genes was done using published algorithm TargetScan (www.targetscan.org). miRpath v.3 (http://diana.imis.athena-innovation.gr/DianaTools/index.php?r=mirpath) was used to perform gene set enriched analysis of miR-148b target genes. The prediction is based on Targetscan parameters such as Context score and Conservation score.

3.2.3 RNA Extraction and Quantitative Real-Time Analysis

Total RNA was extracted using miReasy kit (Qiagen). Real-time quantification to measure miRNAs was performed with the TaqMan miRNA reverse transcription kit and miRNA assay (Life Technology) using Lightcycler 480 (Roche). MiRNAs expression was normalized to the U6 small nucleolar RNA (snRU6). For mRNA analysis, cDNA was amplified by quantitative real-time PCR (qPCR) and normalized to 18S ribosomal RNA. Each reaction was performed in triplicate. Quantification was performed by the 2–ddCt method. qPCR was used to measure the expression of miR-148b (miR-148b-3p Thermo Fisher Scientific, Cat. #4426961), snRU6 (Thermo Fisher Scientific, Cat. #4331182), TGFB2, SMAD2 and 18S rRNA. Primers are pre-designed from Sigma (KiCqStartTM Primers).

3.2.4 Cells transfection, transduction and functional assays

Lipofectamine RNAiMAX (Thermo Fisher Scientific) was used to transfect HUVECs with miR-148b mimic, mimic control (25nM final concentration), according to the manufacturer's instructions. The following functional assays were performed: BrdU incorporation assay using Cell Proliferation colorimetric assay (Roche); migration assay and endothelial barrier function were performed using ECIS machine as described below. Matrigel assay with HUVECs was performed using BD Matrigel Basement Membrane Matrix (BD Biosciences).

3.2.5 ECIS Assays

Confluent HUVECs were transfected with miR-148b mimic and mimic control and plated on the ECIS chip array (8W1E). The migration speed was calculated in μm/h, distance from cells to chip surface in α (Ω0.5cm).

3.2.6 Western-Blot analyses

Proteins were extracted from cultured cells or muscles by using ice-cold buffer A (50mM Hepes, 150mM NaCl, 1mM EDTA, 1mM EGTA, 25mM NaF, 5mM NaPPi, 1%Triton, 1% NP40, 1 mM Na3VO4, 0,25% sodium deoxycholate, 0.5mM Na-orthovanadate, 1 mM benzamidine, 0.1mM phenylmethylsulfonyl fluoride). Protein concentration was determined using the Bio-Rad Protein Assay Reagent (Bio-Rad Laboratories, UK). Detection of proteins by Western blot analyses was done following separation of whole cell extracts (20μg) on SDS-polyacrylamide gels. Proteins were transferred to nitrocellulose membranes and probed with the following antibodies: TGFβ2 (Abcam Ltd. ab36495, 1:1000), SMAD2 (SantaCruz Biotechnology, Santa Cruz, CA, USA; #3102, 1:1000) and β-actin (Abcam Ltd., ab16039, 1:4000). For detection, we

used secondary antibodies conjugated to horseradish peroxidase which were rabbit anti-mouse (Abcam Ltd., ab97046, 1:5000) and goat anti-rabbit (Abcam Ltd., ab6721, 1:10000). Detection was developed by chemiluminescence reaction (ECL) (Immunoblot, Millipore, 23225).

3.2.7 Luciferase assay

TGFB2 3'-UTR and SMAD2 3'-UTR vectors were cloned in pMIR-Reporter (Life Technology). Primers are used for the cloning are: TGFβ2 3′UTR: Forward 5′-ATAAAGCTTATTTGCCACATCATTGCAGA-3′, Reverse 5′-ATAACTAGTGGGAATAAAAAGACGGCACA-3′; SMAD2 3′UTR: Forward 5′-ATAAAGCTTTGATCCAGCTAAGGTAACTGATGTT-3′, Reverse 5′-ATAACTAGTTGGTAAACAACTCAAATGGCTTTC-3′ TGFβ2 3′UTR mut: Forward 5′-ATAAAGCTTATTTGCCACATCATTGCAGA-3′, Reverse 5′-ATAACTAGTCCTATCTGAGAGGAAAATGTCTGC-3′; SMAD2 3′UTR mut: Forward 5′- ATAAAGCTTTGATCCAGCTAAGGTAACTGATGTT-3′, Reverse 5′- ATAACTAGTGGACTTCCAGAGGGAAACAA-3′. Luciferase constructs were transfected into HEK293T cells together with miR-148b mimics or p-SV-beta –Gal control vector. Cells were cultured for 48h and assayed with the Luciferase and β-Galactosidase Reporter Assay Systems (Promega). Luciferase values were normalized to protein concentration and β-galactosidase activity.

3.2.8 Animal experiments

All experiments involving mice were performed in accordance with the guidance and the operation of Animals (Scientific Procedures) Act 1986 and prior approval of the UK Home Office and the University of Edinburgh ethic committee. CD-1 female mice (7–10 weeks old) were randomly assigned a treatment group and anaesthetized with isofluorane. Two full-thickness

excisional wounds were made to the shaved dorsal skin. Full-thickness excisional wounds were made by picking up a fold of skin and using a sterile, disposable 5-mm biopsy punch (Kai Industries), resulting in generation of one wound on each side of the midline. Control oligonucleotides (scramble sequence) and miR-148b mimic (1 ug/wound) were delivered topically by pipette into the wound cavity immediately after wounding and every two days (20μl in a vehicle of 30% Pluronic F-127 gel [is liquid at 4°C but solidifies at body temperature]; Sigma Aldrich). Wounds were photographed using an Olympus camera on days 0, 2, 4, 6, and 7 after wounding. To this aim, two perpendicular diameters of the wound were measured by using a Vernier caliper and wound area was calculated using a standard formula for the area of an ellipse (semi-major diameter X semi-minor diameter X Pi).

3.2.9 Histology

At days 5 or 7 post-wounding, wounds were harvested and fixed in 10% buffered formalin (16h at 4oC, Sigma) for embedding in paraffin. Sectioning was done through the wound beyond the midpoint and wound centres as identified by staining with Haematoxylin and Eosin (Sigma). Sections were deparaffinised, rehydrated and stained with rat anti-mouse polyclonal CD31 (Abcam, ab28364, 1:50) and Cy3-conjugated α-vascular smooth actin (Sigma) all antibodies overnight at 4oC.

3.2.10 Statistical analysis

Comparisons between different conditions were assessed using 2-tailed Student's t test. Differences among groups were elicited using ANOVA statistical test followed by Bonferroni post-hoc analyses as appropriate. Continuous data are expressed as mean ± SD of three independent experiments, each performed in triplicate or quintuplicate. P value <0.05 was

considered statistically significant. Analyses were performed using GraphPad Prism v5.0.

3.3 RESULTS

3.3.1 Identification of miR-148b putative targets

Using gene set enriched analysis miRpath (Vlachos et al., 2015), one of the pathways regulated by miR-148b was the TGF-β pathway (Fig. 3.1 a). Moreover, the Targetscan algorithm predicted *TGFB2* and *SMAD2* to be direct targets of miR-148b. Specifically, both genes contain one a single conserved binding sequence for miR-148b in their 3′ untranslated region (UTR) (Fig. 3.1 b). Moreover, according to miRpath algorithm, *TGFB2* hasn't been yet supported experimentally to be a direct target of miR-148b. Thus, *TGFB2* and *SMAD2* were selected for subsequent *in vitro* validation.

a

#	Gene Name	Gene Ensembl id	Interactions	Score	Experimentally Supported
1.	ROCK1	ENSG00000067900	see interaction	0.980	Yes
2.	INHBB	ENSG00000163083	see interaction	0.996	Yes
3.	BMPR1B	ENSG00000138696	see interaction	0.830	No
4.	SKP1	ENSG00000113558	see interaction	0.803	No
5.	SMAD5	ENSG00000113658	see interaction	0.809	Yes
6.	GDF6	ENSG00000156466	see interaction	0.938	No
7.	TGFB2	ENSG00000092969	see interaction	0.973	No
8.	NOG	ENSG00000183691	see interaction	0.990	No
9.	BMPR2	ENSG00000204217	see interaction	0.818	No

b

Figure 3.1| MiR-148b *in silico* targets analysis. a. Analysis of miR-148b target genes using miRpath software. Table shows Context Score and whether the targets have been

experimentally validated. **b.** In silico analysis of *TGFB2* and *SMAD2* 3'UTR with Targetscan identifies putative miR-148b-binding sites (blue).

3.3.2 Experimental validation of TGFB2 and SMAD2 as direct miR-148b targets

To see if miR-148b overexpression modulates other predicted miR-148b target genes a qPCR was run to test the expression of selected candidates, including *SMAD5*, *GADD45B*, *BCL2L11*, *p27*, *SNAI1*, *MEOX2*, *TNRC6A*, *AGO1*, *S1PR1* and *COPZ1*, which is also a miR-148b host gene. As a result, it is evident that miR-148b modulates the expression of all of these predicted targets (Fig. 3.2 f). Nevertheless, due to the fact that *TGFB2* and *SMAD2* act at the same signalling pathway, these candidates were chosen for further analysis. To investigate whether miR-148b directly binds the 3'UTR of *TGFB2* and *SMAD2*, luciferase reporter assay was performed, in which luciferase reporter gene was fused to the wild-type 3'UTR of *TGFB2* or *SMAD2*, respectively. Overexpression of miR-148b decreased luciferase activity for each of the putative target genes (Fig. 3.2 a). Moreover, the elevated levels of miR-148b did not affect the luciferase activity of the targets, in which the 3'UTR has been truncated, deleting the seed sequence (Fig. 3.2 a). This date validates *TGFB2* and *SMAD2* as direct target genes of miR-148b. In order to see whether miR-148b is able to modulate the expression of *TGFB2* and *SMAD2* in endothelial cells, HUVECs were transfected with miR-148b mimic and control. Overexpression of miR-148b (Fig. 3.2 b) reduced both target gene mRNA (Fig. 3.2 c) and protein levels (Fig. 3.2 d, e), confirming miR-148b regulation of *TGFB2* and *SMAD2 in vitro*. Together, these findings demonstrate that *TGFB2* and *SMAD2* are direct targets of miR-148b, which can downregulate their expression in the endothelial cells.

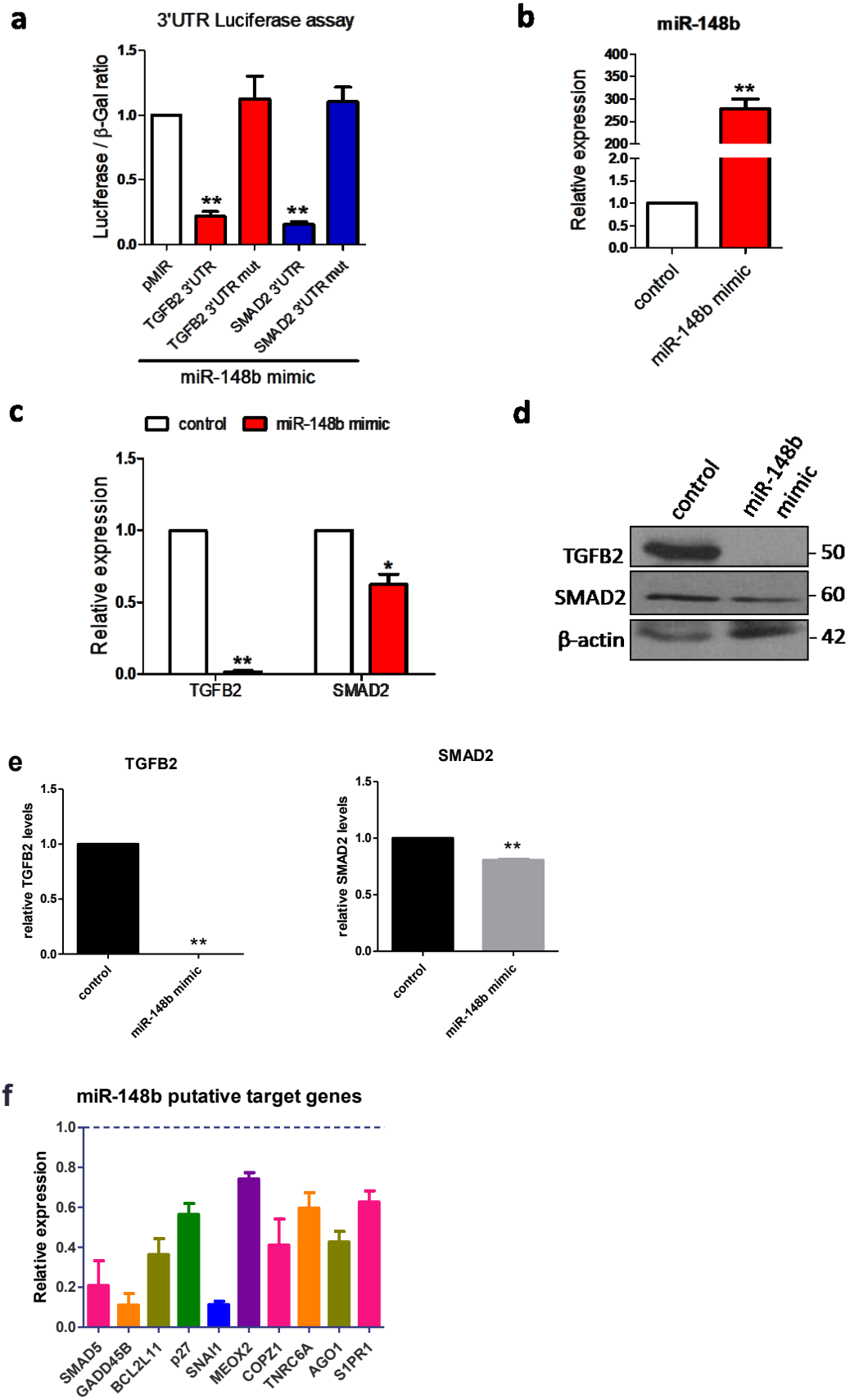
a
3'UTR Luciferase assay
Luciferase / β-Gal ratio
1.5
1.0
0.5
0.0
**
**
pMIR
TGFB2 3'UTR
TGFB2 3'UTR mut
SMAD2 3'UTR
SMAD2 3'UTR mut
miR-148b mimic
b
miR-148b
Relative expression
400
350
300
250
200
2.0
1.5
1.0
0.5
0.0
**
control
miR-148b mimic
c
control
miR-148b mimic
Relative expression
1.5
1.0
0.5
0.0
**
*
TGFB2
SMAD2
d
control
miR-148b mimic
TGFB2
SMAD2
β-actin
50
60
42
e
TGFB2
relative TGFB2 levels
1.5
1.0
0.5
0.0
**
control
miR-148b mimic
SMAD2
relative SMAD2 levels
1.5
1.0
0.5
0.0
**
control
miR-148b mimic
f
miR-148b putative target genes
Relative expression
1.0
0.8
0.6
0.4
0.2
0.0
SMAD5
GADD45B
BCL2L11
p27
SNAI1
MEOX2
COPZ1
TNRC6A
AGO1
S1PR1

Figure 3.2| *In vitro* validation of *TGFB2* and *SMAD2* as direct miR-148b targets. a. Luciferase activity expressed as luciferase/β-Gal ratio at 48h post-co-transfection of HEK293T cells with both miR-148b and the following plasmids: 3'-UTR-TGFB2. 3'-UTR-SMAD2 and pMIR as empty plasmid (n=5); **b.** qPCR showing miR-148b expression levels after miR mimic transfection; average Ct values: miR-148b (control: 30; miR-148b mimic: 22). **c.** qPCR showing relative gene expression of *TGFB2* and *SMAD2*, after miR-148b overexpression (n=3); average Ct values: *TGFB2* (control: 23; miR-148b mimic: 30), *SMAD2* (control: 22; miR-148b mimic: 24); **d.** Western blot analysis of TGFB2 and SMAD2 in samples transfected with miR-148b mimic vs control; β-actin is used as a loading control at dilution 1:4000 (n=3); antibody dilutions for anti-TGFB2 and anti-SMAD2 are 1:1000; **e.** Quantification of TGFB2 and SMAD2 western blots; **f.** qPCR showing relative gene expression of putative miR-148b target genes after miR-148b overexpression (n=2); average Ct values: *SMAD5* (control: 22; miR-148b mimic: 27), *GADD45B* (control: 22, miR-148b mimic: 28), *BCL2L11* (control: 25; miR-148b mimic: 30), *p27* (control: 23; miR-148b mimic: 26), *SNAI1* (control: 26; miR-148b mimic: 32*)*, *MEOX2* (control: 24; miR-148b mimic: 25), *COPZ1* (control: 25; miR-148b mimic: 27), *TNRC6A* (control: 25; miR-148b mimic: 26), *AGO1* (control: 30; miR-148b mimic: 31), *SP1PR1* (control: 24; miR-148b mimic: 25); HUVECs were transfected with miR-148b mimic or control oligonucleotides for 48hrs; For miRNA qPCR U6 was used as a house-keeping control; For target gene qPCR 18s was used as a house-keeping control; Values are means±SEM *P<0.05; **P<0.01 vs control and pMIR vector in experiment b. Unpaired two-tailed Student's t-test was applied.

3.3.4 MiR-148b induces HUVEC proliferation, migration and *in vitro* angiogenesis

To better understand the effect of miR-148b on cellular phenotype, functional cellular assays have been performed with the HUVECs transfected with miR-148b mimic and control. Specifically, miR-148b overexpression significantly increased the proliferation of HUVEC, as demonstrated by BrdU incorporation assay (Fig. 3.3 a). Next, in order to elucidate miR-148b effect on *in vitro* angiogenesis, two pro-angiogenic properties of HUVEC were analysed: migration and cellular network formation. The migration capacity of HUVECs transfected with a miR-148b mimic was significantly elevated (Fig.

3.3 b), along with their ability to form tube-like structures in an *in vitro* Matrigel assay (Fig. 3.3 c). Together, these results illustrate that miR-148b is able to induce *in vitro* angiogenesis via enhancing HUVEC proliferation, migration and cell network formation.

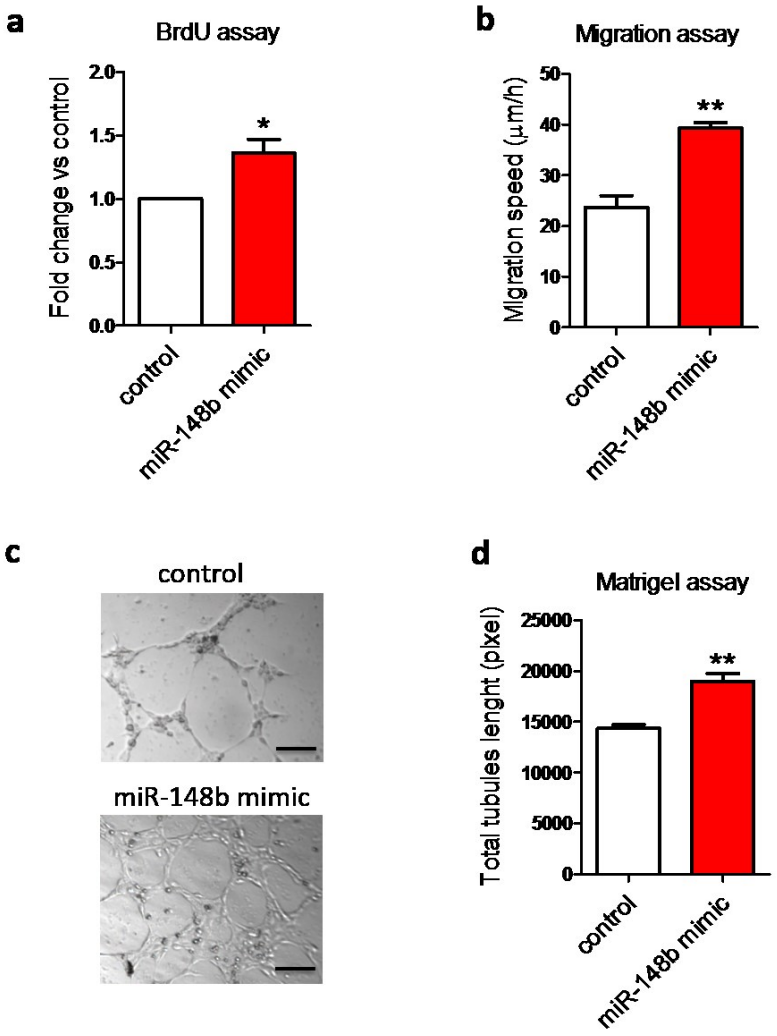

Figure 3.3| MiR-148b overexpression enhances proliferation and *in vitro* angiogenesis. a. EC proliferation was analysed by BrdU incorporation assay and expressed as a fold change in absorbance (n=3); **b.** ECIS migration assay using 8W2LE array reported as migration speed (µm/h) (n=3); **c.** Representative Matrigel assay pictures and **d.** quantification as total tubules length expressed as pixel density (n=3); Values are means±SEM *P<0.05; **P<0.01 vs control. Unpaired two-tailed Student's t-test was applied.

3.3.5 Topical miR-148b delivery facilitates angiogenesis and promotes wound healing *in vivo*

In order to determine whether overexpression of miR-148b is also able to induce angiogenic response *in vivo*, a model of mouse wound healing angiogenesis has been used due to the fact that this is an ideal model to analyse angiogenesis because of its easy accessibility to control and modulate the process (Eming et al., 2007). Notably, in the skin of the healthy mice miR-148b expression was reduced significantly 3 days after wound induction (Fig. 3.4 a). Next, the topical delivery of miR-148b mimics, within Pluronic gel, increased miR-148b expression 7 days after injury (Fig. 3.4 b). Expression levels of both targets, *TGFB2* and *SMAD2*, were considerably reduced in the wounds following the treatment with miR-148b mimics (Fig. 3.4 b). Moreover, miR-148b overexpression significantly accelerated wound closure (Fig. 3.4 c, d) and enhanced the wound perfusion detected by Doppler analysis (Fig. 3.4 e). Finally, delivery of miR-148b mimics has also increased vascularization in the wound as shown by considerable enhancement of CD31 positive vessels (Fig. 3.4 f). Overall, these data indicate that miR-148b overexpression via topical miR mimics delivery is able to inhibit *TGFB2* and *SMAD2* expression while promoting angiogenesis and wound healing *in vivo*.

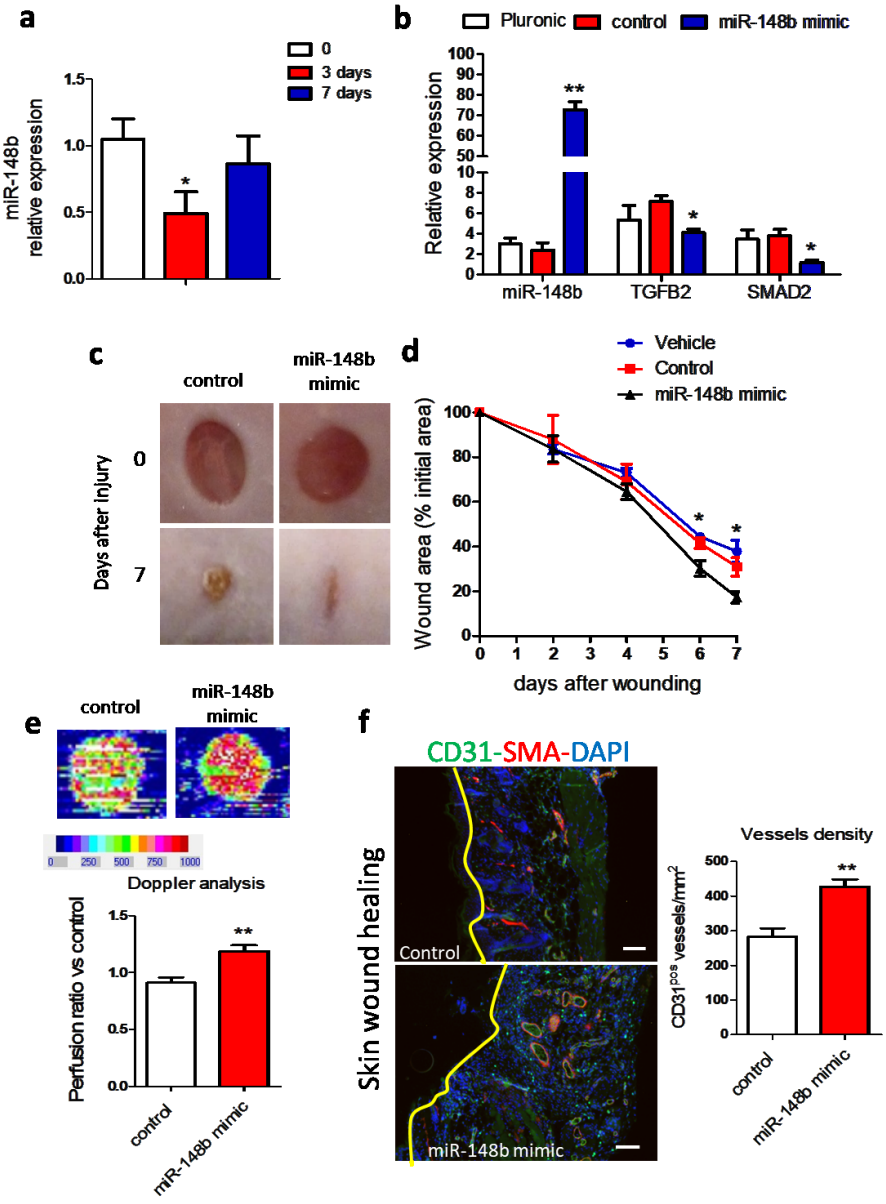

Figure 3.4| MiR-148b facilitates angiogenesis and wound healing *in vivo*. a. qPCR showing expression of miR-148b at 3 and 7 days after wounding, relative to unwounded skin (n = 5); average Ct values: miR-148b (0 d: 29, 3 d: 31, 7 d: 30); **b.** qPCR showing relative gene expression of miR-148b, *TGFB2* and *SMAD2* in dermal wound after delivering of miR-148b mimic or control oligonucleotides for 5 days**;** average Ct values: miR-148b (pluronic: 27, control: 28, miR-148b mimic: 23), *TGFB2* (pluronic: 25, control: 24, miR-148b mimic: 26), *SMAD2* (pluronic: 24, control: 23, miR-148b mimic: 27) **c.** Representative images of control and miR-148b mimic treated wounds at 0 and 7 days post wound injury, scale bar=5mm; **d.** Level of wound closure expressed in percentage of wound area from the initial area (n=8); **e.** Representative colour laser Doppler images are taken at 5 days post wounds. Chart shows level of wounds perfusion

in mice (calculated as the ratio between treated and control blood flow; n=8 per group); **f.** Immunohistochemistry for CD31 (antibody dilution 1:50), α-SMA (antibody dilution 1:100) in miR-148b mimic-treated or control-treated skin wounds; scale bar=100μm (magnification 400x); yellow line determine wound edge. Quantification of vessel density expressed as CD31 positive vessels/mm2 (n=8); For miRNA qPCR U6 was used as a house-keeping control; For target gene qPCR 18s was used as a house-keeping control; Values are means±SEM *P<0.05; **P<0.01 vs control. Unpaired two-tailed Student's t-test was applied.

3.4 DISCUSSION

Here, this chapter shows for the first time that miR-148b is a modulator of endothelial cells function and angiogenesis. Moreover, this chapter provides novel evidence that miR-148b is targeting the expression of *TGFB2* and *SMAD2* genes, which are part of one signalling cascade. Finally, these data elucidates for the first time that role of miR-148b in promoting the wound repair as well as *in vivo* angiogenesis.

3.4.1 MiR-148b targets TGF-β pathway and upregulates *in vitro* angiogenesis

There has been no scientific data in the literature to date discussing the role of miR-148b in endothelial cell biology. The high-throughput phenotypic screen carried out prior to this study has elucidated for the first time that miR-148b overexpression in HUVEC is able to induce cell proliferation. To follow up on the preliminary data, the migration and *in vitro* angiogenesis assays in this chapter have confirmed the proangiogenic properties of miR-148b. Recently, Yang et al. has carried out a similar high-throughput miRNA screen in order to identify miRNAs that could target the expression of *Nox2* gene (Yang et al., 2017), which is a strong inducer of reactive oxygen species (ROS) production in infarcted myocardium (Cave et al., 2006). Interestingly, the study has identified miR-148b along with miR-204 and miR-106b to be potent modulators of *Nox2* expression in human macrophages (THP-1 cells). Moreover, all three miRNAs were able to decrease ROS production in the macrophages as well as reduce the secretion of pro-inflammatory cytokines (Yang et al., 2017).

Further, the miRNA pathway analysis software has predicted miR-148b to potently modulate TGF-β cascade. The target validation experiments in this chapter have confirmed *TGFB2* and *SMAD2* to be direct miR-148b targets with

a strong regulation in HUVECs. These results can explain the increase in proliferation as well as *in vitro* angiogenesis because TGF-β pathway has been reported before to negatively regulate the proliferation of endothelial cells and angiogenesis via ALK5 activation (Goumans et al., 2002) and VEGF insensitivity (Viloria-Petit et al., 2013). In the analogous study, Dews et al. suggested that miR-17~92 cluster, upregulated by c-Myc, is able to promote angiogenesis via blocking the expression of the components of TGF-β signalling cascade – *TGFBR2* and *SMAD4* (Dews et al., 2010).

Interestingly, the downregulation levels of *TGFB2* and *SMAD2* in response to miR-148b overexpression are different: the expression of *TGFB2* is completely silenced, whereas *SMAD2* is only ~65% downregulated. This discrepancy can be explained by the fact that the interaction between miR-148b and *TGFB2* forms the 8mer, which is the exact match to the seed sequence of mature miR-148b. On the other hand, miR-148b:*SMAD2* is a 7mer with incomplete binding of miR-148b. As a result, the interaction between TGFB2 mRNA and miR-148b is stronger and downregulation is more significant than of *SMAD2*. It could also be speculated that *TGFB2* is expressed in a higher abundance than *SMAD2* mRNA resulting in "sponge out" effect on miR-148b.

Importantly, miR-148b overexpression leads to consistent downregulation of other putative target genes, *SMAD5*, *GADD45B*, *BCL2L11*, *p27*, *SNAI1*, *MEOX2*, *TNRC6A*, *AGO1*, *S1PR1* and a miR-148b host gene *COPZ1*. Interestingly, *SMAD5* is involved in an antagonising pathway to the TGFβ2 pathway. It is possible to speculate that the ability of miR-148b to modulate *SMAD5* is part of the feedback mechanism to balance out the effect of TGFβ2-SMAD2 downregulation. What is more, *GADD45B*, *BCL2L11*, *p27*, *TNRC6A* and *S1PR1* are all antiangiogenic genes. It is therefore logical to assume that the strong pro-angiogenic effect of miR-148b is also partially attribute to

downregulation of this genes. Notably, *AGO1* is involved in miRISC assemble and, thus, its silencing by miR-148b could also be a feedback negative mechanism to diminish the production of mature miR-148b-3p, when the levels of its precursor are too high. Similarly, miR-148b targeting of its host gene *COPZ1* suggest another mechanism of automodulation to control miR-148b levels in the cell.

Overall, the *in vitro* part of this chapter demonstrated that miR-148b is able to enhance HUVEC proliferation, migration and angiogenesis *in vitro*, possibly by targeting specifically TGFβ2-ALK5-SMAD2/3 axe.

3.4.2 Topical miR-148b delivery enhances *in vivo* angiogenesis and wound repair

For this study, mouse wound healing model has been chosen for the *in vivo* experiments due to several practical reasons. Not only it is easily obtainable, but it also provides an accelerated model of healing, which can be easily managed and manipulated molecularly and genetically (Perez and Davis, 2008). In the context of this chapter, the mouse wound healing model is particularly useful due to the fact that it minimizes the systemic off-target effects of miRNA therapy due to the topical local delivery directly on the wounds. Specifically, due to the fact that miR-148b overexpression was able to induce *in vitro* angiogenesis, the mouse wound repair method provides a well visualizable model for *in vivo* angiogenic response that can be modulated by miRNA mimic delivery. For the purpose of this chapter, a Pluronic F-127 polymeric gel (Escobar-Chavez et al., 2006) is used as a delivery vehicle of miR-148b mimic and control oligonucleotides. Using this method, the data in this chapter demonstrates for the first time that the successful miR-148b mimics delivery on the wounds is able to target TGF-β pathway *in vivo* and

significantly enhance the dermal angiogenic response and accelerate the wound repair.

It is clear now that miRNA are becoming important modulators of wound healing process (Sen and Roy, 2008). Interestingly, in 2006 it has been reported that Dicer is expressed in mouse skin and is required for dermal morphogenesis (Andl et al., 2006). There is a significant number of miRNAs that are expressed in the skin, the most abundant being miR-200, miR-19/20 family and miR-199 (Yi et al., 2006). It is important to note that the wound repair process involves a number of stages: the inflammatory phase, the proliferation phase, which includes epithelisation, angiogenesis and granulation tissue formation, and remodelling phase characterized by the deposition of collagen that continues after wound closure. Specifically, within one hour of the injury the haemostasis process is taking place, which is characterized by clotting and vasoconstriction, acting simultaneously to prevent prolonged haemorrhage, followed by vasodilation phase that allows the migration of immune cells. After the first hour the inflammatory phase is initiated via migration of leukocytes to the wound site; it is characterized by phagocytosis of bacteria as well as wound debris and secretion of chemokines and cytokines, which attract fibroblasts and endothelial cells to the wound. Within one day of the injury the proliferative phase begins that can act up until one month post-injury. During this phase endothelial cells as well as fibroblast start to proliferate and secrete ECM accompanied by angiogenesis and granulation tissue formation. Finally, a remodelling stage is initiated by the contraction of the wound due to activation of myofibroblasts, followed by subsequent wound maturation lasting for months post-injury (Greaves et al., 2013).

Notably, each stage in the wound healing process is characterized by expression of different genes and is regulated by different sets of miRNAs (Banerjee et al., 2011). Examples of miRNAs regulating the inflammatory phase of wound healing are: miR-105 modulating the expression of Toll-like receptor 2 (*TLR2*) (Benakanakere et al., 2009) as well as miR-146a and miR-125b regulating TNF-α pathway (Sonkoly et al., 2008). The keratinocyte migration and proliferation during proliferation phase of wound healing is orchestrated by pro-migratory miR-205 and anti-proliferative miR-210 targeting *SHIP2* phosphatase (Yu et al., 2010) and transcription factor *E2F3* (Biswas et al., 2010), respectively. Moreover, recent study demonstrated that non-healing ulcers-associated miR-21 and miR-130a negatively regulate the granulation phase of the wound healing (Pastar et al., 2012)

However, there is not much known about miRNAs regulating angiogenic phase of wound healing. This chapter focused specifically on the angiogenic stage of the wound repair during the proliferation phase. MiR-148b was able to promote angiogenesis *in vitro* and in the wound, consistently, possibly by silencing the components of TGF-β pathway.

Interestingly, it has been demonstrated that reduction of the translation of TGF-β in human epidermal keratinocytes resulted in increased secretion of pro-angiogenic VEGF (Riedel et al., 2007). Taking together the data from this chapter, it is therefore possible to speculate that by decreasing the expression of *TGFB2* in the wound tissue, the keratinocytes become less subjected to TGF-β2 stimulus and thereby start to secrete more VEGF, that in turn upregulates endothelial cell proliferation and migration even more, creating a feed-forward positive loop of angiogenic response.

It is important to note that the findings in this chapter directly present the translational significance of the research carried out. The *in vitro* part of the investigation perfectly aligns with the mice study, sharing the same targets of miR-148b and the model of angiogenesis. Both the cellular angiogenic as well as mouse wound healing models prove that miR-148b is able to efficiently enhance angiogenesis and ultimately lead to the closure of the wounds, concluding the pre-clinical part of the study. One possible strategy for the clinical study would be to use miR-148b mimic delivery to enhance the closure of non-healing ulcers in diabetic patients. More work should be done at the *ex vivo* level to generate the proof-of-concept data that miR-148b topical delivery is able to induce wound closure in the skin from patients with diabetes. Importantly, this chapter provides a solid foundation for the initiation of human studies and opens up the avenue for possible therapeutic utilization of miR-148b.

3.4.3 Limitations

The main limitation of this chapter is the lack of direct link between *TGFB2* and *SMAD2* silencing by miR-148b and enhancement of angiogenesis. It is clear from the data that miR-148b also targets other strong anti-angiogenic genes, downregulation of which, together with *TGFB2* and *SMAD2*, could explain such a marginal pro-angiogenic effect of miR-148b.

3.4.4 Conclusion

This chapter introduces the novelty into the research field of miRNA, angiogenesis and wound healing. Specifically, the data in this chapter identifies a novel function of miR-148b to induce angiogenesis in endothelial cells *in vitro* and presents the evidence that *in vivo* topical delivery of miR-148b mimic in the mouse wound is able to facilitate faster wound closure and

perfusion via enhancing *in vivo* angiogenic response. This chapter also discusses a significance of these findings, particularly, in the setting of miRNA therapeutics and the possibility to use miR-148b as a potential therapeutic agent for wound treatment and tissue regeneration.

CHAPTER 4: THE EFFECT OF MIR-148B INHIBITION ON ENDOTHELIAL-TO-MESENCHYMAL TRANSITION

4.1 INTRODUCTION

Initially described as a passive barrier, the endothelium is now appreciated as a complex tissue with multiple functions, with endothelial cells acting as vascular transducers of physical and chemical stimuli within the circulation (Adams and Alitalo, 2007). It has been demonstrated numerously that endothelial cells exhibit high level of adaptation in response to external stimuli, as well as high plasticity which is an integral part of various developmental and pathological processes (Dejana et al., 2017). One type of plasticity is endothelial-to-mesenchymal transition (EndMT), which is a physiologically vital mechanism during development that can become pathological in the adult body. EndMT is characterized by the loss of endothelial-specific markers from the endothelial cells and the adaptation of a mesenchymal-like phenotype along with mesenchymal-specific molecular composition. In particular, vascular endothelial cadherin (VE-cadherin) and platelet-endothelial cell adhesion molecule 1 (PECAM-1, CD31) are being replaced by of α-SMA, vimentin, N-cadherin and extracellular matrix (ECM) proteins such as collagen type I and III (Piera-Velazquez and Jimenez, 2012). Moreover, cytoskeletal rearrangement is also observed in the cells enduring EndMT, which leads to a change in cell polarity giving them a stretched and more fibroblast-like morphology (Piera-Velazquez and Jimenez, 2012). The process of EndMT is vital during the embryonic stages of cardiac and pulmonary artery development (Arciniegas et al., 2005, Armstrong and Bischoff, 2004). However, the transition program is abnormal during post-natal stages leading to a number of disorders such as growth and progression of tumours (Zeisberg et al., 2007a), fibrosis of the heart (Zeisberg et al., 2007b) and renal systems (Zeisberg et al., 2008).

Accumulating studies over the past few years have also revealed that activation of TGF-β pathway regulates endothelial cell phenotypic plasticity and its activation can lead to EndMT induction (Dejana et al., 2017). It is also well known that TGF-β signalling pathway is a crucial regulator of both normal and irregular vascular function (Goumans and Ten Dijke, 2017). During canonical activation of TGF-β pathway, TGF-β binds to the heteromeric receptor complex formed by the activin-like kinase 5 (ALK5, also known as TGF-β type I receptor, TGF-βR1) and the TGFβ type II receptor (TGF-βR2). Phosphorylation of ALK5 by the kinase TGF-βR2, activates its catalytic domain, facilitating the induction of the receptor-regulated Smad proteins (i.e. SMAD2 and SMAD3), which then translocate to the nucleus. Finally, nuclear-localized Smads modulate the transcription of specific target genes (van Meeteren and ten Dijke, 2012).

MicroRNAs are characterized as post-transcriptional gene silencers, which interact with their complementary mRNA transcripts (Ha and Kim, 2014). Their capacity to simultaneously knock down the expression of number of different mRNAs leads to efficient amplification of biological responses (Li and Rana, 2014). Recent investigations have described the important roles of miRNAs as therapeutic agents in regulating either physiological or pathological angiogenesis, particularly through the regulation of endothelial cell function (reviewed in (Caporali and Emanueli, 2011, Caporali and Emanueli, 2012)).

Recently, a number of miRNAs have been identified as modulators of the elements of TGF-β/Smad signalling axis (Kurakula et al., 2015), and ultimately, as regulators of EndMT process (Ghosh et al., 2012a). Despite the fact that the role of TGF-β signalling in modulating endothelial cell homeostasis and plasticity is now well known (van Meeteren and ten Dijke, 2012), there is not

much evidence on the mechanisms regulating the molecular cascade. The rational for this chapter came from the bioinformatic analysis using the miRNA target prediction tools, where it was found that miR-148b target genes are strongly enriched for the components of TGF-β pathway. Moreover, the data in previous chapter has confirmed that miR-148b directly targets the expression of *TGFB2* and *SMAD2* genes, which both are key members of TGF-β signalling cascade as well as are potent inducers of EndMT. MiR-148b together with miR-148a and miR-152 comprise the miR-148/152 family (Chen et al., 2013). Abnormal expression of miR-148/152 family has been reported in tumours, but also in non-cancer diseases such as IgA nephropathy (Serino et al., 2012) and atherosclerotic lesions (Bidzhekov et al., 2012). Nevertheless, miR-148b has never been observed to modulate TGF-β pathway, nor to participate in EndMT.

4.1.1 Hypothesis

Taking in account the data generated from bioinformatic analysis as well as results from the previous chapter on miR-148b-specific regulation of *TGFB2* and *SMAD2*, the main goal of this chapter was to the hypothesis that:

"Downregulation of miR-148b induces TGF-β signalling and facilitates EndMT"

4.1.2 Aims

The aims of this chapter were:

1. Identify the effect of miR-148b inhibition on *TGFB2* and *SMAD2* expression

2. Determine whether miR-148b downregulation changes HUVEC proliferation, migration and cellular network formation *in vitro*

3. Determine if inhibition of miR-148b changes HUVEC morphology and/or induces EndMT *in vitro*

4. Investigate whether knockdown of miR-148b is able to induce EndMT *in vivo*

4.2 METHODS

4.2.1 Cells and Cell Culture

Human umbilical vein ECs (HUVECs; Lonza) were grown in EGM-2 (comprising EBM-2 with growth factors and other supplements) with 2% Foetal Bovine Serum.

4.2.2 miR-148b Target Analysis

Computational prediction of miR-148b target genes was done using published algorithm TargetScan (www.targetscan.org). miRpath v.3 (http://diana.imis.athena-innovation.gr/DianaTools/index.php?r=mirpath) was used to perform gene set enriched analysis of miR-148b target genes. The prediction is based on Targetscan parameters such as Context score and Conservation score.

4.2.3 RNA Extraction and Quantitative Real-Time Analysis

Total RNA was extracted using miReasy kit (Qiagen). Real-time quantification to measure miRNAs was performed with the TaqMan miRNA reverse transcription kit and miRNA assay (Life Technology) using Lightcycler 480 (Roche). MiRNAs expression was normalized to the U6 small nucleolar RNA (snRU6). For mRNA analysis, cDNA was amplified by quantitative real-time PCR (qPCR) and normalized to 18S ribosomal RNA. Each reaction was performed in triplicate. Quantification was performed by the 2–ddCt method. qPCR was used to measure the expression of miR-148b (miR-148b-3p Thermo Fisher Scientific, Cat. #4426961), snRU6 (Thermo Fisher Scientific, Cat. #4331182), TGFB2, SMAD2, CD31, VE-Cadherin, COL1A1 and 18S rRNA. Primers are pre-designed from Sigma (KiCqStartTM Primers).

4.2.4 Cells transfection, transduction and functional assays

Lipofectamine RNAiMAX (Thermo Fisher Scientific) was used to transfect HUVECs with LNA anti-miR-148b and LNA anti-miR control (75nM final concentration), according to the manufacturer's instructions. The following functional assays were performed: BrdU incorporation assay using Cell Proliferation colorimetric assay (Roche); migration assay and endothelial barrier function were performed using ECIS machine as described below. Matrigel assay with HUVECs was performed using BD Matrigel Basement Membrane Matrix (BD Biosciences).

4.2.5 ECIS Assays

Confluent HUVECs were transfected with LNA anti-miR-148b and LNA anti-miR control and plated on the ECIS chip array (8W1E or 8W10E). The migration speed was calculated in μm/h, distance from cells to chip surface in α (Ω0.5cm) and capacitance of the plasma membrane is Cm (μF/cm2).

4.2.6 Western-Blot analyses

Proteins were extracted from cultured cells or muscles by using ice-cold buffer A (50mM Hepes, 150mM NaCl, 1mM EDTA, 1mM EGTA, 25mM NaF, 5mM NaPPi, 1%Triton, 1% NP40, 1 mM Na3VO4, 0,25% sodium deoxycholate, 0.5mM Na-orthovanadate, 1 mM benzamidine, 0.1mM phenylmethylsulfonyl fluoride). Protein concentration was determined using the Bio-Rad Protein Assay Reagent (Bio-Rad Laboratories, UK). Detection of proteins by Western blot analyses was done following separation of whole cell extracts (20μg) on SDS-polyacrylamide gels. Proteins were transferred to nitrocellulose membranes and probed with the following antibodies: TGFβ2 (Abcam Ltd. ab36495, 1:1000), SMAD2 (SantaCruz Biotechnology, Santa Cruz, CA, USA;

#3102, 1:1000), CD31 (Abcam Ltd., 1:1000), VE-Cadherin (Abcam Ltd. ab33168, 1:1000), COL1A1 (Abcam Ltd., ab138492, 1:200), β-actin (Abcam Ltd., ab16039, 1:4000) HDAC3 (GeneTex GTX113303, 1:1000) and GAPDH (GeneTex, GT239, 1:1000) (used as loading control). For detection, we used secondary antibodies conjugated to horseradish peroxidase which were rabbit anti-mouse (Abcam Ltd., ab97046, 1:5000) and goat anti-rabbit (Abcam Ltd., ab6721, 1:10000). Detection was developed by chemiluminescence reaction (ECL) (Immunoblot, Millipore, 23225).

4.2.7 Immunofluorescence

Cells were fixed using 4% paraformaldehyde in PBS at room temperature for 15 min. For intracellular staining, fixed cells were permeabilized using 0.5% Triton X-100 in PBS (Sigma-Aldrich) or 0.1% Saponin in PBS at room temperature for 10 min. The blocking of specific antibody activity was performed using 3% bovine serum albumin (BSA) in PBS for 1 hour. Samples were incubated with antibodies to CD31 (Abcam Ltd., 1:50), VE-cadherin (Abcam Ltd. ab33168, 1:100) and COL1A1 (Abcam Ltd., ab138492, 1:100) in PBS containing 1% BSA at 4°C overnight. Samples were washed extensively with PBS and incubated with Alexa-Fluor-488-conjugated antibodies to rabbit IgG (Life Technologies, Carlsbad, CA, # A11070) and Alexa-Fluor-594-conjugated antibodies to rabbit IgG (Life Technologies, Carlsbad, CA, #A11072) in DAPI with PBS with 1% BSA at room temperature for 1 h. Image analysis was performed on Zeiss LSM 780 confocal microscope.

4.2.8 Animal experiments

All experiments involving mice were performed in accordance with the guidance and the operation of Animals (Scientific Procedures) Act 1986 and prior approval of the UK Home Office and the University of Edinburgh ethic

committee. CD-1 female mice (7–10 weeks old) were randomly assigned a treatment group and anaesthetized with isofluorane. Two full-thickness excisional wounds were made to the shaved dorsal skin. Full-thickness excisional wounds were made by picking up a fold of skin and using a sterile, disposable 5-mm biopsy punch (Kai Industries), resulting in generation of one wound on each side of the midline. Control oligonucleotides (scramble sequence), anti-miR-148b (1 μg/wound) and SMAD2 siRNA (1 μg/wound) were delivered topically by pipette into the wound cavity immediately after wounding and every two days (20μl in a vehicle of 30% Pluronic F-127 gel [is liquid at 4°C but solidifies at body temperature]; Sigma Aldrich). Wounds were photographed using an Olympus camera on days 0, 2, 4, 6, and 7 after wounding. To this aim, two perpendicular diameters of the wound were measured by using a Vernier caliper and wound area was calculated using a standard formula for the area of an ellipse (semi-major diameter X semi-minor diameter X Pi).

4.2.9 Histology

At days 5 or 7 post-wounding, wounds were harvested and fixed in 10% buffered formalin (16h at 4oC, Sigma) for embedding in paraffin. Sectioning was done through the wound beyond the midpoint and wound centres as identified by staining with Haematoxylin and Eosin (Sigma). Sections were deparaffinised, rehydrated and stained with rat anti-mouse polyclonal CD31 (Abcam, ab28364, 1:50) and Cy3-conjugated α-vascular smooth actin (Sigma) all antibodies overnight at 4oC.

4.2.10 Statistical analysis

Comparisons between different conditions were assessed using 2-tailed Student's t test. Differences among groups were elicited using ANOVA

statistical test followed by Bonferroni post-hoc analyses as appropriate. Continuous data are expressed as mean ± SD of three independent experiments, each performed in triplicate or quintuplicate. P value <0.05 was considered statistically significant. Analyses were performed using GraphPad Prism v5.0.

4.3 RESULTS

4.3.1 MiR-148b silencing unlocks the expression of on *TGFB2* and *SMAD2*

In order to downregulate miR-148b expression, HUVECs were transfected with LNA anti-miR-148b and LNA anti-miR control oligos for 6 days. As a result, the anti-miR-148b transfection decreased the expression of miR-148b (Fig. 4.1 a). MiR-148b downregulation resulted in increase in the expression of its target genes *TGFB2* and *SMAD2*, which was also confirmed by the western blot analysis (Fig. 4.1). Together, this data confirms that miR-148b knockdown is able to induce the components of TGF-β signalling pathway, *TGFB2* and *SMAD2*.

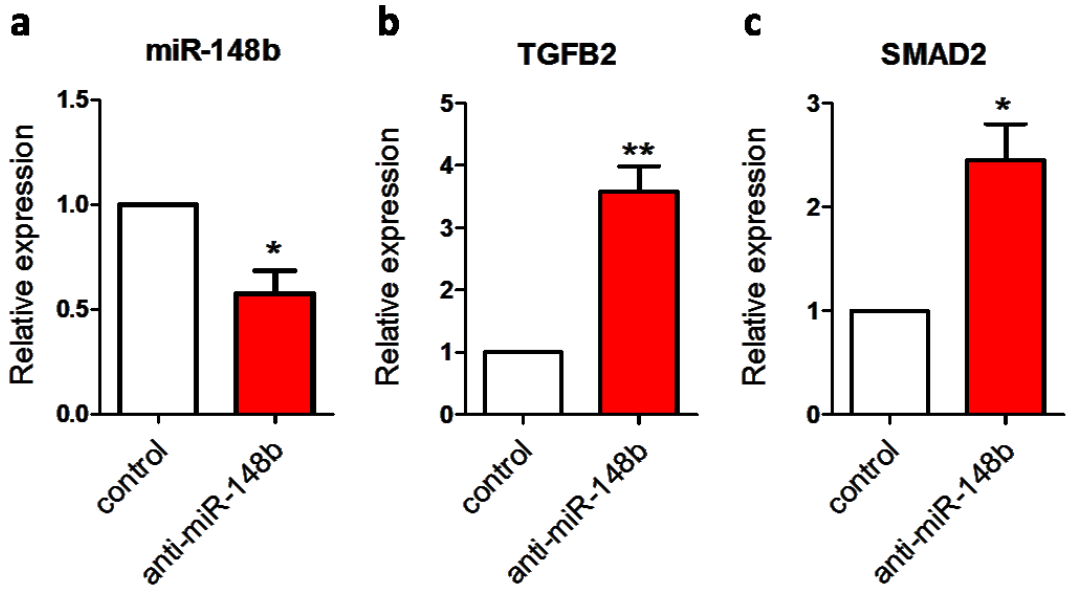

Figure 4.1| MiR-148b inhibition modulates the components of TGF-β signalling. a. qPCR showing miR-148b expression levels after anti-miR transfection; average Ct values: miR-148b (control: 28; anti-miR-148b: 29); **b**. qPCR showing relative gene expression of *TGFB2* and **c.** *SMAD2*, after miR-148b inhibition (n=3); average Ct values: *TGFB2* (control: 27; anti-miR-148b: 25), *SMAD2* (control: 24, anti-miR-148b: 21); HUVECs were transfected with LNA anti-miR-148b or LNA anti-miR control oligonucleotides for 6 days; For miRNA qPCR U6 was used as a house-keeping control; For target gene qPCR 18s was used as a house-keeping control;

Values are means±SEM *P<0.05; **P<0.01 vs control. Unpaired two-tailed Student's t-test was applied.

4.3.2 MiR-148b downregulation reduces HUVEC proliferation and increases membrane capacitance while having to effect on *in vitro* angiogenesis

Next, the downregulation of miR-148b expression was assessed in the context of regulating endothelial cell function. Firstly, the BrdU incorporation assay has demonstrated that HUVECs transfected with anti-miR-148b exhibit diminished cellular proliferation (Fig. 4.2 a). Interestingly, the inhibition of miR-148b expression had no effect on HUVEC migration (Fig. 4.2 b) and cellular network formation on Matrigel (Fig. 4.2 b). In order, to better understand the possible morphological change that miR-148b downregulation could have on HUVECs, the cells were subjected to a very high-sensitivity membrane capacitance (Cm) assay, changes in which reflect structural changes in the plasma membrane and rearrangement of the cytoskeleton (Giaever and Keese, 1991a). Strikingly, downregulation of miR-148b elevated membrane capacitance of HUVECs, which is reflects on the morphological change (Fig. 4.2 d). Overall, these results demonstrate that miR-148b inhibition causes the decrease in endothelial cell proliferation, has no effect on *in vitro* angiogenesis properties and leads to structural change reflected by increase in membrane capacitance.

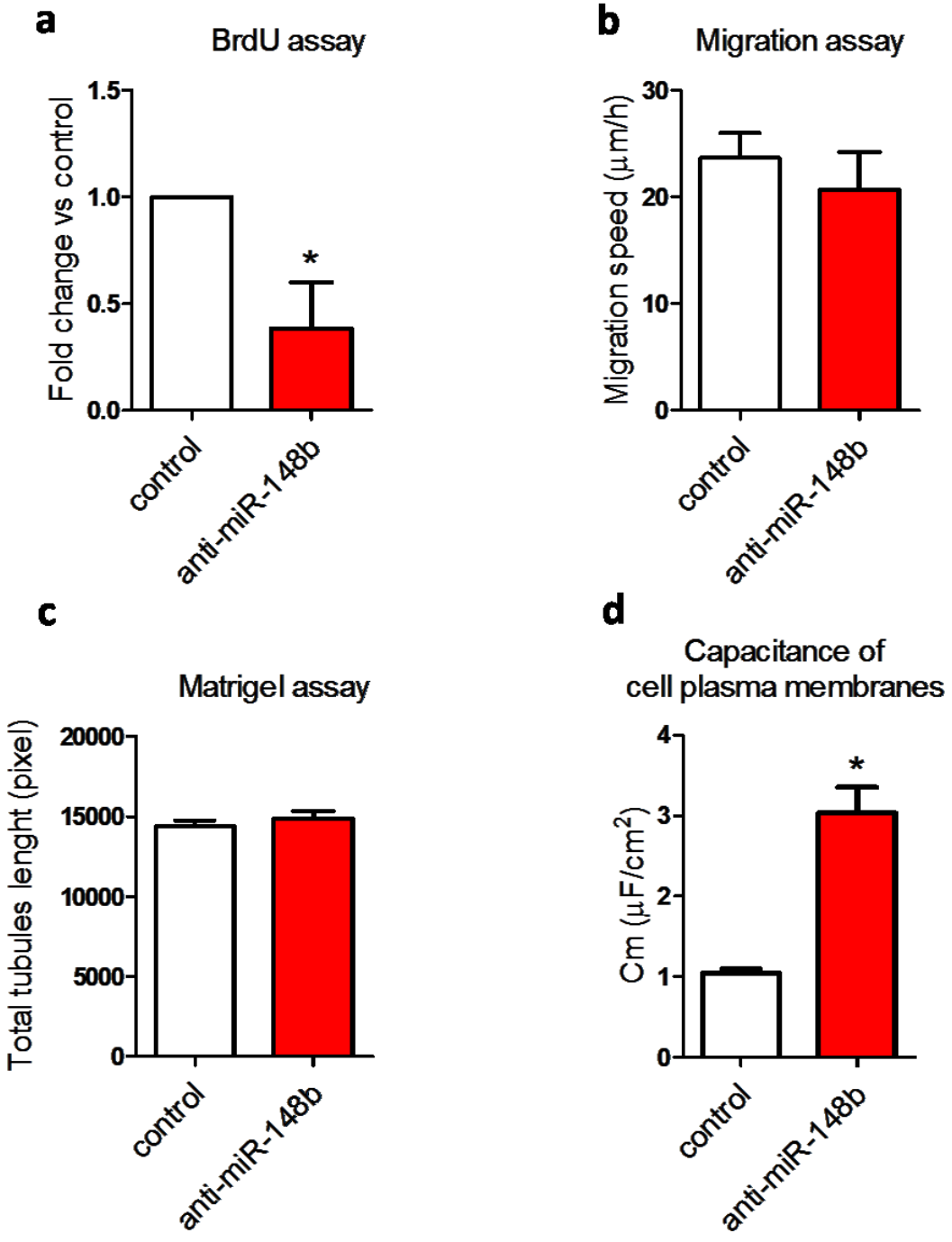

Figure 4.2| MiR-148b inhibition differentially modulates endothelial cell function and leads to the structural change of endothelial cells. a. EC proliferation was analyzed by BrdU incorporation assay and expressed as a fold change in absorbance (n=3); **b.** ECIS migration assay reported as migration speed on 8W2LE array (µm/h) (n=3); **c.** Matrigel assay quantification as total tubules length and expressed as pixel density (n=3); **d**. Quantification of cell membrane capacitance in HUVECs knock-down for miR-148b or control expressed as

μF/cm², 8W10E+ array was used (n=5); Values are means±SEM *P<0.05; **P<0.01 vs control. Unpaired two-tailed Student's t-test was applied.

4.3.3 MiR-148b inhibition promotes EndMT *in vitro*

Due to the fact that miR-148b downregulation increased cell membrane capacitance, and thus altered cellular structure, and enhanced TGF-β pathway, which is directly involved in EndMT, cells were analyzed for the expression of endothelial- and mesenchymal-specific markers. In particular, a significant decrease in gene expression of both endothelial markers, *CD31* and *VE-Cadherin*, was observed upon miR-148b downregulation (Fig. 4.3 a), further validated by reduction in the protein levels of both markers (Fig. 4.3 b). On the other hand, HUVEC exhibiting low miR-148b levels started to highly express pro-mesenchymal COL1A1 (Fig. 4.3 a, b). Furthermore, immunofluorescence staining revealed that control-treated HUVECs display a typically rounded/cobblestone morphology that was lost in anti-miR-148b treated cells. Anti-miR-148b treatment also resulted in a pronounced decrease in CD31 and VE-cadherin and increase in COL1A1 immunoreactivity (Fig. 4.3 c). Taken together, this data shows that loss of miR-148b function facilitates to EndMT program in endothelial cells.

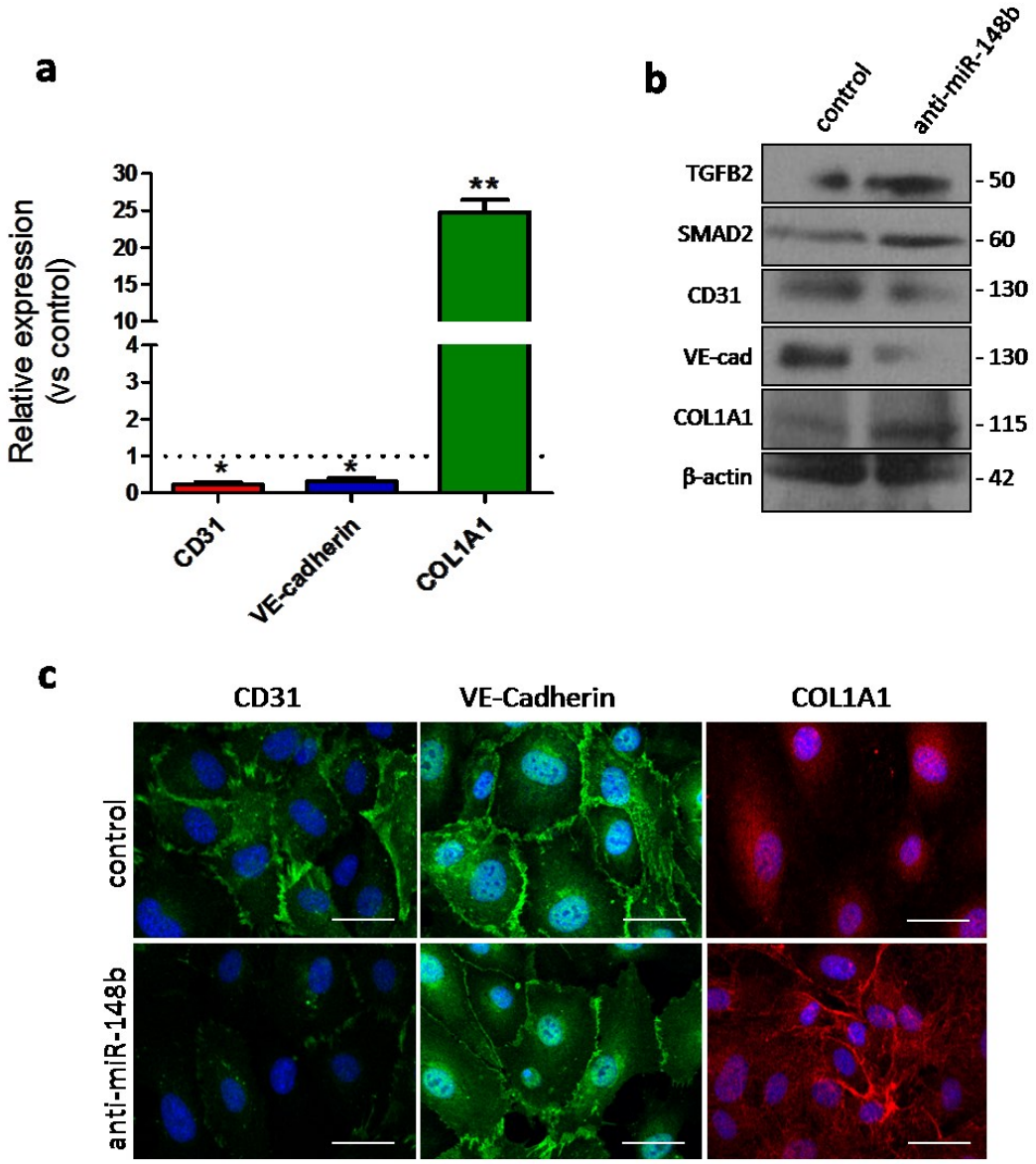

Figure 4.3| MiR-148b downregulation induces EndMT program. a. qPCR showing relative gene expression of *CD31*, *VE-Cadherin* and *COL1A1* after anti-miR-148b transfection; average Ct values: *CD31* (control: 21; anti-miR-148b: 22), *VE-Cadherin* (control: 20; anti-miR-148b: 22), *COL1A1* (control: 38; anti-miR-148: 34); the dotted line represents the relative gene expression in HUVECs transfected with control anti-miR (n=3); **b.** Western blot analysis of TGFB2 (antibody dilution 1:1000), SMAD2 (antibody dilution 1:1000), CD31 (antibody dilution 1:1000), VE-Cadherin (antibody dilution 1:1000) and COL1A1 (antibody dilution 1:200); β-actin is used as a loading control (1:4000) (n=3); **c.** Immunofluorescence images showing localization of CD31 (1:50), VE-Cadherin (1:100) and COL1A1 (1:100) in anti-miR-148b or control transfected cells (n=3); scale bar=50μm; For target gene qPCR 18s was used as a house-

keeping control; Values are means±SEM *P<0.05; **P<0.01 vs control. Unpaired two-tailed Student's t-test was applied.

4.3.4 *In vivo* inhibition of miR-148b induces EndMT in the wound and impairs wound closure

In order to understand whether miR-148b downregulation also induces EndMT *in vivo*, again a mouse model of wound healing has been employed. Specifically, a Pluronic gel was used as a delivery vehicle for the control and anti-miR-148b oligonucleotides onto the dermal wounds. Delivery of anti-miR-148b, or control oligonucleotides immediately after wounding, and every two days thereafter, resulted in increased expression of *TGFB2* and *SMAD2* target genes mRNA in the wounds (Fig. 4.4 a). Macroscopic analysis showed that wound closure was significantly attenuated in anti-miR-148b-treated wounds (Fig. 4.4 c, d). Nevertheless, inhibition of miR-148b did not have any effect on the wound perfusion as shown by Doppler analysis (Fig. 4.4 e). In order to test for the presence of EndMT in the wound edge, wounds were stained with CD31 and fibroblast-specific protein-1 (FSP-1) antibodies. Confocal analysis has demonstrated that, while control-oligonucleotide-treated wounds contained only CD31-positive vessels, the wounds treated with anti-miR-148b-treated were comprised of CD31-FSP-1 double-positive vessels, consistent with the occurrence of EndMT (Fig. 4.5 a, b). Furthermore, the delivery of anti-miR-148b has led to the strong increase in FSP-1 single-positive cells in the wounds (Fig. 4.5 c). Next, in order to confirm that loss-of-miR-148b-mediated EndMT occurs through TGF-β2-SMAD2 axis, a siRNA for *SMAD2* was used to silence *SMAD2* in the anti-miR-148b treated wounds. The resulting SMAD2 knockdown (Fig. 4.4 b) was able to rescue the anti-miR-148b-attenuated wound closure to the control level (Fig. 4.4 c, d) without changing the perfusion (Fig. 4.4 e). Moreover, silencing of *SMAD2* reduced the

percentage of vessels positive for both CD31 and FSP-1 and decreased the total number of FSP-1 positive cells in the wounds treated with anti-miR-148b (Fig. 4.5 a, b and c). Together, this data demonstrates that inhibition of miR-148b *in vivo* is able to attenuate wound healing and facilitate EndMT on the wound edge via *SMAD2* upregulation.

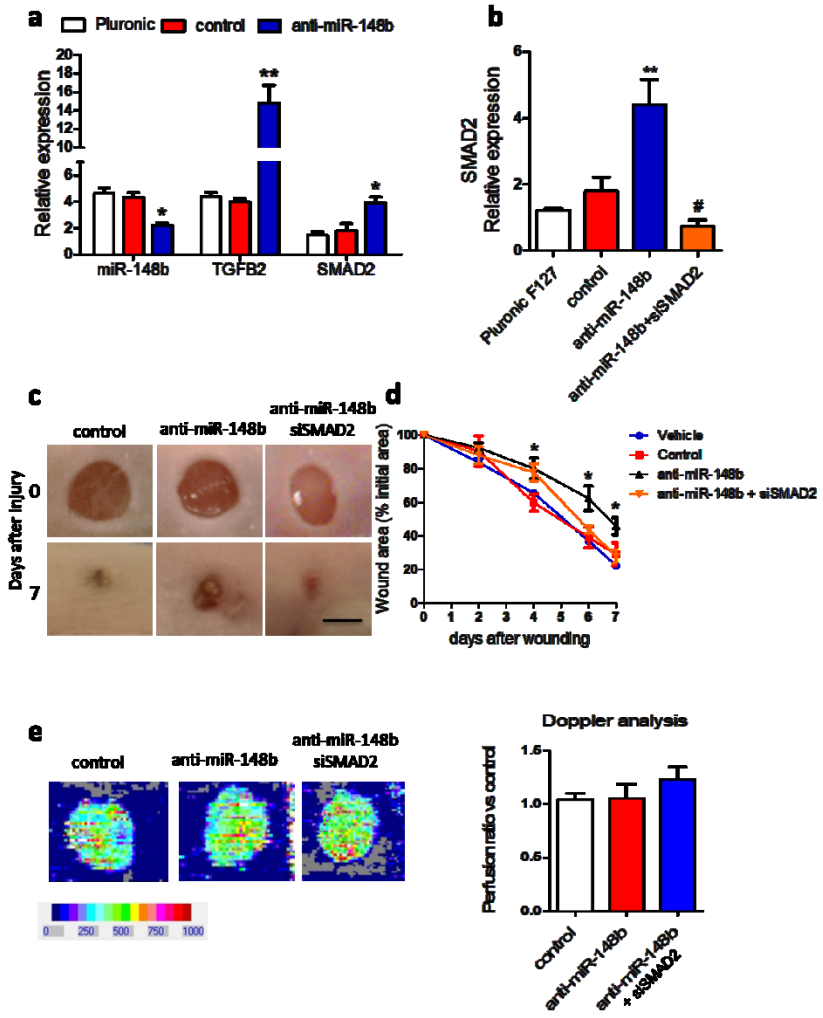

Figure 4.4| Inhibition of miR-148b delays wound closure and has no effect on perfusion. Dermal wounds were treated with control-oligonucleotides and anti-miR-148b or *SMAD2* siRNA for 7 days. **a.** qPCR showing relative expression of miR-148b, *TGFB2* and *SMAD2* (n=5); average Ct values: miR-148b (pluronic: 27; control: 28; anti-miR-148b: 30), *TGFB2* (pluronic: 25; control: 27; anti-miR-148b: 24), *SMAD2* (pluronic: 26; control: 27; anti-miR-148: 25) **b.** qPCR showing relative *SMAD2* expression in dermal wounds treated (n=5); average

Ct values: *SMAD2* (pluronic: 26; control: 27; anti-miR-148b: 25; anti-miR-148b+siSMAD2: 28) **c**. Representative images of treated wounds at 0 and 7 days post wound injury, scale bar=5mm; **d.** Level of wound closure expressed in percentage of wound area from the initial wound area (n=8); **e.** Representative colour laser Doppler images are taken at 5 days post wounds. Chart shows level of wounds perfusion in mice (calculated as the ratio between treated and control blood flow; n=8 per group). For miRNA qPCR U6 was used as a house-keeping control; For target gene qPCR 18s was used as a house-keeping control; Values are means±SEM. *P<0.05; **P<0.01 vs control; #P<0.05 vs anti-miR-148b. Unpaired two-tailed Student's t-test and one-way ANOVA statistical test followed by Bonferroni post-hoc analyses were applied.

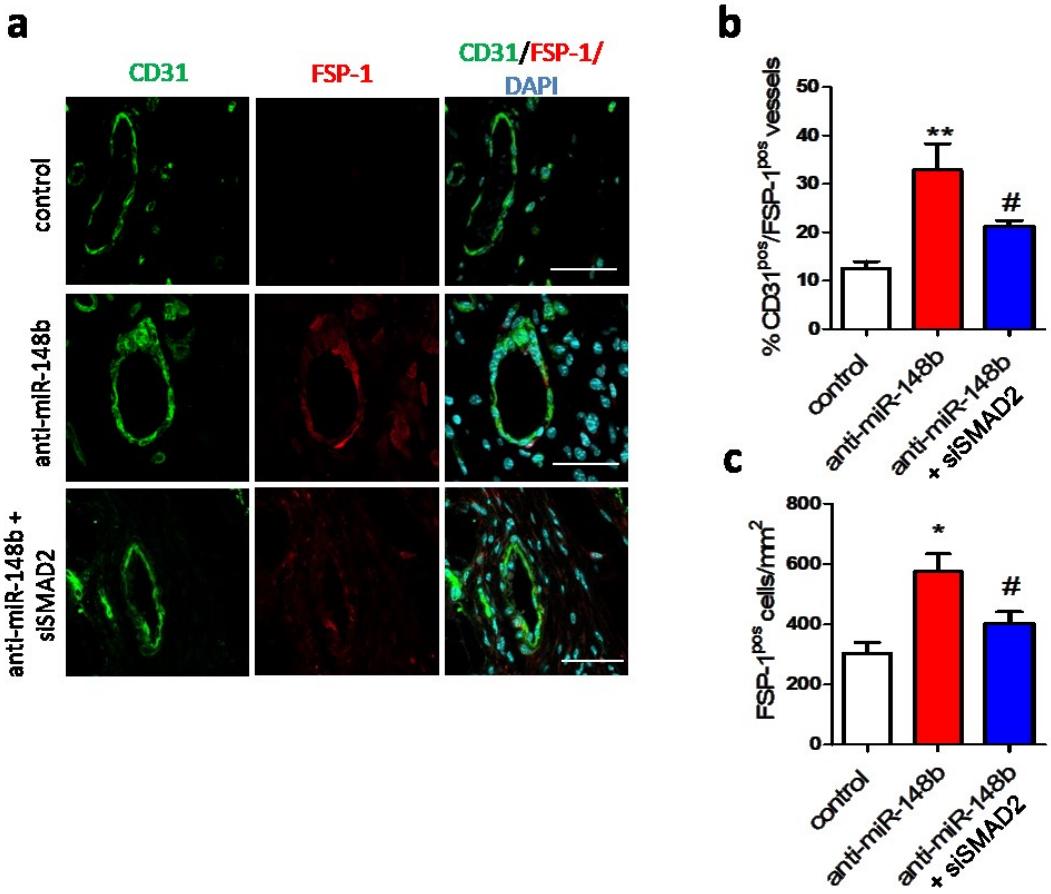

Figure 4.5| Inhibition of miR-148b induces EndMT in a mouse model of wound healing. Dermal wounds were treated with control-oligonucleotides and anti-miR-148b or *SMAD2* siRNA for 7 days. **a.** Immunohistochemistry localization of CD31 (1:50) and FSP-1 (1:50) in the wound vessels; scale bar=25μm (magnification 630x) (n=8); **b**. Quantification of

CD31/FSP-1 double positive vessels and **c.** FSP-1 positive vessels in the wounds; n=8 per each group; Values are means±SEM. *P<0.05; **P<0.01 vs control. #P<0.05 vs anti-miR-148b Unpaired two-tailed Student's t-test and one-way ANOVA statistical test followed by Bonferroni post-hoc analyses were applied.

4.4 DISCUSSION

The data presented in this chapter shows for the first time that downregulation of miR-148b is able to affect endothelial cell plasticity. Specifically, this chapter provides novel evidence that miR-148b inhibition upregulates the expression of *TGFB2* and *SMAD2* genes, thus activating TGF-β signalling cascade and leading to EndMT program. Finally, these findings provide the evidence that *in vivo* silencing of miR-148b expression causes poor wound repair in mice due to induction of EndMT.

4.4.1 MiR-148b inhibition promotes EndMT on the cellular level while having no effect on *in vitro* angiogenesis

Based on the data from the previous chapter, where it has been demonstrated that miR-148b overexpression boosts endothelial cell proliferation the *in vitro* angiogenic response, it was expected that inhibition of miR-148b would attenuate angiogenesis *in vitro*. Nevertheless, the findings in this chapter showed that miR-148b knockdown is sufficient to decrease endothelial cell proliferation without affecting endothelial cell migration and cellular network formation. Notably, this data separates miR-148b effect on cellular proliferation and angiogenic response, which occurred simultaneously in the previous chapter. To elucidate the effect of miR-148b inhibition on the cellular level, an ECIS model has been employed, which is able to pick up sensitive changes in cellular electrical impedance parameters (Giaever and Keese, 1991b). The use of ECIS model in endothelial cells has been described before and changes in impedance have been attributed to the endothelial function and morphology (Szulcek et al., 2014). After applying this model to the cells transfected with anti-miR-148b, it was found that one of the impedance parameters, cell membrane capacitance (Cm), was significantly increased.

Based on the fact that different cell types exhibit different values of Cm (Giaever and Keese, 1991b), it has been concluded that miR-148b downregulation exerts a phenotypic change on HUVECs. Interestingly, it has been recently reported that increase in cell membrane capacitance occurs during cellular differentiation (Qi et al., 2015).

Furthermore, miR-148b silencing upregulated its target genes, *TGFB2* and *SMAD2*, which are central components of TGF-β signalling cascade. Activation of this pathway has been numerously reporter to play a key role in inducing EndMT program (Dejana et al., 2017). Together with increase in membrane capacitance, activation of TGF-β signalling, reduction of endothelial-specific markers, CD31 and VE-Cadherin and upregulation of fibroblast-specific COL1A1, this chapter demonstrates for the first time that miR-148b downregulation promotes EndMT program.

Interestingly, since Ghosh et al. has reported the first evidence of miRNA involvement in EndMT (Ghosh et al., 2012b), miRNAs are now known to modulate EndMT through different mechanisms. *In vitro* and *in vivo* studies demonstrated that decreased FGF signalling leads to reduction in *let-7* expression and initiation of TGF-β-dependent EndMT (Chen et al., 2012). Recently, miR-20a was shown to target multiple genes in TGF-β signalling such as *ALK5*, *TGFBR2* and *SARA*, thereby negatively regulating EndMT. The expression of miR-20a, which is normally downregulated during EndMT, is rescued by FGF2 (Correia et al., 2016). The study also specifies that miR-20a regulates EndMT on the receptor level. On the other hand, this chapter shows that miR-148b modulates the transition program on receptor (targeting *TGFB2*) and signal transduction levels (targeting *SMAD2*). Contrary to the previous studies, Kumarswamy et al. showed that miR-21 upregulation in response to TGF-β2 treatment is able to induce EndMT via silencing

phosphatase and tensin homolog (*PTEN*) in endothelial cells, resulting in activation of the Akt-pathway (Kumarswamy et al., 2012). Opposite to the results from this chapter, downregulation of miR-21 leads to inhibition of EndMT and partial restoration of pro-endothelial phenotype, which is a consequence of *PTEN* upregulation and reduction in Akt signalling. In agreement with this study, a recent investigation reported that TGF-β-induced miR-27b overexpression causes EndMT via silencing *Elk1* in mouse pancreatic microvascular endothelial cells. Interestingly, it was also found that one of miR-27b target genes is *VAV3*, a regulator of actin remodeling, which is also modulated by another EndMT-promoting miRNA, miR-31, suggesting a potential combinatorial regulation (Suzuki et al., 2017). This important point is also true in the context of this chapter as *SMAD2* is also a target of EndMT-facilitating miR-20a, which could potentially act in a synergic manner with miR-148b.

Up until now, here has been no scientific evidence to date discussing the role of miR-148b in endothelial cell plasticity and EndMT. The data in this chapter provides novel evidence on a new regulatory player in induction of EndMT program *in vitro*. Together with other miRNAs such as *let-7*, miR-20a and others, miR-148b may constitute a larger post-transcriptional regulatory network modulating endothelial cell plasticity.

4.4.2 MiR-148b inhibition attenuates wound repair by inducing EndMT in mice wounds

Due to the successful utilization of mouse wound healing angiogenesis model in the previous chapter, the same approach was used in this chapter. As previously described, the Pluronic gel delivery system is sufficient to deliver

anti-miR-148b oligos in mouse wounds, thus leading to poor wound closure and induction of EndMT program.

The occurrence of EndMT postnatally has been associated with different types of fibrotic disease such as that in kidney (Zeisberg et al., 2008) and heart (Zeisberg et al., 2007c), both of which are associated with excessive collagen expression and deposition. Previous studies reported the importance of EndMT in dermal fibrosis, showing that delay in wound closure is associated with excessive collagen deposition (Manetti et al., 2017a).

This chapter has demonstrated for the first time that induction of EndMT in response to miR-148b downregulation has a detrimental influence on skin wound healing. Following delivery of anti-miR-148b to the wounds, EndMT accounted for around 20% of skin vessels that were undergoing mesenchymal transition. This is highly important as cells going through transition program can be expected to secrete large amounts of collagen and other ECM proteins, which could contribute to fibrosis. In addition, the acquisition of mesenchymal phenotype by the dermal endothelial cells is likely to lead to endothelial dysfunction, seen through decreased cellular migration or dysregulation of inflammatory cell recruitment. The data in this chapter also elucidates the mechanism of EndMT induction in the current model, which is mainly based on activation of *SMAD2* as demonstrated by the reduction of EndMT *in vivo* using siRNA for *SMAD2*.

Interestingly, the downregulation of miR-148b did not affect wound perfusion, which is supported by *in vitro* data showing that miR-148b inhibition does not attenuate angiogenesis. The uninvolvement of angiogenesis further confirms that the impairment of wound repair is a result of endothelial cells switching to mesenchymal cell lineage. The argument that

wound healing is attenuated due to possible excess of collagen deposition following EndMT induction in the wounds is supported by findings that fibrosis and TGF-β pathway activation are central causes of the pathology of scleroderma (Varga, 2002a), which is a disorder characterized by thickened skin and poor wound healing (Moran, 2014). Due to the fact that not only does miR-148b inhibition activate TGF-β pathway *in vivo*, but also leads to wound repair impairment and EndMT, it is therefore plausible to speculate that miR-148b downregulation could play role in the pathology of scleroderma. It has been recently demonstrated that it is possible to treat scleroderma using miRNA therapy approach. In particular, a topical antagomir approach has been utilized to downregulate miR-155 levels in mice, which resulted in decreased fibrosis, skin thickening and activated fibroblasts, which are the hallmarks of scleroderma (Yan et al., 2016). Furthermore, it has been shown before that TGF-β pathway is upregulated in skin scars (Xie et al., 2008, Scott et al., 1995, Wang et al., 2000), which are also characterized by increased deposition of ECM proteins (Gauglitz et al., 2011). In line with similarities with the model of wound healing in this chapter it is possible to speculate that decreased levels of miR-148b could be a characteristic of scarring, due to its effects on TGF-β cascade upregulation and poor wound repair. Moreover, it has been demonstrated that by diminishing TGF-β signalling using antisense oligonucleotide approach it is possible to decrease the scarring in the adult wounds (Choi et al., 1996). Combining the data from both chapters it is logical to assume that topical modulation of miR-148b in the skin could revert the detrimental scarring.

Overall, the data presented in this chapter supports the involvement of miR-148b in skin wound healing and induction of EndMT *in vivo*. These findings

also open up new avenues for miR-148b-based therapies for disorders such as scleroderma and scarring.

4.4.3 Limitations

One limitation of this chapter is a technical challenge in quantifying the secreted COL1A1 due to the fact that it is insoluble. This data would be a good indication of the fibrotic potential of anti-miR-148b. Another limitation is inability of the *in vivo* model to detect the cells which have completely lost the endothelial phenotype and became mesenchymal. The lineage (endothelial) tracing mice would be able to solve this challenge.

4.4.4 Conclusion

The chapter provides new data on the molecular mechanism of EndMT, linking it's induction to the previously unreported miR-148b in endothelial cell biology. In particular, the results presented in this chapter elucidate the important function of miR-148b on the differentiation of endothelial cells, where its downregulation can lead to the mesenchymal switch, governed by upregulation of *TGFB2* and *SMAD2* expression. The induction of EndMT *in vivo* and its detrimental effect on wound healing process further confirms the importance of miR-148b in endothelial cell biology and vascular homeostasis.

CHAPTER 5: THE EFFECT OF MIR-148B ON INFLAMMATION-INDUCED ENDOTHELIAL-TO-MESENCHYMAL TRANSITION

5.1 INTRODUCTION

Endothelial-to-mesenchymal transition (EndMT) is a process by which endothelial cells (ECs) significantly lose endothelial features and gain mesenchymal fibroblast-like phenotype, which is characterized by elevated expression of α-SMA, vimentin, N-cadherin and acquisition of "spindle-shaped" cellular morphology due to cytoskeleton rearrangement (Medici and Kalluri, 2012). In addition to its important role during embryogenesis, such as cardiac and pulmonary artery development (Armstrong and Bischoff, 2004, Arciniegas et al., 2005), EndMT also occurs in adult organism in response to pathological stimuli, such as inflammation, leading to pathologies such as cardiac (Zeisberg et al., 2007b) and renal fibrosis (Zeisberg et al., 2008), vascular remodelling (Cooley et al., 2014) and atherosclerosis (Evrard et al., 2016).

Inflammation is maintained by specific plasma molecules, mediators of inflammation, which act as propagators of the inflammatory response by local as well as systemic action. Inflammatory mediators largely consist of pro-inflammatory cytokines, such as interleukin-1 beta (IL-1b) and tumor necrosis factor alpha (TNF-a), growth factors, reactive oxygen species (ROS) as well as bacterial endotoxins. Importantly, it has been demonstrated that mediators of inflammation are able to induce endothelial cell differentiation into activated fibroblasts, thus linking inflammation to EndMT (Pérez et al., 2017). Data reported in the mid-1980s showed that human umbilical vein endothelial cells (HUVECs), cultured in the activated peripheral blood mononuclear leukocyte supernatants, underwent morphological changes, producing mesenchymal-like morphology instead of the typical endothelial cobblestone appearance (Montesano et al., 1984). It is believed that inflammatory cytokines induce

EndMT program in endothelial cells via activation of NF-κB transcription factor, however the precise mechanism is still not understood.

Non-coding microRNAs are post-transcriptional repressors of gene expression and are often dysregulated in pathological processes (Quiat and Olson, 2013). MiRNAs are able to exert diverse functions on endothelial cells, including the regulation of proliferation, migration and *in vitro* angiogenesis (Wu et al., 2009). Moreover, recent studies on endothelial cell plasticity have shown that miRNAs can also play a key role in the modulation of EndMT (Chen et al., 2012, Cao et al., 2014). Interestingly, Chen et al. has demonstrated that inflammatory cytokines are able to induce the EndMT program in HUVECs via indirect reduction of *let-7* miRNA expression and activation of the TGF-β signalling (Chen et al., 2012).

In the previous chapter it has been found that miR-148b holds the capacity to modulate TGF-β signalling and its downregulation leads to the induction of EndMT. Due to the profound phenotypic effect of miR-148b on endothelial cell function and phenotype the following chapter will focus on the mechanism of regulation of miR-148b expression.

5.1.1 Hypothesis

In light of the findings from the previous chapter on induction of TGF-β signalling and EndMT in response of miR-148b downregulation and the published literature stating that inflammation is a link between two processes, the main goal of this chapter was to the hypothesis that:

"Pro-inflammatory cytokines induce EndMT via modulation of miR-148b expression"

5.1.2 Aims

The aims of this chapter were:

1. Identify pro-inflammatory stimuli regulating miR-148b expression

2. Determine whether induction of inflammation can facilitate EndMT

3. Determine whether exogenous modulation of miR-148b expression can alter the effect of inflammation on endothelial cells

5.2 METHODS

5.2.1 Cells and Cell Culture

Human umbilical vein ECs (HUVECs; Lonza) were grown in EGM-2 (comprising EBM-2 with growth factors and other supplements) with 2% Foetal Bovine Serum. Confluent HUVECs were treated with 10 ng/ml TNF-α, IL-1β, TGF-β2 (PeproTech); medium and cytokines were changed every two days. SB 431542 (Tocris) has been used at the dose of 10μM.

5.2.2 Cells transfection, transduction and functional assays

Lipofectamine RNAiMAX (Thermo Fisher Scientific) was used to transfect HUVECs treated with TNF-α/IL-1β with miR-148b mimic, mimic control (25nM final concentration), siRNA SMAD2 and siRNA control (10nm final concentration) according to the manufacturer's instructions.

5.2.3 RNA Extraction and Quantitative Real-Time Analysis

Total RNA was extracted using miReasy kit (Qiagen). Real-time quantification to measure miRNAs was performed with the TaqMan miRNA reverse transcription kit and miRNA assay (Life Technology) using Lightcycler 480 (Roche). MiRNAs expression was normalized to the U6 small nucleolar RNA (snRU6). For mRNA analysis, cDNA was amplified by quantitative real-time PCR (qPCR) and normalized to 18S ribosomal RNA. Each reaction was performed in triplicate. Quantification was performed by the 2–ddCt method. qPCR was used to measure the expression of miR-148b (miR-148b-3p Thermo Fisher Scientific, Cat. #4426961), snRU6 (Thermo Fisher Scientific, Cat. #4331182), TGFB2, SMAD2, CD31, VE-Cadherin, COL1A1 and 18S rRNA. Primers are pre-designed from Sigma (KiCqStartTM Primers).

5.2.4 Western-Blot analyses

Proteins were extracted from cultured cells or muscles by using ice-cold buffer A (50mM Hepes, 150mM NaCl, 1mM EDTA, 1mM EGTA, 25mM NaF, 5mM NaPPi, 1%Triton, 1% NP40, 1 mM Na3VO4, 0,25% sodium deoxycholate, 0.5mM Na-orthovanadate, 1 mM benzamidine, 0.1mM phenylmethylsulfonyl fluoride). Protein concentration was determined using the Bio-Rad Protein Assay Reagent (Bio-Rad Laboratories, UK). Detection of proteins by Western blot analyses was done following separation of whole cell extracts (20μg) on SDS-polyacrylamide gels. Proteins were transferred to nitrocellulose membranes and probed with the following antibodies: TGFβ2 (Abcam Ltd. ab36495, 1:1000), SMAD2 (SantaCruz Biotechnology, Santa Cruz, CA, USA; #3102, 1:1000), CD31 (Abcam Ltd., 1:1000), VE-Cadherin (Abcam Ltd. ab33168, 1:1000), COL1A1 (Abcam Ltd., ab138492, 1:200), β-actin (Abcam Ltd., ab16039, 1:4000) (used as loading control). For detection, we used secondary antibodies conjugated to horseradish peroxidase which were rabbit anti-mouse (Abcam Ltd., ab97046, 1:5000) and goat anti-rabbit (Abcam Ltd., ab6721, 1:10000). Detection was developed by chemiluminescence reaction (ECL) (Immunoblot, Millipore, 23225).

5.2.5 Immunofluorescence

Cells were fixed using 4% paraformaldehyde in PBS at room temperature for 15 min. For intracellular staining, fixed cells were permeabilized using 0.5% Triton X-100 in PBS (Sigma-Aldrich) or 0.1% Saponin in PBS at room temperature for 10 min. The blocking of specific antibody activity was performed using 3% bovine serum albumin (BSA) in PBS for 1 hour. Samples were incubated with antibodies to CD31 (Abcam Ltd., 1:50), VE-cadherin (Abcam Ltd. ab33168, 1:100) and COL1A1 (Abcam Ltd., ab138492, 1:100) in

PBS containing 1% BSA at 4°C overnight. Samples were washed extensively with PBS and incubated with Alexa-Fluor-488-conjugated antibodies to rabbit IgG (Life Technologies, Carlsbad, CA, # A11070) and Alexa-Fluor-594-conjugated antibodies to rabbit IgG (Life Technologies, Carlsbad, CA, #A11072) in DAPI with PBS with 1% BSA at room temperature for 1 h. Image analysis was performed on Zeiss LSM 780 confocal microscope.

5.2.6 ELISA assay

Cell culture medium collected from HUVECs stimulated with TNF-α and IL-1β 6 days after stimulation. Then, the culture medium medium was collected and a commercially available sandwich ELISA kit (R&D Systems #DB250) was used to measure the secretion of TGF-β2 in the medium. The absorbance (450 nm) for each sample was analyzed by a microplate reader Infinite® M1000 PRO (Tecan) and was interpolated with a standard curve.

5.2.7 Statistical analysis

Comparisons between different conditions were assessed using 2-tailed Student's t test. Differences among groups were elicited using ANOVA statistical test followed by Bonferroni post-hoc analyses as appropriate. Continuous data are expressed as mean ± SD of three independent experiments, each performed in triplicate or quintuplicate. P value <0.05 was considered statistically significant. Analyses were performed using GraphPad Prism v5.0.

5.3 RESULTS

5.3.1 Combination of TNF-α, IL-1β reduce miR-148b expression *in vitro*

In order to investigate whether cytokine treatment is able to affect the expression of miR-148b, HUVECs were treated for 6 days with the following cytokines: TNF-α, IL-1β, TGF-β1, TGF-β2 and a combination of TNF-α/IL-1β. The single delivery of cytokines did not exert any significant effects on miR-148b expression (Fig. 5.1 a-d). Interestingly, the combination of TNF-α and IL-1β pro-inflammatory cytokines has led to the inhibition of miR-148b expression 3 days post-treatment with the sharpest decrease after 6 days (Fig. 5.1 e). This data shows that only the simultaneous stimulation of HUVECs with TNF-α and IL-1β leads to reduction in miR-148b expression after 3 days post-treatment.

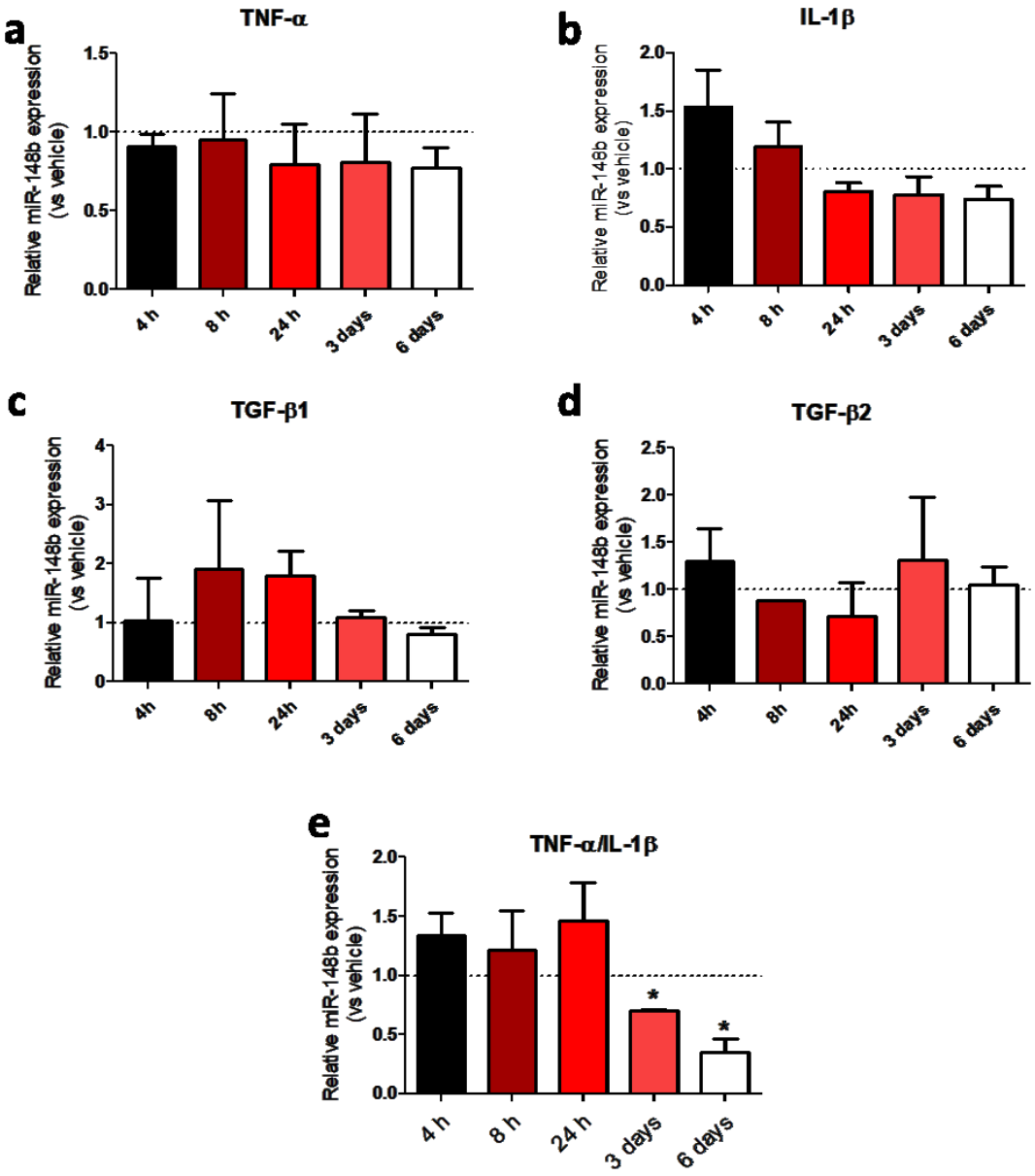

Figure 5.1| The combination of pro-inflammatory cytokines downregulates the expression of miR-148b. qPCR showing relative miR-148b expression after treatment of HUVECs with 10 ng/ml of: **a.** TNF-α (average Ct values of all time points 28); **b.** IL-1β (average Ct values of time points 28 (4-8h) and 29 (24h-6 days)); **c.** TGF-β1 (average Ct values of 4h, 3 days and 6 days 32, 8 h-24 h - 31); **d.** TGF-β2 (average Ct values of all time points 31) and **e.** TNF-α/ IL-1β (average Ct values of 4-24 h – 30; 3 days: 31; 6 days: 32) for 6 days; the dotted line represents relative miR-148b expression in vehicle treated HUVECs (n=3): U6 was used as a house-keeping control in the qPCR; Values are means±SEM *P<0.05 vs control. Unpaired two-tailed Student's t-test was applied.

5.3.2 TNF-α/IL-1β-induced inflammation promotes EndMT

To test if inflammation, induced by the combination of TNF-α and IL-1β, is able to promote EndMT, stimulated HUVECs were analysed for the panel of transition markers employed in the previous chapter. Specifically, the expression of *TGFB2* and *SMAD2*, which are also miR-148b targets, was significantly increased at mRNA and protein levels, accompanied by the increase in TGF-β2 secretion (Fig. 5.2 a-c). Notably, the level of phosphorylated SMAD2 (p-SMAD2), which represent the activated variant of the protein, increased markedly following cytokine stimulation (Fig. 5.2 b). Moreover, consistent with an induction of EndMT, both mRNA and protein expression of the endothelial-specific markers, CD31 and VE-Cadherin, were decreased after cytokines stimulation, while COL1A1 was markedly elevated (Fig 5.2 a, b). These findings were further confirmed by immunofluorescence staining of HUVECs showing the reduction in CD31 and VE-Cadherin and increase in COL1A1 immunoreactivity (Fig. 5.2 d). Together, this data demonstrates that chronic inflammation facilitated by TNF-α/IL-1β stimulation induces EndMT.

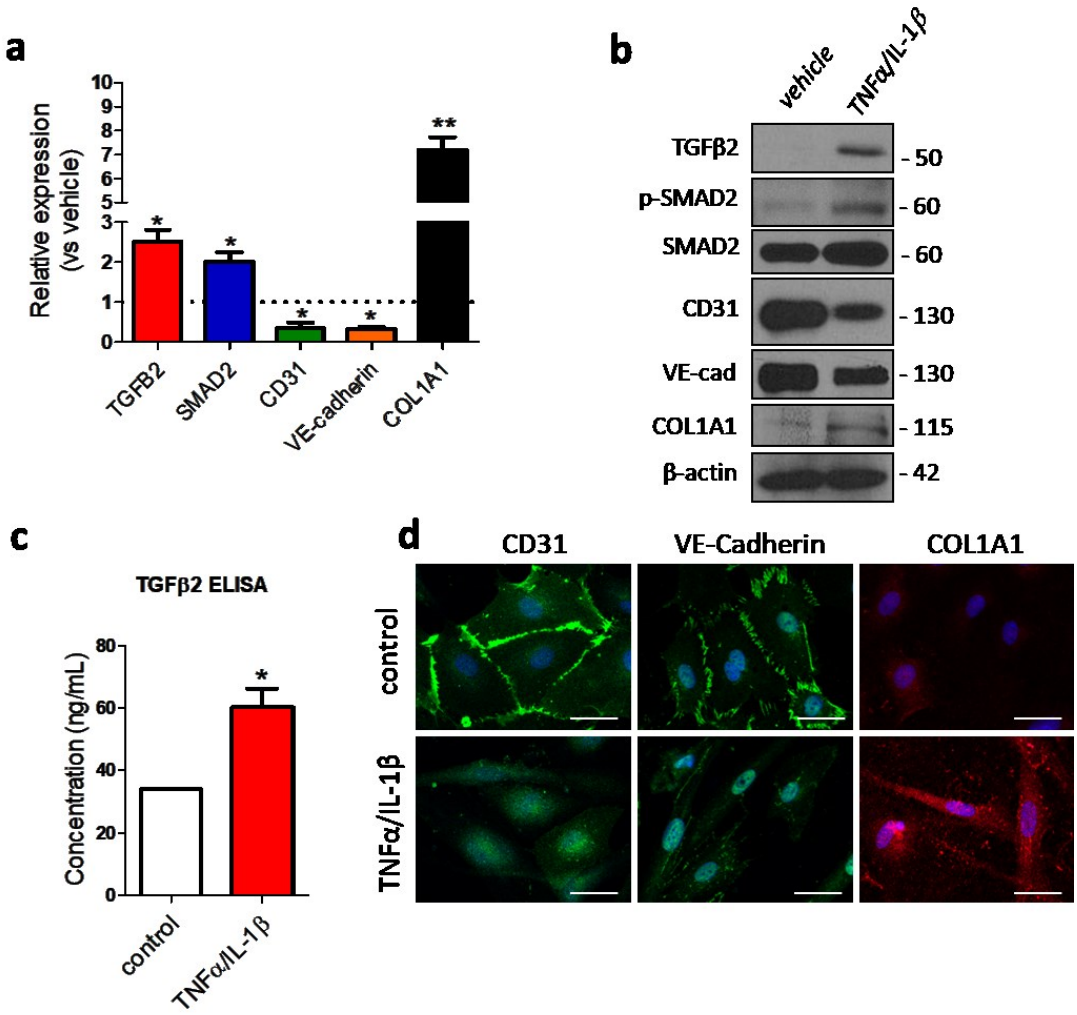

Figure 5.2| Chronic inflammation induces EndMT *in vitro*. HUVECs were stimulated with a combination of TNF-α and IL-1β for 6 days. **a.** qPCR showing relative expression of *TGFB2* (average Ct: vehicle: 27; TNF-α/IL-1β: 25), *SMAD2* (average Ct: vehicle: 27; TNF-α/IL-1β: 26), *CD31* (average Ct: vehicle: 22; TNF-α/IL-1β: 24), *VE-cadherin* (average Ct: vehicle: 23; TNF-α/IL-1β: 24) and *COL1A1* (average Ct: vehicle: 37; TNF-α/IL-1β: 40); the dotted line represents the relative gene expression in vehicle treated HUVECs (n=3); **b.** Western blot analysis of TGFB2, p-SMAD2, SMAD2, CD31, VE-Cadherin and COL1A1; β-actin was used as a loading control; **c.** Quantification of TGF-β2 ELISA experiment expressed in TGF-β2 concentration (ng/mL) in TNF-α/IL-1β treated samples vs the control; **d.** Immunofluorescence images showing localization of CD31 (1:50), VE-Cadherin (1:100) and COL1A1 (1:100) in TNF-α/IL-1β treated cells; scale bar=50μm (magnification 40x); 18s was used as a house-keeping control in the qPCR; Values are means±SEM. *P<0.05; **P<0.01 vs vehicle. Unpaired two-tailed Student's t-test was applied.

5.3.3 MiR-148b gain-of-function inhibits EndMT and maintains endothelial phenotype after cytokine treatment

The next question to address was whether exogenous overexpression of miR-148b could preserve the endothelial phenotype of HUVECs and attenuate EndMT induced by inflammation. To do that, HUVECs were simultaneously transfected with miR-148b mimic and stimulated with TNF-α and IL-1β. Firstly, a strong increase in miR-148b levels was observed in cells with miR-148b gain-of-function (Fig. 5.3 a) in collaboration with decrease in its targets, *TGFB2* and *SMAD2*, which were elevated in response to inflammation (Fig. 5.3 a, b). Importantly, miR-148b gain-of-function was sufficient to block SMAD2 phosphorylation (Fig. 5.3 b), thus preventing the activation of pro-EndMT signalling. The secretion of TGF-β2 was also markedly attenuated by the cells transfected with miR-148b mimic (Fig. 5.3 c). Importantly, miR-148b gain-of-function was sufficient to rescue the endothelial phenotype of HUVECs, as shown by the increased CD31 and VE-Cadherin and reduced COL1A1 expression and immunofluorescence signals (Fig. 5.3 a, b, d). Together, these findings demonstrate that miR-148b overexpression in the HUVEC model of chronic inflammation leads to the inhibition of EndMT program.

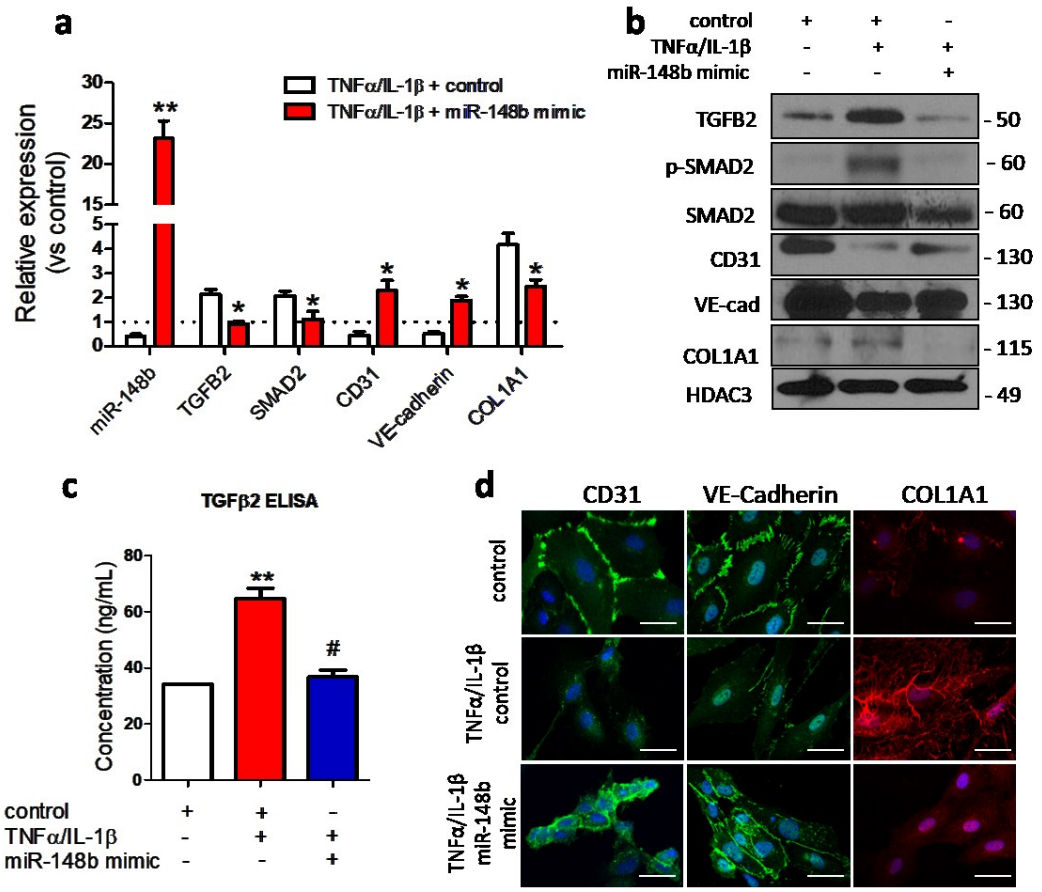

Figure 5.3| MiR-148b gain-of-function inhibits cytokines-induced EndMT. HUVECs were transfected with miR-148b mimic stimulated with a combination of TNF-α and IL-1β for 6 days. **a.** qPCR showing relative expression of miR-148b (average Ct: vehicle: 28; TNF-α/IL-1β + control: 27; TNF-α/IL-1β + miR-148b mimic: 22), *TGFB2* (average Ct: vehicle: 27; TNF-α/IL-1β + control: 26; TNF-α/IL-1β + miR-148b mimic: 27), *SMAD2* (average Ct: vehicle: 26; TNF-α/IL-1β + control: 25; TNF-α/IL-1β + miR-148b mimic: 26), *CD31* (average Ct: vehicle: 23; TNF-α/IL-1β + control: 24; TNF-α/IL-1β + miR-148b mimic: 22), *VE-cadherin* (average Ct: vehicle: 23; TNF-α/IL-1β + control: 24; TNF-α/IL-1β + miR-148b mimic: 22) and *COL1A1* (average Ct: vehicle: 35; TNF-α/IL-1β + control: 33; TNF-α/IL-1β + miR-148b mimic: 34); the dotted line represents the relative gene expression in vehicle treated HUVECs (n=3); **b.** Western blot analysis of TGFB2, p-SMAD2, SMAD2, CD31, VE-Cadherin and COL1A1; GAPDH was used as a loading control instead of β-actin due to the fact that it was constant; **c.** Quantification of TGFβ2 ELISA experiment expressed in TGFβ2 concentration (ng/mL) in miR-148b gain-of-function and/or TNFα/IL-1β treated samples vs the control; **d.** Immunofluorescence images

showing localization of CD31 (1:50), VE-Cadherin (1:100) and COL1A1 (1:100) in miR-148b or control transfected HUVECS and/or treated with TNF-α/IL-1β; scale bar=50μm (magnification 40x) (n=3). For miRNA qPCR U6 was used as a house-keeping control; For target gene qPCR 18s was used as a house-keeping control; Values are means±SEM. *P<0.05; **P<0.01 vs vehicle and/or TNFα/IL-1β together with control mimic. Unpaired two-tailed Student's t-test was applied.

5.3.4 Inflammation-induced EndMT occurs partially via SMAD2

In order to better understand the involvement of miR-148b target genes in the mechanism of inflammation-induced EndMT, two methods of TGF-β pathway interference were employed: an inhibitor of receptor kinase ALK5, SB431542 and siRNA for *SMAD2*. Interestingly, treatment of HUVECs, stimulated with inflammatory cytokines, was not sufficient to completely prevent SMAD2 phosphorylation and, thus, did not increase the expression of endothelial-specific markers CD31 and VE-Cadherin (Fig. 5.4 a, b). Conversely, *SMAD2* silencing in HUVECs treated with TNF-α/IL-1β increased the expression of *CD31* and *VE-Cadherin* (Fig. 5.4 c). Further, SMAD2 knockdown as well as increase in CD31 and VE-Cadherin and reduction in COL1A1 were confirmed at protein level (Fig. 5.4 d). Finally, immunocytochemistry validated a partial increase in CD31 and VE-Cadherin and a significant decrease in COL1A1 in stimulated HUVECs with *SMAD2* knockdown (Fig. 5.4 e). Together, this data demonstrates that *SMAD2* silencing is able to partially preserve the endothelial phenotype, suggesting that EndMT induced by chronic inflammation occurs, at least in part, via SMAD2-dependent pathway.

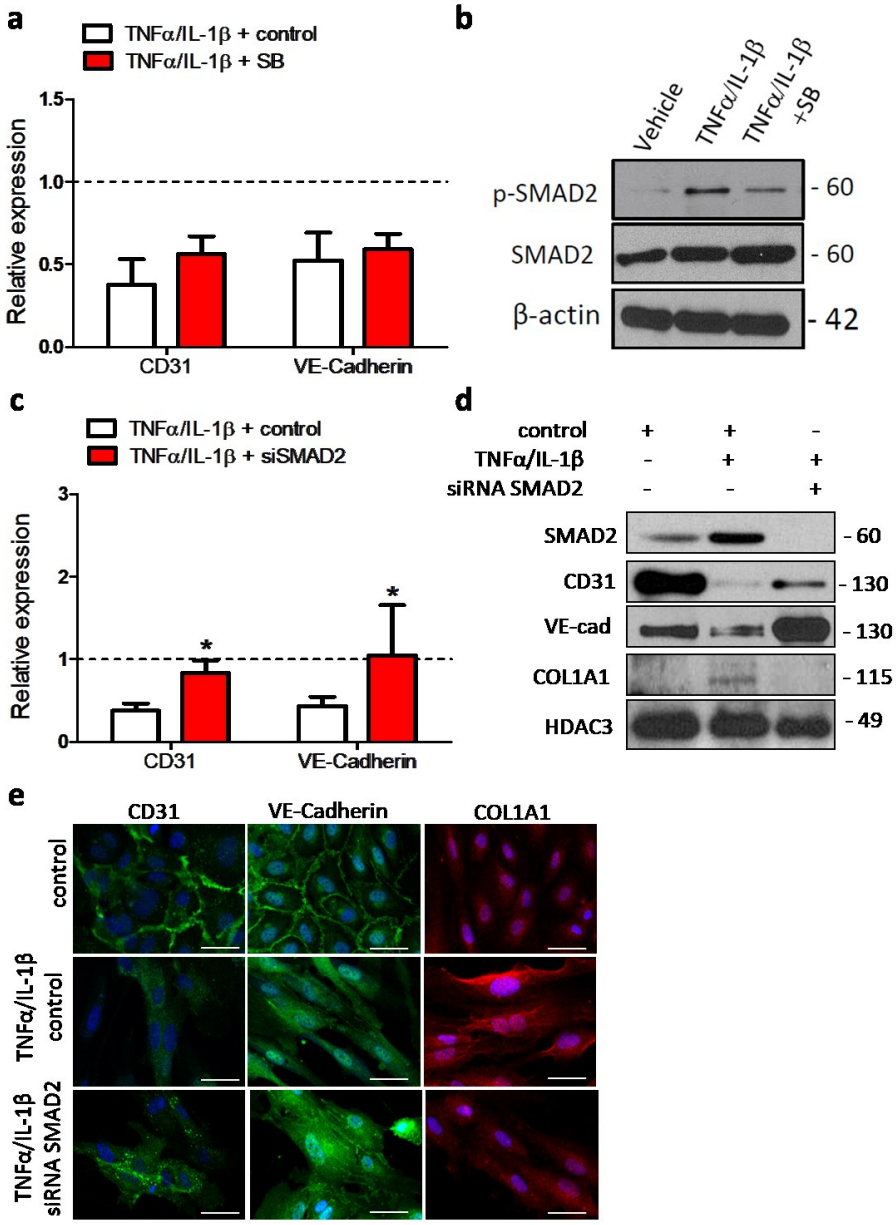

Figure 5.4| *SMAD2* silencing partially inhibits cytokines-induced EndMT. HUVECs were treated with ALK5 inhibitor SB431542 or transfected with *SMAD2* siRNA and stimulated with a combination of TNF-α and IL-1β for 6 days. **a.** qPCR showing relative expression *CD31* and *VE-Cadherin* following treatment with ALK5 inhibitor SB431542 and/or TNFα/IL-1β (average Cts are constant for all conditions 23-24); the dotted line represents the relative gene expression in vehicle treated HUVECs (n=3); **b.** Western blot analysis of p-SMAD2 (1:1000) and SMAD2 (1:1000) following treatment with ALK5 inhibitor SB431542 and/or TNFα/IL-1β; β-actin (1:4000) is used as a loading control; **c.** qPCR showing relative expression CD31 and VE-Cadherin following transfection with *SMAD2* siRNA and/or TNFα/IL-1β (average Cts for

CD31 24 vs 23; VE-Cadherin: 25 vs 23); the dotted line represents the relative gene expression in vehicle treated HUVECs (n=3); **d.** Western blot analysis of SMAD2 (1:1000), CD31 (1:1000), VE-Cadherin (1:1000) and COL1A1 (1:1000) following transfection with *SMAD2* siRNA and/or TNFα/IL-1β; HDAC3 (1:500) is used as a loading control instead of β-actin because the latter for changing; **e.** Immunofluorescence images showing localization of CD31 (1:50), VE-Cadherin (1:100) and COL1A1 (1:100) in *SMAD2* siRNA or control transfected HUVECS and/or treated with TNF-α/IL-1β, scale bar=50μm (magnification 400x); 18s was used as a house-keeping control in the qPCR; Values are means±SEM. *P<0.05 vs TNFα/IL-1β treated and control siRNA transfected. Unpaired two-tailed Student's t-test was applied.

5.4 DISCUSSION

The data presented in this chapter demonstrates for the first time the role of miR-148b as a mediator between inflammation and EndMT. Specifically, this chapter shows that chronic inflammation, induced by TNF-α and IL-1β, reduces the expression of miR-148b, thus causing the initiation of EndMT program. The chapter further confirms this data by providing the evidence that miR-148b gain-of-function is able to restore the endothelial phenotype post-stimulation with inflammatory cytokines. Finally, the results in the current chapter confirm the inflammation-miR-148b-TGF-β-EndMT axis, where the inflammation-induced transition program occurs via SMAD2-dependent mechanism.

5.4.1 Chronic inflammation induces EndMT via miR-148b downregulation

One of the first studies describing the inflammation-dependent regulation of miRNA expression came from Chen et al., demonstrating the importance of *let-7* miRNA in EndMT (Chen et al., 2012). Specifically, the investigation has proposed a novel model of EndMT, where inflammation induced by IFN-γ, TNF-α and IL-1β leads to suppression of FGF signalling, which in turn decreases *let-7* expression, thus promoting transition program (Chen et al., 2012). Notably, this chapter discusses the model of chronic inflammation induced by the combination of TNF-α and IL-1β cytokines for 6 days. As in the study before, induction of inflammation targets the expression of miR-148b and leads to EndMT due to resulting overexpression of *SMAD2*. It is important to note that in addition to the upregulation of *TGFB2* and *SMAD2* expression, the inflammatory environment also led to the marginal increase in TGF-β2 secretion, suggesting the possible autocrine as well as paracrine feed-forward loop of EndMT regulation.

Furthermore, the model of EndMT discussed in this chapter has been supported by another study, demonstrating the potency of different cytokines to induce the transition program in human intestinal microvascular endothelial cells (HIMEC) (Rieder et al., 2011). Specifically, it has been shown that only the combination of inflammatory cytokines such as TNF-α and IL-1β was able to exert the strongest EndMT phenotype, with a slight enhancement by the addition of TGF-β1 (Rieder et al., 2011). Importantly, this supports the data presented in this chapter that the strongest downregulation of miR-148b was observed when combining both TNF-α and IL-1β. Due to the fact that TGF-β1 and TGF-β2 were not able to affect miR-148b expression, it can be speculated that miR-148b-modulated EndMT is inflammation dependent. Moreover, the investigation also pointed out that the chronic treatment of endothelial cells with TNF-α, IL-1β and TGF-β1 resulted into marginal increase in collagen 1 expression and intestinal fibrosis (Rieder et al., 2011). Due to the fact that inflammation-induced EndMT via miR-148b downregulation led to strong enhancement of COL1A1 in the current model, it is possible to speculate that reduction of miR-148b by chronic inflammation could be a source of EndMT in different fibrotic pathologies.

5.4.2 MiR-148b gain-of-function attenuates EndMT induced by chronic inflammation via *SMAD2* silencing

One of the pioneering studies in the involvement of miRNA in EndMT has demonstrated that inhibition of miR-21 in TGF-β-induced model of transition is sufficient to partially block EndMT (Kumarswamy et al., 2012). Later, another investigation has shown that miR-20a gain-of-function exerts a protective anti-EndMT effect on endothelial cells, comparable to FGF2 stimulation (Correia et al., 2016). In agreement with the study above, miR-148b gain-of-function in the model presented in this chapter, efficiently abrogated

EndMT and rescued the endothelial phenotype. Importantly, due to the fact that EndMT was inhibited in response to simultaneous miR-148b overexpression and induction of inflammation, it therefore suggests that miR-148b is able to block EndMT initiation step. Moreover, the reduction of TGF-β2 secretion after miR-148b gain-of-function demonstrates that miR-148b can block the potential autocrine and paracrine EndMT regulation. Taking together the decrease in *SMAD2* and *TGFB2* gene expression as well as inhibition of TGF-β2 release, it is reasonable to assign miR-148b a role of potent negative regulator of EndMT. Additionally, Correia et al. demonstrates that miR-20a blocks EndMT through different levels: targeting the expression of *SMADs*, *ALK5*, *TGFBR2* and *SARA* (Correia et al., 2016). Concordantly, Targetscan miRNA target prediction analysis shows that other players in TGF-β pathway, such as *TGFBRAP1* and *SMURF2*, are putative miR-148b target genes, suggesting that miR-148b prevents EndMT by potently targeting different stages of TGF-β signalling.

The study above suggests that the mechanism of EndMT inhibition is achieved due to combinatorial silencing of several genes in TGF-β pathway by miR-20a (Correia et al., 2016). The data in this chapter has shown that the effect of miR-148b-induced block of EndMT is achieved mainly through *SMAD2* silencing. In particular, inhibition of TGF-βR1 was not sufficient to block EndMT and rescue the endothelial phenotype in response to inflammatory cytokines. As was shown by subsequent western blot analysis the ALK5 inhibitor was not able to prevent phosphorylation of SMAD2 significantly, and the remaining p-SMAD2 levels were sufficient to induce the EndMT program. It can also be speculated, that in the current model of chronic inflammation, SMAD2 is being alternatively phosphorylated. Specifically, it has been reported before that Toll-Like Receptor 4 (TLR4) signalling is able to induce SMAD2

phosphorylation in the presence of activated TGF-β pathway (Bhattacharyya et al., 2013). Notably, mammalian TLRs share the same cytoplasmic domains with IL-1 receptor family and, thus, exert similar cascades of signal transduction (Lin and Yeh, 2005). Moreover, it has been demonstrated that TNF-α signalling can activate SMAD2 phosphorylation by itself during epithelial-to-mesenchymal transition (Camara and Jarai, 2010). Taking into account these findings, it is possible to speculate that both TNF-α and IL-1β can induce ALK5-independent SMAD2 phosphorylation, which facilitates EndMT even in the presence of TGF-βR1 inhibitor.

5.4.3 Limitations

The main limitation in this chapter is the activity of the cytokines. In particular, TGF-β cytokines need to be activated by MMPs because the inactive form will not have any downstream effects. Other inflammatory cytokines are fragile and the activity may be decreasing over time. Another technical limitation is the fact that coating the coverslips with fibronectin increases the matrix stiffness leading to change in cell behaviour, such as increase in proliferation and fibrosis, which could contribute to the increase in collagen.

5.4.4 Conclusion

The important novelty of this chapter is the introduction of the link between inflammation, miR-148b and EndMT. The chapter proposes a model, where a physiological inflammatory stimuli, such as TNF-α and IL-1β, lead to reduction of miR-148b, thus facilitating EndMT program. Notably, this data demonstrates that pharmacological overexpression of miR-148b using mimics is sufficient to block the physiological induction of EndMT preserving the endothelial integrity. This chapter provides further mechanistic evidence,

showing that SMAD2 is at least partially responsible for induction of EndMT in the proposed model.

CHAPTER 6: CONCLUSIONS AND FUTURE DIRECTIONS

6.1 GENERAL DISCUSSION AND CONCLUSIONS

This thesis has explored and demonstrated for the first time that miR-148b plays a vital role in determining endothelial cell function and plasticity via targeting and regulating the TGF-β pathway. Overexpression of miR-148b reduces the expression of *TGFB2* and *SMAD2* and facilitates the acquisition of a pro-endothelial cell phenotype, enhancing EC proliferation, migration as well as *in vitro* angiogenesis. The topical *in vivo* delivery of miR-148b mimics onto injured skin significantly induces dermal angiogenesis and leads to a faster wound healing process. On the other hand, the silencing of endogenous miR-148b turns on the EndMT program in the endothelial cells via upregulation of *TGFB2* and *SMAD2*. The effect of the pharmacological miR-148b inhibition can be phenocopied by the physiological inflammatory stimuli such as TNF-α and IL-1β. Ultimately, miR-148b loss-of-function *in vivo* leads to induction of dermal EndMT attenuating the wound closure.

Importantly, the work presented in this thesis demonstrated the correlation between *in vitro* and *in vivo* functions of miR-148b. The increase in endothelial cell proliferation, migration and *in vitro* angiogenic response has been validated in cellular HUVEC model and could be possibly attributed to the interference with *TGFB2* and *SMAD2* expression. This data is also backed up by the previous literature stating that the TGF-β/ALK5 pathway inhibits endothelial cell migration and proliferation (Goumans et al., 2002), which can explain the enhancing effects of miR-148b on endothelial cell function. The proangiogenic effects of miR-148b overexpression are replicated in the *in vivo* model of wound healing angiogenesis. It is important to note that in the current model, following the wound induction, the peak of neovascularization occurs between days 4 and 8 after skin puncture. Therefore, the angiogenic response can be studied during this timeframe (Simons et al., 2015). In this

work, not only did miR-148b upregulation lead to the increase in *in vivo* angiogenesis and wound perfusion, but also markedly accelerated the wound closure in mice. It is proposed in this work that accelerated wound healing occurred due to miR-148b-induced TGF-β pathway inhibition, mainly due to *SMAD2* downregulation, as shown experimentally. Indeed, in accordance with this thesis, it has been demonstrated in the literature that *SMAD3* antisense oligonucleotides accelerated wound healing and reduced scarring in a mouse excisional wound model (Hong et al., 2008). It has been shown previously that 1-3 days after skin injury, there is a strong inflammatory response happening in the wound, characterized by high levels of cytokines, including TNF-α and IL-1β (Reinke and Sorg, 2012). Taking into account that TNF-α/IL-1β treatment reduces miR-148b expression *in vitro*, it is therefore possible to assume that miR-148b downregulation 3 days after skin injury is due to physiological inflammatory response in the wound. Interestingly, 7 days after wounding, miR-148b levels go up in the skin, which correlates well with the proliferation stage of the wound healing that occurs after 3-10 days (Reinke and Sorg, 2012). Overall, this thesis has demonstrated that exogenous delivery of miR-148b mimics is able to initiate angiogenesis and faster wound perfusion, thus accelerating the wound healing process.

The next part of this thesis was exploring miR-148b loss-of-function to understand its role in endothelial biology further. One of the key messages of the thesis is that miR-148b downregulation leads to the induction of EndMT. Moreover, this work has dissected the mechanism of miR-148b-dependent EndMT induction both *in vitro* and *in vivo*, showing that the effect is achieved through activation of TGF-β signalling, mostly via *SMAD2* upregulation. Importantly, this investigation presented a pioneering data of EndMT occurrence in the *in vivo* model of wound healing due to miR-148b inhibition.

Previous studies reported the importance of EndMT in dermal fibrosis, showing that delay in wound closure is associated with excessive collagen deposition (Manetti et al., 2017b). The data in this thesis has demonstrated that miR-148b silencing in the skin results in expression of the fibroblast-specific FSP-1 marker in 30% of skin vessels. These findings are clinically relevant because upon transition, the cells in these FSP-1 positive vessels can be expected to secrete large amounts of collagen and other ECM proteins, which could contribute to fibrotic skin disease. However, the current acute model of wound healing is not suitable for exploring the differences in fibrosis due to the fact that fibrotic response is initiated in the skin after 10 days post wounding (Patel et al., 2018). Under normal physiological conditions, the deposition of ECM proteins is a transient process, which is terminated once a sufficient amount of matrix is accumulated in the wound bed (Faler et al., 2006). The silencing of miR-148b leads to the over-activation of TGF-β in the wound, potentially enhancing the probability of development of fibrotic disease. One such disease is scleroderma, characterized by pathological skin fibrosis, poor wound closure and enhanced TGF-β signalling (Maeda et al., 2016, Varga, 2002b).

Clearly, EndMT has established itself to play an important role in different pathologies, such as atherosclerosis (Evrard et al., 2016), vein graft failure (Chen et al., 2012) and contributes significantly to tissue fibrosis, including cardiac and kidney fibrosis (Zeisberg et al., 2007b, Zeisberg et al., 2008, Zeisberg et al., 2007a). Nevertheless, there are studies suggesting that tissue fibrosis originates primarily from the activation and proliferation of the myofibroblasts and only 10% comes from EndMT (LeBleu et al., 2013). More studies are needed to identify the significance of EndMT in human physiology. However, it is safe to say that during complex diseases, including tissue

fibrosis, a number of different pathological processes are occurring simultaneously, inducing each other in a feed-forward loop.

Importantly, the effects of miR-148b downregulation by anti-miR-148b, such as induction of TGF-β signalling and EndMT were phenocopied by physiological inflammatory stimuli, TNF-α and IL-1β. In a number of studies it has been shown that TNF-α and IL-1β can trigger EndMT through NF-κB translocation to the nucleus (Rieder et al., 2011, Mahler et al., 2013). In the model proposed in this thesis, TNF-α/IL-1β-mediated NF-κB activation might function directly on miR-148b expression or on miR-148b maturation from pri- or pre-miR-148b, thus boosting the TGF-β cascade and inducing the EndMT program. Using the rescue experiment, this thesis confirmed that TNF-α/IL-1β-mediated EndMT occurs via miR-148b downregulation and partially via *SMAD2* signalling. Interestingly, the TGF-βR1 (ALK5) inhibitor was not able to prevent SMAD2 phosphorylation and block EndMT. This thesis has that, in this model, SMAD2 is partially phosphorylated via ALK5-independent mechanism, such as TLR4 signalling, TNF-α-dependent phosphorylation or by Mps1, which is a component of the mitotic spindle checkpoint that is functional during oxidative stress (Zhu et al., 2007, Yu et al., 2016). The fact that miR-148b gain-of-function is able to prevent the transition program and can preserve the endothelial phenotype confirms that miR-148b is a key player in TNF-α/IL-1β-induced EndMT. Interestingly in a recent study it has been shown that the serum from Kawasaki disease patients, which is rich in inflammatory cytokines, reduces the expression of miR-483 and induces EndMT. Moreover, in agreement with this thesis, miR-483 gain-of-function was able to rescue the endothelial phenotype and suppress EndMT (He et al., 2017). Overall, the final results chapter identified the way miR-148b is

regulated under physiological inflammatory conditions, leading to the pathological EndMT.

6.1 Future work

Potential future experiments in the *in vitro* part of the study would be carried out to elucidate the mechanism of EndMT induced by the inflammatory cytokines. It has been shown in this work that 6 days treatment with TNF-α/IL-1β is able to downregulate miR-148b, which in turn promotes the transition program. It is therefore important to understand the signalling cascade that occurs in between cytokine binding to their receptors and miR-148b downregulation. The most likely possibility is that TNF-α and IL-1β, upon interaction with their membrane receptors, induce NF-kB translocation to the nucleus, which then leads to miR-148b downregulation. To do this, HUVECs would be transfected with siRNA NF-kB and the treated with TNF-α/IL-1β for 6 days. If, after that, the EndMT is prevented, it would show that miR-148b downregulation is NF-kB-dependent.

The current data shows that TNF-α/IL-1β stimulation downregulates miR-148b. However, it is unclear whether the cytokines decreases the transcription of miR-148b or maturation step. It has been reported before that p-SMAD2/3 is able to interact directly with Dicer and promote maturation of miRNA (Garcia et al., 2015). In the model presented in the thesis there is high level of SMAD2 phosphorylation. Thus, it is important to test whether p-SMAD2 is able to affect miR-148b maturation. To do that the qPCR should be carried on the RNA extract from stimulated HUVECs with primers targeting pri-miR-148b, which is a primary transcript form of miR-148b, and compare the expression with the control cells. This will show if there is a difference in miR-148b transcription. To understand whether the cytokines affect the maturation

of miR-148b, the northern blot can be carried out to compare the levels of pre-miR-148b and mature miR-148b between stimulated and control HUVECs after transfection with pre-miR-148b. The possible increase in pre-miR-148b in stimulated cells vs control could mean that the maturation step is blocked after cytokine treatment.

Next interesting *in vitro* experiment would be to understand whether the transition in our model is complete or reversible. To do this, HUVECs should be treated with cytokines for 6 days and then, at day 6, the medium should be changed to complete endothelium growth medium. At the selected time points, cells should be harvested and tested for the EndMT markers, which would show whether HUVECs differentiated completely into mesenchymal cells or the effect is reversible. Another variation of this experiment would be to transfect TNF-α/IL-1β-stimulated cells with miR-148b mimic after 6 days of treatment and not at day 0. The results from this experiment would also suggest whether miR-148b can block EndMT initiation or progression. Interestingly, Correia et al. has carried out a similar study, where endothelial cells, undergoing TGF-β-induced EndMT, were transfected with miR-20a at day 0 and after 72 hours post-treatment. Specifically, it has been found that miR-20a can only have an effect, when introduced at day 0, where it can limit the number of cells acquiring mesenchymal phenotype (Correia et al., 2016).

Further, it's essential to determine the physiological stimuli, which can induce the expression of miR-148b in the endothelial cells. There are a number of studies demonstrating that FGF is able to attenuate EndMT and rescue the endothelial phenotype (Chen et al., 2012, Correia et al., 2016). It is, therefore, reasonable to test whether HUVEC stimulation with FGF would upregulate miR-148b. It is well known that FGF promotes endothelial cell proliferation and is a strong inducer of angiogenesis (Ucuzian et al., 2010, Seghezzi et al.,

1998). It is therefore interesting to see if miR-148b silencing using anti-miR in the stimulated HUVECs with FGF would attenuate pre-angiogenic effects of FGF. In that case, it would mean that FGF is acting via miR-148b dependent pathway.

In this study, it has been demonstrated that miR-148b targets two key members of TGF-β pathway, *TGFB2* and *SMAD2*. This shows that miR-148b is able to regulate the cascade at different levels. It would be interesting to see what other genes within TGF-β signalling can be modulated by miR-148b. For this, a specific TGF-β signalling array can be used to see which genes in the pathway are downregulated by miR-148b mimic. Indeed, TargetScan and MirPath analyses predict different components of TGF-β pathway, such as *TGFBRAP1*, *GDF6*, *BMPR1B* and others, to be miR-148b target genes. The whole miR-148b regulatory network could be identified by carrying out Ago2 pulldown and then doing RNA sequencing to find all RNA molecules, which are bound to miR-148b-3p.

In the *in vivo* part of the study there are two main experiments that could be carried out in the future. As mentioned previously, the wound healing model in this thesis is not long enough to see the fibrotic response. Therefore, it would be interesting to prolong the model and compare the collagen levels between control and anti-miR-148b treated wounds at later time points. Another output of wound healing process is scar formation. Notably, it has been reported that EndMT contributes to scar formation in the wounds (Patel et al., 2018). It would, thus, be interesting to investigate whether anti-miR-148b treatment would enhance the scarring in the wound. On the other hand, it is possible to assume that miR-148b mimic delivery would decrease the scar formation due to enhanced regenerative response.

Finally, it has been reported that angiogenesis is attenuated in the diabetic non-healing ulcers (Okonkwo and DiPietro, 2017, Drinkwater et al., 2002). Currently, there is no efficient treatment for this detrimental condition, which can ultimately lead to severe complications, including leg amputations. It is therefore important to understand whether miR-148b treatment could improve the closure of diabetic non-healing wounds. For this, an *ex vivo* model of wounding on the skin of diabetic patients can be employed, where miR-148b mimics would be delivered to the induced wounds. The possible positive results from this study could initiate Phase I clinical trials, investigating the safety of miR-148-based therapy, preparing for the later efficacy studies. Current challenges with miRNA-based therapies include possible off-target effects, especially when miRNA therapeutics are delivered systemically. With this method, the pathological off-target effects are minimized due to a localized topical delivery directly to the wounds.

Potentially, it might be also possible to use miR-148b-based therapy within other disease models such as myocardial infarction. After acute myocardial infarction, a significant ischemic injury occurs in the myocardium, which determines the size of the infarct. The restoration of the coronary blood flow using the stent implantation or coronary artery bypass surgery improves the outcome of the patients. However, the ischemic post-MI heart exerts microvascular rarefaction and dysfunction, which impairs the perfusion of the whole myocardium (Cochain et al., 2013). Thus, a pro-angiogenic therapy post-MI would be beneficial to restore the blood supply of the myocardium. In this context miR-148b-based therapeutics could prove to be effective in the perfusion of the infarcted myocardium. In order to remove the possible pathological system off-target effects, miR-148b oligos could be delivered locally during the angioplasty, either in free form or coupled to nanoparticles.

At the moment, the UK priority patent application has been filed to protect the intellectual property generated in this thesis. The technology of miR-148b-based gene therapy could be licenced out to RNA delivery companies such as miRagen Therapeutics and Regulus Therapeutics, which can take this technology further, generating potential treatments and introducing them into clinical practice.

Overall, the work presented in this thesis has identified the new role of miR-148b in endothelial cell biology, emphasising its proangiogenic properties, which accelerate the wound healing process. Inhibition of miR-148b has been shown to have a detrimental effect on endothelium, promoting EndMT and attenuating the wound closure. The data from this study can be used further to generate miR-148b-based therapy for promoting wound repair, reducing scar formation and treating non-healing ulcers in diabetic patients.

REFERENCES

ABDALLA, S. A. & LETARTE, M. 2006. Hereditary haemorrhagic telangiectasia: current views on genetics and mechanisms of disease. *Journal of Medical Genetics,* 43**,** 97-110.

ADAMS, R. H. & ALITALO, K. 2007. Molecular regulation of angiogenesis and lymphangiogenesis. *Nat Rev Mol Cell Biol,* 8**,** 464-78.

ALBINSSON, S., SUAREZ, Y., SKOURA, A., OFFERMANNS, S., MIANO, J. M. & SESSA, W. C. 2010. MicroRNAs are necessary for vascular smooth muscle growth, differentiation, and function. *Arterioscler Thromb Vasc Biol,* 30**,** 1118-26.

AMERES, S. L. & ZAMORE, P. D. 2013. Diversifying microRNA sequence and function. *Nat Rev Mol Cell Biol,* 14**,** 475-88.

ANANIA, M. C., CETTI, E., LECIS, D., TODOERTI, K., GULINO, A., MAURO, G., DI MARCO, T., CLERIS, L., PAGLIARDINI, S., MANENTI, G., BELMONTE, B., TRIPODO, C., NERI, A. & GRECO, A. 2017. Targeting COPZ1 non-oncogene addiction counteracts the viability of thyroid tumor cells. *Cancer Lett,* 410**,** 201-211.

ANDL, T., MURCHISON, E. P., LIU, F., ZHANG, Y., YUNTA-GONZALEZ, M., TOBIAS, J. W., ANDL, C. D., SEYKORA, J. T., HANNON, G. J. & MILLAR, S. E. 2006. The miRNA-processing enzyme dicer is essential for the morphogenesis and maintenance of hair follicles. *Curr Biol,* 16**,** 1041-9.

ARCINIEGAS, E., CARRILLO, L. M., DE SANCTIS, J. B. & CANDELLE, D. 2008. Possible role of NFkappaB in the embryonic vascular remodeling and the endothelial mesenchymal transition process. *Cell Adh Migr,* 2**,** 17-29.

ARCINIEGAS, E., FRID, M. G., DOUGLAS, I. S. & STENMARK, K. R. 2007. Perspectives on endothelial-to-mesenchymal transition: potential contribution to vascular remodeling in chronic pulmonary hypertension. *Am J Physiol Lung Cell Mol Physiol,* 293**,** L1-8.

ARCINIEGAS, E., NEVES, C. Y., CARRILLO, L. M., ZAMBRANO, E. A. & RAMIREZ, R. 2005. Endothelial-mesenchymal transition occurs during embryonic pulmonary artery development. *Endothelium,* 12**,** 193-200.

ARCINIEGAS, E., SUTTON, A. B., ALLEN, T. D. & SCHOR, A. M. 1992. Transforming growth factor beta 1 promotes the differentiation of endothelial cells into smooth muscle-like cells in vitro. *J Cell Sci,* 103 (Pt 2)**,** 521-9.

ARMSTRONG, E. J. & BISCHOFF, J. 2004. Heart valve development: endothelial cell signaling and differentiation. *Circ Res,* 95**,** 459-70.

BAEYENS, N. & SCHWARTZ, M. A. 2016. Biomechanics of vascular mechanosensation and remodeling. *Molecular Biology of the Cell,* 27**,** 7-11.

BANERJEE, J., CHAN, Y. C. & SEN, C. K. 2011. MicroRNAs in skin and wound healing. *Physiol Genomics,* 43**,** 543-56.

BARTEL, D. P. 2009. MicroRNAs: target recognition and regulatory functions. *Cell,* 136**,** 215-33.

BARTEL, D. P. 2018. Metazoan MicroRNAs. *Cell,* 173**,** 20-51.

BECK, R., RAWET, M., WIELAND, F. T. & CASSEL, D. 2009. The COPI system: molecular mechanisms and function. *FEBS Lett,* 583**,** 2701-9.

BELLER, M., SZTALRYD, C., SOUTHALL, N., BELL, M., JACKLE, H., AULD, D. S. & OLIVER, B. 2008. COPI complex is a regulator of lipid homeostasis. *PLoS Biol,* 6**,** e292.

BENAKANAKERE, M. R., LI, Q., ESKAN, M. A., SINGH, A. V., ZHAO, J., GALICIA, J. C., STATHOPOULOU, P., KNUDSEN, T. B. & KINANE, D. F. 2009. Modulation of TLR2 protein expression by miR-105 in human oral keratinocytes. *J Biol Chem,* 284**,** 23107-15.

BHATTACHARYYA, S., KELLEY, K., MELICHIAN, D. S., TAMAKI, Z., FANG, F., SU, Y., FENG, G., POPE, R. M., BUDINGER, G. R., MUTLU, G. M., LAFYATIS, R., RADSTAKE, T., FEGHALI-BOSTWICK, C. & VARGA, J. 2013. Toll-like receptor 4 signaling augments transforming growth factor-beta responses: a novel mechanism for maintaining and amplifying fibrosis in scleroderma. *Am J Pathol,* 182**,** 192-205.

BIDZHEKOV, K., GAN, L., DENECKE, B., ROSTALSKY, A., HRISTOV, M., KOEPPEL, T. A., ZERNECKE, A. & WEBER, C. 2012. microRNA expression signatures and parallels between monocyte subsets and atherosclerotic plaque in humans. *Thromb Haemost,* 107**,** 619-25.

BIRDSEY, G. M., SHAH, A. V., DUFTON, N., REYNOLDS, L. E., OSUNA ALMAGRO, L., YANG, Y., ASPALTER, I. M., KHAN, S. T., MASON, J. C., DEJANA, E., GOTTGENS, B., HODIVALA-DILKE, K., GERHARDT, H., ADAMS, R. H. & RANDI, A. M. 2015. The endothelial transcription factor ERG promotes vascular stability and growth through Wnt/beta-catenin signaling. *Dev Cell,* 32**,** 82-96.

BISWAS, S., ROY, S., BANERJEE, J., HUSSAIN, S. R., KHANNA, S., MEENAKSHISUNDARAM, G., KUPPUSAMY, P., FRIEDMAN, A. & SEN, C. K. 2010. Hypoxia inducible microRNA 210 attenuates keratinocyte proliferation and impairs closure in a murine model of ischemic wounds. *Proc Natl Acad Sci U S A,* 107**,** 6976-81.

BOBIK, A. 2006. Transforming growth factor-betas and vascular disorders. *Arterioscler Thromb Vasc Biol,* 26**,** 1712-20.

BOBIK, A., AGROTIS, A., KANELLAKIS, P., DILLEY, R., KRUSHINSKY, A., SMIRNOV, V., TARARAK, E., CONDRON, M. & KOSTOLIAS, G. 1999a. Distinct patterns of transforming growth factor-beta isoform and receptor expression in human atherosclerotic lesions. Colocalization implicates TGF-beta in fibrofatty lesion development. *Circulation,* 99**,** 2883-91.

BOBIK, A., AGROTIS, A., KANELLAKIS, P., DILLEY, R., KRUSHINSKY, A., SMIRNOV, V., TARARAK, E., CONDRON, M. & KOSTOLIAS, G. 1999b. Distinct Patterns of Transforming Growth Factor-β Isoform and Receptor Expression in Human Atherosclerotic Lesions. *Colocalization Implicates TGF-β in Fibrofatty Lesion Development,* 99**,** 2883-2891.

BOHNSACK, M. T., CZAPLINSKI, K. & GORLICH, D. 2004. Exportin 5 is a RanGTP-dependent dsRNA-binding protein that mediates nuclear export of pre-miRNAs. *Rna,* 10**,** 185-91.

BONAUER, A., CARMONA, G., IWASAKI, M., MIONE, M., KOYANAGI, M., FISCHER, A., BURCHFIELD, J., FOX, H., DOEBELE, C., OHTANI, K., CHAVAKIS, E., POTENTE, M., TJWA, M., URBICH, C., ZEIHER, A. M. & DIMMELER, S. 2009. MicroRNA-92a controls angiogenesis and functional recovery of ischemic tissues in mice. *Science,* 324**,** 1710-3.

BRAVI, L., RUDINI, N., CUTTANO, R., GIAMPIETRO, C., MADDALUNO, L., FERRARINI, L., ADAMS, R. H., CORADA, M., BOULDAY, G., TOURNIER-LASSERVE, E., DEJANA, E. & LAMPUGNANI, M. G. 2015. Sulindac metabolites decrease cerebrovascular malformations in CCM3-knockout mice. *Proc Natl Acad Sci U S A,* 112**,** 8421-6.

BRIDEAU, C., GUNTER, B., PIKOUNIS, B. & LIAW, A. 2003. Improved statistical methods for hit selection in high-throughput screening. *J Biomol Screen,* 8**,** 634-47.

CALLIS, T. E., PANDYA, K., SEOK, H. Y., TANG, R.-H., TATSUGUCHI, M., HUANG, Z.-P., CHEN, J.-F., DENG, Z., GUNN, B., SHUMATE, J., WILLIS, M. S., SELZMAN, C. H. & WANG, D.-Z. 2009a. MicroRNA-208a is a regulator of cardiac hypertrophy and conduction in mice. *The Journal of Clinical Investigation,* 119.

CALLIS, T. E., PANDYA, K., SEOK, H. Y., TANG, R. H., TATSUGUCHI, M., HUANG, Z. P., CHEN, J. F., DENG, Z., GUNN, B., SHUMATE, J., WILLIS, M. S., SELZMAN, C. H. & WANG, D. Z. 2009b. MicroRNA-208a is a regulator of cardiac hypertrophy and conduction in mice. *J Clin Invest,* 119**,** 2772-86.

CAMARA, J. & JARAI, G. 2010. Epithelial-mesenchymal transition in primary human bronchial epithelial cells is Smad-dependent and enhanced by fibronectin and TNF-alpha. *Fibrogenesis Tissue Repair,* 3**,** 2.

CAO, Y., FENG, B., CHEN, S., CHU, Y. & CHAKRABARTI, S. 2014. Mechanisms of Endothelial to Mesenchymal Transition in the Retina in Diabetes. *Investigative Ophthalmology & Visual Science,* 55**,** 7321-7331.

CAPORALI, A. & EMANUELI, C. 2011. MicroRNA regulation in angiogenesis. *Vascul Pharmacol,* 55**,** 79-86.

CAPORALI, A. & EMANUELI, C. 2012. MicroRNAs in Postischemic Vascular Repair. *Cardiol Res Pract,* 2012**,** 486702.

CAPORALI, A., MELONI, M., VOLLENKLE, C., BONCI, D., SALA-NEWBY, G. B., ADDIS, R., SPINETTI, G., LOSA, S., MASSON, R., BAKER, A. H., AGAMI, R., LE SAGE, C., CONDORELLI, G., MADEDDU, P., MARTELLI, F. & EMANUELI, C. 2011. Deregulation of microRNA-503 contributes to diabetes mellitus-induced impairment of endothelial function and reparative angiogenesis after limb ischemia. *Circulation,* 123**,** 282-91.

CARE, A., CATALUCCI, D., FELICETTI, F., BONCI, D., ADDARIO, A., GALLO, P., BANG, M.-L., SEGNALINI, P., GU, Y., DALTON, N. D., ELIA, L., LATRONICO, M. V. G., HOYDAL, M., AUTORE, C., RUSSO, M. A., DORN, G. W., ELLINGSEN, O., RUIZ-LOZANO, P., PETERSON, K. L., CROCE, C. M., PESCHLE, C. & CONDORELLI, G. 2007. MicroRNA-133 controls cardiac hypertrophy. *Nat Med,* 13**,** 613-618.

CARMELIET, P. & JAIN, R. K. 2011. Molecular mechanisms and clinical applications of angiogenesis. *Nature,* 473**,** 298-307.

CAVE, A. C., BREWER, A. C., NARAYANAPANICKER, A., RAY, R., GRIEVE, D. J., WALKER, S. & SHAH, A. M. 2006. NADPH oxidases in cardiovascular health and disease. *Antioxid Redox Signal,* 8**,** 691-728.

CHANG, H., ZHOU, X., WANG, Z. N., SONG, Y. X., ZHAO, F., GAO, P., CHIANG, Y. & XU, H. M. 2012. Increased expression of miR-148b in ovarian carcinoma and its clinical significance. *Mol Med Rep,* 5**,** 1277-80.

CHAUDHURI, V., ZHOU, L. & KARASEK, M. 2007. Inflammatory cytokines induce the transformation of human dermal microvascular endothelial cells into myofibroblasts: a potential role in skin fibrogenesis. *J Cutan Pathol,* 34**,** 146-53.

CHEN, J. F., MURCHISON, E. P., TANG, R., CALLIS, T. E., TATSUGUCHI, M., DENG, Z., ROJAS, M., HAMMOND, S. M., SCHNEIDER, M. D., SELZMAN, C. H., MEISSNER, G., PATTERSON, C., HANNON, G. J. & WANG, D. Z. 2008. Targeted deletion of Dicer in the heart leads to dilated cardiomyopathy and heart failure. *Proc Natl Acad Sci U S A,* 105**,** 2111-6.

CHEN, P. Y., QIN, L., BAEYENS, N., LI, G., AFOLABI, T., BUDATHA, M., TELLIDES, G., SCHWARTZ, M. A. & SIMONS, M. 2015. Endothelial-to-mesenchymal transition drives atherosclerosis progression. *J Clin Invest,* 125**,** 4514-28.

CHEN, P. Y., QIN, L., BARNES, C., CHARISSE, K., YI, T., ZHANG, X., ALI, R., MEDINA, P. P., YU, J., SLACK, F. J., ANDERSON, D. G., KOTELIANSKI, V., WANG, F., TELLIDES, G. & SIMONS, M. 2012. FGF regulates TGF-beta signaling and endothelial-to-mesenchymal transition via control of let-7 miRNA expression. *Cell Rep,* 2**,** 1684-96.

CHEN, P. Y. & SIMONS, M. 2016. When endothelial cells go rogue. *EMBO Mol Med,* 8**,** 1-2.

CHEN, Y., SONG, Y. X. & WANG, Z. N. 2013. The microRNA-148/152 family: multi-faceted players. *Mol Cancer,* 12**,** 43.

CHENG, Y., LIU, X., YANG, J., LIN, Y., XU, D.-Z., LU, Q., DEITCH, E. A., HUO, Y., DELPHIN, E. S. & ZHANG, C. 2009. MicroRNA-145, a Novel Smooth Muscle Cell Phenotypic Marker and Modulator, Controls Vascular Neointimal Lesion Formation. *Circulation Research,* 105**,** 158-166.

CHOI, B. M., KWAK, H. J., JUN, C. D., PARK, S. D., KIM, K. Y., KIM, H. R. & CHUNG, H. T. 1996. Control of scarring in adult wounds using antisense transforming growth factor-beta 1 oligodeoxynucleotides. *Immunol Cell Biol,* 74**,** 144-50.

CHUNG, A. S. & FERRARA, N. 2011. Developmental and pathological angiogenesis. *Annu Rev Cell Dev Biol,* 27**,** 563-84.

CIMINO, D., DE PITTA, C., ORSO, F., ZAMPINI, M., CASARA, S., PENNA, E., QUAGLINO, E., FORNI, M., DAMASCO, C., PINATEL, E., PONZONE, R., ROMUALDI, C., BRISKEN, C., DE BORTOLI, M., BIGLIA, N., PROVERO, P., LANFRANCHI, G. & TAVERNA, D. 2013. miR148b is a major coordinator of breast cancer progression in a relapse-associated microRNA signature by targeting ITGA5, ROCK1, PIK3CA, NRAS, and CSF1. *Faseb j,* 27**,** 1223-35.

CIPOLLONE, F., FAZIA, M., MINCIONE, G., IEZZI, A., PINI, B., CUCCURULLO, C., UCCHINO, S., SPIGONARDO, F., DI NISIO, M., CUCCURULLO, F., MEZZETTI, A. & PORRECA, E. 2004. Increased Expression of Transforming Growth Factor-β1 as a Stabilizing Factor in Human Atherosclerotic Plaques. *Stroke,* 35**,** 2253-2257.

COCHAIN, C., CHANNON, K. M. & SILVESTRE, J. S. 2013. Angiogenesis in the infarcted myocardium. *Antioxid Redox Signal,* 18**,** 1100-13.

COMPTON, L. A., POTASH, D. A., BROWN, C. B. & BARNETT, J. V. 2007. Coronary vessel development is dependent on the type III transforming growth factor beta receptor. *Circ Res,* 101**,** 784-91.

COOLEY, B. C., NEVADO, J., MELLAD, J., YANG, D., ST HILAIRE, C., NEGRO, A., FANG, F., CHEN, G., SAN, H., WALTS, A. D., SCHWARTZBECK, R. L., TAYLOR, B., LANZER, J. D., WRAGG, A., ELAGHA, A., BELTRAN, L. E., BERRY, C., FEIL, R., VIRMANI, R., LADICH, E., KOVACIC, J. C. & BOEHM, M. 2014. TGF-beta signaling mediates endothelial-to-mesenchymal transition (EndMT) during vein graft remodeling. *Sci Transl Med,* 6**,** 227ra34.

CORREIA, A. C., MOONEN, J. R., BRINKER, M. G. & KRENNING, G. 2016. FGF2 inhibits endothelial-mesenchymal transition through microRNA-20a-mediated repression of canonical TGF-beta signaling. *J Cell Sci,* 129**,** 569-79.

COSTA, C., INCIO, J. & SOARES, R. 2007. Angiogenesis and chronic inflammation: cause or consequence? *Angiogenesis,* 10**,** 149-166.

COUCKE, P. J., WILLAERT, A., WESSELS, M. W., CALLEWAERT, B., ZOPPI, N., DE BACKER, J., FOX, J. E., MANCINI, G. M. S., KAMBOURIS, M., GARDELLA, R., FACCHETTI, F., WILLEMS, P. J., FORSYTH, R., DIETZ, H. C., BARLATI, S., COLOMBI, M., LOEYS, B. & DE PAEPE, A. 2006. Mutations in the facilitative glucose transporter GLUT10 alter angiogenesis and cause arterial tortuosity syndrome. *Nat Genet,* 38**,** 452-457.

DAS, S., KUMAR, M., NEGI, V., PATTNAIK, B., PRAKASH, Y. S., AGRAWAL, A. & GHOSH, B. 2014. MicroRNA-326 regulates profibrotic functions of transforming growth factor-beta in pulmonary fibrosis. *Am J Respir Cell Mol Biol,* 50**,** 882-92.

DAVIS, B. N., HILYARD, A. C., LAGNA, G. & HATA, A. 2008. SMAD proteins control DROSHA-mediated microRNA maturation. *Nature,* 454**,** 56-61.

DAVIS, G. E., STRATMAN, A. N., SACHARIDOU, A. & KOH, W. 2011. Molecular basis for endothelial lumen formation and tubulogenesis during vasculogenesis and angiogenic sprouting. *Int Rev Cell Mol Biol,* 288**,** 101-65.

DE VAL, S. & BLACK, B. L. 2009. Transcriptional control of endothelial cell development. *Dev Cell,* 16**,** 180-95.

DE VAL, S., CHI, N. C., MEADOWS, S. M., MINOVITSKY, S., ANDERSON, J. P., HARRIS, I. S., EHLERS, M. L., AGARWAL, P., VISEL, A., XU, S. M., PENNACCHIO, L. A., DUBCHAK, I., KRIEG, P. A., STAINIER, D. Y. & BLACK, B. L. 2008. Combinatorial regulation of endothelial gene expression by ets and forkhead transcription factors. *Cell,* 135**,** 1053-64.

DEJANA, E., HIRSCHI, K. K. & SIMONS, M. 2017. The molecular basis of endothelial cell plasticity. *Nat Commun,* 8**,** 14361.

DENTELLI, P., ROSSO, A., ORSO, F., OLGASI, C., TAVERNA, D. & BRIZZI, M. F. 2010. microRNA-222 controls neovascularization by regulating signal transducer and activator of transcription 5A expression. *Arterioscler Thromb Vasc Biol,* 30**,** 1562-8.

DENZLER, R., MCGEARY, S. E., TITLE, A. C., AGARWAL, V., BARTEL, D. P. & STOFFEL, M. 2016. Impact of MicroRNA Levels, Target-Site Complementarity, and Cooperativity on Competing Endogenous RNA-Regulated Gene Expression. *Mol Cell,* 64**,** 565-579.

DEWS, M., FOX, J. L., HULTINE, S., SUNDARAM, P., WANG, W., LIU, Y. Y., FURTH, E., ENDERS, G. H., EL-DEIRY, W., SCHELTER, J. M., CLEARY, M. A. & THOMAS-TIKHONENKO, A. 2010. The myc-miR-17~92 axis blunts TGF{beta} signaling and production of multiple TGF{beta}-dependent antiangiogenic factors. *Cancer Res,* 70**,** 8233-46.

DIEZ, M., MUSRI, M. M., FERRER, E., BARBERA, J. A. & PEINADO, V. I. 2010. Endothelial progenitor cells undergo an endothelial-to-mesenchymal transition-like process mediated by TGFbetaRI. *Cardiovasc Res,* 88**,** 502-11.

DOEBELE, C., BONAUER, A., FISCHER, A., SCHOLZ, A., REISS, Y., URBICH, C., HOFMANN, W.-K., ZEIHER, A. M. & DIMMELER, S. 2010. Members of the microRNA-17-92 cluster exhibit a cell-intrinsic antiangiogenic function in endothelial cells. *Blood,* 115**,** 4944-4950.

DRAHEIM, K. M., FISHER, O. S., BOGGON, T. J. & CALDERWOOD, D. A. 2014. Cerebral cavernous malformation proteins at a glance. *Journal of Cell Science,* 127**,** 701-707.

DRINKWATER, S. L., SMITH, A., SAWYER, B. M. & BURNAND, K. G. 2002. Effect of venous ulcer exudates on angiogenesis in vitro. *Br J Surg,* 89**,** 709-13.

DUNN, L., PROSSER, H. C., TAN, J. T., VANAGS, L. Z., NG, M. K. & BURSILL, C. A. 2013. Murine model of wound healing. *J Vis Exp***,** e50265.

EDDAHIBI, S., MORRELL, N., D'ORTHO, M.-P., NAEIJE, R. & ADNOT, S. 2002. Pathobiology of pulmonary arterial hypertension. *European Respiratory Journal,* 20**,** 1559-1572.

EICHHORN, STEPHEN W., GUO, H., MCGEARY, SEAN E., RODRIGUEZ-MIAS, RICARD A., SHIN, C., BAEK, D., HSU, S.-H., GHOSHAL, K., VILLÉN, J. & BARTEL, DAVID P. 2014. mRNA Destabilization Is the Dominant Effect of Mammalian MicroRNAs by the Time Substantial Repression Ensues. *Molecular Cell,* 56**,** 104-115.

ELTZSCHIG , H. K. & CARMELIET , P. 2011. Hypoxia and Inflammation. *New England Journal of Medicine,* 364**,** 656-665.

EMING, S. A., BRACHVOGEL, B., ODORISIO, T. & KOCH, M. 2007. Regulation of angiogenesis: Wound healing as a model. *Progress in Histochemistry and Cytochemistry,* 42**,** 115-170.

ESCOBAR-CHAVEZ, J. J., LOPEZ-CERVANTES, M., NAIK, A., KALIA, Y. N., QUINTANAR-GUERRERO, D. & GANEM-QUINTANAR, A. 2006. Applications of thermo-reversible pluronic F-127 gels in pharmaceutical formulations. *J Pharm Pharm Sci,* 9**,** 339-58.

EVRARD, S. M., LECCE, L., MICHELIS, K. C., NOMURA-KITABAYASHI, A., PANDEY, G., PURUSHOTHAMAN, K. R., D'ESCAMARD, V., LI, J. R., HADRI, L., FUJITANI, K., MORENO, P. R., BENARD, L., RIMMELE, P., COHAIN, A., MECHAM, B., RANDOLPH, G. J., NABEL, E. G., HAJJAR, R., FUSTER, V., BOEHM, M. & KOVACIC, J. C. 2016. Endothelial to mesenchymal transition is common in atherosclerotic lesions and is associated with plaque instability. *Nat Commun,* 7**,** 11853.

FABIAN, M. R. & SONENBERG, N. 2012. The mechanics of miRNA-mediated gene silencing: a look under the hood of miRISC. *Nat Struct Mol Biol,* 19**,** 586-93.

FALER, B. J., MACSATA, R. A., PLUMMER, D., MISHRA, L. & SIDAWY, A. N. 2006. Transforming growth factor-beta and wound healing. *Perspect Vasc Surg Endovasc Ther,* 18**,** 55-62.

FASANARO, P., D'ALESSANDRA, Y., DI STEFANO, V., MELCHIONNA, R., ROMANI, S., POMPILIO, G., CAPOGROSSI, M. C. & MARTELLI, F. 2008. MicroRNA-210 modulates endothelial cell response to hypoxia and inhibits the receptor tyrosine kinase ligand Ephrin-A3. *J Biol Chem,* 283**,** 15878-83.

FASANARO, P., GRECO, S., LORENZI, M., PESCATORI, M., BRIOSCHI, M., KULSHRESHTHA, R., BANFI, C., STUBBS, A., CALIN, G. A., IVAN, M., CAPOGROSSI, M. C. & MARTELLI, F. 2009. An integrated approach for experimental target identification of hypoxia-induced miR-210. *J Biol Chem,* 284**,** 35134-43.

FERNANDEZ, L. A., SANZ-RODRIGUEZ, F., BLANCO, F. J., BERNABEU, C. & BOTELLA, L. M. 2006. Hereditary hemorrhagic telangiectasia, a vascular dysplasia affecting the TGF-beta signaling pathway. *Clin Med Res,* 4**,** 66-78.

FIERRO-FERNANDEZ, M., BUSNADIEGO, O., SANDOVAL, P., ESPINOSA-DIEZ, C., BLANCO-RUIZ, E., RODRIGUEZ, M., PIAN, H., RAMOS, R., LOPEZ-CABRERA, M., GARCIA-BERMEJO, M. L. & LAMAS, S. 2015. miR-9-5p suppresses pro-fibrogenic transformation of fibroblasts and prevents organ fibrosis by targeting NOX4 and TGFBR2. *EMBO Rep,* 16**,** 1358-77.

FISCHER, A., ZALVIDE, J., FAUROBERT, E., ALBIGES-RIZO, C. & TOURNIER-LASSERVE, E. 2013. Cerebral cavernous malformations: from CCM genes to endothelial cell homeostasis. *Trends Mol Med,* 19**,** 302-8.

FISH, J. E., SANTORO, M. M., MORTON, S. U., YU, S., YEH, R. F., WYTHE, J. D., IVEY, K. N., BRUNEAU, B. G., STAINIER, D. Y. & SRIVASTAVA, D. 2008. miR-126 regulates angiogenic signaling and vascular integrity. *Dev Cell,* 15**,** 272-84.

FLEISSNER, F., JAZBUTYTE, V., FIEDLER, J., GUPTA, S. K., YIN, X., XU, Q., GALUPPO, P., KNEITZ, S., MAYR, M., ERTL, G., BAUERSACHS, J. & THUM, T. 2010. Asymmetric Dimethylarginine Impairs Angiogenic Progenitor Cell Function in Patients With Coronary Artery Disease Through a MicroRNA-21–Dependent Mechanism. *Circulation Research*.

FRID, M. G., KALE, V. A. & STENMARK, K. R. 2002. Mature vascular endothelium can give rise to smooth muscle cells via endothelial-mesenchymal transdifferentiation: in vitro analysis. *Circ Res,* 90**,** 1189-96.

FRIEDMAN, R. C., FARH, K. K., BURGE, C. B. & BARTEL, D. P. 2009. Most mammalian mRNAs are conserved targets of microRNAs. *Genome Res,* 19**,** 92-105.

FUKUNAGA, R., HAN, B. W., HUNG, J. H., XU, J., WENG, Z. & ZAMORE, P. D. 2012. Dicer partner proteins tune the length of mature miRNAs in flies and mammals. *Cell,* 151**,** 533-46.

GARCIA, R., NISTAL, J. F., MERINO, D., PRICE, N. L., FERNANDEZ-HERNANDO, C., BEAUMONT, J., GONZALEZ, A., HURLE, M. A. & VILLAR, A. V. 2015. p-SMAD2/3 and DICER promote pre-miR-21 processing during pressure overload-associated myocardial remodeling. *Biochim Biophys Acta,* 1852**,** 1520-30.

GAUGLITZ, G. G., KORTING, H. C., PAVICIC, T., RUZICKA, T. & JESCHKE, M. G. 2011. Hypertrophic scarring and keloids: pathomechanisms and current and emerging treatment strategies. *Mol Med,* 17**,** 113-25.

GEBERT, L. F. R. & MACRAE, I. J. 2019. Regulation of microRNA function in animals. *Nat Rev Mol Cell Biol,* 20**,** 21-37.

GHOSH, A. K., NAGPAL, V., COVINGTON, J. W., MICHAELS, M. A. & VAUGHAN, D. E. 2012a. Molecular basis of cardiac endothelial-to-mesenchymal transition (EndMT): differential expression of microRNAs during EndMT. *Cell Signal,* 24**,** 1031-6.

GHOSH, A. K., NAGPAL, V., COVINGTON, J. W., MICHAELS, M. A. & VAUGHAN, D. E. 2012b. Molecular basis of cardiac endothelial-to-

mesenchymal transition (EndMT): Differential expression of microRNAs during EndMT. *Cellular Signalling,* 24**,** 1031-1036.
GIAEVER, I. & KEESE, C. R. 1991a. Micromotion of mammalian cells measured electrically. *Proc Natl Acad Sci U S A,* 88**,** 7896-900.
GIAEVER, I. & KEESE, C. R. 1991b. Micromotion of mammalian cells measured electrically. *Proceedings of the National Academy of Sciences,* 88**,** 7896-7900.
GONZALEZ-NUNEZ, M., MUNOZ-FELIX, J. M. & LOPEZ-NOVOA, J. M. 2013. The ALK-1/Smad1 pathway in cardiovascular physiopathology. A new target for therapy? *Biochim Biophys Acta,* 1832**,** 1492-510.
GORDON, K. J. & BLOBE, G. C. 2008. Role of transforming growth factor-beta superfamily signaling pathways in human disease. *Biochim Biophys Acta,* 1782**,** 197-228.
GOUMANS, M. J. & TEN DIJKE, P. 2017. TGF-beta Signaling in Control of Cardiovascular Function. *Cold Spring Harb Perspect Biol*.
GOUMANS, M. J., VALDIMARSDOTTIR, G., ITOH, S., ROSENDAHL, A., SIDERAS, P. & TEN DIJKE, P. 2002. Balancing the activation state of the endothelium via two distinct TGF-beta type I receptors. *Embo j,* 21**,** 1743-53.
GRAINGER, D. J., WITCHELL, C. M. & METCALFE, J. C. 1995. Tamoxifen elevates transforming growth factor-beta and suppresses diet-induced formation of lipid lesions in mouse aorta. *Nat Med,* 1**,** 1067-73.
GREAVES, N. S., ASHCROFT, K. J., BAGUNEID, M. & BAYAT, A. 2013. Current understanding of molecular and cellular mechanisms in fibroplasia and angiogenesis during acute wound healing. *J Dermatol Sci,* 72**,** 206-17.
GRIVENNIKOV, S. I., GRETEN, F. R. & KARIN, M. 2010. Immunity, Inflammation, and Cancer. *Cell,* 140**,** 883-899.
GUZIK, T., KORBUT, R. & ADAMEK-GUZIK, T. 2003. Nitric oxide and superoxide in inflammation and immune regulation. *J Physiol Pharmacol,* 54**,** 469-487.
HA, M. & KIM, V. N. 2014. Regulation of microRNA biogenesis. *Nat Rev Mol Cell Biol,* 15**,** 509-24.
HE, J., XU, Y., KOYA, D. & KANASAKI, K. 2013. Role of the endothelial-to-mesenchymal transition in renal fibrosis of chronic kidney disease. *Clin Exp Nephrol,* 17**,** 488-97.
HE, M., CHEN, Z., MARTIN, M., ZHANG, J., SANGWUNG, P., WOO, B., TREMOULET, A. H., SHIMIZU, C., JAIN, M. K., BURNS, J. C. & SHYY, J. Y. 2017. miR-483 Targeting of CTGF Suppresses Endothelial-to-Mesenchymal Transition: Therapeutic Implications in Kawasaki Disease. *Circ Res,* 120**,** 354-365.

HE, W., DORN, D. C., ERDJUMENT-BROMAGE, H., TEMPST, P., MOORE, M. A. & MASSAGUE, J. 2006. Hematopoiesis controlled by distinct TIF1gamma and Smad4 branches of the TGFbeta pathway. *Cell,* 125**,** 929-41.

HESSE, M. & ARENZ, C. 2014. MicroRNA maturation and human disease. *Methods Mol Biol,* 1095**,** 11-25.

HEUSSCHEN, R., VAN GINK, M., GRIFFIOEN, A. W. & THIJSSEN, V. L. 2010. MicroRNAs in the tumor endothelium: novel controls on the angioregulatory switchboard. *Biochim Biophys Acta,* 1805**,** 87-96.

HOLDERFIELD, M. T. & HUGHES, C. C. 2008. Crosstalk between vascular endothelial growth factor, notch, and transforming growth factor-beta in vascular morphogenesis. *Circ Res,* 102**,** 637-52.

HONG, H. J., JIN, S. E., PARK, J. S., AHN, W. S. & KIM, C. K. 2008. Accelerated wound healing by smad3 antisense oligonucleotides-impregnated chitosan/alginate polyelectrolyte complex. *Biomaterials,* 29**,** 4831-7.

HUANG, C., XIAO, X., YANG, Y., MISHRA, A., LIANG, Y., ZENG, X., YANG, X., XU, D., BLACKBURN, M. R., HENKE, C. A. & LIU, L. 2017. MicroRNA-101 attenuates pulmonary fibrosis by inhibiting fibroblast proliferation and activation. *J Biol Chem,* 292**,** 16420-16439.

HUMINIECKI, L., GOLDOVSKY, L., FREILICH, S., MOUSTAKAS, A., OUZOUNIS, C. & HELDIN, C. H. 2009. Emergence, development and diversification of the TGF-beta signalling pathway within the animal kingdom. *BMC Evol Biol,* 9**,** 28.

HUNTZINGER, E. & IZAURRALDE, E. 2011. Gene silencing by microRNAs: contributions of translational repression and mRNA decay. *Nat Rev Genet,* 12**,** 99-110.

HUSE, M., MUIR, T. W., XU, L., CHEN, Y.-G., KURIYAN, J. & MASSAGUÉ, J. 2001. The TGFβ Receptor Activation Process. *Molecular Cell,* 8**,** 671-682.

IVEY, K. N., MUTH, A., ARNOLD, J., KING, F. W., YEH, R. F., FISH, J. E., HSIAO, E. C., SCHWARTZ, R. J., CONKLIN, B. R., BERNSTEIN, H. S. & SRIVASTAVA, D. 2008. MicroRNA regulation of cell lineages in mouse and human embryonic stem cells. *Cell Stem Cell,* 2**,** 219-29.

JONAS, S. & IZAURRALDE, E. 2015. Towards a molecular understanding of microRNA-mediated gene silencing. *Nat Rev Genet,* 16**,** 421-433.

KALLURI, R. & WEINBERG, R. A. 2009. The basics of epithelial-mesenchymal transition. *The Journal of Clinical Investigation,* 119**,** 1420-1428.

KANG, Y., CHEN, C. R. & MASSAGUE, J. 2003. A self-enabling TGFbeta response coupled to stress signaling: Smad engages stress response factor ATF3 for Id1 repression in epithelial cells. *Mol Cell,* 11**,** 915-26.
KLUGE, A., ZIMMERMANN, R., MÜNKEL, B., MOHRI, M., SACK, S., SCHAPER, J. & SCHAPER, W. 1995. Insulin-like growth factor I is involved in inflammation linked angiogenic processes after microembolisation in porcine heart. *Cardiovascular Research,* 29**,** 407-415.
KNIGHT, S. W. & BASS, B. L. 2001. A Role for the RNase III Enzyme DCR-1 in RNA Interference and Germ Line Development in Caenorhabditis elegans. *Science,* 293**,** 2269-2271.
KOKUDO, T., SUZUKI, Y., YOSHIMATSU, Y., YAMAZAKI, T., WATABE, T. & MIYAZONO, K. 2008. Snail is required for TGFbeta-induced endothelial-mesenchymal transition of embryonic stem cell-derived endothelial cells. *J Cell Sci,* 121**,** 3317-24.
KONG, P., CHRISTIA, P., SAXENA, A., SU, Y. & FRANGOGIANNIS, N. G. 2013. Lack of specificity of fibroblast-specific protein 1 in cardiac remodeling and fibrosis. *Am J Physiol Heart Circ Physiol,* 305**,** H1363-72.
KONISTI, S., KIRIAKIDIS, S. & PALEOLOG, E. M. 2012. Hypoxia[mdash]a key regulator of angiogenesis and inflammation in rheumatoid arthritis. *Nat Rev Rheumatol,* 8**,** 153-162.
KOTAKE, Y., NAKAGAWA, T., KITAGAWA, K., SUZUKI, S., LIU, N., KITAGAWA, M. & XIONG, Y. 2010. Long non-coding RNA ANRIL is required for the PRC2 recruitment to and silencing of p15INK4B tumor suppressor gene. *Oncogene,* 30**,** 1956.
KRENNING, G., BARAUNA, V. G., KRIEGER, J. E., HARMSEN, M. C. & MOONEN, J. R. 2016. Endothelial Plasticity: Shifting Phenotypes through Force Feedback. *Stem Cells Int,* 2016**,** 9762959.
KRIEG, T., ABRAHAM, D. & LAFYATIS, R. 2007. Fibrosis in connective tissue disease: the role of the myofibroblast and fibroblast-epithelial cell interactions. *Arthritis Res Ther,* 9 Suppl 2**,** S4.
KRUG, E. L., RUNYAN, R. B. & MARKWALD, R. R. 1985. Protein extracts from early embryonic hearts initiate cardiac endothelial cytodifferentiation. *Developmental Biology,* 112**,** 414-426.
KUHNERT, F., MANCUSO, M. R., HAMPTON, J., STANKUNAS, K., ASANO, T., CHEN, C. Z. & KUO, C. J. 2008. Attribution of vascular phenotypes of the murine Egfl7 locus to the microRNA miR-126. *Development,* 135**,** 3989-93.
KULKARNI, A. B. & KARLSSON, S. 1993. Transforming growth factor-beta 1 knockout mice. A mutation in one cytokine gene causes a dramatic inflammatory disease. *Am J Pathol,* 143**,** 3-9.

KUMARSWAMY, R., VOLKMANN, I., JAZBUTYTE, V., DANGWAL, S., PARK, D. H. & THUM, T. 2012. Transforming growth factor-beta-induced endothelial-to-mesenchymal transition is partly mediated by microRNA-21. *Arterioscler Thromb Vasc Biol,* 32**,** 361-9.

KUNDU, J. K. & SURH, Y.-J. 2012. Emerging avenues linking inflammation and cancer. *Free Radical Biology and Medicine,* 52**,** 2013-2037.

KURAKULA, K., GOUMANS, M. J. & TEN DIJKE, P. 2015. Regulatory RNAs controlling vascular (dys)function by affecting TGF-ss family signalling. *EXCLI J,* 14**,** 832-50.

LAKOS, G., TAKAGAWA, S., CHEN, S. J., FERREIRA, A. M., HAN, G., MASUDA, K., WANG, X. J., DIPIETRO, L. A. & VARGA, J. 2004. Targeted disruption of TGF-beta/Smad3 signaling modulates skin fibrosis in a mouse model of scleroderma. *Am J Pathol,* 165**,** 203-17.

LAMOUILLE, S., MALLET, C., FEIGE, J. J. & BAILLY, S. 2002. Activin receptor-like kinase 1 is implicated in the maturation phase of angiogenesis. *Blood,* 100**,** 4495-501.

LANDSKRONER-EIGER, S., MONEKE, I. & SESSA, W. C. 2013. miRNAs as modulators of angiogenesis. *Cold Spring Harb Perspect Med,* 3**,** a006643.

LEBLEU, V. S., TADURI, G., O'CONNELL, J., TENG, Y., COOKE, V. G., WODA, C., SUGIMOTO, H. & KALLURI, R. 2013. Origin and function of myofibroblasts in kidney fibrosis. *Nat Med,* 19**,** 1047-53.

LEE, Y., AHN, C., HAN, J., CHOI, H., KIM, J., YIM, J., LEE, J., PROVOST, P., RADMARK, O., KIM, S. & KIM, V. N. 2003. The nuclear RNase III Drosha initiates microRNA processing. *Nature,* 425**,** 415-9.

LEE, Y., KIM, M., HAN, J., YEOM, K. H., LEE, S., BAEK, S. H. & KIM, V. N. 2004. MicroRNA genes are transcribed by RNA polymerase II. *Embo j,* 23**,** 4051-60.

LI, Z. & RANA, T. M. 2014. Therapeutic targeting of microRNAs: current status and future challenges. *Nat Rev Drug Discov,* 13**,** 622-38.

LIANG, H., XU, C., PAN, Z., ZHANG, Y., XU, Z., CHEN, Y., LI, T., LI, X., LIU, Y., HUANGFU, L., LU, Y., ZHANG, Z., YANG, B., GITAU, S., LU, Y., SHAN, H. & DU, Z. 2014. The antifibrotic effects and mechanisms of microRNA-26a action in idiopathic pulmonary fibrosis. *Mol Ther,* 22**,** 1122-1133.

LIAO, Y. H., CHANG, Y. H., SUNG, L. Y., LI, K. C., YEH, C. L., YEN, T. C., HWANG, S. M., LIN, K. J. & HU, Y. C. 2014. Osteogenic differentiation of adipose-derived stem cells and calvarial defect repair using baculovirus-mediated co-expression of BMP-2 and miR-148b. *Biomaterials,* 35**,** 4901-10.

LIN, E. A., KONG, L., BAI, X. H., LUAN, Y. & LIU, C. J. 2009a. miR-199a, a bone morphogenic protein 2-responsive MicroRNA, regulates

chondrogenesis via direct targeting to Smad1. *J Biol Chem,* 284**,** 11326-35.
LIN, W. J. & YEH, W. C. 2005. Implication of Toll-like receptor and tumor necrosis factor alpha signaling in septic shock. *Shock,* 24**,** 206-9.
LIN, Z., MURTAZA, I., WANG, K., JIAO, J., GAO, J. & LI, P. F. 2009b. miR-23a functions downstream of NFATc3 to regulate cardiac hypertrophy. *Proc Natl Acad Sci U S A,* 106**,** 12103-8.
LIU, G., FRIGGERI, A., YANG, Y., MILOSEVIC, J., DING, Q., THANNICKAL, V. J., KAMINSKI, N. & ABRAHAM, E. 2010. miR-21 mediates fibrogenic activation of pulmonary fibroblasts and lung fibrosis. *J Exp Med,* 207**,** 1589-97.
LIU, N., WILLIAMS, A. H., KIM, Y., MCANALLY, J., BEZPROZVANNAYA, S., SUTHERLAND, L. B., RICHARDSON, J. A., BASSEL-DUBY, R. & OLSON, E. N. 2007. An intragenic MEF2-dependent enhancer directs muscle-specific expression of microRNAs 1 and 133. *Proc Natl Acad Sci U S A,* 104**,** 20844-9.
LOEYS, B. L., CHEN, J., NEPTUNE, E. R., JUDGE, D. P., PODOWSKI, M., HOLM, T., MEYERS, J., LEITCH, C. C., KATSANIS, N., SHARIFI, N., XU, F. L., MYERS, L. A., SPEVAK, P. J., CAMERON, D. E., DE BACKER, J., HELLEMANS, J., CHEN, Y., DAVIS, E. C., WEBB, C. L., KRESS, W., COUCKE, P., RIFKIN, D. B., DE PAEPE, A. M. & DIETZ, H. C. 2005. A syndrome of altered cardiovascular, craniofacial, neurocognitive and skeletal development caused by mutations in TGFBR1 or TGFBR2. *Nat Genet,* 37**,** 275-81.
LOPEZ-OROZCO, J., PARE, J. M., HOLME, A. L., CHAULK, S. G., FAHLMAN, R. P. & HOBMAN, T. C. 2015. Functional analyses of phosphorylation events in human Argonaute 2. *Rna,* 21**,** 2030-8.
LU, R., JI, Z., LI, X., QIN, J., CUI, G., CHEN, J., ZHAI, Q., ZHAO, C., ZHANG, W. & YU, Z. 2015. Tumor suppressive microRNA-200a inhibits renal cell carcinoma development by directly targeting TGFB2. *Tumour Biol,* 36**,** 6691-700.
LUND, E., GUTTINGER, S., CALADO, A., DAHLBERG, J. E. & KUTAY, U. 2004. Nuclear export of microRNA precursors. *Science,* 303**,** 95-8.
MACHADO, R. D., ALDRED, M. A., JAMES, V., HARRISON, R. E., PATEL, B., SCHWALBE, E. C., GRUENIG, E., JANSSEN, B., KOEHLER, R., SEEGER, W., EICKELBERG, O., OLSCHEWSKI, H., ELLIOTT, C. G., GLISSMEYER, E., CARLQUIST, J., KIM, M., TORBICKI, A., FIJALKOWSKA, A., SZEWCZYK, G., PARMA, J., ABRAMOWICZ, M. J., GALIE, N., MORISAKI, H., KYOTANI, S., NAKANISHI, N., MORISAKI, T., HUMBERT, M., SIMONNEAU, G., SITBON, O., SOUBRIER, F., COULET, F., MORRELL, N. W. & TREMBATH, R. C.

2006. Mutations of the TGF-beta type II receptor BMPR2 in pulmonary arterial hypertension. *Hum Mutat,* 27**,** 121-32.

MADDALUNO, L., RUDINI, N., CUTTANO, R., BRAVI, L., GIAMPIETRO, C., CORADA, M., FERRARINI, L., ORSENIGO, F., PAPA, E., BOULDAY, G., TOURNIER-LASSERVE, E., CHAPON, F., RICHICHI, C., RETTA, S. F., LAMPUGNANI, M. G. & DEJANA, E. 2013. EndMT contributes to the onset and progression of cerebral cavernous malformations. *Nature,* 498**,** 492-6.

MAEDA, T., YAMAMOTO, T., IMAMURA, T. & TSUBOI, R. 2016. Impaired wound healing in bleomycin-induced murine scleroderma: a new model of wound retardation. *Arch Dermatol Res,* 308**,** 87-94.

MAHLER, G. J., FARRAR, E. J. & BUTCHER, J. T. 2013. Inflammatory cytokines promote mesenchymal transformation in embryonic and adult valve endothelial cells. *Arterioscler Thromb Vasc Biol,* 33**,** 121-30.

MAHMOUD, M. M., SERBANOVIC-CANIC, J., FENG, S., SOUILHOL, C., XING, R., HSIAO, S., MAMMOTO, A., CHEN, J., ARIAANS, M., FRANCIS, S. E., VAN DER HEIDEN, K., RIDGER, V. & EVANS, P. C. 2017. Shear stress induces endothelial-to-mesenchymal transition via the transcription factor Snail. *Sci Rep,* 7**,** 3375.

MALESZEWSKA, M., MOONEN, J. R., HUIJKMAN, N., VAN DE SLUIS, B., KRENNING, G. & HARMSEN, M. C. 2013. IL-1beta and TGFbeta2 synergistically induce endothelial to mesenchymal transition in an NFkappaB-dependent manner. *Immunobiology,* 218**,** 443-54.

MALLAT, Z., GOJOVA, A., MARCHIOL-FOURNIGAULT, C., ESPOSITO, B., KAMATE, C., MERVAL, R., FRADELIZI, D. & TEDGUI, A. 2001. Inhibition of transforming growth factor-beta signaling accelerates atherosclerosis and induces an unstable plaque phenotype in mice. *Circ Res,* 89**,** 930-4.

MANETTI, M., ROMANO, E., ROSA, I., GUIDUCCI, S., BELLANDO-RANDONE, S., DE PAULIS, A., IBBA-MANNESCHI, L. & MATUCCI-CERINIC, M. 2017a. Endothelial-to-mesenchymal transition contributes to endothelial dysfunction and dermal fibrosis in systemic sclerosis. *Annals of the Rheumatic Diseases*.

MANETTI, M., ROMANO, E., ROSA, I., GUIDUCCI, S., BELLANDO-RANDONE, S., DE PAULIS, A., IBBA-MANNESCHI, L. & MATUCCI-CERINIC, M. 2017b. Endothelial-to-mesenchymal transition contributes to endothelial dysfunction and dermal fibrosis in systemic sclerosis. *Ann Rheum Dis,* 76**,** 924-934.

MARCELO, K. L., GOLDIE, L. C. & HIRSCHI, K. K. 2013. Regulation of endothelial cell differentiation and specification. *Circ Res,* 112**,** 1272-87.

MASSAGUE, J. 2012. TGFbeta signalling in context. *Nat Rev Mol Cell Biol,* 13**,** 616-30.

MATYAS, G., ARNOLD, E., CARREL, T., BAUMGARTNER, D., BOILEAU, C., BERGER, W. & STEINMANN, B. 2006. Identification and in silico analyses of novel TGFBR1 and TGFBR2 mutations in Marfan syndrome-related disorders. *Hum Mutat,* 27**,** 760-9.

MEDICI, D. & KALLURI, R. 2012. Endothelial-mesenchymal transition and its contribution to the emergence of stem cell phenotype. *Semin Cancer Biol,* 22**,** 379-84.

MEDICI, D., POTENTA, S. & KALLURI, R. 2011. Transforming growth factor-beta2 promotes Snail-mediated endothelial-mesenchymal transition through convergence of Smad-dependent and Smad-independent signalling. *Biochem J,* 437**,** 515-20.

MEIJER, HEDDA A., SMITH, EWAN M. & BUSHELL, M. 2014. Regulation of miRNA strand selection: follow the leader? *Biochemical Society Transactions,* 42**,** 1135-1140.

MONTESANO, R., MOSSAZ, A., RYSER, J. E., ORCI, L. & VASSALLI, P. 1984. Leukocyte interleukins induce cultured endothelial cells to produce a highly organized, glycosaminoglycan-rich pericellular matrix. *J Cell Biol,* 99**,** 1706-15.

MONTEYS, A. M., SPENGLER, R. M., WAN, J., TECEDOR, L., LENNOX, K. A., XING, Y. & DAVIDSON, B. L. 2010. Structure and activity of putative intronic miRNA promoters. *Rna,* 16**,** 495-505.

MOONEN, J. R., LEE, E. S., SCHMIDT, M., MALESZEWSKA, M., KOERTS, J. A., BROUWER, L. A., VAN KOOTEN, T. G., VAN LUYN, M. J., ZEEBREGTS, C. J., KRENNING, G. & HARMSEN, M. C. 2015. Endothelial-to-mesenchymal transition contributes to fibro-proliferative vascular disease and is modulated by fluid shear stress. *Cardiovasc Res,* 108**,** 377-86.

MOORE-MORRIS, T., GUIMARAES-CAMBOA, N., BANERJEE, I., ZAMBON, A. C., KISSELEVA, T., VELAYOUDON, A., STALLCUP, W. B., GU, Y., DALTON, N. D., CEDENILLA, M., GOMEZ-AMARO, R., ZHOU, B., BRENNER, D. A., PETERSON, K. L., CHEN, J. & EVANS, S. M. 2014. Resident fibroblast lineages mediate pressure overload-induced cardiac fibrosis. *J Clin Invest,* 124**,** 2921-34.

MORAN, M. E. 2014. Scleroderma and evidence based non-pharmaceutical treatment modalities for digital ulcers: a systematic review. *J Wound Care,* 23**,** 510-6.

MULLEN, A. C., ORLANDO, D. A., NEWMAN, J. J., LOVEN, J., KUMAR, R. M., BILODEAU, S., REDDY, J., GUENTHER, M. G., DEKOTER, R. P.

& YOUNG, R. A. 2011. Master transcription factors determine cell-type-specific responses to TGF-beta signaling. *Cell,* 147**,** 565-76.
NEHLS, V. & DRENCKHAHN, D. 1995. A microcarrier-based cocultivation system for the investigation of factors and cells involved in angiogenesis in three-dimensional fibrin matrices in vitro. *Histochem Cell Biol,* 104**,** 459-66.
OKONKWO, U. A. & DIPIETRO, L. A. 2017. Diabetes and Wound Angiogenesis. *Int J Mol Sci,* 18.
OZSOLAK, F., POLING, L. L., WANG, Z., LIU, H., LIU, X. S., ROEDER, R. G., ZHANG, X., SONG, J. S. & FISHER, D. E. 2008. Chromatin structure analyses identify miRNA promoters. *Genes Dev,* 22**,** 3172-83.
PADUA, D., ZHANG, X. H., WANG, Q., NADAL, C., GERALD, W. L., GOMIS, R. R. & MASSAGUE, J. 2008. TGFbeta primes breast tumors for lung metastasis seeding through angiopoietin-like 4. *Cell,* 133**,** 66-77.
PALMIERI, A., PEZZETTI, F., BRUNELLI, G., MARTINELLI, M., SCAPOLI, L., ARLOTTI, M., MASIERO, E. & CARINCI, F. 2008. Medpor regulates osteoblast's microRNAs. *Biomed Mater Eng,* 18**,** 91-7.
PANNU, H., AVIDAN, N., TRAN-FADULU, V. & MILEWICZ, D. M. 2006. Genetic basis of thoracic aortic aneurysms and dissections: potential relevance to abdominal aortic aneurysms. *Ann N Y Acad Sci,* 1085**,** 242-55.
PASTAR, I., KHAN, A. A., STOJADINOVIC, O., LEBRUN, E. A., MEDINA, M. C., BREM, H., KIRSNER, R. S., JIMENEZ, J. J., LESLIE, C. & TOMIC-CANIC, M. 2012. Induction of specific microRNAs inhibits cutaneous wound healing. *J Biol Chem,* 287**,** 29324-35.
PATEL, J., BAZ, B., WONG, H. Y., LEE, J. S. & KHOSROTEHRANI, K. 2018. Accelerated Endothelial to Mesenchymal Transition Increased Fibrosis via Deleting Notch Signaling in Wound Vasculature. *J Invest Dermatol,* 138**,** 1166-1175.
PEREZ, L., MUNOZ-DURANGO, N., RIEDEL, C. A., ECHEVERRIA, C., KALERGIS, A. M., CABELLO-VERRUGIO, C. & SIMON, F. 2017. Endothelial-to-mesenchymal transition: Cytokine-mediated pathways that determine endothelial fibrosis under inflammatory conditions. *Cytokine Growth Factor Rev,* 33**,** 41-54.
PÉREZ, L., MUÑOZ-DURANGO, N., RIEDEL, C. A., ECHEVERRÍA, C., KALERGIS, A. M., CABELLO-VERRUGIO, C. & SIMON, F. 2017. Endothelial-to-mesenchymal transition: Cytokine-mediated pathways that determine endothelial fibrosis under inflammatory conditions. *Cytokine & Growth Factor Reviews,* 33**,** 41-54.

PEREZ, R. & DAVIS, S. C. 2008. Relevance of animal models for wound healing. *Wounds,* 20**,** 3-8.

PFEFFER, S., SEWER, A., LAGOS-QUINTANA, M., SHERIDAN, R., SANDER, C., GRASSER, F. A., VAN DYK, L. F., HO, C. K., SHUMAN, S., CHIEN, M., RUSSO, J. J., JU, J., RANDALL, G., LINDENBACH, B. D., RICE, C. M., SIMON, V., HO, D. D., ZAVOLAN, M. & TUSCHL, T. 2005. Identification of microRNAs of the herpesvirus family. *Nat Methods,* 2**,** 269-76.

PIERA-VELAZQUEZ, S. & JIMENEZ, S. A. 2012. Molecular mechanisms of endothelial to mesenchymal cell transition (EndoMT) in experimentally induced fibrotic diseases. *Fibrogenesis Tissue Repair,* 5**,** S7.

PIERA-VELAZQUEZ, S., LI, Z. & JIMENEZ, S. A. 2011. Role of endothelial-mesenchymal transition (EndoMT) in the pathogenesis of fibrotic disorders. *Am J Pathol,* 179**,** 1074-80.

POLISENO, L., TUCCOLI, A., MARIANI, L., EVANGELISTA, M., CITTI, L., WOODS, K., MERCATANTI, A., HAMMOND, S. & RAINALDI, G. 2006. MicroRNAs modulate the angiogenic properties of HUVECs. *Blood,* 108**,** 3068-71.

PONCE, M. L. 2009. Tube formation: an in vitro matrigel angiogenesis assay. *Methods Mol Biol,* 467**,** 183-8.

POTENTE, M., GERHARDT, H. & CARMELIET, P. 2011. Basic and therapeutic aspects of angiogenesis. *Cell,* 146**,** 873-87.

QI, X.-Y., HUANG, H., ORDOG, B., LUO, X., NAUD, P., SUN, Y., WU, C.-T., DAWSON, K., TADEVOSYAN, A., CHEN, Y., HARADA, M., DOBREV, D. & NATTEL, S. 2015. Fibroblast Inward-Rectifier Potassium Current Upregulation in Profibrillatory Atrial RemodelingNovelty and Significance. *Circulation Research,* 116**,** 836-845.

QUIAT, D. & OLSON, E. N. 2013. MicroRNAs in cardiovascular disease: from pathogenesis to prevention and treatment. *J Clin Invest,* 123**,** 11-8.

QURESHI, A. T., MONROE, W. T., DASA, V., GIMBLE, J. M. & HAYES, D. J. 2013. miR-148b-nanoparticle conjugates for light mediated osteogenesis of human adipose stromal/stem cells. *Biomaterials,* 34**,** 7799-810.

RANE, S., HE, M., SAYED, D., VASHISTHA, H., MALHOTRA, A., SADOSHIMA, J., VATNER, D. E., VATNER, S. F. & ABDELLATIF, M. 2009. Downregulation of miR-199a derepresses hypoxia-inducible factor-1alpha and Sirtuin 1 and recapitulates hypoxia preconditioning in cardiac myocytes. *Circ Res,* 104**,** 879-86.

RAZI, M., CHAN, E. Y. & TOOZE, S. A. 2009. Early endosomes and endosomal coatomer are required for autophagy. *J Cell Biol,* 185**,** 305-21.

REINKE, J. M. & SORG, H. 2012. Wound repair and regeneration. *Eur Surg Res,* 49**,** 35-43.

REUTER, S., GUPTA, S. C., CHATURVEDI, M. M. & AGGARWAL, B. B. 2010. Oxidative stress, inflammation, and cancer: How are they linked? *Free Radical Biology and Medicine,* 49**,** 1603-1616.

RIEDEL, K., RIEDEL, F., GOESSLER, U. R., GERMANN, G. & SAUERBIER, M. 2007. TGF-β Antisense Therapy Increases Angiogenic Potential in Human Keratinocytes In Vitro∗. *Archives of Medical Research,* 38**,** 45-51.

RIEDER, F., KESSLER, S. P., WEST, G. A., BHILOCHA, S., DE LA MOTTE, C., SADLER, T. M., GOPALAN, B., STYLIANOU, E. & FIOCCHI, C. 2011. Inflammation-induced endothelial-to-mesenchymal transition: a novel mechanism of intestinal fibrosis. *Am J Pathol,* 179**,** 2660-73.

RISAU, W. 1997. Mechanisms of angiogenesis. *Nature,* 386**,** 671-4.

ROMERO, L. I., ZHANG, D. N., HERRON, G. S. & KARASEK, M. A. 1997. Interleukin-1 induces major phenotypic changes in human skin microvascular endothelial cells. *J Cell Physiol,* 173**,** 84-92.

RUDEL, S., WANG, Y., LENOBEL, R., KORNER, R., HSIAO, H. H., URLAUB, H., PATEL, D. & MEISTER, G. 2011. Phosphorylation of human Argonaute proteins affects small RNA binding. *Nucleic Acids Res,* 39**,** 2330-43.

RÜEGG, C. 2006. Leukocytes, inflammation, and angiogenesis in cancer: fatal attractions. *Journal of Leukocyte Biology,* 80**,** 682-684.

SANFORD, L. P., ORMSBY, I., GITTENBERGER-DE GROOT, A. C., SARIOLA, H., FRIEDMAN, R., BOIVIN, G. P., CARDELL, E. L. & DOETSCHMAN, T. 1997. TGFbeta2 knockout mice have multiple developmental defects that are non-overlapping with other TGFbeta knockout phenotypes. *Development,* 124**,** 2659-70.

SCHIRLE, N. T. & MACRAE, I. J. 2012. The crystal structure of human Argonaute2. *Science,* 336**,** 1037-40.

SCOTT, P. G., DODD, C. M., TREDGET, E. E., GHAHARY, A. & RAHEMTULLA, F. 1995. Immunohistochemical localization of the proteoglycans decorin, biglycan and versican and transforming growth factor-beta in human post-burn hypertrophic and mature scars. *Histopathology,* 26**,** 423-31.

SEGHEZZI, G., PATEL, S., REN, C. J., GUALANDRIS, A., PINTUCCI, G., ROBBINS, E. S., SHAPIRO, R. L., GALLOWAY, A. C., RIFKIN, D. B. & MIGNATTI, P. 1998. Fibroblast growth factor-2 (FGF-2) induces vascular endothelial growth factor (VEGF) expression in the

endothelial cells of forming capillaries: an autocrine mechanism contributing to angiogenesis. *J Cell Biol,* 141**,** 1659-73.

SEN, C. K. & ROY, S. 2008. microRNA in Cutaneous Wound Healing. *In:* YING, S.-Y. (ed.) *Current Perspectives in microRNAs (miRNA).* Dordrecht: Springer Netherlands.

SERINO, G., SALLUSTIO, F., COX, S. N., PESCE, F. & SCHENA, F. P. 2012. Abnormal miR-148b expression promotes aberrant glycosylation of IgA1 in IgA nephropathy. *J Am Soc Nephrol,* 23**,** 814-24.

SHOVLIN, C. L. & LETARTE, M. 1999. Hereditary haemorrhagic telangiectasia and pulmonary arteriovenous malformations: issues in clinical management and review of pathogenic mechanisms. *Thorax,* 54**,** 714-729.

SIMONS, M., ALITALO, K., ANNEX, B. H., AUGUSTIN, H. G., BEAM, C., BERK, B. C., BYZOVA, T., CARMELIET, P., CHILIAN, W., COOKE, J. P., DAVIS, G. E., EICHMANN, A., IRUELA-ARISPE, M. L., KESHET, E., SINUSAS, A. J., RUHRBERG, C., WOO, Y. J. & DIMMELER, S. 2015. State-of-the-Art Methods for Evaluation of Angiogenesis and Tissue Vascularization: A Scientific Statement From the American Heart Association. *Circ Res,* 116**,** e99-132.

SMALL, E. M. & OLSON, E. N. 2011. Pervasive roles of microRNAs in cardiovascular biology. *Nature,* 469**,** 336-342.

SONG, Y., XU, Y., WANG, Z., CHEN, Y., YUE, Z., GAO, P., XING, C. & XU, H. 2012. MicroRNA-148b suppresses cell growth by targeting cholecystokinin-2 receptor in colorectal cancer. *Int J Cancer,* 131**,** 1042-51.

SONG, Y. X., YUE, Z. Y., WANG, Z. N., XU, Y. Y., LUO, Y., XU, H. M., ZHANG, X., JIANG, L., XING, C. Z. & ZHANG, Y. 2011. MicroRNA-148b is frequently down-regulated in gastric cancer and acts as a tumor suppressor by inhibiting cell proliferation. *Mol Cancer,* 10**,** 1.

SONKOLY, E., STAHLE, M. & PIVARCSI, A. 2008. MicroRNAs: novel regulators in skin inflammation. *Clin Exp Dermatol,* 33**,** 312-5.

STENVERS, K. L., TURSKY, M. L., HARDER, K. W., KOUNTOURI, N., AMATAYAKUL-CHANTLER, S., GRAIL, D., SMALL, C., WEINBERG, R. A., SIZELAND, A. M. & ZHU, H. J. 2003. Heart and liver defects and reduced transforming growth factor beta2 sensitivity in transforming growth factor beta type III receptor-deficient embryos. *Mol Cell Biol,* 23**,** 4371-85.

SUZUKI, H. I., KATSURA, A., MIHIRA, H., HORIE, M., SAITO, A. & MIYAZONO, K. 2017. Regulation of TGF-beta-mediated endothelial-mesenchymal transition by microRNA-27. *J Biochem,* 161**,** 417-420.

SZULCEK, R., BOGAARD, H. J. & VAN NIEUW AMERONGEN, G. P. 2014. Electric Cell-substrate Impedance Sensing for the Quantification of Endothelial Proliferation, Barrier Function, and Motility. e51300.

TAN, Z., RANDALL, G., FAN, J., CAMORETTI-MERCADO, B., BROCKMAN-SCHNEIDER, R., PAN, L., SOLWAY, J., GERN, J. E., LEMANSKE, R. F., NICOLAE, D. & OBER, C. 2007. Allele-specific targeting of microRNAs to HLA-G and risk of asthma. *Am J Hum Genet,* 81**,** 829-34.

TANG, T., WILSON, P. G., THOMPSON, J. C., NELSON, C., YODER, M. H. & TANNOCK, L. R. 2013. Prevention of TGFβ induction attenuates angII-stimulated vascular biglycan and atherosclerosis in Ldlr−/− mice. *Journal of Lipid Research,* 54**,** 2255-2264.

TELLIDES, G. & POBER, J. S. 2015. Inflammatory and immune responses in the arterial media. *Circ Res,* 116**,** 312-22.

THUM, T., GROSS, C., FIEDLER, J., FISCHER, T., KISSLER, S., BUSSEN, M., GALUPPO, P., JUST, S., ROTTBAUER, W., FRANTZ, S., CASTOLDI, M., SOUTSCHEK, J., KOTELIANSKY, V., ROSENWALD, A., BASSON, M. A., LICHT, J. D., PENA, J. T., ROUHANIFARD, S. H., MUCKENTHALER, M. U., TUSCHL, T., MARTIN, G. R., BAUERSACHS, J. & ENGELHARDT, S. 2008. MicroRNA-21 contributes to myocardial disease by stimulating MAP kinase signalling in fibroblasts. *Nature,* 456**,** 980-4.

UCUZIAN, A. A., GASSMAN, A. A., EAST, A. T. & GREISLER, H. P. 2010. Molecular mediators of angiogenesis. *J Burn Care Res,* 31**,** 158-75.

VAN MEETEREN, L. A. & TEN DIJKE, P. 2012. Regulation of endothelial cell plasticity by TGF-beta. *Cell Tissue Res,* 347**,** 177-86.

VAN ROOIJ, E., QUIAT, D., JOHNSON, B. A., SUTHERLAND, L. B., QI, X., RICHARDSON, J. A., KELM JR, R. J. & OLSON, E. N. 2009. A Family of microRNAs Encoded by Myosin Genes Governs Myosin Expression and Muscle Performance. *Developmental Cell,* 17**,** 662-673.

VAN ROOIJ, E., SUTHERLAND, L. B., QI, X., RICHARDSON, J. A., HILL, J. & OLSON, E. N. 2007. Control of stress-dependent cardiac growth and gene expression by a microRNA. *Science,* 316**,** 575-9.

VAN ROOIJ, E., SUTHERLAND, L. B., THATCHER, J. E., DIMAIO, J. M., NASEEM, R. H., MARSHALL, W. S., HILL, J. A. & OLSON, E. N. 2008. Dysregulation of microRNAs after myocardial infarction reveals a role of miR-29 in cardiac fibrosis. *Proc Natl Acad Sci U S A,* 105**,** 13027-32.

VAN SOLINGEN, C., SEGHERS, L., BIJKERK, R., DUIJS, J. M., ROETEN, M. K., VAN OEVEREN-RIETDIJK, A. M., BAELDE, H. J., MONGE, M., VOS, J. B., DE BOER, H. C., QUAX, P. H., RABELINK, T. J. & VAN

ZONNEVELD, A. J. 2009. Antagomir-mediated silencing of endothelial cell specific microRNA-126 impairs ischemia-induced angiogenesis. *J Cell Mol Med,* 13**,** 1577-85.

VAN THIENEN, J. V., FLEDDERUS, J. O., DEKKER, R. J., ROHLENA, J., VAN IJZENDOORN, G. A., KOOTSTRA, N. A., PANNEKOEK, H. & HORREVOETS, A. J. 2006. Shear stress sustains atheroprotective endothelial KLF2 expression more potently than statins through mRNA stabilization. *Cardiovasc Res,* 72**,** 231-40.

VARGA, J. 2002a. Scleroderma and Smads: Dysfunctional Smad family dynamics culminating in fibrosis. *Arthritis & Rheumatism,* 46**,** 1703-1713.

VARGA, J. 2002b. Scleroderma and Smads: dysfunctional Smad family dynamics culminating in fibrosis. *Arthritis Rheum,* 46**,** 1703-13.

VERRECCHIA, F. & MAUVIEL, A. 2007. Transforming growth factor-beta and fibrosis. *World J Gastroenterol,* 13**,** 3056-62.

VILORIA-PETIT, A., RICHARD, A., ZOURS, S., JARAD, M. & COOMBER, B. L. 2013. Role of Transforming Growth Factor Beta in Angiogenesis. *In:* MEHTA, J. L. & DHALLA, N. S. (eds.) *Biochemical Basis and Therapeutic Implications of Angiogenesis.* New York, NY: Springer New York.

VLACHOS, I. S., ZAGGANAS, K., PARASKEVOPOULOU, M. D., GEORGAKILAS, G., KARAGKOUNI, D., VERGOULIS, T., DALAMAGAS, T. & HATZIGEORGIOU, A. G. 2015. DIANA-miRPath v3.0: deciphering microRNA function with experimental support. *Nucleic Acids Res,* 43**,** W460-6.

WAHLE, E. & WINKLER, G. S. 2013. RNA decay machines: deadenylation by the Ccr4-not and Pan2-Pan3 complexes. *Biochim Biophys Acta,* 1829**,** 561-70.

WANG, R., GHAHARY, A., SHEN, Q., SCOTT, P. G., ROY, K. & TREDGET, E. E. 2000. Hypertrophic scar tissues and fibroblasts produce more transforming growth factor-beta1 mRNA and protein than normal skin and cells. *Wound Repair Regen,* 8**,** 128-37.

WANG, S., AURORA, A. B., JOHNSON, B. A., QI, X., MCANALLY, J., HILL, J. A., RICHARDSON, J. A., BASSEL-DUBY, R. & OLSON, E. N. 2008. The Endothelial-Specific MicroRNA miR-126 Governs Vascular Integrity and Angiogenesis. *Developmental Cell,* 15**,** 261-271.

WINTER, J., JUNG, S., KELLER, S., GREGORY, R. I. & DIEDERICHS, S. 2009. Many roads to maturity: microRNA biogenesis pathways and their regulation. *Nat Cell Biol,* 11**,** 228-34.

WRANA, J. L., ATTISANO, L., WIESER, R., VENTURA, F. & MASSAGUE, J. 1994. Mechanism of activation of the TGF-beta receptor. *Nature,* 370**,** 341-7.

WU, F., YANG, Z. & LI, G. 2009. Role of specific microRNAs for endothelial function and angiogenesis. *Biochem Biophys Res Commun,* 386**,** 549-53.

WU, Q., HAN, L., YAN, W., JI, X., HAN, R., YANG, J., YUAN, J. & NI, C. 2016. miR-489 inhibits silica-induced pulmonary fibrosis by targeting MyD88 and Smad3 and is negatively regulated by lncRNA CHRF. *Sci Rep,* 6**,** 30921.

WU, Y., LIU, G. L., LIU, S. H., WANG, C. X., XU, Y. L., YING, Y. & MAO, P. 2012. MicroRNA-148b enhances the radiosensitivity of non-Hodgkin's Lymphoma cells by promoting radiation-induced apoptosis. *J Radiat Res,* 53**,** 516-25.

XI, Q., WANG, Z., ZAROMYTIDOU, A. I., ZHANG, X. H., CHOW-TSANG, L. F., LIU, J. X., KIM, H., BARLAS, A., MANOVA-TODOROVA, K., KAARTINEN, V., STUDER, L., MARK, W., PATEL, D. J. & MASSAGUE, J. 2011. A poised chromatin platform for TGF-beta access to master regulators. *Cell,* 147**,** 1511-24.

XIE, J. L., QI, S. H., PAN, S., XU, Y. B., LI, T. Z., LIU, X. S. & LIU, P. 2008. Expression of Smad protein by normal skin fibroblasts and hypertrophic scar fibroblasts in response to transforming growth factor beta1. *Dermatol Surg,* 34**,** 1216-24; discussion 1224-5.

YAN, Q., CHEN, J., LI, W., BAO, C. & FU, Q. 2016. Targeting miR-155 to Treat Experimental Scleroderma. *Scientific Reports,* 6**,** 20314.

YANG, B., LIN, H., XIAO, J., LU, Y., LUO, X., LI, B., ZHANG, Y., XU, C., BAI, Y., WANG, H., CHEN, G. & WANG, Z. 2007. The muscle-specific microRNA miR-1 regulates cardiac arrhythmogenic potential by targeting GJA1 and KCNJ2. *Nat Med,* 13**,** 486-491.

YANG, J., BROWN, M. E., ZHANG, H., MARTINEZ, M., ZHAO, Z., BHUTANI, S., YIN, S., TRAC, D., XI, J. J. & DAVIS, M. E. 2017. High-throughput screening identifies microRNAs that target Nox2 and improve function after acute myocardial infarction. *Am J Physiol Heart Circ Physiol,* 312**,** H1002-h1012.

YANG, M., HAASE, A. D., HUANG, F. K., COULIS, G., RIVERA, K. D., DICKINSON, B. C., CHANG, C. J., PAPPIN, D. J., NEUBERT, T. A., HANNON, G. J., BOIVIN, B. & TONKS, N. K. 2014. Dephosphorylation of tyrosine 393 in argonaute 2 by protein tyrosine phosphatase 1B regulates gene silencing in oncogenic RAS-induced senescence. *Mol Cell,* 55**,** 782-90.

YI, R., O'CARROLL, D., PASOLLI, H. A., ZHANG, Z., DIETRICH, F. S., TARAKHOVSKY, A. & FUCHS, E. 2006. Morphogenesis in skin is governed by discrete sets of differentially expressed microRNAs. *Nat Genet,* 38**,** 356-62.

YU, J., PENG, H., RUAN, Q., FATIMA, A., GETSIOS, S. & LAVKER, R. M. 2010. MicroRNA-205 promotes keratinocyte migration via the lipid phosphatase SHIP2. *Faseb j,* 24**,** 3950-9.

YU, Z. C., HUANG, Y. F. & SHIEH, S. Y. 2016. Requirement for human Mps1/TTK in oxidative DNA damage repair and cell survival through MDM2 phosphorylation. *Nucleic Acids Res,* 44**,** 1133-50.

ZEISBERG, E. M., POTENTA, S., XIE, L., ZEISBERG, M. & KALLURI, R. 2007a. Discovery of endothelial to mesenchymal transition as a source for carcinoma-associated fibroblasts. *Cancer Res,* 67**,** 10123-8.

ZEISBERG, E. M., POTENTA, S. E., SUGIMOTO, H., ZEISBERG, M. & KALLURI, R. 2008. Fibroblasts in kidney fibrosis emerge via endothelial-to-mesenchymal transition. *J Am Soc Nephrol,* 19**,** 2282-7.

ZEISBERG, E. M., TARNAVSKI, O., ZEISBERG, M., DORFMAN, A. L., MCMULLEN, J. R., GUSTAFSSON, E., CHANDRAKER, A., YUAN, X., PU, W. T., ROBERTS, A. B., NEILSON, E. G., SAYEGH, M. H., IZUMO, S. & KALLURI, R. 2007b. Endothelial-to-mesenchymal transition contributes to cardiac fibrosis. *Nat Med,* 13**,** 952-61.

ZEISBERG, E. M., TARNAVSKI, O., ZEISBERG, M., DORFMAN, A. L., MCMULLEN, J. R., GUSTAFSSON, E., CHANDRAKER, A., YUAN, X., PU, W. T., ROBERTS, A. B., NEILSON, E. G., SAYEGH, M. H., IZUMO, S. & KALLURI, R. 2007c. Endothelial-to-mesenchymal transition contributes to cardiac fibrosis. *Nat Med,* 13**,** 952-961.

ZENG, X., HUANG, C., SENAVIRATHNA, L., WANG, P. & LIU, L. 2017. miR-27b inhibits fibroblast activation via targeting TGFbeta signaling pathway. *BMC Cell Biol,* 18**,** 9.

ZERNECKE, A., BIDZHEKOV, K., NOELS, H., SHAGDARSUREN, E., GAN, L., DENECKE, B., HRISTOV, M., KÖPPEL, T., JAHANTIGH, M. N., LUTGENS, E., WANG, S., OLSON, E. N., SCHOBER, A. & WEBER, C. 2009. Delivery of MicroRNA-126 by Apoptotic Bodies Induces CXCL12-Dependent Vascular Protection. *Science Signaling,* 2**,** ra81-ra81.

ZHAO, G., ZHANG, J. G., LIU, Y., QIN, Q., WANG, B., TIAN, K., LIU, L., LI, X., NIU, Y., DENG, S. C. & WANG, C. Y. 2013. miR-148b functions as a tumor suppressor in pancreatic cancer by targeting AMPKalpha1. *Mol Cancer Ther,* 12**,** 83-93.

ZHAO, Y., RANSOM, J. F., LI, A., VEDANTHAM, V., VON DREHLE, M., MUTH, A. N., TSUCHIHASHI, T., MCMANUS, M. T., SCHWARTZ, R. J. & SRIVASTAVA, D. 2007. Dysregulation of cardiogenesis, cardiac conduction, and cell cycle in mice lacking miRNA-1-2. *Cell,* 129**,** 303-17.

ZHAO, Y., SAMAL, E. & SRIVASTAVA, D. 2005. Serum response factor regulates a muscle-specific microRNA that targets Hand2 during cardiogenesis. *Nature,* 436**,** 214-20.

ZHU, S., WANG, W., CLARKE, D. C. & LIU, X. 2007. Activation of Mps1 promotes transforming growth factor-beta-independent Smad signaling. *J Biol Chem,* 282**,** 18327-38.

APPENDIX I: PERMISSIONS

nature publishing group

Thank you for your order!

Dear Mr. Vladislav Miscianinov,

Thank you for placing your order through Copyright Clearance Center's RightsLink® service.

Order Summary

Order Date:	May 3, 2017
Order Number:	4101370620605
Publication:	Nature
Title:	Molecular mechanisms and clinical applications of angiogenesis
Type of Use:	reuse in a dissertation / thesis
Order Total:	0.00 GBP

View or print complete details of your order and the publisher's terms and conditions.

Sincerely,

Copyright Clearance Center

APPENDIX II: WESTERN BLOT SCANS

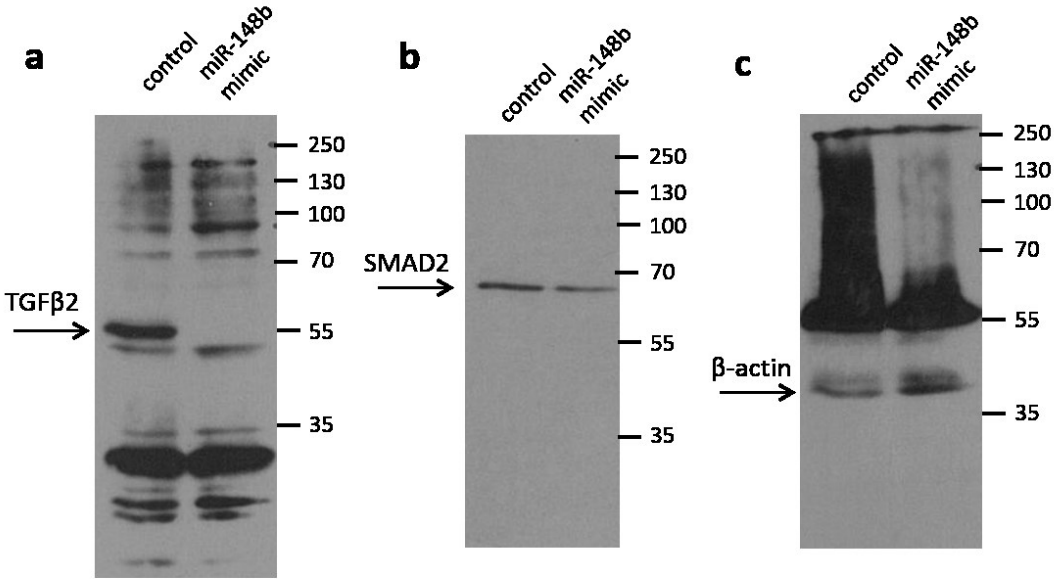

a. TGFβ2 MW=50 kDa; **b.** SMAD2 MW=60 kDa; **c.** β-actin MW=42 kDa

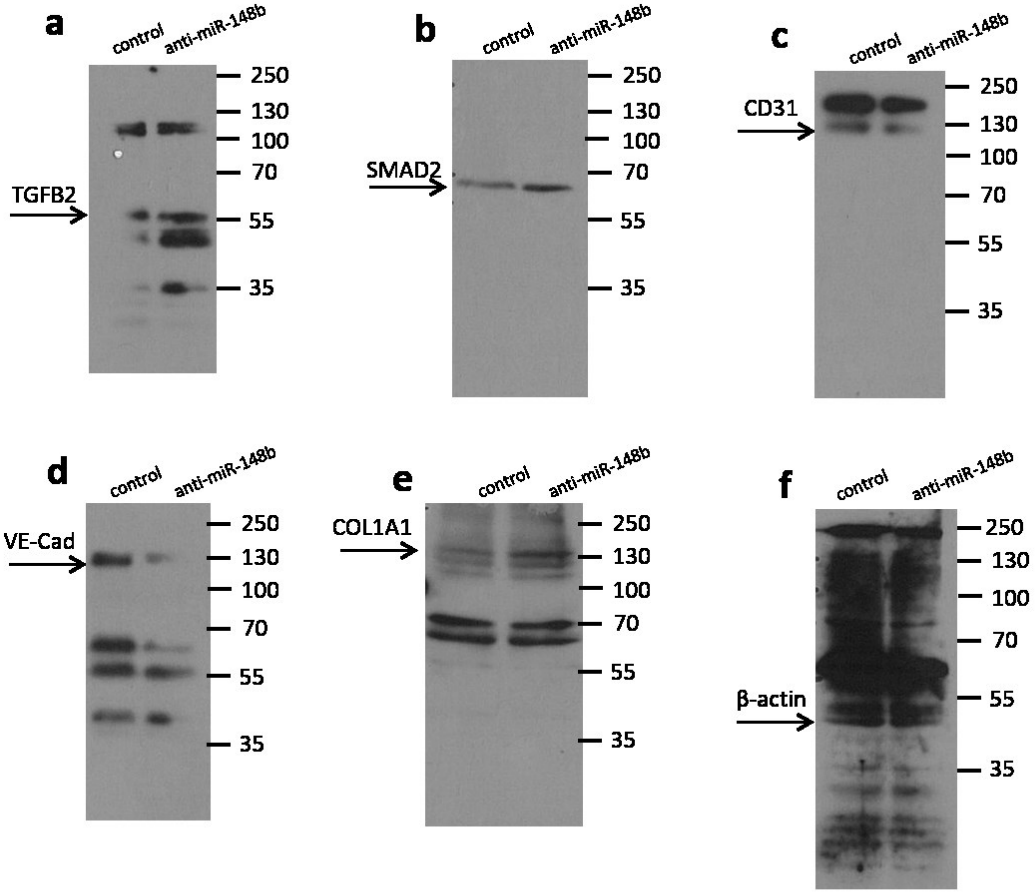

a. TGFB2 MW=50 kDa; **b.** SMAD2 MW=60 kDa; **c.** CD31 MW=130 kDa; **d.** VE-Cadherin MW=130 kDa; **e.** COL1A1 MW=139 kDa; **f.** β-actin MW=42 kDa

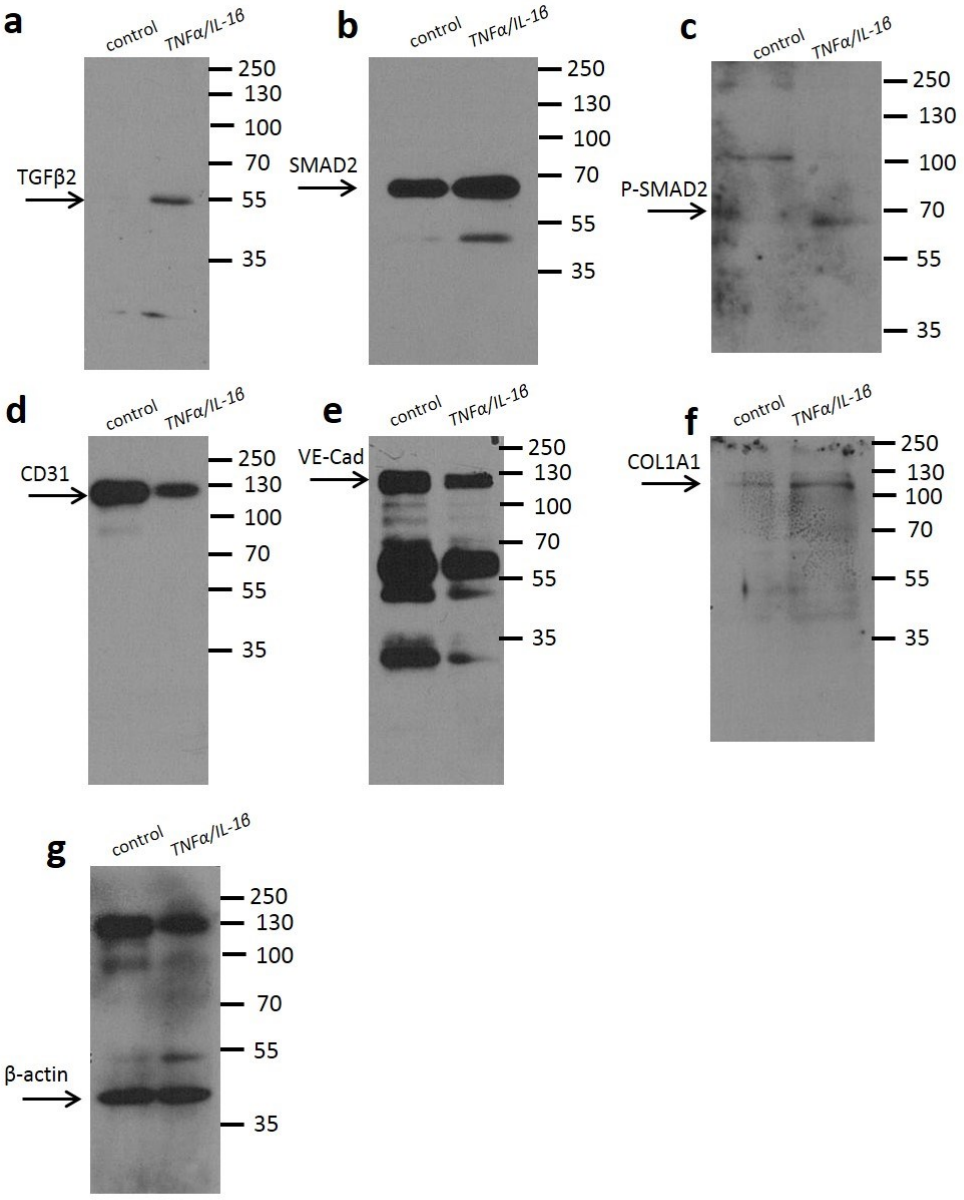

a. TGFβ2 MW=50 kDa; **b.** SMAD2 MW=60 kDa; **c.** P-SMAD2 MW=60 kDa; **d.** CD31 MW=130 kDa; **e.** VE-Cadherin MW=130 kDa; **f.** COL1A1 MW=115 kDa; **g.** β-actin MW=42 kDa

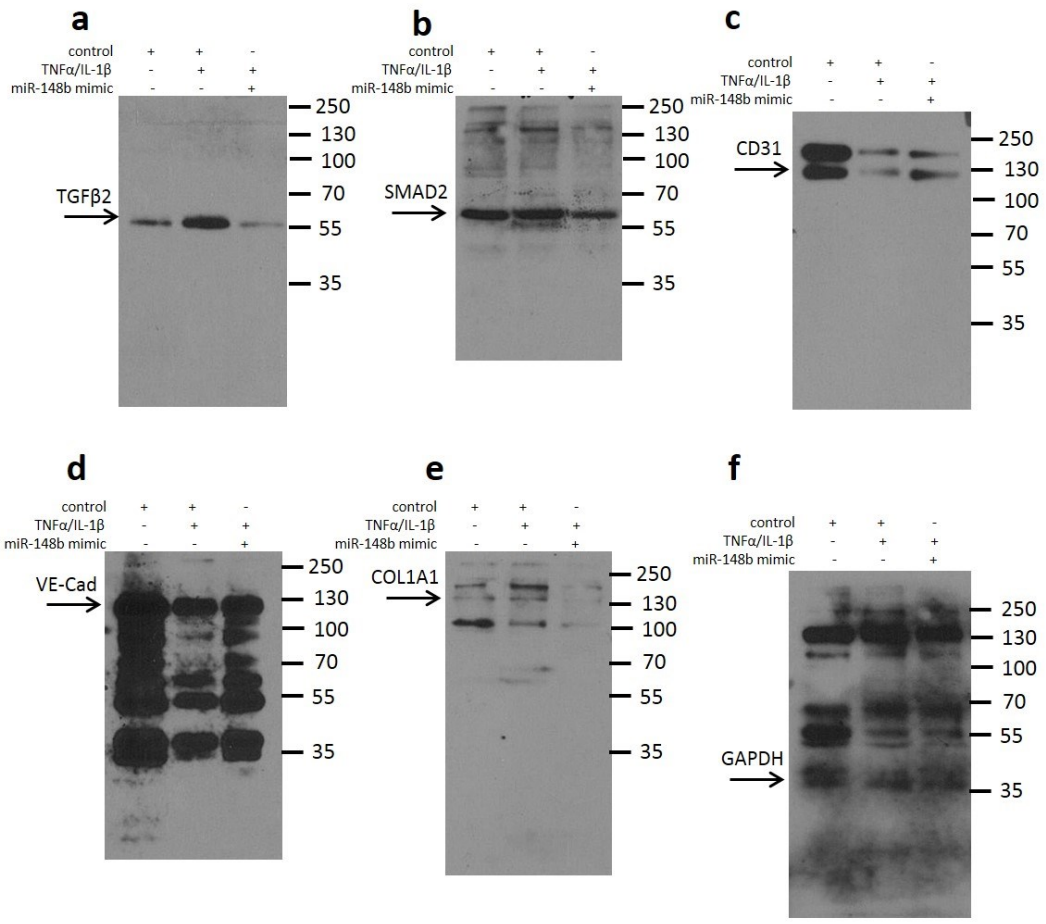

a. TGFβ2 MW=50 kDa; **b.** SMAD2 MW=60 kDa; **c.** CD31 MW=130 kDa; **d.** VE-Cadherin MW=130 kDa; **e.** COL1A1 MW=139 kDa **f.** GAPDH MW=37 kDa

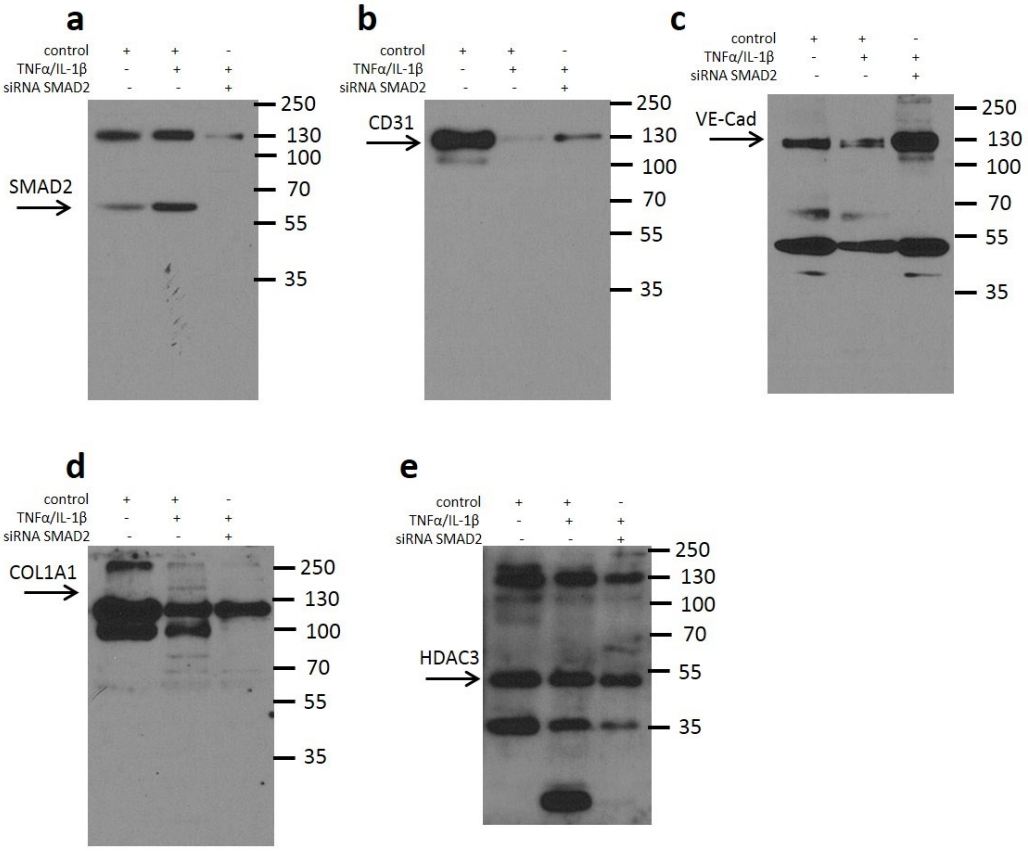

a. SMAD2 MW=60 kDa; **b.** CD31 MW=130 kDa; **c.** VE-Cadherin MW=130 kDa; **d.** COL1A1 MW=139 kDa **e.** HDAC3 MW=49 kDa

APPENDIX III: PUBLICATION

Molecular Therapy
Original Article

MicroRNA-148b Targets the TGF-β Pathway to Regulate Angiogenesis and Endothelial-to-Mesenchymal Transition during Skin Wound Healing

Vladislav Miscianinov,[1] Andrea Martello,[1] Lorraine Rose,[1] Elisa Parish,[1] Ben Cathcart,[1] Tijana Mitić,[1] Gillian A. Gray,[1] Marco Meloni,[1] Ayman Al Haj Zen,[2] and Andrea Caporali[1]

[1]University/British Heart Foundation Centre for Cardiovascular Science, QMRI, University of Edinburgh, Edinburgh EH16 4TJ, UK; [2]British Heart Foundation Centre of Research Excellence, Wellcome Trust Centre for Human Genetics, Division of Cardiovascular Medicine, Radcliffe Department of Medicine, University of Oxford, Oxford OX3 7BN, UK

Transforming growth factor beta (TGF-β) is crucial for regulation of the endothelial cell (EC) homeostasis. Perturbation of TGF-β signaling leads to pathological conditions in the vasculature, causing cardiovascular disease and fibrotic disorders. The TGF-β pathway is critical in endothelial-to-mesenchymal transition (EndMT), but a gap remains in our understanding of the regulation of TGF-β and related signaling in the endothelium. This study applied a gain- and loss-of function approach and an *in vivo* model of skin wound healing to demonstrate that miR-148b regulates TGF-β signaling and has a key role in EndMT, targeting *TGFB2* and *SMAD2*. Overexpression of miR-148b increased EC migration, proliferation, and angiogenesis, whereas its inhibition promoted EndMT. Cytokine challenge decreased miR-148b levels in ECs while promoting EndMT through the regulation of SMAD2. Finally, in a mouse model of skin wound healing, delivery of miR-148b mimics promoted wound vascularization and accelerated closure. In contrast, inhibition of miR-148b enhanced EndMT in wounds, resulting in impaired wound closure that was reversed by SMAD2 silencing. Together, these results demonstrate for the first time that miR-148b is a key factor controlling EndMT and vascularization. This opens new avenues for therapeutic application of miR-148b in vascular and tissue repair.

INTRODUCTION

It is well known that the transforming growth factor beta (TGF-β) signaling pathway plays a crucial role in the regulation of vascular function in health and disease.[1] During canonical activation of the TGF-β pathway, TGF-β binds to the heteromeric receptor complex formed by the activin-like kinase 5 (ALK5, also known as the TGF-β type I receptor, TGFBR1) and the TGF-β type II receptor (TGFBR2). Phosphorylation of ALK5 by TGFBR2 kinase activates its catalytic kinase domain allowing the activation of the receptor-regulated Smads (i.e., SMAD2 and SMAD3), which translocate to the nucleus, where they regulate the transcription of specific target genes.[2]

Activation of the TGF-β pathway in endothelial cells (ECs) during angiogenesis is reported to have pro-angiogenic, as well as anti-angiogenic effects. Discrepancies might be explained by the variations in ligand concentration, culture conditions, cell type, and developmental or disease stage *in vivo*. In addition, the effects of TGF-β signaling depend on the interplay between different members of the TGF-β family.[3] Accumulating evidence over the past few years is revealing the role of the TGF-β pathway in regulation of cellular plasticity, thus including the control of EC phenotype.[4] EC plasticity is represented by the endothelial-to-mesenchymal transition (EndMT), allowing the endothelium to not only alter its fate but to provide a potentially important additional source of mesenchymal cells for participation in fibrosis.[5,6] During the EndMT process, ECs lose their endothelial specification and acquire a mesenchymal-like phenotype. Specifically, loss of vascular endothelial cadherin (VE-cadherin) and platelet-EC adhesion molecule 1 (PECAM-1, CD31) are observed along with elevated expression of α-smooth muscle actin (α-SMA), vimentin (VIM), N-cadherin, and extracellular matrix (ECM) proteins like collagen type I and III.[7] ECs undergoing EndMT also exhibit cytoskeletal rearrangement, resulting in a change in cell polarity whereby they acquire a stretched and more fibroblast-like morphology.[7] Recently, EndMT has been reported to play an important role during the embryonic stages of cardiac and pulmonary artery development.[8,9] In addition, EndMT has a pathological role through promoting tumor growth and progression,[10] contributing to cardiac[11] and renal fibrosis[12] as well as vascular remodelling[13] and atherosclerosis.[14]

MicroRNAs (miRNAs) are post-transcriptional inhibitory regulators of gene expression that bind to complementary mRNA transcripts.[15] Their capacity to simultaneously inhibit many different mRNAs

Received 22 September 2017; accepted 4 May 2018;
https://doi.org/10.1016/j.ymthe.2018.05.002.

Correspondence: Andrea Caporali, PhD, University/British Heart Foundation Centre for Cardiovascular Science, The Queen's Medical Research Institute, University of Edinburgh, Edinburgh EH16 4TJ, UK.
E-mail: a.caporali@ed.ac.uk

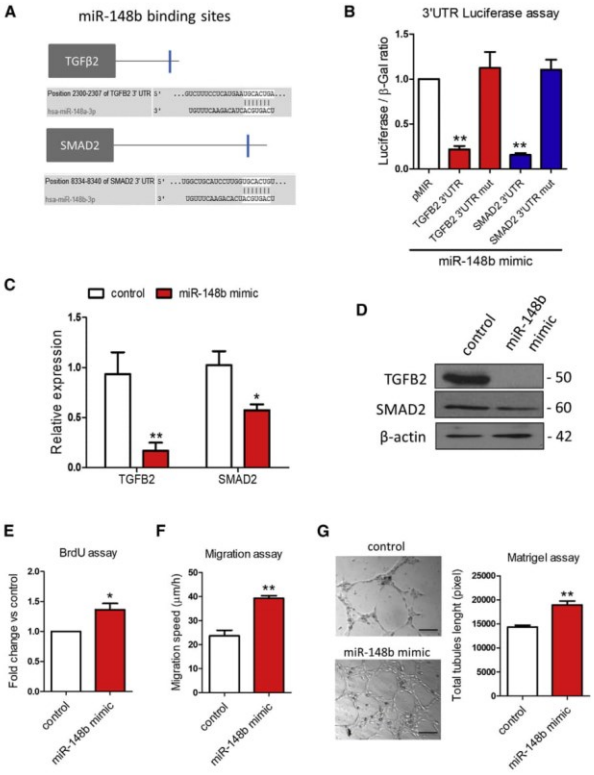

Figure 1. TGFB2 and SMAD2 Are miR-148b Target Genes

(A) *In silico* analysis of TGFB2 and SMAD2 3′ UTR with TargetScan identifies putative miR-148b-binding sites (blue). (B) Luciferase activity at 48 hr post-co-transfection of HEK293T cells with both miR-148b and the following plasmids: 3′ UTR-TGFB2, 3′ UTR-SMAD2, and pMIR as empty plasmid (n = 5). (C) Relative gene expression of TGFB2 and SMAD2 after miR-148b overexpression (n = 3). (D) Western blot analysis of TGFB2 and SMAD2 in samples transfected with miR-148b mimic versus control; β-actin is used as a loading control (n = 3); HUVECs were transfected with miR-148b mimic or control oligonucleotides for 48 hr. (E) EC proliferation was analyzed by BrdU incorporation assay (n = 5). (F) EC migration reported as migration speed (μm/hr) (n = 5). (G) Representative Matrigel assay images and quantification as total tubule length (n = 5); values are means ± SEM. *$p < 0.05$; **$p < 0.01$ versus control and pMIR vector in experiment b. Unpaired two-tailed Student's t test was applied.

allows for efficient amplification of biological responses.[16] Recent studies have revealed important roles for miRNAs as therapeutic tools in regulating physiological and pathological angiogenesis, through the regulation of EC function (reviewed in Caporali and Emanueli[17,18]).

Several miRNAs have been identified that target elements of the TGF-β/Smad signaling axis[19] and, more recently, contribute to the EndMT process.[20] Although the role of TGF-β signaling in the regulation and maintenance of adult EC homeostasis and plasticity is now well established,[2] less is known about the mechanisms that regulate the TGF-β signaling pathway. Using miRNA target-prediction analysis, we have found that miR-148b targets are strongly enriched for the components of TGF-β pathway. The present study aims to investigate how this miRNA regulates EC function and how it impacts on TGF-β signaling in these cells. miR-148b, together with miR-148a and miR-152, comprises the miR-148/152 family.[21] Although aberrant expression of the miR-148/152 family has been observed in tumors, and in non-tumor diseases such as immunoglobulin A (IgA) nephropathy[22] and atherosclerotic lesions;[23] its function has not been explored in ECs.

Here, we establish that in ECs, miR-148b plays a critical role in promoting angiogenesis and that its inhibition promotes EndMT process through regulation of the target genes, *TGFB2* and *SMAD2*. Furthermore, we demonstrate, in an *in vivo* model of wound healing, that overexpression of miR-148b increases vascularization and accelerates wound closure, whereas miR-148b inhibition leads to an enhanced EndMT in the wound, resulting in impaired closure.

RESULTS

miR-148b Targets TGFB2 and SMAD2 and Regulates EC Functions

Gene set enriched analysis (miRpath[24]) has identified components of the TGF-β pathway as putative targets of miR-148b (Figure S1A). Moreover, the TargetScan algorithm[25] predicted *TGFB2* and *SMAD2* to be direct targets of miR-148b (Figure 1A). Accordingly, both gene targets were predicted to contain a single conserved binding sequence for miR-148b in their 3′ UTR (Figure 1A). To investigate whether miR-148b directly binds the 3′ UTR of *TGFB2* and *SMAD2*, we performed a luciferase reporter assay in which luciferase reporter gene was fused to the wild-type 3′ UTR of *TGFB2* or *SMAD2*,

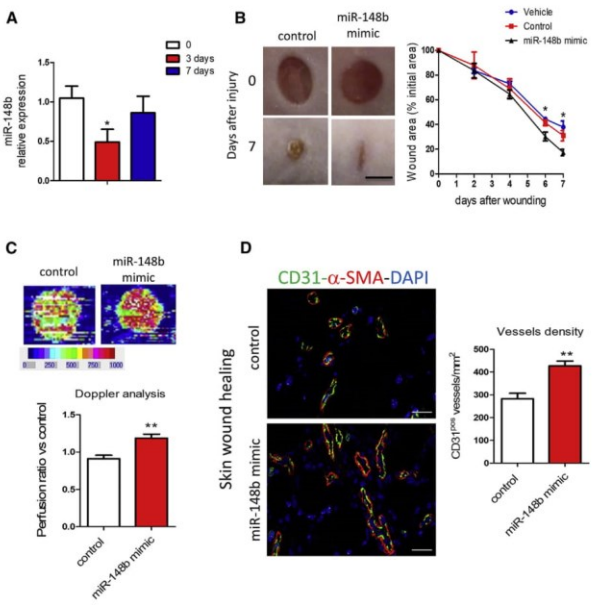

Figure 2. miR-148b Regulates Angiogenesis and Accelerates Wound Healing

(A) Expression of miR-148b at 3 and 7 days after wounding, relative to unwounded skin (n = 5). (B) Left, representative images of control and miR-148b mimic-treated wounds at 0 and 7 days post-wound-injury; scale bar, 5 mm. Right, the level of wound closure is expressed as a percentage of initial wound area (n = 8). (C) Representative color laser Doppler images are taken at 5 days post-wounding. The chart shows the level of wound perfusion in mice (calculated as the ratio between treated and control blood flow; n = 8 per group). (D) Left, immunohistochemistry for CD31 and α-SMA in miR-148b mimic-treated or control-oligonucleotide-treated skin wounds; scale bars, 100 μm (magnification 400×). Right, quantification of vessel density expressed as CD31-positive vessels/mm^2 (n = 8). Values are means ± SEM. *p < 0.05; **p < 0.01 versus control. Unpaired two-tailed Student's t test was applied.

respectively. Overexpression of miR-148b decreased luciferase activity for each of the putative target genes, whereas mutation of the binding sites restored it (Figures 1B and S1B). In addition, miR-148b mimics, at the dose of 25 nM, reduced both target gene mRNA (Figures 1C, S1C, and S1D) and protein levels (Figure 1D). Notably, miR-148b upregulation did not affect the expression of *ACVR1* and *ROCK1*, previously identified target genes of miR-148/152 cluster[26,27] (Figure S1E). We then investigated the role of miR-148b on the functional properties of ECs. miR-148b overexpression significantly increased the proliferation of human umbilical vein EC (HUVECs), as demonstrated by bromodeoxyuridine (BrdU) incorporation (Figure 1E). The migration capacity of HUVECs transfected with a miR-148b mimic was also significantly elevated (Figure 1F), along with their ability to form tubes in an *in vitro* Matrigel assay (Figure 1G).

miR-148b Promotes Angiogenesis and Accelerates Skin Wound Healing

To follow up the *in vitro* results, we asked whether miR-148b could influence angiogenesis in a mouse model of wound healing. In this model, following skin puncture, the peak of neovascularization occurs between days 4 and 8 after wounding. Vessel density generally returns to initial levels around 3 weeks later. Thus, before, and at the peak of vascularization, this model characterizes the angiogenic response.[28]

Three days after wound injury, the expression of miR-148b was found to be downregulated, going back to basal level after 7 days (Figure 2A). The analysis of Cy3-labeled miR-148b mimics in the wounds demonstrated that the mimics could reach the endothelium *in vivo* (Figure S2A).

Topical delivery of miR-148b mimics starting at day 3 after wounding increased the expression of miR-148b and decreased the expression levels of both targets at day 7 after wounding (Figure S2B). Moreover, miR-148b overexpression also accelerated wound closure (Figure 2B) and led to a significant increase in wound perfusion detected by Doppler analysis (Figure 2C) and vessel density (Figure 2D). These data indicate that treatment with miR-148b mimics promotes angiogenesis and accelerates wound healing in *vivo*.

Loss of Function of miR-148b Promotes Endothelial-Mesenchymal Transition

To analyze the phenotypic effect of miR-148b loss-of-function on ECs, HUVECs were transfected with anti-miR-148b oligonucleotides (Figure S1F). The inhibition of miR-148b expression decreased the proliferation of HUVECs (Figure 3A); however, it did not cause a change in EC migration or tubulogenesis (Figures 3B and 3C). Next, we examined the capacitance of the EC membrane, changes in which reflect structural changes in the plasma membrane and rearrangement of the cytoskeleton (the capacitance of ECs is ~1.1 μF/cm^2, whereas for mesenchymal cells, it is ~3.0 μF/cm^2).[29] Knockdown of miR-148b in ECs increased the membrane capacitance, consistent with the occurrence of transition from an endothelial-to-mesenchymal phenotype (Figure 3D). In line with this, miR-148b loss-of-function increased the expression of its target genes, *TGFB2* and *SMAD2* and the expression of collagen 1A1

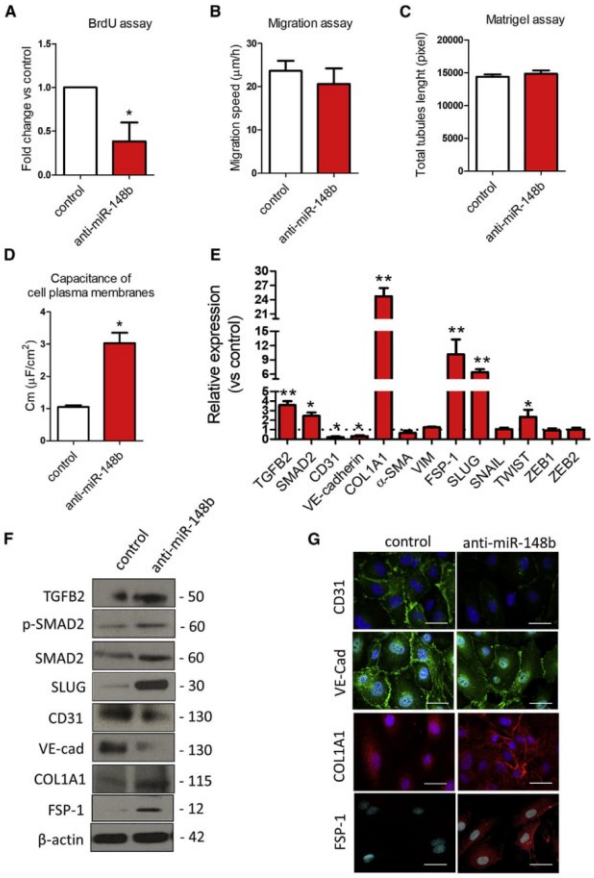

Figure 3. Inhibition of miR-148b Induces EndMT

HUVECs were transfected with anti-miR-148b or control oligonucleotides for 48 hr. (A) EC proliferation was analyzed by BrdU incorporation assay (n = 5). (B) EC migration reported as migration speed (μm/hr) (n = 5). (C) Matrigel assay quantification as total tubules length (n = 5). (D) Quantification of cell membrane capacitance in HUVEC knockdown for miR-148b or control (n = 5). (E) Relative gene expression of TGFB2, SMAD2, CD31, VE-cadherin COL1A1, SNAIL, SLUG, TWIST, ZEB1/2, VIM, FSP-1, and α-SMA (n = 3). (F) Western blot analysis of TGFB2, SMAD2, p-SMAD2, SLUG, CD31, VE-cadherin, COL1A1, and FSP-1; β-actin is used as a loading control (n = 3). (G) Immunofluorescence images showing localization of CD31, VE-cadherin, COL1A1, and FSP-1 in anti-miR-148b- or control-transfected cells (n = 3); scale bars, 50 μm (magnification 400×). Values are means ± SEM. *$p < 0.05$; **$p < 0.01$ versus control. Unpaired two-tailed Student's t test was applied.

(*COL1A1*) and fibroblast-specific protein 1 (*FSP-1*) but decreased the expression of *CD31* and *VE-Cadherin*, without detectable changes in *α-SMA* or *VIM* levels (Figure 3E). Moreover, expression analysis of the transcription factors involved in EndMT, such as *SNAIL*, *SLUG*, *TWIST*, and *ZEB1/2*, showed strong upregulation of SLUG after miR-148b inhibition (Figure 3E). Western blot analysis confirmed the upregulation of TGFB2, SMAD2 and its phosphorylation, the appearance of mesenchymal marker COL1A1, FSP-1, along with suppression of CD31 and endothelial VE-cadherin and the upregulation of SLUG in ECs lacking miR-148b (Figure 3F). Furthermore, immunofluorescence staining revealed that control-treated HUVECs display a typically rounded/cobblestone morphology that was lost in anti-miR-148b-treated cells. Anti-miR-148b treatment also resulted in a pronounced decrease in CD31 and VE-cadherin and increase in COL1A1 and FSP-1 immunoreactivity (Figure 3G). Taken together, these data show that loss of miR-148b function leads to EndMT.

Pro-inflammatory Cytokines Promote EndMT via Downregulation of miR-148b

It has been reported that EndMT is closely linked to inflammation and high levels of pro-inflammatory cytokines.[30] To investigate whether cytokine treatment could reduce the expression of miR-148b, thus triggering EndMT, we treated HUVECs with TNF-α, interleukin-1β (IL-1β), TGF-β1, or TGF-β2, as well as with a combination of cytokines for 6 days (Figures S3A–S3D). Interestingly, we found that only the combination of TNF-α- and IL-1β-inhibited miR-148b expression after 3 days, with its strongest downregulation at 6 days (Figure 4A). This was accompanied by significantly increased expression of TGFB2 and SMAD2, at both mRNA and protein levels (Figures 4B and 4C), phosphorylation of SMAD2 (Figure 4C), and increased secretion of TGF-β2 (Figure S4A). To test whether cytokine-induced miR-148b downregulation governs EndMT, we analyzed endothelial- and fibroblast-specific markers after the treatment with TNF-α/IL-1β. Consistent with enhancement of EndMT, both mRNA and protein expression of the endothelial markers CD31 and VE-cadherin were decreased (Figures 4B and 4C). These findings were further

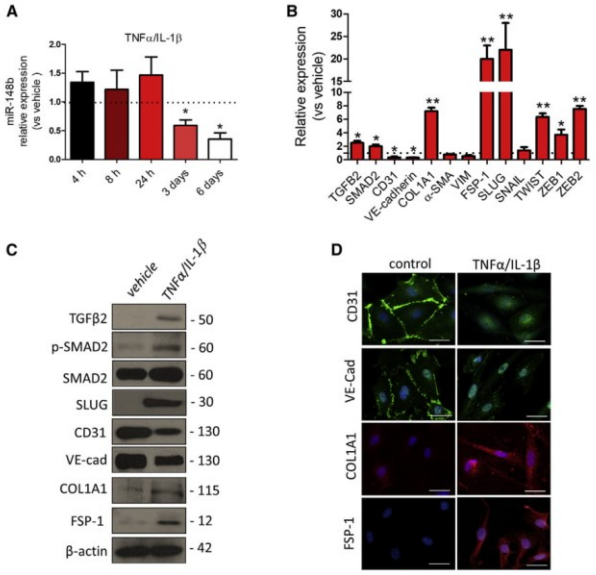

Figure 4. Chronic Inflammation Downregulates miR-148b in ECs

HUVECs were treated with a combination of TNF-α and IL-1β for 6 days. (A) miR-148b expression levels after TNF-α/IL-1β treatment. (B) Relative expression of miR-148b, TGFB2, SMAD2, CD31, VE-cadherin, SNAIL, SLUG, TWIST, ZEB1/2, VIM, FSP-1, α-SMA, and COL1A1. (C) Western blot analysis of TGFB2, p-SMAD2, SMAD2, CD31, VE-cadherin, SLUG, FSP-1, and COL1A1; β-actin was used as a loading control. (D) Immunofluorescence images showing localization of CD31, VE-cadherin, COL1A1, and FSP-1 in TNF-α/IL-1β-treated cells; scale bars, 50 μm (magnification 400×). Values are means ± SEM. *$p < 0.05$; **$p < 0.01$ versus vehicle. Unpaired two-tailed Student's t test was applied.

confirmed by immunofluorescence staining of HUVECs treated with TNF-α/IL-1β (Figure 4D). In contrast, mRNA expression and protein levels of fibroblast-specific COL1A1 and FSP-1 (Figures 4B and 4C) were increased 6 days after TNF-α/IL-1β treatment, corroborated by an increase in cellular and extracellular immunofluorescence signals (Figure 4D). Moreover, upregulation of SLUG was confirmed at mRNA and protein levels in cytokine-treated ECs (Figures 4B and 4C). Notably, HUVECs cultured for 14 days in the presence of TNF-α/IL-1β maintained the downregulation of miR-148b and acquired expression of α-SMA, in addition to other markers of EndMT (Figures S5A and S5B).

Finally, we analyzed the expression of let-7b and miR-20a, miRNAs involved in the EndMT process.[31,32] While miR-20a and let-7b were both downregulated *in vivo* during wound healing (Figure S6A), only miR-20a was downregulated by cytokine treatment in ECs (Figure S6B).

miR-148b Overexpression Rescues Cytokine-Mediated EndMT

We next examined whether miR-148b gain of function could rescue the endothelial phenotype and reduce cytokine-induced EndMT. In response to a miR-148b mimic, we observed a decreased in TGFB2, SMAD2, SLUG, FSP-1, COL1A1, and a reduced phosphorylation of SMAD2 in HUVECs treated with TNF-α/IL-1β, whereas expression of CD31 and VE-cadherin at mRNA and protein levels was rescued (Figures S4B, S7A, and 5A). The maintenance of endothelial markers CD31 and VE-cadherin on EC membrane and the decrease of COL1A1 and FSP-1 staining was also confirmed by immunostaining (Figure 5B).

To better understand the contribution of target genes in this model of EndMT, we interfered with the TGF-β pathway using a TGF-β receptor (ALK5) inhibitor (SB431542) or small interfering RNA (siRNA) for SMAD2. Knockdown of SMAD2 in HUVECs treated with cytokines partially restored *CD31* and *VE-cadherin* expression, whereas blocking of ALK5 reduced the level of SMAD2 phosphorylation but did not rescue endothelial marker expression (Figures S7B and S7C). We next confirmed at protein level that the SMAD2 siRNA partially restores the level of CD31 and VE-cadherin in cytokine-treated ECs, whereas decreased SLUG, FSP-1, and COL1A1 (Figure 5C). Changes in expression of CD31 and VE-cadherin, FSP-1, and COL1A1 were further confirmed by immunocytochemistry (Figure 5D).

miR-148b Loss of Function Attenuates Wound Repair by Enabling EndMT in a Skin-Wound-Healing Model

Next, we investigated whether miR-148b-mediated EndMT also occurs *in vivo* in the mouse model of skin wound healing. Delivery of anti-miR-148b or control oligonucleotides immediately after wounding and every 2 days thereafter resulted in increased mRNA expression of *TGFB2* and *SMAD2* targets in the wounds (Figure S8A). Macroscopic analysis showed that wound closure was markedly attenuated in anti-miR-148b-treated wounds (Figure 6A) without influencing wound perfusion and vessel density (Figures S7C and S7D). There was not a significant improvement in wound closure detected following SMAD2 siRNA only (Figures 6A and S8B). Next, to investigate EndMT at the wound edge, wounds were stained with CD31 and FSP-1 and SLUG antibodies (Figures 6B and 6C). Confocal analysis showed that while

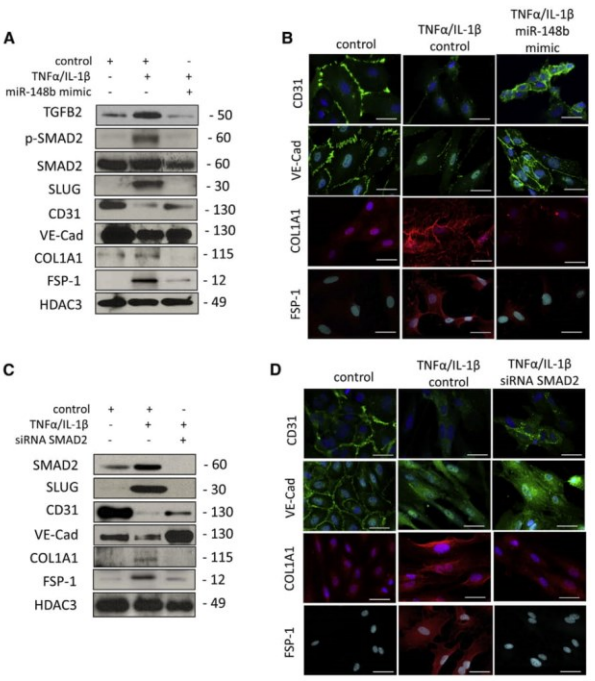

Figure 5. Overexpression of miR-148b Rescues Cytokine-Induced EndMT

HUVECs were transfected with miR-148b mimic, SMAD2 siRNA, or control and treated with TNF-α/IL-1β for 6 days. (A) Representative western blot analysis of TGFB2, SMAD2, p-SMAD2 CD31, VE-cadherin, SLUG, FSP-1, and COL1A1; HDAC3 is used as a loading control (n = 3). (B) Immunofluorescence images showing localization of CD31, VE-cadherin, COL1A1, and FSP-1 in miR-148b- or control-transfected HUVECS and/or treated with TNF-α/IL-1β; scale bars, 50 μm (magnification 400×) (n = 3). (C) Representative western blot analysis of SMAD2, CD31, VE-cadherin, SLUG, COL1A1, and FSP-1; HDAC3 is used as a loading control (n = 3). (D) Immunofluorescence images showing localization of CD31, VE-cadherin, COL1A1, and FSP-1 in SMAD2 siRNA or control-transfected HUVECS and/or treated with TNF-α/IL-1β; scale bars, 50 μm (magnification 400×) (n = 3).

control-oligonucleotide-treated wounds contained only CD31-positive vessels, anti-miR-148b-treated wounds were comprised of CD31-FSP-1 or CD31-SLUG double-positive vessels, consistent with the occurrence of EndMT (Figure 6D). Moreover, anti-miR-148b-treated wounds showed an increase in the total number of FSP-1-positive cells compared with the control oligonucleotide-treated wounds (Figure 6D), whereas staining with PicroSirius Red did not detect any increase of collagen deposition in the wounds (Figure S8E). Finally, to confirm that loss of miR-148b-mediated EndMT occurs through SMAD2 regulation, we knocked down SMAD2 by siRNA *in vivo* in the anti-miR-148b-treated wounds (Figure S8B). Knocking down SMAD2 in this model promotes wound closure (Figure 6A) without significantly promoting wound perfusion and vessel density (Figures S8C and S8D). Moreover, SMAD2 siRNA reduced the percentage of vessels double positive for CD31-FSP-1 and CD31-SLUG and decreased the total number of FSP-1-positive cells in the wounds treated with anti-miR-148b (Figure 6D). Overall, these results show that inhibition of miR-148b *in vivo* impaired wound healing and promoted EndMT on the wound edge via SMAD2.

DISCUSSION

We have comprehensively explored and been able to demonstrate for the first time that miR-148b has a crucial role in determining EC function and plasticity by regulating the TGF-β pathway. Overexpression of miR-148b enhances EC proliferation, migration, and *in vitro* angiogenesis via targeting *TGFB2* and *SMAD2*. *In vivo* delivery of miR-148b to injured skin promotes angiogenesis and accelerates wound closure. In contrast, miR-148b inhibition promotes the acquisition of a mesenchymal phenotype by ECs by unlocking the expression of *TGFB2* and *SMAD2*. This is associated with poor *in vivo* skin wound closure and activation of EndMT in dermal vessels.

One of the first indications of the involvement of miRNAs in EndMT came from Ghosh et al.,[20] who reported differential expression of a specific set of miRNAs during transition of mouse cardiac ECs to a mesenchymal phenotype. Since then, miRNAs have been linked to regulation of EndMT through different mechanisms. *In vitro* and *in vivo* studies demonstrated that decreased fibroblast growth factor (FGF) signaling leads to reduction in let-7 expression and initiation of TGF-β-dependent Endo-MT.[31] Recently, miR-20a was shown to target multiple genes in TGF-β signaling, such as ALK5, TGF-βR2, and SARA, thereby negatively regulating EndMT. The expression of miR-20a, which is normally downregulated during EndMT, is rescued by FGF2.[32] In our study, both miR-20a and let-7b are downregulated *in vivo* in the model of wound healing, whereas only miR-20a is also downregulated by cytokine treatment in HUVECs. Interestingly, further bioinformatic analysis demonstrated that the three miRNAs target a different set of genes of the TGF-β pathway with minimal (2 on 20 genes between miR-148b and let-7b) or no overlapping

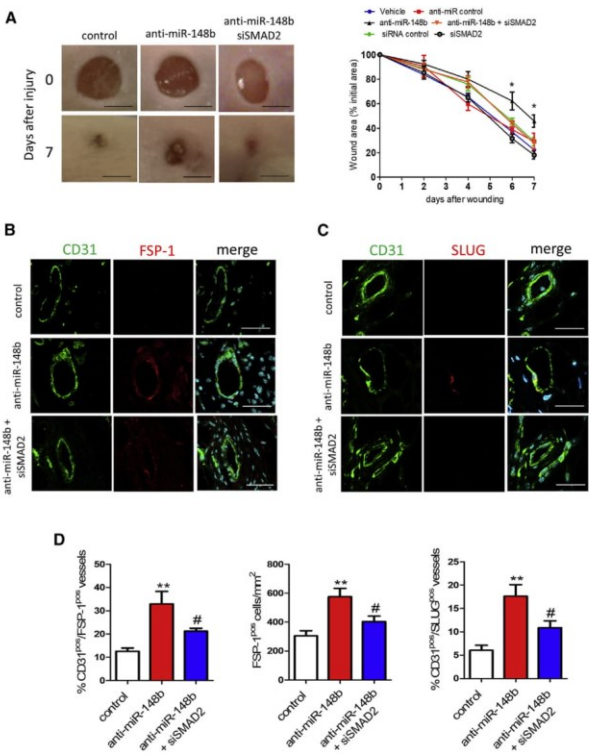

Figure 6. Inhibition of miR-148b Delays Wound Closure and Promotes EndMT in a Model of Wound Healing

Dermal wounds were treated with anti-miR control or siRNA control oligonucleotides and anti-miR-148b and/or SMAD2 siRNA for 7 days. (A) Left, representative images of treated wounds at 0 and 7 days post-wound-injury; scale bar, 5 mm. Right, level of wound closure is expressed as a percentage of wound area from the initial wound area (n = 8). (B) Immunohistochemical localization of CD31 (green) and FSP-1 (red) in the wound vessels; scale bars, 25 μm (magnification 630×) (n = 8), nuclei are stained with DAPI (blue). (C) Immunohistochemical localization of CD31 and SLUG in wound vessels; scale bars, 25 μm (magnification 630×) (n = 8), nuclei are stained with DAPI (blue). (D) Quantification of CD31/FSP-1 double-positive vessels and FSP-1-positive cells and CD31/SLUG double-positive vessels in the wounds; n = 8 per each group. Values are expressed as means ± SEM. $^{*}p < 0.05$; $^{**}p < 0.01$ versus anti-miR control. $^{\#}p < 0.05$ versus anti-miR-148b. Unpaired two-tailed Student's t test and one-way ANOVA statistical test followed by Bonferroni post-hoc analyses were applied.

(between miR-148b and miR-20a) targets. Therefore, miR-20a, let-7b, and miR-148b can interfere at different levels of the TGF-β pathway, permitting a possible synergic effect during skin wound healing.

The occurrence of EndMT post-natally has been associated with different types of fibrotic disease such as that in kidney[12] and heart,[11] both of which are associated with excessive collagen expression and deposition. Previous studies reported the importance of EndMT in dermal fibrosis, showing that delay in wound closure is associated with excessive collagen deposition.[33] In the present study, anti-miR-148b-mediated EndMT have a detrimental influence on skin wound closure, showing that around 30% of skin vessels are double positive for CD31 and FSP-1. This is highly important because, so transformed, these cells can be expected to secrete large amounts of collagen and other ECM proteins, which could contribute to fibrosis. In line with this, in our model we detected an increase in the recruitment of FSP-1-positive cells in wound treated with anti-miR-148b. However, analysis with PicroSirius Red did not show any accumulation of collagen in the wounds treated with anti-miR-148b at day 7 after wounding.

EndMT may lead to ECs acquiring a variety of different mesenchymal fates through different stages of differentiation.[4] The early endothelial response is characterized by a partial downregulation of endothelial markers, junction dismantling, and upregulation of some early mesenchymal markers. At later times, expression of endothelial markers further declines while more mesenchymal markers, including matrix proteins, are upregulated.[4] An abnormally increased inflammatory environment is often linked with phenotypic changes in ECs.[34] Chronic treatment of ECs with a combination of TNF-α and IL-1β over 6 days decreased the expression of miR-148b in ECs while it increased the expression and secretion of TGF-β2. In addition, the acquisition of a mesenchymal phenotype due to inflammation by dermal ECs is likely to lead to endothelial dysfunction, seen through decreased EC migration or dysregulation of inflammatory cell recruitment.[33]

Inflammation is sufficient to induce all events required for EndMT except for *de novo* acquisition of α-SMA, which is strictly dependent on TGF-β [30]. In our experiments, cytokine treatment or miR-148b inhibition increases the release of TGF-β2, as a direct target, which drives the EndMT process, perhaps partly or incompletely at least after 6 days. Consequently, EndMT appeared complete after 14 days of

TNF-α/IL-1β exposure. By this point, ECs have acquired α-SMA in addition to other markers of EndMT.

Recent reports show that inflammatory cytokines such as TNF-α and IL1-β can also trigger EndMT via binding to their receptors and by inducing nuclear factor κB (NF-κB) translocation to the nucleus, driving the expression of EndMT-specific genes.[30,35] Such inflammatory signals facilitate EndMT by increasing endogenous TGF-β expression in an NFκB-dependent manner, creating a feed-forward signaling mechanism.[36] Interestingly, treatment with the miR-148b mimics inhibited EndMT progression in cytokine-treated ECs. In agreement with this, a recent study demonstrated that pro-inflammatory molecules present in the serum of patients with Kawasaki syndrome induce EndMT through downregulation of miR-483 in ECs, whereas the overexpression of miR-483 using mimic oligonucleotides suppresses EndMT and restores EC function.[37]

In our *in vitro* model, the mechanism is based on activation of SMAD2, as demonstrated by rescue of EndMT using SMAD2 antisense. Alternatively, we have used SB43152, a specific inhibitor of ALK5, at the dose of 10 μM to inhibit SMAD2 phosphorylation and inhibit EndMT progression. However, SB43152 did not restore endothelial markers in the same manner as miR-148b mimics and SMAD2 siRNA. Discrepancy in outcomes is likely to be explained by an action of the miR-148b mimic or SMAD2 siRNA through SMAD2 mRNA degradation. In addition, another possible explanation of lack of activity of the inhibitor of ALK5 is that SMAD2 could be phosphorylated independently of ALK5 signaling by the mitotic kinase Mps1.[38]

In the *in vivo* model of wound healing, SMAD2 siRNA rescued anti-miR-148b-mediated EndMT and increased wound closure rate at day 7. However, at the same time point SMAD2 siRNA alone had no effect on wound closure rate. The discrepancy of these results could be explained by a role for other SMAD-independent pathways during wound closure and EndMT. For example, TGF-β and inflammatory cytokines have been shown to activate diverse non-SMAD parallel downstream pathways, such as extra-cellular signal-regulated kinase (ERK), c-Jun NH2-terminal kinase (JNK), p38 mitogen-activated protein (MAP) kinase.[39] Moreover, a recent study that analyzed the impact of EndMT on the skin wounds showed the existence of Notch-mediated EndMT during skin wound healing.[40]

The participation of EndMT during wound healing merits further confirmation and validation in future studies from individuals with recognized clinical pathological conditions, such as diabetic non-healing wounds. Such confirmation should lead to a change in the paradigm of the origin of cells involved in the fibrotic process. Furthermore, identification of the source of TGF-β and other active ligands that can initiate EndMT and increased understanding of the molecular mechanisms that regulate EndMT will be of great value in providing cellular targets amenable to therapeutic intervention for fibrotic disease. In our experience, the skin-wound-healing model is an excellent model to assess the potential impact of EndMT on the vessels that have formed during the wound-healing process. The excisional wounds rapidly close, with the active tissue remodelling of the wound area occurring in a reproducible way at specific time points. The use of an endothelial lineage-tracing mouse model during wound healing[40] has recently further corroborated our data and highlighted the critical role of EndMT during skin wound healing.

The TGF-β signaling pathway is considered a promising target for the treatment of many diseases, including pathological skin conditions. Most of the components of the TGF-β pathway have been targeted for drug development through various strategies. Several, such as oligonucleotide antisense, have been developed through pre-clinical to clinical trials.[41] Indeed, TGF-β antisense oligonucleotides reduced scarring and improved surgical outcome in animal models.[42] Moreover, Smad3 antisense oligonucleotides accelerated wound healing and reduced scarring in a mouse excisional wound model.[43] In this context, the benefit of miRNA-based therapy is the possibility of interfering with the regulation of multiple genes. Several miRNAs have already been used as therapeutic tools in vascular disease[17,18] to regulate different steps of the skin-wound-healing process.[44] Considering this, we have demonstrated that miR-148b mimics impact on different components of TGF-β pathway, thus amplifying its therapeutic potential in a model of skin wound healing.

An important factor that we have considered in our *in vivo* experiments is also at which stage of the wound-healing process treatment with miR-148b mimics could be beneficial. Several studies have previously reported that reducing TGF-β pathway at later stages during skin wound healing improved scarring outcome.[45] Based on these observations, skin wounds in the present study were treated from 3 days after wounding, when expression of miR-148b decreased, thus avoiding early inhibition of TGF-β signaling during the inflammatory phase, when it is required to start the healing process.[46]

In summary, the data presented here identify miR-148b as a novel regulator of TGF-β signaling and EC plasticity and a potential therapeutic target for promotion of tissue repair.

MATERIALS AND METHODS

Cells and Cell Culture

HUVECs (Lonza) were grown in endothelial growth medium-2 (EGM-2) (comprising endothelial basal medium-2 [EBM-2] with growth factors and other supplements) with 2% fetal bovine serum (FBS). Confluent HUVECs were treated with 10 ng/mL TNF-α, IL-1β, and TGF-β2 (PeproTech); medium and cytokines were changed every 2 days. SB431542 (Tocris) has been used at the dose of 10 μM. HEK293T cells (ATCC, CRL-11268) were cultured in DMEM with 10% FBS (Life Technologies).

miR-148b Target Analysis

Computational prediction of miR-148b target genes was done using published algorithm TargetScan (http://www.targetscan.org). miRpath v.3 (http://diana.imis.athena-innovation.gr/DianaTools/index.php?r=mirpath) was used to perform gene set enriched analysis of

miR-148b target genes. The prediction is based on TargetScan parameters such as Context score and Conservation score. The Context score for a specific site is the sum of the contribution of 14 features of the 3′ UTR structure;[47] the Conservation score is the probability of conserved targeting.[48] TargetScan considers matches to human 3′ UTRs and their orthologs, as defined by UCSC whole-genome alignments. Lowest Context score shows a more favorable binding. Higher conservation score represents a broad conservation of the binding sites between the species.

RNA Extraction and Quantitative Real-Time Analysis

Total RNA was extracted using an miReasy kit (QIAGEN). Real-time quantification to measure miRNA was performed with the TaqMan miRNA reverse transcription kit and miRNA assay (Life Technologies) using Lightcycler 480 (Roche). miRNA expression was normalized to the U6 small nucleolar RNA (snRU6). For mRNA analysis, cDNA was amplified by quantitative real-time PCR (real-time qPCR) and normalized to 18S ribosomal RNA. Each reaction was performed in triplicate. Quantification was performed by the $2^{-\Delta\Delta Ct}$ method.[49] Real-time qPCR was used to measure the expression of miR-148b (miR-148b-3p Thermo Fisher Scientific, cat. #4426961), snRU6 (Thermo Fisher Scientific, cat. #4331182), TGF-β2, SMAD2, CD31, VE-cadherin, COL1A1, α-SMA, SLUG, VIM, SNAIL, TWIST, ZEB1/2, and 18S rRNA. Pre-optimized primers were obtained from Sigma (KiCqStart Primers).

Cell Transfection, Transduction, and Functional Assays

Lipofectamine RNAiMAX (Thermo Fisher Scientific) was used to transfect HUVECs with miR-148b mimic, anti-miR-148b, and mimic or anti-miR control (25 nM and 75 mM, respectively, final concentration) or with siRNA targeting SMAD2 (20 nM final concentration), according to the manufacturer's instructions. jetPEI-HUVECs (Polyplus) was used to transfect HUVECs with DNA plasmids. The following functional assays were performed: BrdU incorporation assay using Cell Proliferation colorimetric assay (Roche); Matrigel assay with HUVECs was performed as previously described using BD Matrigel Basement Membrane Matrix (BD Biosciences).[50]

ECIS Assays: Migration Assay and Plasma Membrane Capacitance Analysis

Confluent HUVECs were transfected with controls or miR-148b mimic or anti-miR-148b and plated on the electric cell-substrate impedance sensing (ECIS) chip array (8W1E or 8W10E). The migration speed was calculated in μm/hr, capacitance of the plasma membrane is capacitance ($\mu F/cm^2$) as reported in Giaever and Keese.[29]

Western Blot Analyses

Proteins were extracted from cultured cells or muscles by using ice-cold buffer A (50 mM HEPES, 150 mM NaCl, 1 mM EDTA, 1 mM EGTA, 25 mM sodium fluoride [NaF], 5 mM sodium pyrophosphate [$Na_4P_2O_7$], 1% Triton, 1% NP40, 1 mM sodium orthovanadate [Na3VO4], 0.25% sodium deoxycholate, 0.5 mM Na-orthovanadate, 1 mM benzamidine, 0.1 mM phenylmethylsulfonyl fluoride). Protein concentration was determined using the Bio-Rad Protein Assay Reagent (Bio-Rad, UK). Detection of proteins by western blot analyses was done following separation of whole-cell extracts (20 μg) on SDS-polyacrylamide gels. Proteins were transferred to nitrocellulose membranes and probed with the following antibodies: TGF-β2 (Abcam, ab36495; 1:1,000), SMAD2 (Santa Cruz Biotechnology, Santa Cruz, CA, USA, #3102, 1:1,000), p-SMAD2 (465/467) (Cell Signaling, #3108; 1:1,000); CD31 (Abcam, 1:1,000), VE-cadherin (Abcam, ab33168; 1:1,000), COL1A1 (Abcam, ab138492; 1:200), FSP-1 (S100A4; Abcam, ab41532; 1:1,000), SLUG (Abcam, ab27568; 1:1000), β-actin (Abcam, ab16039; 1:4,000), HDAC3 (GeneTex GTX113303; 1:1,000), and GAPDH (GeneTex, GT239; 1:1,000) (both used as loading control). For detection, we used secondary antibodies conjugated to horseradish peroxidase, which were rabbit anti-mouse (Abcam, ab97046; 1:5,000) and goat anti-rabbit (Abcam, ab6721; 1:10,000). Detection was developed by enhanced chemiluminescence reaction (ECL) (Immunoblot, Millipore, 23225).

Immunofluorescence

Cells were fixed using 4% paraformaldehyde in PBS at room temperature for 15 min. For intracellular staining, fixed cells were permeabilized using 0.5% Triton X-100 in PBS (Sigma-Aldrich) or 0.1% Saponin in PBS at room temperature for 10 min. The blocking of specific antibody activity was performed using 3% BSA in PBS for 1 hr. Samples were incubated with antibodies to CD31 (Abcam, ab28364; 1:50), VE-cadherin (Abcam, ab33168; 1:100), FSP-1 (Abcam, ab41532; 1:200) and COL1A1 (Abcam, ab138492; 1:100) in PBS containing 1% BSA at 4°C overnight. Samples were washed extensively with PBS and incubated with Alexa Fluor 488-conjugated antibodies to rabbit immunoglobulin G (IgG) (Life Technologies, Carlsbad, CA, #A11070) and Alexa Fluor 594-conjugated antibodies to rabbit IgG (Life Technologies, Carlsbad, CA, #A11072) in DAPI with PBS with 1% BSA at room temperature for 1 hr. Image analysis was performed on Zeiss LSM 780 confocal microscope.

Luciferase Assay

Luciferase assay has been performed as previously described.[50] TGFB2 3′ UTR and SMAD2 3′ UTR vectors were cloned in pMIR-Reporter (Life Technologies). Primers are used for the cloning are as follows: TGF-β2 3′ UTR, forward 5′-ATAAAGCTTATTTGCCA CATCATTGCAGA-3′, reverse 5′-ATAACTAGTGGGAATAAAAA GACGGCACA-3′; SMAD2 3′ UTR, forward 5′-ATAAAGCTTT GATCCAGCTAAGGTAACTGATGTT-3′; reverse 5′-ATAACTAG TTGGTAAACAACTCAAATGGCTTTC-3′. Primers for 3′ UTR mutation are as follows: TGFB2, forward 5′-ATAAAGCTTATTTG CCACATCATTGCAGA-3′ and reverse 5′-ATAACTAGTCCTATC TGAGAGGAAAATGTCTGC-3′; SMAD2, forward 5′-ATAAAGC TTTGATCCAGCTAAGGTAACTGATGTT-3′ and reverse 5′-ATA ACTAGTGGACTTCCAGAGGGAAACAA-3′. Luciferase constructs were transfected into HEK293T cells or HUVECs together with miR-148b mimics or p-SV-β-gal control vector. Cells were cultured for 48 hr and assayed with the Luciferase and β-Galactosidase Reporter Assay Systems (Promega). Luciferase values were normalized to protein concentration and β-galactosidase activity.

Animal Experiments

All experiments involving mice were performed in accordance with the guidance and the operation of Animals (Scientific Procedures) Act 1986 and prior approval of the UK Home Office and the University of Edinburgh Animal Welfare and Ethical Review Board. The skin-wound-healing protocol was performed as described previously.[51–53] CD-1 female mice (7 to 9 weeks old) (n = 8 per group) were randomly assigned to a treatment group and anaesthetized with isofluorane. Two full-thickness excisional wounds were made to the shaved dorsal skin. Full-thickness excisional wounds were made in a midline skin fold using a sterile, disposable 5-mm biopsy punch (Kai Industries), resulting in generation of one wound on each side of the midline. Control oligonucleotides (scramble sequence), miR-148b mimic, Cy3-labeled miR-148b mimic, or anti-miR-148b or SMAD2 siRNA (1 μg/wound) were delivered topically by pipette into the wound cavity (10 μL in a vehicle of 30% Pluronic F-127 gel [that is, liquid at 4°C but solidifies at body temperature]; Sigma-Aldrich). Mimics were initially delivered after 3 days, whereas anti-miR and siRNA were delivered immediately after wounding. The treatment was repeated every second day for 7 days. Wounds were photographed using an Olympus camera on days 0, 2, 4, 6, and 7 after wounding. Wound areas were calculated as previously described.[51,52] In brief, wound diameter was measured using a Vernier caliper, and wound area was calculated using a standard formula for the area of an ellipse (semi-major diameter × semi-minor diameter × Pi). The superficial blood flow of the wounds was sequentially analyzed by color laser Doppler (Color Laser Doppler, Moor, UK), and the ratio of blood flow between the mimic or anti-miR or siRNA-treated and the control-treated wounds was calculated. Wound size and Doppler analysis were performed in blinded fashion.

Histology and Image Analysis

Wounds were harvested, prepared, and analyzed as previously described.[51–53] At days 5 or 7 post-wounding, wounds were harvested and fixed in 10% buffered formalin (16 hr at 4°C, Sigma) for embedding in paraffin. Sections were deparaffinized, rehydrated, and stained with rat anti-mouse polyclonal CD31 (Abcam, ab28364; 1:50), α-SMA (Sigma, A2547; 1:100), rabbit anti-mouse FSP-1 (Abcam, ab41532; 1:50), and SLUG (Abcam, ab28364; 1:200); all antibodies were used overnight at 4°C. Stained slides were photographed and analyzed in a blinded fashion using a Zeiss LSM 780 Confocal Microscope (Zeiss). Vascular density in wounds was counted after immunostaining for CD31 and α-SMA. Ten fields per section/animal (n = 8 animal; 400× magnification) were randomly examined and averaged to analyze the number of CD31-positive blood vessels in the wound edges. Image analysis was performed using ImageJ software as previously reported.[51] Vascular density is expressed per square millimeter. EndMT of ECs was assessed by FSP-1 and SLUG immunostaining combined with CD31 staining. CD31-FSP-1 and CD31-SLUG double-positive vessels are expressed as percentage of positive vessels. For analysis of fibrosis, slides were stained with PicroSirius Red (PSR) then photographed and analyzed in a blinded fashion using a light microscope (Axioscope 2; Zeiss). Six images per slide were captured at 400× magnification for PSR histological staining. Color deconvolution in ImageJ software was used to evaluate the percentage of red staining, which indicates the presence of collagen fibers in the tissue. The area of collagen was measured as the percentage of total pixels in each image, using the Threshold option in ImageJ software.

Statistical Analysis

Comparisons between two different conditions were assessed using two-tailed Student's t test. Differences among groups of more than two were tested using one-way ANOVA, followed by Bonferroni post-hoc analyses as appropriate. Data are expressed as mean ± SEM of three independent experiments, each performed in triplicate or quintuplicate, as reported in the figure legends. A p value < 0.05 was considered statistically significant. Analyses were performed using GraphPad Prism v5.0.

SUPPLEMENTAL INFORMATION

Supplemental Information includes eight figures and can be found with this article online at https://doi.org/10.1016/j.ymthe.2018.05.002.

AUTHOR CONTRIBUTIONS

V.M. acquired and analyzed the data and drafted the manuscript; M.M., T.M., A.A.H.Z., A.M., L.R., B.C., G.A.G., and E.P. participated in acquiring and analyzing the data and revised the manuscript; A.C. designed the study and drafted the manuscript.

CONFLICTS OF INTEREST

The authors declare no competing interest.

ACKNOWLEDGMENTS

V.M. is sponsored by a University of Edinburgh Chancellor's Fellow studentship and A.C. is a British Heart Foundation (BHF) Intermediate Research Fellow and a University of Edinburgh Chancellor's Fellow. This study was supported by grants from the British Heart Foundation (BHF) (FS/11/52/29018 and PG/16/58/32275 to A.C. and FS/14/7/30574 to A.M.). B.C. is supported by the Edinburgh BHF PhD Program, A.A.H.Z. is supported by the Intermediate Fellowship awarded by the Oxford British Heart Foundation (BHF) Centre of Research Excellence (RE/08/004/23915), and T.M. is supported by BHF Career Re-entry Fellow (FS/16/38/32351). A.C. acknowledges the Edinburgh BHF Research Excellence Award.

REFERENCES

1. Goumans, M.J., and Ten Dijke, P. (2018). TGF-beta signaling in control of cardiovascular function. Cold Spring Harb. Perspect. Biol. *10*, a022210.
2. van Meeteren, L.A., and ten Dijke, P. (2012). Regulation of endothelial cell plasticity by TGF-β. Cell Tissue Res. *347*, 177–186.
3. Akhurst, R.J. (2012). The paradoxical TGF-β vasculopathies. Nat. Genet. *44*, 838–839.
4. Dejana, E., Hirschi, K.K., and Simons, M. (2017). The molecular basis of endothelial cell plasticity. Nat. Commun. *8*, 14361.
5. Piera-Velazquez, S., Mendoza, F.A., and Jimenez, S.A. (2016). Endothelial to mesenchymal transition (EndoMT) in the pathogenesis of human fibrotic diseases. J. Clin. Med. *5*, e45.

6. Kovacic, J.C., Mercader, N., Torres, M., Boehm, M., and Fuster, V. (2012). Epithelial-to-mesenchymal and endothelial-to-mesenchymal transition: from cardiovascular development to disease. Circulation *125*, 1795–1808.

7. Piera-Velazquez, S., and Jimenez, S.A. (2012). Molecular mechanisms of endothelial to mesenchymal cell transition (EndoMT) in experimentally induced fibrotic diseases. Fibrogenesis Tissue Repair *5* (*Suppl 1*), S7.

8. Arciniegas, E., Neves, C.Y., Carrillo, L.M., Zambrano, E.A., and Ramírez, R. (2005). Endothelial-mesenchymal transition occurs during embryonic pulmonary artery development. Endothelium *12*, 193–200.

9. Armstrong, E.J., and Bischoff, J. (2004). Heart valve development: endothelial cell signaling and differentiation. Circ. Res. *95*, 459–470.

10. Zeisberg, E.M., Potenta, S., Xie, L., Zeisberg, M., and Kalluri, R. (2007). Discovery of endothelial to mesenchymal transition as a source for carcinoma-associated fibroblasts. Cancer Res. *67*, 10123–10128.

11. Zeisberg, E.M., Tarnavski, O., Zeisberg, M., Dorfman, A.L., McMullen, J.R., Gustafsson, E., Chandraker, A., Yuan, X., Pu, W.T., Roberts, A.B., et al. (2007). Endothelial-to-mesenchymal transition contributes to cardiac fibrosis. Nat. Med. *13*, 952–961.

12. Zeisberg, E.M., Potenta, S.E., Sugimoto, H., Zeisberg, M., and Kalluri, R. (2008). Fibroblasts in kidney fibrosis emerge via endothelial-to-mesenchymal transition. J. Am. Soc. Nephrol. *19*, 2282–2287.

13. Cooley, B.C., Nevado, J., Mellad, J., Yang, D., Hilaire, C.S., Negro, A., Fang, F., Chen, G., San, H., Walts, A.D., et al. (2014). TGF-β signaling mediates endothelial-to-mesenchymal transition (EndMT) during vein graft remodeling. Sci. Transl. Med. *6*, 227ra34.

14. Evrard, S.M., Lecce, L., Michelis, K.C., Nomura-Kitabayashi, A., Pandey, G., Purushothaman, K.R., d'Escamard, V., Li, J.R., Hadri, L., Fujitani, K., et al. (2016). Endothelial to mesenchymal transition is common in atherosclerotic lesions and is associated with plaque instability. Nat. Commun. *7*, 11853.

15. Ha, M., and Kim, V.N. (2014). Regulation of microRNA biogenesis. Nat. Rev. Mol. Cell Biol. *15*, 509–524.

16. Li, Z., and Rana, T.M. (2014). Therapeutic targeting of microRNAs: current status and future challenges. Nat. Rev. Drug Discov. *13*, 622–638.

17. Caporali, A., and Emanueli, C. (2011). MicroRNA regulation in angiogenesis. Vascul. Pharmacol. *55*, 79–86.

18. Caporali, A., and Emanueli, C. (2012). MicroRNAs in postischemic vascular repair. Cardiol. Res. Pract. *2012*, 486702.

19. Kurakula, K., Goumans, M.J., and Ten Dijke, P. (2015). Regulatory RNAs controlling vascular (dys)function by affecting TGF-β family signalling. EXCLI J. *14*, 832–850.

20. Ghosh, A.K., Nagpal, V., Covington, J.W., Michaels, M.A., and Vaughan, D.E. (2012). Molecular basis of cardiac endothelial-to-mesenchymal transition (EndMT): differential expression of microRNAs during EndMT. Cell. Signal. *24*, 1031–1036.

21. Chen, Y., Song, Y.X., and Wang, Z.N. (2013). The microRNA-148/152 family: multi-faceted players. Mol. Cancer *12*, 43.

22. Serino, G., Sallustio, F., Cox, S.N., Pesce, F., and Schena, F.P. (2012). Abnormal miR-148b expression promotes aberrant glycosylation of IgA1 in IgA nephropathy. J. Am. Soc. Nephrol. *23*, 814–824.

23. Bidzhekov, K., Gan, L., Denecke, B., Rostalsky, A., Hristov, M., Koeppel, T.A., Zernecke, A., and Weber, C. (2012). microRNA expression signatures and parallels between monocyte subsets and atherosclerotic plaque in humans. Thromb. Haemost. *107*, 619–625.

24. Vlachos, I.S., Zagganas, K., Paraskevopoulou, M.D., Georgakilas, G., Karagkouni, D., Vergoulis, T., Dalamagas, T., and Hatzigeorgiou, A.G. (2015). DIANA-miRPath v3.0: deciphering microRNA function with experimental support. Nucleic Acids Res. *43* (W1), W460–W466.

25. Grimson, A., Farh, K.K., Johnston, W.K., Garrett-Engele, P., Lim, L.P., and Bartel, D.P. (2007). MicroRNA targeting specificity in mammals: determinants beyond seed pairing. Mol. Cell *27*, 91–105.

26. Song, H., Wang, Q., Wen, J., Liu, S., Gao, X., Cheng, J., and Zhang, D. (2012). ACVR1, a therapeutic target of fibrodysplasia ossificans progressiva, is negatively regulated by miR-148a. Int. J. Mol. Sci. *13*, 2063–2077.

27. Zhang, J., Ying, Z.Z., Tang, Z.L., Long, L.Q., and Li, K. (2012). MicroRNA-148a promotes myogenic differentiation by targeting the ROCK1 gene. J. Biol. Chem. *287*, 21093–21101.

28. Simons, M., Alitalo, K., Annex, B.H., Augustin, H.G., Beam, C., Berk, B.C., Byzova, T., Carmeliet, P., Chilian, W., Cooke, J.P., et al.; American Heart Association Council on Basic Cardiovascular Sciences and Council on Cardiovascular Surgery and Anesthesia (2015). State-of-the-art methods for evaluation of angiogenesis and tissue vascularization: a scientific statement from the American Heart Association. Circ. Res. *116*, e99–e132.

29. Giaever, I., and Keese, C.R. (1991). Micromotion of mammalian cells measured electrically. Proc. Natl. Acad. Sci. USA *88*, 7896–7900.

30. Rieder, F., Kessler, S.P., West, G.A., Bhilocha, S., de la Motte, C., Sadler, T.M., Gopalan, B., Stylianou, E., and Fiocchi, C. (2011). Inflammation-induced endothelial-to-mesenchymal transition: a novel mechanism of intestinal fibrosis. Am. J. Pathol. *179*, 2660–2673.

31. Chen, P.Y., Qin, L., Barnes, C., Charisse, K., Yi, T., Zhang, X., Ali, R., Medina, P.P., Yu, J., Slack, F.J., et al. (2012). FGF regulates TGF-β signaling and endothelial-to-mesenchymal transition via control of let-7 miRNA expression. Cell Rep. *2*, 1684–1696.

32. Correia, A.C., Moonen, J.R., Brinker, M.G., and Krenning, G. (2016). FGF2 inhibits endothelial-mesenchymal transition through microRNA-20a-mediated repression of canonical TGF-β signaling. J. Cell Sci. *129*, 569–579.

33. Manetti, M., Romano, E., Rosa, I., Guiducci, S., Bellando-Randone, S., De Paulis, A., Ibba-Manneschi, L., and Matucci-Cerinic, M. (2017). Endothelial-to-mesenchymal transition contributes to endothelial dysfunction and dermal fibrosis in systemic sclerosis. Ann. Rheum. Dis. *76*, 924–934.

34. Romero, L.I., Zhang, D.N., Herron, G.S., and Karasek, M.A. (1997). Interleukin-1 induces major phenotypic changes in human skin microvascular endothelial cells. J. Cell. Physiol. *173*, 84–92.

35. Mahler, G.J., Farrar, E.J., and Butcher, J.T. (2013). Inflammatory cytokines promote mesenchymal transformation in embryonic and adult valve endothelial cells. Arterioscler. Thromb. Vasc. Biol. *33*, 121–130.

36. Liu, R.M., and Gaston Pravia, K.A. (2010). Oxidative stress and glutathione in TGF-beta-mediated fibrogenesis. Free Radic. Biol. Med. *48*, 1–15.

37. He, M., Chen, Z., Martin, M., Zhang, J., Sangwung, P., Woo, B., Tremoulet, A.H., Shimizu, C., Jain, M.K., Burns, J.C., and Shyy, J.Y. (2017). miR-483 targeting of CTGF suppresses endothelial-to-mesenchymal transition: therapeutic implications in Kawasaki disease. Circ. Res. *120*, 354–365.

38. Zhu, S., Wang, W., Clarke, D.C., and Liu, X. (2007). Activation of Mps1 promotes transforming growth factor-beta-independent Smad signaling. J. Biol. Chem. *282*, 18327–18338.

39. Derynck, R., and Zhang, Y.E. (2003). Smad-dependent and Smad-independent pathways in TGF-beta family signalling. Nature *425*, 577–584.

40. **Patel, J, Baz, B, Wong, HY, Lee, JS, and Khosrotehrani, K (2017). Accelerated endothelial to mesenchymal transition increased fibrosis via deleting Notch signalling in wound vasculature.**

41. Akhurst, R.J., and Hata, A. (2012). Targeting the TGFβ signalling pathway in disease. Nat. Rev. Drug Discov. *11*, 790–811.

42. Choi, B.M., Kwak, H.J., Jun, C.D., Park, S.D., Kim, K.Y., Kim, H.R., and Chung, H.T. (1996). Control of scarring in adult wounds using antisense transforming growth factor-beta 1 oligodeoxynucleotides. Immunol. Cell Biol. *74*, 144–150.

43. Cordeiro, M.F., Mead, A., Ali, R.R., Alexander, R.A., Murray, S., Chen, C., York-Defalco, C., Dean, N.M., Schultz, G.S., and Khaw, P.T. (2003). Novel antisense oligonucleotides targeting TGF-beta inhibit in vivo scarring and improve surgical outcome. Gene Ther. *10*, 59–71.

44. Mulholland, E.J., Dunne, N., and McCarthy, H.O. (2017). MicroRNA as therapeutic targets for chronic wound healing. Mol. Ther. Nucleic Acids *8*, 46–55.

45. Finnson, K.W., McLean, S., Di Guglielmo, G.M., and Philip, A. (2013). Dynamics of transforming growth factor beta signaling in wound healing and scarring. Adv. Wound Care (New Rochelle) *2*, 195–214.

46. Finnson, K.W., Arany, P.R., and Philip, A. (2013). Transforming growth factor beta signaling in cutaneous wound healing: lessons learned from animal studies. Adv. Wound Care (New Rochelle) *2*, 225–237.

47. Agarwal, V., Bell, G.W., Nam, J.W., and Bartel, D.P. (2015). Predicting effective microRNA target sites in mammalian mRNAs. eLife *4*, eLife.05005.

48. Friedman, R.C., Farh, K.K., Burge, C.B., and Bartel, D.P. (2009). Most mammalian mRNAs are conserved targets of microRNAs. Genome Res. *19*, 92–105.

49. Schmittgen, T.D., and Livak, K.J. (2008). Analyzing real-time PCR data by the comparative C(T) method. Nat. Protoc. *3*, 1101–1108.

50. Caporali, A., Meloni, M., Völlenkle, C., Bonci, D., Sala-Newby, G.B., Addis, R., Spinetti, G., Losa, S., Masson, R., Baker, A.H., et al. (2011). Deregulation of microRNA-503 contributes to diabetes mellitus-induced impairment of endothelial function and reparative angiogenesis after limb ischemia. Circulation *123*, 282–291.

51. Al Haj Zen, A., Nawrot, D.A., Howarth, A., Caporali, A., Ebner, D., Vernet, A., Schneider, J.E., and Bhattacharya, S. (2016). The retinoid agonist tazarotene promotes angiogenesis and wound healing. Mol. Ther. *24*, 1745–1759.

52. Caporali, A., Meloni, M., Miller, A.M., Vierlinger, K., Cardinali, A., Spinetti, G., Nailor, A., Faglia, E., Losa, S., Gotti, A., et al. (2012). Soluble ST2 is regulated by p75 neurotrophin receptor and predicts mortality in diabetic patients with critical limb ischemia. Arterioscler. Thromb. Vasc. Biol. *32*, e149–e160.

53. Barcelos, L.S., Duplaa, C., Kränkel, N., Graiani, G., Invernici, G., Katare, R., Siragusa, M., Meloni, M., Campesi, I., Monica, M., et al. (2009). Human CD133^{+} progenitor cells promote the healing of diabetic ischemic ulcers by paracrine stimulation of angiogenesis and activation of Wnt signaling. Circ. Res. *104*, 1095–1102.